Early Events in Tumour Development: a study based on mouse models of human colorectal cancer

by

Rungtiva Kongkanuntn

A thesis submitted for the degree of
Doctor of philosophy
University of Edinburgh
2000

Declaration

This thesis has been composed by myself and the experiments reported in this thesis were carried out by myself unless stated otherwise in the text.

Rungtiva Kongkanuntn

Edinburgh,

January, 2000

Abstract

Mutation in the *APC* gene is present in over 80% of sporadic human colorectal cancer tumours, both benign and malignant. It is responsible, when inherited in the germ line, for the mendelian dominant condition of familial adenomatous polyposis (FAP). Germ-line mutation in nucleotide mismatch repair genes, in contrast, is responsible for the familial disorder of hereditary, non-polyposis colorectal cancer, and functional deficiency in this group of genes is clonally present in around 15% of sporadic tumour. Although these two types of genetic deficiency are both associated with colorectal cancer, their roles appear to be very different: whereas deficiency in *Apc* facilitates development of adenomas with a low transition frequency to cancer, deficiency in mismatch repair genes is associated with malignant tumours which evolve rapidly from precursor benign lesions, or perhaps may arise *de novo*. APC is a multifunctional protein whose known functions include interaction with microtubules and the signalling protein β-catenin, a component of the Wnt-dependent transcriptional activation pathway. Its precise role in initiating adenoma formation is, however, not clear. Use of murine models of human colorectal cancer will lead to a further understanding of how the *APC*, mismatch repair and *p53* genes interact with each other in the process of cancer development. Furthermore, these models should elucidate the role played by β-catenin, a mediator of the Wnt pathway. β-Catenin is known to be modulated by APC and involved subsequently in the activation of downstream target genes. However, it is still unclear how mutations affecting β-catenin interact with mismatch repair gene mutations. This thesis, therefore, seeks to examine the cell biology of the earliest manifestations of neoplasia in mice congenitally deficient in *Apc* or mismatch repair (*Msh2* $^{-/-}$) function.

I have investigated the pattern of β-catenin staining in a spectrum of apparently normal epithelium from animals bearing mutations in *Apc* (the *Min* mouse), *p53* and *Msh2* and compared this with patterns of Apc and E-cadherin protein immunohistochemistry staining. In general, β-catenin and E-cadherin expression was found at the lateral intercellular membrane in all types of epithelium, whereas Apc

staining was found in the cytoplasm of epithelial cells in each organ but also showed strong positivity at the apical surface in intestinal epithelium. In animals bearing heterozygous mutation of Apc, enhanced β-catenin expression was identified in intestinal and pancreatic lesions in *Apc* $^{Min+/-}$ and (*Apc* $^{Min+/-}$/*p53* $^{-/-}$) mice and in a subset of intestinal lesions in *Msh2* $^{-/-}$ mice.

This thesis characterised in detail the pattern of β-catenin expression in intestinal and pancreatic lesions arising in mice singly or multiply mutant for *Apc*, *p53* and *Msh2*. These lesions were first graded on the basis of morphology. Overexpression of β-catenin was found in the majority of early intestinal lesions arising on an *Apc* $^{Min+/-}$ background. In all categories of lesion studied mosaic patterns of β-catenin expression were observed with the proportion of cells showing a decrease in staining intensity associated with increasing lesion size. *p53* status did not have any effects on these patterns. Mice mutant for the mismatch repair gene, *Msh2*, also showed increased expression of β-catenin in intestinal adenomas and microadenomas. However, in contrast with *Apc* $^{Min+/-}$ mice, a subset of these lesions retained apparently normal expression. β-Catenin upregulation was also found in the pancreas in foci of histologically abnormal cells in *Apc* $^{Min+/-}$ and (*Apc* $^{Min+/-}$/*p53* $^{-/-}$) mice. PCR analysis of microdissected materials confirmed that β-catenin overexpression was consistently associated with loss of the remaining wild type *Apc* allele. Subsequently analysis of these foci (see below) confirmed these cells to be dysplastic, based on their aberrant nuclear volume. In the (*Apc* $^{Min+/-}$/*p53* $^{-/-}$) mice both adenomas and adenocarcinomas of the pancreas arose and were characterised by an increased staining intensity of β-catenin. Taken together, these findings demonstrated that increased expression of β-catenin is an efficient marker of early neoplastic change in both murine intestine and pancreas in *Apc* mutant mice. However, they also showed that dysregulation of β-catenin is not an obligate step in the development of earliest intestinal preneoplastic lesions: genetic events other than complete loss of *Apc* function appear competent to initiate the transition from normal to neoplastic epithelium.

I have further analysed the nuclear volume of cells within lesions both in the intestine and pancreas because an increase in nuclear size was noted in the first part of study. This

was performed using both three-dimensional (3D) and two-dimensional (2D) imaging. The nuclear volume analysis of intestinal lesions in all genotypes of mice showed only small differences in nuclear volume in all types of lesions compared to wild type mice and normal intestinal crypt nuclei ($p<0.05$). In contrast, there was a marked difference in nuclear volume of cells within pancreatic lesions arising in each mutant background when compared to wild type and adjacent normal pancreatic nuclei ($p<0.05$). The largest increase in nuclear volume was associated with mice doubly mutant for *Apc* and *p53* (*Apc* $^{Min+/-}$/*p53* $^{-/-}$). These mice showed significant increases in nuclear volume in all sizes of pancreatic lesions. The increase in nuclear volume observed in all genotypes was most extreme in small lesions but the increase was less prominent in larger lesions ($p< 0.05$), suggesting that lesions pass through a critical stage of instability during their growth. The change in nuclear volume is extrapolated to reflect an increase in chromosome ploidy, which is an early cellular event in carcinogenesis. In summary, an increase in nuclear size is an early cellular phenomenon in carcinogenesis, which is influenced by mutation of both *Apc* and *p53* genes.

Acknowledgement

My PhD study was funded by the Thai Government, and was supervised by Professor Andrew H. Wyllie, to whom I am very grateful for his kindness, support and encouragement.

Special thanks to Dr. Vivien J. Bubb and Professor Alan R. Clarke for very helpful, kind advises and discussions.

Thanks to Dr. Peter G. Bush for his advice in three-dimensional image analysis.

I would like to thank Scott Cunningham, Francis Rae, Steven MacKey, Stuart McKenzei and every one working in the Department of Pathology for supporting my work during the past three years and a half.

Final thanks to my husband who always encourages and gives a moral support to me and thank to my parents and my family.

Table of Contents

Abbreviations

AMP	adenosine mono-phosphate
AP	alkaline phosphatase
APC	adenomatous polyposis coli protien, human
APC	adenomatous polyposis coli gene, human
Apc	adenomatous polyposis coli protein, mouse
Apc	adenomatous polyposis coli gene, mouse
ATP	adenosine tri-phosphate
BrdU	bromodeoxyuridine
CLSM	confocal laser scanning microscope
DAB	3,3-diaminobenzidine
DNA	deoxyribonucleic acid
DNTPs	deoxyribonucleotide triphosphates
EDTA	diamino tetra acetic acid
FAP	familial adenomatous polyposis
GSK	glycogen synthase kinase
HCl	hydrocloric acid
H_2O_2	hydrogen peroxide
HNPCC	hereditary non-polyposis colon cancer
HOME	highly optimised microscope environment
HRP	horseradish peroxidase
Ig	immunoglobulin
Mg	magnesium
Min	multiple intestinal neoplasia
MMR	mismatch repair gene
PCR	polymerase chain reaction
RNA	ribonucleic acid

RT	room temperature
SDS	sodium dodesyl sulfate
TBE	tris-borate/EDTA electrophoresis buffer
TBS	tris buffered saline
TE	tris/EDTA buffer
UV	ultraviolet light

Chapter 1

Introduction

This thesis provides a new view of the role in carcinogenesis of the oncosuppressor protein Adenomatous Polyposis Coli (APC). The evidence for this view, unfolded in the following chapters, is drawn from observations in mice bearing germ-line defects in *Apc* and other genes, and studied by immunohistochemical, morphometric and molecular pathological techniques. The underlying motive in these studies, however, is the profound social and medical implications of disorders of *APC* in man, and in particular their roles in the causation of colorectal cancer.

1.1. Human colorectal cancer

1.1.1. Incidence and Epidemiology

Adenocarcinoma of the colon and rectum is the second commonest malignant tumour in males and the third commonest in females in the Western world. In Scotland, a country of around 5 million inhabitants, there are 27,000 new cases every year (HMSO 1989) a situation that has remained unchanged for the past 2 decades. The overall survival of affected patients has also remained unchanged, despite many high technologies in diagnostic methods and in surgery, which is the mainstay of treatment. In world wide, it has been estimates that there are at least half a million new cases every year, but colorectal cancer is much rarer in the Southeast Asian countries which are different in environmental factors associated with colorectal cancer risk. In the 1950's, epidemiological studied of immigrants from Japan (at that time a low incidence area) to Hawaii (a western community with dietary and social habits close to those of the United States) showed the strong influence of environmental factors in the pathogenesis of this disease. The incidence of colorectal cancer in the Southeast Asian communities has risen steadily. Age-adjusted incidence, male and female ratio; in Japan is now 14.8:10.1 per 100,000; in Singaporean Chinese is 20.2:18.1 per 100,000; in Singaporean Malays is

6.9:5.5 per 100,000; in Hong Kong Chinese is 21.7:16.7 per 100,000; figures close to those of UK (17.1:14.6 per 100,000) and USA (32.1:22.6 per 100,000) (Parkin *et al* 1992). In Thailand, the incidence (5.5:3.7 per 100,000) is still much lower (Vatanasapt *et al* 1993). Incidence in India is 3.2:2.6 (Parkin *et al* 1992). These data clearly demonstrated the existence of environmental agents in the genesis of the disease, most probably in the diet.

Adenomas are uncommon before the age of 30, but occur with increasing frequency as progressively older. The average age at diagnosis is about 50 years. Adenomas are more common in males in all regions of colon whereas adenomas in the right colon have been noted to show more severe dysplasia in females (Morson *et al* 1990). Up to the age of 55, cancer of the colon is more common in females and becomes slightly more common in males after the age of 55. In high-risk areas the incidence of right-sided colon cancer may be higher in females of all ages.

1.1.2. Natural history and histopathology

In the west, approximately 60% of primary colorectal cancers arise in the sigmoid colon or rectum (Damjanov *et al* 1996). The transverse colon accounts for a further 25%. The ascending colon is a predilection site and it appears that the incidence of cancer in the right colon is increasing. The tumours are most commonly moderately differentiated adenocarcinomas, but a significant proportion usually situated in the caecum or ascending colon, which are mucin secreting or poorly differentiated. Directly metastasise to the local lymph nodes and by haematogenous routes to the liver occasionally or other organs. At the time of diagnosis, approximately 15% of tumours in patients are restricted to the mucosa, 35% have not completely penetrated the muscle wall, 35% have affected lymph nodes identifiable after surgical removal and the remainders more distant metastases (Morson *et al* 1990). Prognosis is dependent upon the stage of the tumour at the time of detection. Very few patients with distant metastases survive, indicating the generally ineffective character of chemotherapy and radiation therapy. In contrast, survival of patients with intramucosal tumours is close to 100%, regardless of stage, this survival is around 30%, but shows no substantial further

reduction after 5 years, which indicates that early, appropriate intervention can effect cure.

There is substantial evidence that almost colorectal adenocarcinomas develop from pre-existing premalignant lesions. The most clearly evidence of these is the adenoma, but intraepithelial dysplasia has also been described, particularly in the relatively rare subgroup of cancers arising in patients with ulcerative colitis. Adenomas are benign tumours arising as local proliferations of intramucosal glands. Initially flat or berry-like, they can compose of a stalk. Histologically, adenomas are classified as tubular, tubulovillous and villous. In surgical material approximately 10% of adenomas are villous, but in autopsy studies only 1% of adenomas are tubulovillous or villous (Damjanov *et al* 1996). Adenomas may show mild or low-grade dysplasia. Adenomas can gradually grow in size and change from a tubular to a villous structure. The cells show severe or high-grade dysplasia followed by malignant change resulting in local invasion with eventual metastasis to distant site.

The evidence that adenomas can develop to carcinomas, and that most carcinomas arise in this way came initially from epidemiological and histological studies. In brief, adenomas are six times as common in surgical specimens of colorectal cancer than in length, age and sex matched colorectal specimens from patients without cancer; adenomas occur at earlier age than carcinomas; adenomas are larger and more numerous in high risk populations for colorectal cancer; a series of adenomas will show all grades of dysplasia ranging from slightly different from normal through to carcinoma *in situ*; and removal of adenomas greatly reduces the incidence of cancer in the intestine. Furthermore, histological analysis of adenoma sometimes shows small foci of adenocarcinoma, while similar analysis of carcinomas shows foci of adenoma. Finally, evidence from patients submitted to repeated sigmoidoscopy but without therapy, was observed progression from adenoma to carcinoma. The most definitive evidence for this progression, however, has come much more recently, though analysis of the molecular genetic events that are associated with adenoma and carcinoma growth.

1.1.3. Molecular genetics of human colorectal cancer

Following the discovery of oncogenes, human colorectal cancer was one of the first human tumours have been analysed in detailed at the molecular level, and still remains unclear. As adenomas enlarge, they accumulate clonal mutations in the *Ki-ras* oncogene, notably when there is villous formation, a histopathological feature associated with risk of progression to malignancy. Evidence of loss of heterozygosity at potential oncosuppressor loci such as *DCC* in 18q, and of trisomy of specific chromosomes (notably chromosome 7) also appears in the larger adenomas (Damjanov *et al* 1996). Dissection of small foci of carcinoma arising inside adenomas shows that this transition is often associated with severe disruption of genomic stability. Carcinomas tend to be aneuploid in DNA content and have multiple sites of LOH. A high proportion shows mutation or allelic loss of the oncosuppressor gene *p53*. These changes are summarised in diagram below.

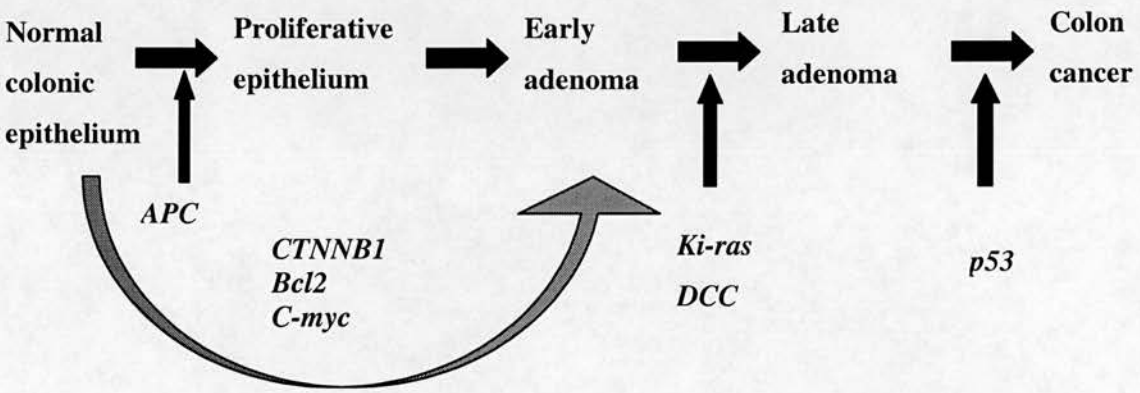

The majority of these observations were from separate analyses of benign and malignant tumours, collected from large numbers of patients, some were collected by microdissected complex tumours that contained both benign and malignant tumour. There was remarkable confirmation of the evolution of carcinoma from adenoma, associated with conservation in the carcinoma of the same mutation in *Ki-ras* as was present in the adenoma, and further genomic changes such as *p53* mutation and aneuploidy.

Outstanding among these changes in molecular genetic is mutation and loss of heterogeneity of the oncosuppressor gene *APC*. This is observed in over 80% of all colorectal tumours, benign or malignant, and with no difference in incidence with tumour progression. The frequency with inactivation of APC function, although clonally expanded defects in both alleles, itself suggests that *APC* deficiency is an essential early step in the pathway leading through the genesis of adenomas to the development of carcinoma. Definitive evidence both for the importance of *APC* deficiency in this circumstance and the possibility that there may be more than one genetic pathway leading to colorectal cancer comes from studies of human syndromes in which susceptibility to colorectal tumours is inherited.

1.1.4. Inherited Colorectal Cancer susceptibility syndromes

1.1.4.1. Familial adenomatous polyposis (FAP)

Familial adenomatous polyposis (FAP) is an autosomal dominantly inherited cancer-predisposition syndrome that is usually linked to mutation of the adenomatous polyposis coli gene (*APC*) that has been localised to 5q21. The disease is classically characterised by the development, usually during the teenage years, of at least 100 adenomatous polyps in the colorectum. Adenomatous polyps are neoplasms that range from small, often pedunculated lesions to large neoplasms that are usually sessile. In FAP, the adenomas develop shortly after puberty. By 17 years of age carcinomas may arise to the larger lesions. By 25 years of age, over 80% of individuals have cancer. By 40, virtually 100% of individual have cancer unless a prior colectomy has been carried out. Males and females are equally affected. All adenomatous lesions arose as the result of epithelial proliferative dysplasia, which ranged from mild to severe as identified as carcinoma *in situ*. Furthermore, there was strong evidence that almost of invasive colorectal adenocarcinomas arose from adenomatous polyps. Patients with FAP may develop gastric fundic gland polyposis (50% of cases), duodenal adenomas and gastric, pancreatic, biliary or distal small intestinal neoplasms (Damjanov *et al* 1996). Numerous extraintestinal lesions related with adenomatous polyposis. These include desmoid tumours, exostoses of the long bones and endostoses (particularly of the mandible),

which have been referred to as osteomas. Congenital hypertrophy of the retinal pigment epithelium (CHRPE) characterised by a hyperpigmentation of the retina caused by increased numbers of large pigment granules, central nervous system neoplasms, and epidermoid cysts. The association of FAP, desmoids, and exostoses has been termed Gardner's syndrome, whereas the combination of cerebral neoplasia and FAP is known as Turcot's syndrome. These two syndromes have been linked to mutation of the *APC* gene.

Familial adenomatous polyposis carries a very high risk of progression to colorectal cancer. In the majority of patients with FAP, one germline allele of *APC* is mutated, insertion or deletion resulting in a truncated and thus inactive *APC* product. A second somatic event involving mutation or less frequently allele deletion of the remaining *APC* allele within a somatic cell results in tumour formation. Somatic mutations of *APC* can be detected in tumour DNA from more than two-thirds of sporadic colorectal neoplasms. Therefore, in addition to a cause of a rare familial syndrome when inherited as a germline mutation, the *APC* gene is an important target for mutation in the common sporadic variety of colorectal cancer.

APC deficiency is associated with adenoma formation, and this is in complete according to the information given earlier about its incidence in sporadic tumours. However, there is another inherited colorectal cancer susceptibility syndrome, which has important implications for our understanding of the genesis of human colorectal cancer in general, and also for the experiments to be described in this thesis. This syndrome is " Hereditary Non-polyposis Colorectal Cancer, HNPCC ".

1.1.4.2. Hereditary Non-polyposis Colorectal Cancer (HNPCC)

Hereditary non-polyposis colon cancer (HNPCC) is a common autosomal dominant syndrome characterised by early onset carcinomas of the colon as well as cancers of the endometrium, stomach, upper urinary tract, small intestine and ovary (Lynch *et al* 1991, 1993, Watson and Lynch 1993). Approximately 5% of cases of colorectal cancer were attributed to two autosomal dominant inherited syndromes, FAP and HNPCC. Most patients with HNPCC had germ-line mutations of one of the mismatch repair genes (MMR) (Liu *et al* 1996).

The process of mismatch repair (MMR) was first proposed to explain the results of experiments on genetic recombination and bacterial mutagenesis. In the subsequent 30 years, a considerable amount of information has accumulated on this process. Mismatch repair has long been commonly accepted to play two major roles in the cell: (1) the repair of errors made during DNA replication, or as the result of some types of chemical damage to DNA and DNA precursors and (2) the processing of recombination intermediates to yield new configurations of genetic markers. More recent studies have suggested that mismatch repair also played additional roles: (1) in the regulation of recombination events between different DNA sequences, which could result in different types of genetic instability (Rayssiguier *et al* 1989); (2) in some types of nucleotide excision repair responsible for repair of physical/chemical damage to DNA and (3) as part of a cell cycle check point control system by recognising certain types of DNA damage and triggering cell cycle arrest. Therefore, the process of mismatch repair is responsible for the recognition and repair of base pair mismatches and single strand insertion/deletion loops (IDLs) that arise in the genome through a variety of mechanisms during DNA replication, recombination or chemical modification.

DNA replication seems to be prone to a process known as slippage, where one DNA strand can ride up over the other, in a manner reminiscent of a zip fastener that becomes snagged because its links are not taken alternately from left and right which results in replicative error of DNA. This slippage is more likely to happen in regions of repetitive sequence and was thought to occur because DNA polymerases were less able to process through these regions. In higher organisms, these repetitive sequences are called microsatellites, they are often found in the protein encoding regions of many eukaryotic genes. Repetition in a microsatellite was based on a single base "poly A", two bases $(CA)_n$ or three or more bases. When there was alteration in microsatellite size somatically in tumour cells compared with normal tissues it was termed "replication error, RER" (Aaltonen *et al* 1993, Peltomaki *et al* 1993, Aaltonen *et al* 1994). However, when multiple microsatellites were seen affected, this process was termed microsatellite instability. The importance of microsatellite instability as a

mechanism in human carcinogenesis first became apparent with the study of a rare dominant cancer predisposition syndrome, hereditary non-polyposis colorectal cancer (HNPCC). DNA mismatch repair (MMR) is the form of DNA repair responsible for the correction of mismatched and/or unmatched bases, as reviewed by Jiricny (1998).

The discovery of microsatellite instability in tumours and cell lines derived from HNPCC patients (Ionov *et al* 1993, Peltomaki *et al* 1993, Aaltonen *et al* 1993, Thibodeau *et al* 1993) and the knowledge that MMR mutations destabilised simple repeats in yeast (Strand *et al* 1993) suggested that mutations in human homologues of MMR components was involved in human cancer. This notion was confirmed when a human homologue of bacterial *mutS* and yeast *MSH2* was cloned and found to be mutated in some HNPCC families (Fishel *et al* 1993, Leach *et al* 1993). Mutations in human *MSH2* were detected in approximately 50% of HNPCC kindreds (Liu *et al* 1996). *hMSH2* is a member of a family of proteins that are homologous to the Escherichia coli MutS protein, which is responsible for the initial recognition of mismatched nucleotides generated during DNA replication (Fishel *et al* 1993, Leach *et al* 1993). It was known that mutations in *hMSH2* were also responsible for the Muir-Torre syndrome (Marra and Boland 1995), a variant of HNPCC characterised by cutaneous tumour manifestations in addition to the tumour types characteristic of the HNPCC syndrome.

Tumours arising in the patients with the hereditary non-polyposis colorectal cancer syndromes (Lynch syndrome) may account for up to 13% of cancers of the colon and rectum. Affected patients do not develop polyposis, but carry a high risk of developing colorectal cancers as well as other neoplasms. A somatic mutation inactivating the remaining normal allele occurs in tumour DNA, resulting in loss of function of the gene and decreased surveillance and repair of DNA mismatches that arise and are propagated upon cell division in a dividing cell. In the Lynch I syndrome, patients develop colon cancer at an average age of 44 years predominantly (70%) in the right colon. Patients with the Lynch II syndrome develop extracolonic malignancies in addition. These include endometrial cancer, transitional carcinoma of ureter and renal pelvis, and adenocarcinoma of stomach, small intestine, ovary,

pancreas and biliary tract. For diagnosis, the Amsterdam criteria for assignment as an HNPCC case: (1) there must be three affected relatives, one of whom is a first-degree relative of the other two; (2) colorectal cancer must be present in at least two generations; (3) one or more of the cancers must have developed before 50 years of age (Damjanov *et al* 1996).

1.1.4.3. Implications of the cancer susceptibility syndromes for colorectal carcinomas in general

The existence of these 2 inherited syndromes, with their very different clinical presentations, posses important questions on the ongoing of colorectal tumours and their progression to malignancy. Do the tumours that arise in HNPCC patients start as adenomas? Why does the tumour syndrome in HNPCC involve adenomas in small numbers only, but sometimes more than one carcinoma, whereas the FAP syndrome is characterised by hundreds or thousands of adenomas before a single carcinoma develop? Are these rapidly progressing and more slowly progressing adenomas? And do these questions have relevance to the evolution of sporadic colorectal cancer also? As these questions lie close to the central themes of this thesis, they are discussed further now.

(i) *APC* is mutated in HNPCC adenomas in man

In HNPCC cancers, somatic mutation or promoter methylation of the wild type allele results in complete loss of mismatch repair function and consequently the cancers, which develop are characterised by microsatellite instability. Loss of mismatch repair results in an increase in the mutation rate and RER^+ tumours. Approximately 10-15% of sporadic colorectal cancers is found to be RER^+. Microsatellite instability is not seen in normal intestinal epithelium in the patients with HNPCC and is present in only 50% of HNPCC associated adenomas as opposed to over 90% of HNPCC colorectal cancers (Aaltonen *et al* 1993, 1994). Thus, loss of mismatch repair function does not give a selective advantage in normal epithelium or in early adenomas. This suggests that tumour initiation and early development involve the usual steps of mutation in *APC*. This appears to be the case, since the frequency of *APC* mutations appears to be similar in both sporadic and HNPCC associated colorectal tumours (Aaltonen *et al* 1993). The pattern of mutation in *APC*

may be different and one study has found significant higher frequencies of mutation at short mononucleotide repeat sequences in the *APC* gene in HNPCC associated cancers (Huang *et al* 1996). This suggests that, somatic mutation or loss or down regulation by methylation of the wild type allele of the mismatch repair gene may have occurred before *APC* mutation.

(ii) *p53* is frequently involved in colorectal cancer

Mutations in *p53* are also associated with the development of aneuploidy. Mutations in *p53* gene are found in colorectal and pulmonary carcinomas in patients with Li-Fraumeni syndrome (Birch 1990). Aneuploidy does not alter gene function but only change gene dosage. Many cellular functions can certainly be radically altered simply by changes in gene dosage but dominant oncogenes and many tumour suppressor gene effects depend on function changing mutations so that chromosomal imbalance itself cannot be the primary mechanism of genetic change in tumour evolution.

(iii) These 2 pathways are represented in sporadic tumours; one with microsatellite instability and mismatch repair gene deficiency; the other with chromosomal instability and often *p53* mutation.

Mutation of *p53* gene has been shown to occur in the adenoma to carcinoma sequence and most probably occur before metastasis. *p53* mutations thus appear to mark the transition from a benign adenoma to a malignant carcinoma and are found in up to 70% of sporadic colorectal cancers.

(iv) These 2 pathways, both involve *APC* mutations, but phenotype, location, histology, and prognosis of patients are different.

One hypothesis to draw together these observations in man may be stated as follows:

- APC is gateway to adenomagenesis
- A higher than normal mutation rate is required for onwards progression to carcinoma
- In the presence of mismatch repair gene deficiency this is achieved through nucleotide mutations, frameshift mutations as a germ line defect, progression to carcinoma will rapidly follow onset of critical APC deficiency that permits adenoma.
- In contrast, other means of acquiring high mutation rate may require separate genetic events. Loss of p53 function, for example, would be permissive for cell survival (and

replication) following double strand breaks, and so increase the likelihood translocation, deletions and amplifications.

This thesis directly addresses the sequence of the assumptions underlying this hypothesis. It asks: (1) Does lose of *APC* itself alter the stability of the genome, or is coincident *p53* null or *Msh2* null status obligatory? (2) Is there an alternative gateway to adenoma formation that does not involve *APC* knockout?

These questions are to be addressed through use of murine models in which there are germ line deficiency of *Apc*, *p53* and *Msh2* alone and in combination. Before discussing these models, however, it is relevant to give more detail of the molecular actions of these 3 genes.

1.2. Molecular actions of *APC*, *p53* and *Msh2*

1.2.1. *APC* gene

a) Structure

The *APC* gene was mapped to human chromosome 5q21 and mouse chromosome 18. *APC* is a large gene originally described as consisting of 16 exons, one noncoding and 15 coding (Groden *et al* 1991), and is expressed in all tissues analysed. The APC is a 310 kDa cytoplasmic protein (Smith *et al* 1993) expressed in epithelial cells in the upper portions of the colonic crypts, suggesting that it functioned in the mature colonocyte (Smith *et al* 1993). Structural analysis of the APC protein reveal it consists of 2844 amino acids organised into several different domains associated with different functions. Amino-terminal 171 amino acids function in oligomerisation, the amino-terminal third of the APC protein contains a series of heptad repeats that are characteristic of amino acid sequences predicted to form coiled-coil structures mediating protein-protein interactions. These repeats have been shown to mediate the oligomerisation of APC *in vitro* (Su *et al* 1993, Joslyn *et al* 1993). The central part of the protein contains 42 amino acid motif that is repeated 13 times. These include heptad repeats and Arm repeats, as well as sites for phosphorylation and for complexing with β-catenin. The sequence of 15 amino acids, repeated three times between APC amino acid 1020-1169, represented a unique motif for β-catenin

binding. The sequence contains a series of 7 motifs of the 20 amino acids represents β-catenin binding and down regulation. The C-terminal third of the APC protein contains approximately 200 amino acids originally referred to as the basic domain. It is the C-terminal region of APC that contained sites that able to bind the tubulin cytoskeleton in epithelial cells (Munemitsu *et al* 1994). This region also contained site for binding EB-1 protein at 284 residues of the C-terminus (Su *et al* 1995), the human homologue of the *Drosophila* discs large tumour suppressor protein (DLG) located at the extreme C-terminus, 72 amino acids, of the C-terminus and possibly $p34^{cdc2}$ (Matsumine *et al* 1996, Trzepacz *et al* 1997).

The spectrum of mutations that occur in FAP and sporadic colorectal cancer reveal more biological information about tumour development. Although mutations of *APC* probably occur along the whole length of the molecule, only those mutations that were advantageous would be selected. Both germline and sporadic *APC* mutations tend to occur in the 5' part of the gene and result in a truncated protein (Nakamura 1993). In sporadic tumours, over 60% of the mutations were found between codons 1286 and 1513 which accounted for less than 10% of the coding part of the gene and is termed the mutation cluster region (MCR) (Nakamura 1993). The MCR is located near the β-catenin binding sites, mutations which occur here resulted in truncated proteins which may bind to, but which are unable to promote degradation of β-catenin (Peifer 1996, Munemitsu *et al* 1995).

Structure of *APC*

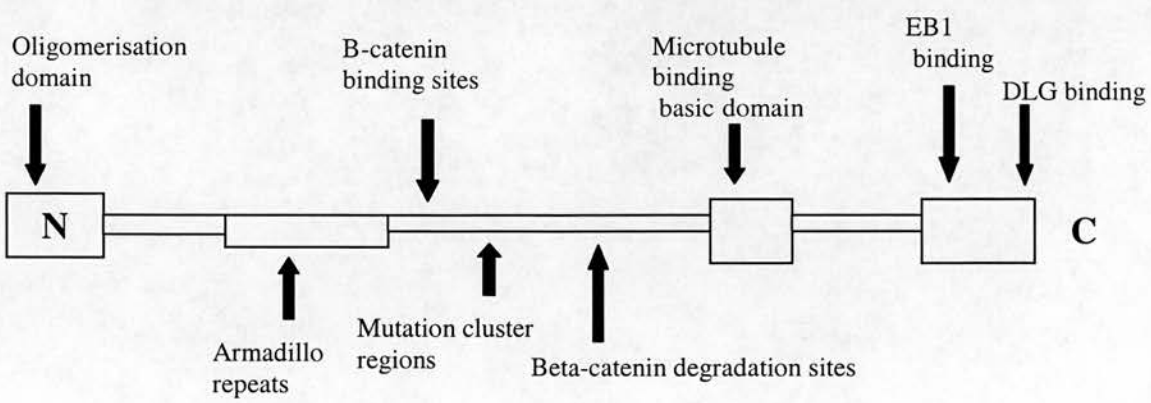

b) Interacting proteins

Cell fractionation studies showed that the APC protein occurred in the cytoplasmic, membrane/skeletal fraction and nuclear fraction (White 1997). By using HT-29, a colorectal cell line contained no intact APC protein and widely used for experimental studies (Morin *et al* 1996), demonstrated that both EB1 and β-catenin were simultaneously bound to full-length APC *in vivo*, strongly imply the functional interaction between these genes. They also found that the expression of APC in HT-29 cells inhibited cell growth through increased apoptosis and the apoptosis observed is *p53*-independent (Morin *et al* 1996).

EB-1 is a 30 to 35 kDa protein. EB1 binds to the carboxyl terminal domain of an APC tumour suppressor protein and has recently been shown to be a component of the microtubule cytoskeleton in mammalian cells and to be associated with the mitotic apparatus. These observations may provide a physiological connection between Apc and cellular division (Berrueta *et al* 1998). EB1 has been shown to be localised both to cytoplasmic microtubules in interphase cells and to the spindle microtubules during mitosis (Berrueta *et al* 1998). Localisation of EB1 with the centrosomes and attachment to microtubules was visualised during prophase and prometaphase and association to cytoplasmic microtubules was observed in anaphase and telophase (Berrueta *et al* 1998, Morrison *et al* 1998).

Rubinfeld *et al* (1996) showed that when β-catenin is present in excess, APC was phosphorylated by GSK3β which resulting in degradation of β-catenin via ubiquitin-proteasome pathway (see details in section 1.4.2).

DLG tumour suppressor protein was identified as the human homologue of the Drosophila discs large tumour suppressor protein. DLG protein was localised to the cell-cell contact in epithelial cells where its interaction with cytoskeletal protein. It was demonstrated that both APC and hDLG were concentrated at sites of synaptic density in rat hippocampal neurons and at sites of cell-cell contact in epithelial cells (Matsumine *et al* 1996), which suggested that the APC-DLG complex may participate in regulation of both cell cycle progression and neuronal function.

c) Function

Although APC function remains unclear there is now evidence that the APC protein participates in a number of cellular processes including cell cycle regulation, apoptosis, cell adhesion, cell migration, microtubule assembly and cell fate determination (Munemitsu *et al* 1996, Baeg *et al* 1995, Rubinfeld *et al* 1995, Morin *et al* 1996, Nathke *et al* 1996). Expression of APC has been reported to inhibit the proliferation of fibroblasts by blocking progression into S phase of the cell cycle (Baeg *et al* 1995), and APC was found to regulate passage through the G_1 phase in human colon cancer cell lines (Heinen and Groden 1999). A role has also been proposed for that APC protein function in regulation of intestinal crypt fission and cell proliferation in both the normal intestine of human familial adenomatous polyposis patients and mice mutant for *Apc* (*Apc* ^{Min}) (Wasan *et al* 1998). The first reports on the intracellular localisation of APC came from experiments using transient overexpression in various cell lines. In these studies the ectopically expressed wild type APC colocalised with the microtubule network, whereas a truncated APC, representative of that expressed in colon cancer cells, did not (Smith *et al* 1994, Munemitsu *et al* 1994). Subsequently, it was reported that wild type APC is present in highly concentrated clusters localised to actively migrating regions of the cell membranes, with microtubules extending into the clusters (Nathke *et al* 1996, Neufeld and White 1997). Others reported the Apc protein to be highly expressed in developing rodent brain and to function in regulating microtubule dynamics (Morrison *et al* 1997). It was concluded that APC might contribute to the process of epithelial cell migration.

APC has also been implicated in the Wnt signalling pathway, through modification of the levels of β-catenin. APC protein forms complex with β-catenin and subsequently is phosphorylated by GSK3β, which enhance the degradation of β-catenin by ubiquitin proteasome pathway. This role of APC in the Wnt signalling is discussed in much greater details in section 1.4.1.

1.2.2. *p53* gene

Roles for the p53 protein have been suggested in many and varied cellular processes, including DNA repair, recombination, differentiation and senescence. A large body of data suggested that p53 suppressed growth through two mechanisms, cell cycle arrest and apoptosis. Loss of function of *p53* gene is associated with many inherited and sporadic forms of malignancy in man.

a) Structure

The *p53* gene is located on human chromosome 17p13 and encodes 53 kDa nuclear phosphoprotein. The p53 protein can be divided into three regions:

a. The amino terminal which contains a large number of acidic residues, no basic residues and a large number of amino acids (including many Pro-Pro pairs);
b. The carboxy terminal which is very hydrophilic and contains many charged residues;
c. The central region of the protein which contains several very hydrophobic regions and very few charged amino acids.

The amino terminal region contains 72 amino acids (Fields and Jang 1990, Raycroft *et al* 1990), which is transcriptional activation domain. The carboxy terminus is a basic region, which is important in facilitating tetramerization. The tetramerization regions composed of two domains, one a α-helix whose hydrophobic amino acids are directly involved in protein-protein interaction, and the other is a basic region, which stabilises the tetramers (Sturzbecher *et al* 1992, Clore *et al* 1994). The tetramerization region also contains one or more nuclear localisation signals, which are important in directing the subcellular compartmentalisation of p53 (Shaulsky *et al* 1990a). Recently, evidence showed that the central region contained the domain that bound to DNA and, more particularly, to the target DNA sequences of *p53*. Thus the central region and carboxy terminal of p53 protein are important in determining and directing the shape and optimal intramolecular interactions needed for DNA binding.

b) Function

The *p53* gene product is a multifunctional protein, which plays roles in modulating gene transcription, recognising cell cycle checkpoints, activating apoptosis, controlling DNA replication and repair, maintaining genomic stability and responding to genetic insults (Elledge and Lee 1995).

Most evidence suggests that *p53* functions as a transcription factor: *p53* possesses sequence-specific DNA-binding activity and can activate the transcription of genes that carry a target element within their promoter (El-Diery *et al* 1992). *p53* activates the transcription of genes involved in the induction of both growth arrest and apoptosis through transcriptional activation of *MDM2, p21/WAF-1/CIP-1* and bax, (White 1996, Oliner *et al* 1992) and perhaps other genes as well. *p53* induces the transcription of its own negative regulator *MDM-2*, which then serves as a negative feedback loop to turn off the activity of *p53* (Momand *et al* 1992) by binding of *MDM2* to the p53 amino domain (Oliner *et al* 1993).

p53 has been shown to induce both growth arrest and apoptosis, although either response has been shown to be influenced by the physiological circumstances or cell type. Thus genotoxic insults such as chemotherapy and radiation are known to induce cell death through *p53*-dependent pathways (Clarke *et al* 1993) but not all cell types exhibit *p53* dependent apoptosis following γ-irradiation induced DNA damage (Clarke *et al* 1994). In addition to the role of *p53* in G_1 growth arrest and apoptosis, *p53* also plays a role in the control both of the G_1 and S checkpoints and the G_2 and M checkpoints of the cell cycle (Mercer *et al* 1990). The response of epithelial stem cells of the small intestine suggested that *p53* might play a role in the deletion of damaged cells with carcinogenic potential, whereas this process was limited in the colon (Merritt *et al* 1994).

At the protein level, the wild type *p53* gene product does not accumulate in amounts that could be detected by immunohistochemistry because of a short half-life of 6-20 minutes. However, it can be stabilised by DNA damage, which extend half-life to 6 hours (Leahy *et al* 1996). Mutant p53, which is functionally inactive and stabilised, could be detected in the nucleus of the cell (Leahy *et al* 1996). It has been

shown that expression of both mutant variants of the mouse *p53* gene significantly increased the cellular resistance of haematopoietic cell lineages to γ-irradiation (Lee and Bernstein 1993).

The cellular localisation of the p53 protein varies during the cell cycle in serum-stimulated, non- transformed Balb/c 3T3 cells. The protein is found in the cytoplasm during G_1, entering the nucleus during the G_1/S transition where it remains until the end of the G_2/M phase. After DNA synthesis, it is found again in the cytoplasm (Shaulky *et al* 1990b). However, in transformed or tumour cells, the p53 protein is predominantly seen localised to the nucleus. These observations suggest that the progression of the cell cycle required p53 protein. Abnormalities in chromosome segregation and mitotic delay following irradiation in *p53* deficient mice was also reported (Bouffler *et al* 1995), which suggested a G_2/M checkpoint role for *p53*.

The *p53* tumour suppressor gene is the most frequently mutated gene in human tumours and reintroduction of *p53* into transformed cells can induce either growth arrest or apoptosis (White 1996). Thus, *p53* aberrations can contribute not only to tumorigenesis but also to resistance to radiation and chemotherapy. However, the resistance to radiation and chemotherapy in rapidly dividing tumours is not solely dependent upon the states of *p53*. For example, *Bcl-2*, which is known to be to involve in cell survival as an anti-apoptotic signal is often highly expressed in tumours which are resistant to chemotherapy, and has been shown to confer resistance to cell death normally induced by a variety of chemotherapeutic agents (cited by Hoffman and Liebermann 1994). In addition, *Bcl-2* suppresses *p53*-dependent as well as *p53*-independent pathways (Wang *et al* 1993). Thus, a pharmacological attack targeted to the checkpoint sites of cell death may be critical for effective cancer therapy.

1.2.3. *MSH2* gene

Mutation of the mismatch repair genes *hMSH2* and *hMLH1* have been found in a high proportion of individuals with hereditary nonpolyposis colon cancer (HNPCC). The pairing of mismatched nucleotides occurs by polymerase misincorporation, by

damage to nucleotide precursors, by damage to DNA and during genetic recombination (Friedberg *et al* 1995). Mismatch repair differs from nucleotide and base excision repair in that the components of the system recognises normal nucleotides that are either mispaired or unpaired, rather than recognising abnormal nucleotides (Fishel and Kolodner 1995). The most extensively characterised MMR system was the DNA adenine methylase instructed MutHLS pathway in *Escherichia coli* (Modrich 1991). In this pathway, mismatches and small insertion/deletion loops (IDLs) were initially recognised and bound by the MutS protein. Mismatch-bound MutS formed a complex with the MutL protein, which was required for the activation of MutH, a latent endonuclease that generates a nick in the newly synthesised DNA strand, from which the excision and repair of the lesion took place. MutL was therefore believed to act as a molecular matchmaker in coupling mismatch recognition by the MutS to MutH activation (Sancar and Hearst 1993). Mutations in components of MMR led to an increase in the spontaneous mutation rate, giving rise to a mutator phenotype. The MutHLS system of bacteria appears to have been conserved throughout evolution (Fishel and Kolodner 1995).

Two lines of experimentation indicate that eukaryotes had a broad-spectrum mismatch repair system related to the bacterial MutHLS system. A series of genetic studies led to the identification of eukaryotic homologues of the bacterial *mutL* and *mutS* gene products (Reenan and Kolodner 1992); and biochemical studies of eukaryotic cells demonstrated *in vitro* nick-directed mismatch repair reactions had mechanisms similar to those catalysed by the *E. coli* MutHLS system (Fang and Modrich 1993). More recently, biochemical fractionation studies have led to the purification of eukaryotic homologues of the bacterial MutL and MutS proteins (Drummond *et al* 1995). In the yeast, *MSH2* recognised mismatched nucleotides as a heterodimer with G/T-binding protein (Drummond *et al* 1995) and *MSH3* and *MSH6* appeared to modify the specificity of this recognition. Furthermore, although they demonstrated binding of *MSH2* alone to DNA containing mismatched nucleotides or lesions binding appeared to be an order of magnitude lower than where *MSH2* was

complexed with either *MSH3* or *MSH6* (Alani *et al* 1995, Fishel *et al* 1994a, Fishel *et al* 1994b).

In human cells, it is clear that the post-meiotic segregation phenotype was closely linked with mismatch repair and thus implied an important role for this process in meiotic recombination. The characterisation of the *S. cerevisiae* MutS and MutL homologues (MSH and MLH respectively) made possible the identification of human MMR genes (Leach *et al* 1993, Fishel *et al* 1994a, 1994b, Nicolaides *et al* 1994, Papadopoulos *et al* 1994, Kolodner *et al* 1995). To date, germ-line mutations in four mismatch repair genes have been shown to be associated with HNPCC: *hMLH1* (Bronner *et al* 1994), *hPMS1* and *hPMS2* (Nicolaides *et al* 1994) and *hMSH2* (Leach *et al* 1993, Fishel *et al* 1993). It has been estimated that approximately 50% of the HNPCC kindreds are associated with germ-line mutations in *hMSH2* (Borresen *et al* 1995, Miyaki *et al* 1995, Froggatt *et al* 1995). Furthermore, it appears that the majority of both HNPCC and sporadic tumours that displayed microsatellite instability had mutations in either *hMSH2* or *hMLH1*, whereas mutation in *hPMS1*, *hPMS2*, *hPMS3*, and *hPMS6* accounted for a small fraction. This leave 10-40% of sporadic microsatellite unstable tumours still unaccounted for (Borresen *et al* 1995, Liu *et al* 1995, Liu *et al* 1996). During the past three years, six components of the human mismatch repair system have been cloned (Fishel *et al* 1993, Leach *et al* 1993, Bronner *et al* 1994, Nicolaides *et al* 1994, Palombo *et al* 1995). These were *hMSH2* (human mutS homologue 2), *hMLH1* (human mutL homologue 1), *hPMS1* and *hPMS2* (human homologues of mutL) and *hMSH6* [a human mutS homologue, originally named GTBP (G/T-binding protein/p160)]. There is other human mutS homologue, *hMSH3* (dup-1), role in mismatch repair is so far unclear (Fujii and Shimada 1989, Fishel and Kolodner 1995, Drummond *et al* 1997, Marra *et al* 1998). All MutS homologues characterised to date are highly conserved at their C-terminal regions, which contain the consensus ATP-binding site. Assuming that, following binding at the mismatch site, hMutSα (heterodimers of *hMsh2* and *hMsh3*) undergoes an ATP-dependent conformational change and translocates along the double helix in a manner similar to the MutS homodimer, thereby generating a looped structure, it

would be predicted that ATPase-defective mutants would be MMR deficient (Iaccarino *et al* 1998).

The recent discovery of MMR defects in hereditary cancer syndromes and in sporadic tumours of various types has provided strong support for the role of mutations in cancer development. Two lines of evidence suggested that *hMSH2* was one of the HNPCC genes. First, it mapped to the same chromosomal position as the markers linked to the disease. Second, phenotypic instability, a characteristic of mismatch repair defects, was found in tumours from these patients. Current data suggested that *hMSH2* was one of the major HNPCC genes, causing 30-40% of all cases (Fishel *et al* 1993, Leach *et al* 1993, Liu *et al* 1996), but three other components of the human mismatch repair have also been cloned and shown to be mutated in the germline of HNPCC patients. The most important of these genes, *hMLH1*, mapped to chromosome arm 3p and accounted for an additional 30% of the germline mutations in HNPCC families (Bronner *et al* 1994, Papadopoulos *et al* 1994, Liu *et al* 1996, Tannergard *et al* 1996). The two *hPMS* genes, which mapped to chromosome arms 2q (*hPMS1*) and 7p (*hPMS2*), have been found mutated in the germline of a few HNPCC patients (Nicolaides *et al* 1994, Liu *et al* 1996).

The use of small animals as models for tumorigenesis in a controlled experimental manner has been a mainstay of cancer research for long period of time. The mouse model may offer the most profound lessons to understanding human cancer. It is now well documented that different mouse strains exhibit markedly different propensities to cancer, whether they are spontaneous or induced. Mouse genetics offer the opportunity to identify the loci and genes responsible for altered penetrance or expressions of cancer phenotypes. However, the development of molecular genetic techniques to identify specific cancer associated gene lesions, combined with breakthroughs in the manipulation of the germ line of mice, have greatly facilitated the generation of powerful new models for understanding the mechanistic roles of specific genes in cancer initiation and progression.

1.3. Murine models of oncosuppressor gene deficiency

There are many strains of mouse developed as model for human colorectal cancer. Much of the attention today in colorectal cancer susceptibility was focused on tumour initiation events. The availability of reliable mouse models for initiation now allows the researchers to focus on genes involved in progression of cancer.

1.3.1. Mouse model for *Apc* gene study: The *Min* mice

The *Min* (multiple intestinal neoplasia) mouse is an important mouse model of human intestinal polyposis syndromes such as familial adenomatous polyposis (FAP) and Gardner's syndrome (Shoemaker *et al* 1997, Moser *et al* 1990). The *Min* mouse is heterozygous for a nonsense allele at codon 850 of *Apc* gene, the mouse homologue of *APC* (Su *et al* 1992). The *Min* mutation was discovered by phenotypic screening after random germ-line point mutagenesis with ethylnitrosourea (ENU), which is point mutagen (Moser *et al* 1990). The allelic *Apc* loss in *Min*-induced adenomas involved somatic hemizygosity of chromosome 18 (Justice *et al* 1992, Luongo *et al* 1993, Luongo *et al* 1994). *Min* mice displayed an anaemic phenotype, which was traced to bleeding from multiple polyps in the intestine (Moser *et al* 1990). The phenotype of these mice differed from the human FAP phenotype in a few aspects. In the *Min* mice, tumours occurred in the small intestine whereas in human FAP patients, the majority of tumours developed in the large intestine (Bilger *et al* 1996). In addition, about 10% of female *Min* mice developed mammary tumours, which has not been seen in human FAP patients (Moser *et al* 1993). The incidence of polyps in *Min* mice varied greatly depending on the strain background and if polyps were left untreated, they become invasive (Moser *et al* 1992). On a C57B1/6 background, *Min* mice developed approximately 30 tumours in their intestine, whereas on a mixed AKR x C57B1/6 background, this number decreased to an average of about six tumours and the mice lived longer. These results suggested that AKR strain of mice carried genes that acted to reduce polyp formation in *Apc* ^{Min} mice. The neoplastic phenotype of *Apc* ^{Min} heterozygotes was expressed in the intestinal epithelium of sensitive animals with 100% penetrance. On resistant

backgrounds, longer-lived animals also developed other types of neoplastic lesions, including mammary adenocarcinomas (Moser *et al* 1993). The penetrance of these lesions was far less than 100% of *Apc* ^{Min} animals. However, the penetrance could be increased even on the short-lived sensitive genetic background by appropriately timed somatic ethylnitrosourea (ENU) treatment (Moser *et al* 1993). A second class of neoplastic lesion in non-endodermal tissue was the desmoid fibrosarcoma, found in the peritoneal muscle wall. In the mouse, as in human a heterozygous defect in the *Apc* or *APC* gene predisposed to a broad range of hyperplastic and neoplastic lesions in an embryonically diverse range of tissues.

Adenomas in human FAP kindreds differ from those in the *Min* mouse in two respects:

1. The loss of function of the normal allele occurs by intragenic inactivating mutations or interstitial deletions in human, but by loss of the entire chromosome in the mouse: and
2. Loss has been detected in no more than 71% of tumours in the human, but in 100% in the mouse.

The overall conclusion from these studies was that adenoma formation in the *Min* mouse required loss of normal *Apc* function. Because *Apc* loss correlated completely with adenoma formation, this gene qualifies as a tumour suppressor gene controlling at least tumour establishment. Accordingly, restoration of wild type activity should prevent tumour formation.

By backcrossing *Min* mice from the AKR x C57B1/6 background to pure C57B1/6 and using simple sequence length polymorphisms (SSLP), the *Min* modifying locus was mapped to chromosome 4 and controlled about 50% of genetic variation in tumour number in two intraspecific backcrosses (Dietrich *et al* 1993). The locus was named *Mom-1* for modifier of *Min 1*, it was found to lie in the region of synteny conservation with human chromosome 1p36-p35, a region of frequent somatic loss of heterozygosity in a variety of human tumours, including colon tumours. When the AKR allele of *Mom-1* was transferred onto the sensitive C57B1/6 background, the tumour incidence in *Apc* ^{Min}; *Mom-1*^{AKR}/*Mom-1*$^{B1/6}$ was reduced

two-fold. When both alleles of *Mom-1* were derived from the AKR strain, the tumour incidence was reduced four-fold (Shoemaker *et al* 1997). In the progeny of a cross-involving *Apc* ^{Min} and a targeted *p53* mutant allele (Donehower *et al* 1992), the multiplicity of adenomas in *Apc* ^{Min} mice was independent of the *p53* genotype (Dove *et al* 1994). Defects in *p53* caused aneuploidy in mouse embryo fibroblast cultures (Carder *et al* 1993). Furthermore, as intestinal tumours progress in the human, *p53* is often mutated. The levels of p53 polypeptide were very low in the intestinal tract and in adenomas (Purdie *et al* 1991), except after ionising radiation (Merritt *et al* 1994).

Other *Apc* mutant mice

Apc-deficient mice have been generated by gene targeting (Fodde *et al* 1994, Oshima *et al* 1995). The targeting resulted in the truncation of the *Apc* gene product at amino acid 716. The heterozygous mice developed multiple polyps throughout the small intestine, which was similar to the phenotype seen in *Min* mice. Tumour analysis indicated that the wild type *Apc* gene was lost during tumorigenesis (Oshima *et al* 1995). The homozygous mice died *in utero* before day 8 of gestation, as has been found in *Min* mice. Shibata *et al* (1997) used a conditional gene targeting system, the Cre-loxP system, recombination mediated by the Cre recombinase deletes a region of Apc encompassing exon 14 and induced a frameshift mutation at codon 580. LoxP sites were inserted in the introns 13 and 14 of the *Apc* gene by targeted mutagenesis and mutant allele was introduced into the mouse germ line. Mice homozygous for *Apc*-loxP insertion were normal. However, upon infection of the colorectal region with an adenovirus encoding the Cre recombinase, which results in excision of *Apc* specifically in Cre-loxP, the mice developed adenomas in the colorectal region within 4 weeks. The adenomas showed deletion of *Apc* exon 14, indicating that the loss of *Apc* function was caused by Cre-loxP-mediated recombination (Shibata *et al* 1997).

Crossing between tumour suppressor gene knockout mice was also generated. Mutation in *Apc* predisposed an individual to colonic adenomas, while *p53* lack was associated with the conversion from adenoma to adenocarcinoma. The ability of mutations in both the *Apc* and *p53* tumour suppressor genes to co-operate in the

induction of induce intestinal tumour in the mouse was examined (Clarke *et al* 1995). Mice heterozygous for *Apc* developed adenomas of both the small and large intestine with a small percentage of cases progressed to adenocarcinomas. (*Apc* ^{Min}*/p53* $^{-/-}$) mice have a shorter survival time because the high incidence of thymic lymphoma, extra-thymic lymphoma, sarcoma and pancreatic abnormalities compared to (*Apc*$^{+/+}$*/p53* $^{-/-}$) and (*Apc* ^{Min}*/p53* $^{-/-}$) mice. Therefore, (*Apc* ^{Min}*/p53* $^{-/-}$) mice have a predisposition to pancreatic abnormalities, either preneoplastic foci/dysplasia or pancreatic acinar cell adenocarcinoma. This is accompanied by loss of heterozygosity (LOH) at the *Apc* locus, which supported a role for *Apc* in the genesis of extracolonic cancers.

Furthermore, Reitmair *et al* (1996) analysed the phenotype of (*Apc* ^{Min}*/Msh2* $^{-/-}$) mice. They demonstrated that mice heterozygous for *Apc* and carrying a germline defect in the *Msh2* mismatch repair gene develop more and faster growing intestinal tumours than mice carrying the *Apc* mutation alone. Additionally, whist adenomas from the *Apc* ^{Min} mice all exhibit deletion of the wild type *Apc* allele while the adenomas from (*Apc* ^{Min}*/Msh2* $^{-/-}$) mice appeared to inactivate the wild type *Apc* allele by somatic mutation. Taken together the above studies indicate that *Apc* is a target of the RER phenotype in colon cancer.

1.3.2. Mouse model for mismatch repair gene, *Msh2* deficiency: The *Msh2* mice

In order to further characterise the function of *Msh2* in a mammalian model system, mice deficient for *Msh2* have been generated using embryonic stem cell technology (de Wind *et al* 1995, Reitmair *et al* 1995). *Msh2* $^{-/-}$ mice are susceptible to lymphoid tumours at an early age (de Wind *et al* 1995, Reitmair *et al* 1995) approximately 30% developed leukaemia/lymphomas between the ages of two to five months and all succumbed to leukaemia/lymphoma within 12 months (Reitmair *et al* 1995). Cells isolated from the lymphoid tumours displayed microsatellite instability as expected for MMR-deficient cells and extracts derived from *Msh2* $^{-/-}$ fibroblast cells lacked mismatch binding activity and acquired microsatellite instability and tolerance to methylating agents (de Wind *et al* 1995), which was present in wild-type

and heterozygous cells. As expected, *Msh2* deficiency resulted in mutator phenotype as well as microsatellite instability in *Msh2* $^{-/-}$ cells and tissues. (The mutator phenotype results from the mutator hypothesis of tumorigenesis which suggests that loss of chromosomal stability or maintenance functions results in elevated mutation rates, leading to the accumulation of the numerous required for multistep carcinogenesis). In spite of the mismatch repair gene (MMR) defect, these mice are known to be viable and fertile for at least three generations. This finding was consistent with the discovery of HNPCC patients that appear to be deficient in MMR throughout their somatic tissues (Parson *et al* 1995). This high incidence of early onset lymphoma might simply reflect the exacerbation of a natural predisposition to lymphoma in this particular inbred background (Teich *et al* 1984). Alternatively, it has been proposed that the high incidence of lymphoma in *Msh2* $^{-/-}$ mice might be partly due to increased translocations in lymphoid tissues due to higher recombination rates between diverged retroviral sequences dispersed throughout the mouse genome (Reitmair *et al* 1995).

Apc ^{Min} mice were crossed with *Msh2* $^{+/-}$ mice to generate offspring bearing defects in *Apc* and *Msh2* gene. Interestingly, approximately 70% of the (*Apc* ^{Min}/*Msh2* $^{-/-}$) mice that survived to six months began to develop gastrointestinal tumours and approximately 7% of the (*Apc* ^{Min}/*Msh2* $^{-/-}$) mice developed keratoacanthoma, which is one type of skin tumours, that were associated with the inactivation of the *Apc* gene (Reitmair *et al* 1996). This mouse model can be used as a model system for HNPCC if the leukaemia/lymphoma phenotype could be suppressed.

Biochemical analyses revealed that on the cellular level one mismatch repair gene mutation (heterozygous condition), as opposed to homozygous inactivation, did not severely affect mismatch repair (Parsons *et al* 1993) and animal studies have shown that *Msh2* $^{-/-}$ mice led to predisposition for cancer (Reitmair *et al* 1995). In addition to colorectal cancer, many families had an excess incidence of adenocarcinoma of the endometrium. Cancer of the stomach, ovary, small intestine and pancreas, as well as transitional cell carcinoma of the ureter and renal pelvis, were found less frequently (Mecklin *et al* 1986, Lynch *et al* 1988, Vasen *et al* 1990, Lynch *et al* 1993, Watson

and Lynch 1993, Lynch and Lynch 1994). *Msh2* deficiency resulted in the development of many colonic aberrant crypt foci, as well as reduced survival of the mice, secondary to both a greater number and more rapidly developing adenomas. In what was assumed to be a direct consequence of failure of this process, microsatellite instability was increased in murine *Msh2* $^{-/-}$ cells. However, the consequences of *Msh2* deficiency were complex, with *Msh2* $^{-/-}$ cells also showing hyper-recombination and increased survival after exposure to methylating agents *in vitro* (de Wind *et al* 1995). This property suggested that *Msh2* status might affect the ability to undergo apoptosis, with increased resistance to methylating agents arising from failure to detect damage and hence initiated apoptosis. Results from several different tumour cell lines deficient in mismatch repair were consistent with this hypothesis (Karran and Bignami 1994). Toft *et al* (1999) characterised an *in vivo Msh2*-deficient apoptotic response to methylating agents and raised the possibility that *Msh2* deficiency might predispose to malignancy not only through failure to repair of mismatch DNA lesions but also through the failure to engage apoptosis. The mechanism of inactivation of the wild type *Apc* allele depended on *Msh2* status (Reitmair *et al* 1996). DNA mismatch repair was a post-replicative process that corrected DNA polymerase insertion errors that have escaped proofreading. It was known to operate in mammalian cells, although the detailed mechanism was best understood in *E. coli.*

1.3.3. Mouse model for *p53* deficiency: The *p53* knockout mouse

The *p53* tumour suppressor gene is more frequently mutated in human cancer than any other known gene. In some types of tumours such as colon carcinomas, *p53* was mutated in greater than 80% of cases (Baker *et al* 1990). Most *p53* mutations occurring in human tumours were point mutations mapping to the DNA binding domain of the p53 protein (Hollstein *et al* 1991). Since the importance of the *p53* gene in cell cycle control and cancer prevention, development of a mouse model was an obvious priority. Three research groups generated *p53* null mouse strains independently by gene targeting techniques (Donehower *et al* 1992, Jacks *et al* 1994,

Purdie *et al* 1994). The majority of *p53* null mice developed normally. However, a fraction of the female null embryos display defects in neural tube closure resulting in an overgrowth of neural tissue in the region of the mid-brain, a condition known as exencephaly (Armstrong *et al* 1995). The first reported *p53* knockout mouse strain was one in which parts of intron 4 and exon 5 of the *p53* gene were replaced with a neo cassette, such that *p53* conserved region II and consequently the DNA-binding domain was disrupted (Donehower *et al* 1992). Other groups created a mutation that deleted the region between *p53* exons 2 and 6, replacing it with a neo gene expression cassette, equivalent to approximately 40% of the coding sequence (Clarke *et al* 1994, Jacks *et al* 1994).

Analysis of all those three strains of *p53* null mice gave rise to the same conclusions (reviewed in Macleod and Jacks 1999):

(1) *p53* was generally not required for normal embryonic development (Donehower *et al* 1992, Jacks *et al* 1994, Purdie *et al* 1994);

(2) *p53* null mice were predisposed to cancer, all three strains of *p53* null mice developed lymphomas predominantly and sarcomas to a lesser extent (Donehower *et al* 1992, Jacks *et al* 1994, Purdie *et al* 1994). Donehower's mice were analysed on 75% C57B1/6: 25% 129/SV genetic background. At 10 months of age all mice had developed tumours or died with an average tumour latency of 4 to 5 months. More than 70% developed either thymic lymphoma or generalised B cell lymphoma. The surviving mice were predominantly affected by sarcomas of varying types such as osteosarcoma, haemangiosarcoma and undifferentiated sarcoma. There were also rare cases of mammary gland carcinoma. Similar results were observed by Jacks *et al* (1994) after deletion of exons 2 to 6 in mice on the same genetic background: 75% C57B1/6: 25% 129/SV. Thymic lymphoma was the predominant tumour type and various types of sarcoma were observed in the remaining mice. However, carcinomas were not observed in these mice, although several cases of teratoma were found. In the third study of *p53* null mice, Purdie *et al* (1994) analysing a similar *p53* null mutant to Jacks *et al* (1994) (deletion exons 2 to 6) in mice on a different genetic background, 129/Ola. Very

similar results were observed despite the difference in genetic background, most mice died from thymic lymphomas and a small number of mice died from sarcomas. There was a slight decrease in tumour latency on the 129/Ola background. However, Purdie *et al* observed pituitary adenocarcinomas in their *p53* null mice these were not seen by Donehower *et al* or Jacks *et al*;

(3) Other genetic events were probably involved in tumour development since the average tumour latency was about 4 to 5 months;

(4) *p53* heterozygotes developed a different spectrum of tumours to *p53* null mice; predominantly sarcomas of varying types and a small number of adenocarcinomas. Lymphomas were observed at a much lower frequency in *p53* heterozygotes than in *p53* null mice (Purdie *et al* 1994).

(5) Reduction in *p53* gene dosage might be enough to drive tumorigenesis in some tissues; Donehower *et al* (1992) and Purdie *et al* (1994) observed that there was only about 50% of tumours in the *p53* heterozygous mice showed LOH at the *p53* locus.

1.3.4. Multistep in carcinogenesis in mouse models

a) *Apc*, *p53* and *Ki-ras* gene interaction

APC inactivation is an early event in the genesis of colorectal cancer followed by activation of *ras* and loss of *p53* and *DCC* or related genes. Mouse models have been used to examine the cooperativity of both oncogenic *ras* and inactivation of *p53* with *APC* mutations in tumour formation. In one study the ectopic expression of oncogenic *Ki-ras* plus inactivation of *p53* resulted in proliferation of gut epithelium but not promote the formation of adenomas (Kim *et al* 1993). When this was superimposed on a mutant *Apc* background, the number of tumours was only modestly increased above that observed with the mutant *Apc* mouse alone. It was suggested that the failure of *Ki-ras* and *p53* inactivation to promote tumorigenesis was due to the continuous process of epithelial cell renewal that occurs in the intestine and the failure of the transgenes to be expressed in the stem cells of intestinal crypts. Initiation of tumours in the intestine of the *Apc* mutant mouse might

occur in the crypt cells and co-operation between various gene defects might have to occur or more specifically, in a stem cell in order to promote tumours.

b) *Apc* and *Msh2* gene interaction

This exclusively of mutations in *APC* and mismatch repair genes led to the proposal of independent pathways to tumour formation, one characterised by microsatellite instability and another in which inactivation of *APC* was involved. However, in a much more extensive sampling involving both cell lines and tumour samples, Huang *et al* (1996) reported an equal propensity for *APC* mutations in cell lines and tumours with or without microsatellite instability. Lengauer *et al* (1997) demonstrated that colorectal tumours without microsatellites instability exhibit a striking effect in chromosome segregation, resulting in gains or loss in excess of 10^{-2} per chromosome per generation. This form of chromosomal instability reflected a continuing cellular defect that persisted throughout the lifetime of the tumour cell and was not related to chromosome number. Thus, persistent genetic instability might be critical for the development of all colorectal cancers. Moreover, their data indicated that the mismatch repair deficiency contributed to the activation of the *APC* gene. This was evident from the significant excess of frameshift mutations in *APC* in the RER background relative to the nonRER background. The frameshift mutations were characteristic of those expected from the RER phenotype as 81% occurred in microsatellite repeat sequence, while this was the case for only 37% of the *APC* frameshift in the nonRER background. By using a mouse model, Reitmair *et al* (1996) also concluded that defected in mismatch repair genes resulted in contributed to mutations in *Apc*. Mice heterozygous for wild type *Apc* and carrying a germline defect in the *Msh2* mismatch repair gene developed more and faster growing adenomas than mice carrying only the *Apc* mutation did as well as reduced survival of the mice. Additionally, adenomas from the Apc^{Min} mice all exhibited deletion of the wild type *Apc* allele while the adenomas from (Apc^{Min} /$Msh2^{-/-}$) mice appeared to inactivate the wild type *Apc* allele by somatic mutation. Taken together the above studies indicated that *Apc* was a target of the RER phenotype in colon cancer.

c) *Apc* and methylating agents

Although hypomethylation was originally proposed as a contributing factor in the multistep progression of colorectal cancer (Fearon and Vogelstein 1990), more recent evidence has demonstrated this to be a protective effect (Laird *et al* 1995). *Apc* ^{Min} mice there were also heterozygous for DNA methyltransferase, were treated with DNA methyltransferase inhibitors and were found to be far less prone to the development of adenomas than control *Apc* ^{Min} mice (Laird *et al* 1995). It was suggested that C to T transitions resulting from methylation of cytosine occurred at a lower frequency in the methyltransferase compromised animals. However, the target for the protective effect of methyltransferase inhibition was not likely to be the wild type *Apc* allele as this was almost always inactivated through loss of the wild type *Apc* allele in the tumours of *Apc* ^{Min} mice and not through point mutation (Luongo *et al* 1994, Oshima *et al* 1995, Levy *et al* 1994, Laird *et al* 1995). It was suggested that *p53* was a possible target since it commonly has C to T transitions but *p53* $^{-/-}$ mice carrying a mutant *Apc* allele were not more prone to polyp formation than *Apc* ^{Min} mice alone. Activation of *APC* gene expression by the DNA methylating agent -- N-methyl-N-nitro-N-nitroguanidine (MNNG) in HCT-116 colon cancer cell line showed the increased nuclear transcription of the *APC* gene and correlated with a concurrent increase in the p53 protein level (Narayan and Jaiswal 1997), which suggested a role for *p53* in a stress response pathway involving APC.

1.4 Wingless/Wnt signalling pathway

1.4.1. Wnt signalling

In *Drosophila*, the *Wingless* pathway mediates anteroposterior patterning within each segment of the fly embryo (Wieschaus and Riggleman 1987). In vertebrates, the *Wnt* pathway important in the induction of the dorsoventral and anteroposterior embryonal axes. Since the initial identification of Wnt-1 as a proto-oncogene (Nusse and Varmus 1992), Wnt-1 and Wnt-related genes have been shown to encode secreted factors involved in cell growth, differentiation, organogenesis and oncogenesis in both vertebrates and invertebrates (Nusse and Varmus 1992, Nusse

1997). In response to a Wnt signal in vertebrates or to a wingless signal in *Drosophila*, a receptor encoded by the *frizzled* gene family (Bhanot *et al* 1996, Yang-Snyder *et al* 1996) is activated and transmitted the signal to cytoplasmic downstream components. These components including dishevelled (dsh), zeste-white 3 kinase (zw3) and armadillo (arm), which were homologous to the vertebrate proteins Dsh (Siegfried *et al* 1992), GSK-3β (He *et al* 1995, Siegfried *et al* 1992) and β-catenin (McCrea *et al* 1991), respectively. β-Catenin, the mammalian homologue of *Drosophila* armadillo protein, was first identified as a cadherin-associated protein at cell-cell junctions (McCrea *et al* 1991).

Binding of a Wnt molecule to a frizzled receptor activates Dishevelled, which inhibits the activity of the APC-Axin-GSK-3β complex of proteins. Dishevelled activation also lead to the activation of JNK kinases. Integrin-linked kinase (ILK) promotes the stabilisation and nuclear import of β-catenin. Overexpression of ILK in epithelial cell lines promotes the nuclear translocation of β-catenin (Novak *et al* 1998) stimulating the activity of a reporter gene with multimerised Lef-1 binding sites. ILK overexpression also disrupts cell-cell adhesion and stimulates both fibronectin matrix assembly and anchorage-independent growth (Wu *et al* 1998, Radeva *et al* 1997). The mechanism by which ILK activation results in nuclear accumulation of β-catenin could involve inactivation of GSK-3β. β-Catenin was also shown to form a complex with processed presenilin proteins in the endoplasmic reticulum, an interaction that resulted in stabilisation of β-catenin. In response to Wnt signalling, β-catenin is translocated and accumulates in the nucleus, binding to -- Lef-1/Tcf proteins, interfering with Lef-1/Tcf acetylation, and perhaps displacing Groucho corepressors. The association of Lef-1/Tcf with β-catenin results in transcriptional activation. The β-catenin regulates gene expression by direct interaction with transcription factors such as Lef-1, providing a molecular mechanism for the transmission of signals from cell-adhesion component or Wnt protein to the nucleus (Behrens *et al* 1996). Recently, *c-myc* oncogene has been identified as a target gene in the Wnt signalling pathway (He *et al* 1998). Further, *AP-1* has been --

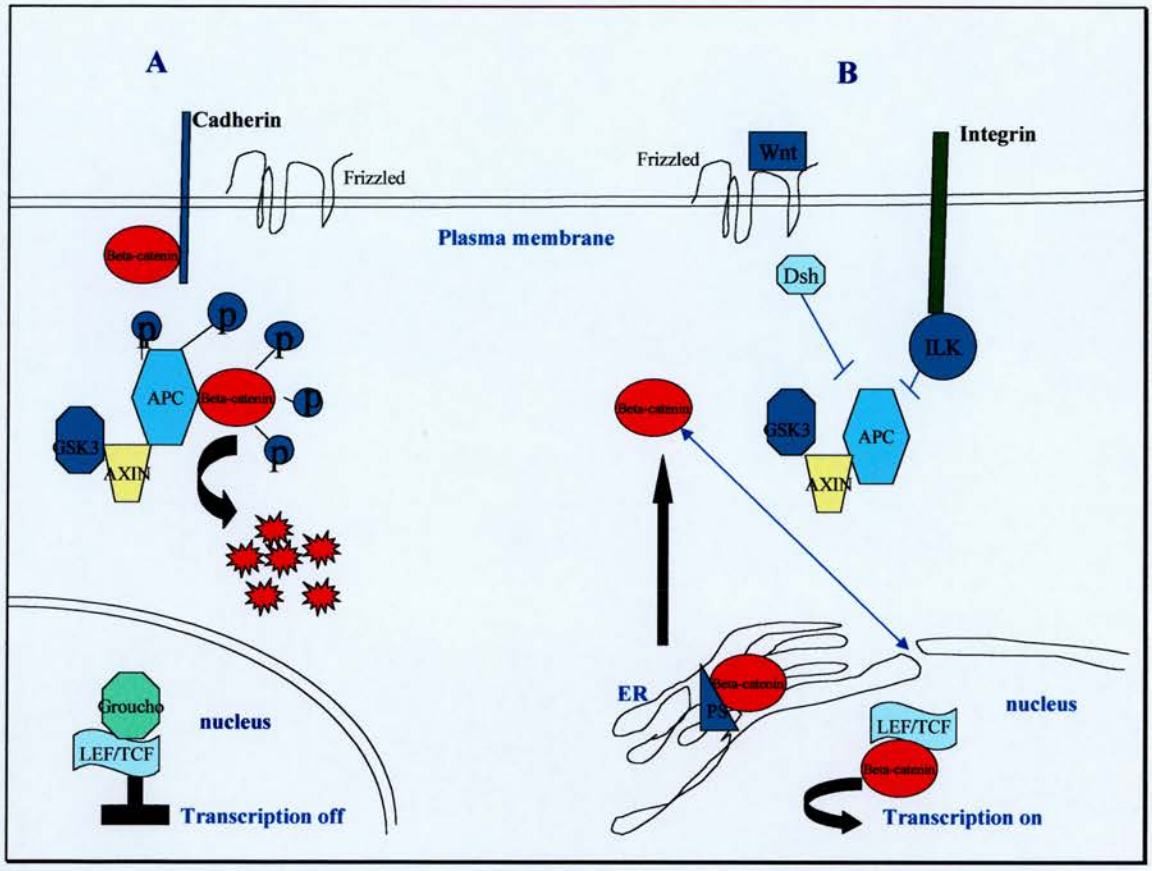

Figure 1.1 Diagram of Wnt signalling pathway and interaction of the components in the pathway

(A) The interactions of Wnt components in the Wnt signalling pathway. At the top, β-catenin binds to cadherins, mediating interactions with the actin cytoskeleton. In the cytoplasm β-catenin interacts with Axin and APC. GSK-3β phosphorylates Axin, which subsequently interacts with β-catenin and APC, leading to the phosphorylation and degradation of β-catenin. Nuclear Lef-1/Tcf interacts with Groucho co-repressors, preventing transcription of Wnt target genes. (B) Signalling events and interactions that stabilise β-catenin, leading to the activation of Lef-1/Tcf-mediated transcription. Binding of a Wnt molecule to Frizzled receptor activates Dishevelled (Dsh), which inhibits the activity of the APC-Axin-GSK-3β complex of proteins. ILK can promote the stabilisation and nuclear import of β-catenin. The mechanism by which ILK activation results in nuclear accumulation of β-catenin could involve inactivation of GSK-3β. β-catenin has also been shown to complex with processed presenilin proteins (PS) in the endoplasmic reticulum (ER), an interaction that results in stabilisation of β-catenin accumulation in the nucleus and the binding of Lef-1/Tcf proteins, which subsequently interfere with Lef-1/Tcf acetylation and perhaps displacing Groucho co-repressors. The association of Lef-1/Tcf with β-catenin results in transcription activation. Adapted from Eastman and Grosschedl 1999.

demonstrated as a target gene of β-catenin-Tcf/Lef signalling in human colorectal carcinomas (Mann *et al* 1999). A model of the Wnt signalling pathway is summarised in Figure 1.1.

1.4.2. β-Catenin

β-Catenin was first identified as one of a small group of proteins that coimmunoprecipitate with the cell adhesion molecule E-cadherin. β-Catenin also plays important roles in cell adhesion and cell signalling. The protein influences adhesion by providing a functional bridge between cadherins and the actin cytoskeleton. β-Catenin has been intensively studied because:

1. The interaction between β-catenin and cadherin adhesion molecules
2. β-Catenin was similar to the Armadillo protein of *Drosophila* which is an important element in the *Wnt/Wingless* signalling pathway and
3. β-Catenin also complexes with the APC protein, the product of a tumour suppressor gene that was mutated in colon cancer.

a) Structure

The β-catenin gene (*CTNNB1*) was mapped to human chromosome 3p21 and mouse chromosome 9. The gene product was a 92 kDa protein, which appeared to be important in the functional activities of both APC and E-cadherin. The *CTNNB1* gene has 16 exons and spans 23.2 kb (Nollet *et al* 1996). Alternative splicing within exon 16 produces a splice variant that is 159 base pairs shorter in the 3-prime untranslated region. The promoter region was shown to be GC-rich and to contain a TATA box (Nollet *et al* 1996). β-Catenin was found to be composed of an N-terminal head domain of about 130 amino acids. The N-terminus of β-catenin contains a consensus phosphorylation site for glycogen synthase kinase 3β (GSK-3β) and point mutations that altered serine or threonine residues within this sequence were sufficient to stabilise the protein (Yost *et al* 1996). The N-terminus is followed by 12 tandem imperfect sequence repeats, each of about 42 amino acids, called armadillo or arm repeats which are also found in many other cytoplasmic proteins. The crystal structure for the 12 arm repeats of β-catenin was

solved recently (Huber *et al* 1997). Structural analysis has revealed that arm repeats were α-helical and pack against one another to form an elongated superhelix of -- α-helices. The groove created by the twisted superhelical structure is highly charged and proposed to be the interacting surface for β-catenin targets. The C-terminal domain of -- β-catenin is composed of about 100 amino acids (McCrea *et al* 1991). The three regions have distinctive charge distributions; the head and tail regions are acidic, whereas the arm repeat region is highly basic.

Structure of β-catenin

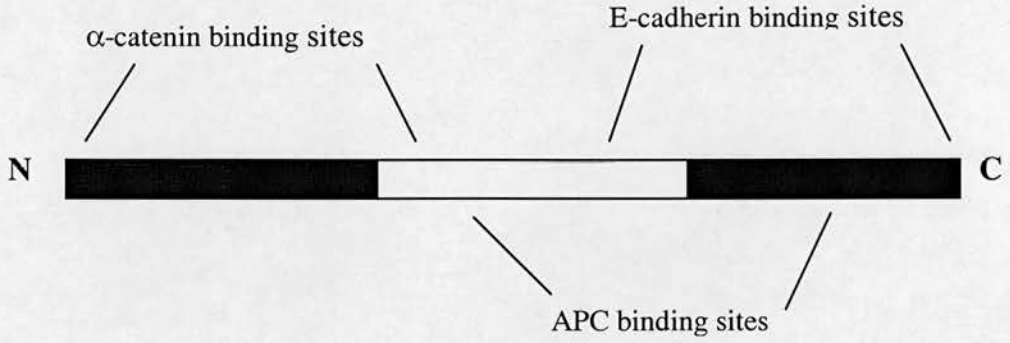

b) Function

β-Catenin is a component of the *Wnt/Wingless* growth factor signalling pathway (*wingless* is the *Drosophila* homologue of *Wnt*) (Gumbiner 1995, Miller and Moon 1996). This pathway plays a key role in development (Willert and Nusse 1998). In *Drosophila*, this pathway was shown to mediate anteroposterior patterning within each segment of the fly embryo (Wieschaus and Riggleman 1987).

β-Catenin was found to be a membrane associated protein, which existed as homodimers. β-Catenin is either localised to the membrane or is found free in the cytoplasm. Separate roles have been proposed for this localisation either in the *Wnt/Wingless* pathway or through interaction with the cadherins. Normally, β-catenin is predominantly located in the cytoplasm as pools of free monomeric protein. The cellular levels of the β-catenin protein as well as subcellular localisation are normally very tightly regulated. In the absence of a *Wnt* signal, GSK3β phosphorylates APC and --

β-catenin (Miller and Moon 1996, Munemitsu *et al* 1996, Yost *et al* 1996, Aberle *et al* 1997, Behrens *et al* 1998, Cadigan and Nusse 1998, Hart *et al* 1998, Ikeda *et al* 1998). Axin facilitates GSK3β phosphorylation of APC and β-catenin *in vitro*. Phosphorylation of β-catenin leads to its ubiquitination and targeting to the proteasome, resulting in -- β-catenin degradation (Aberle *et al* 1997, Salomon *et al* 1997).

In contrast, following stimulation of the *Wnt* pathway, GSK3β is inactivated and leads to the accumulation of free intracellular β-catenin. β-Catenin binds to APC through two motifs located in the central third of the APC proteins, which is either absent or truncated in almost all tumour cells containing mutations in APC (Nakamura 1993, Polakis 1995, Kinzler and Vogelstein 1996). β-Catenin also binds to the *Lef/Tcf* transcription factor (Fagotto 1998). β-Catenin binds to a region within the first 56 amino acids of all known *Lef/Tcf* transcription factors (Behrens *et al* 1996, Huber *et al* 1996, Molenaar *et al* 1996). *Lef/Tcf* transcription factors are sequence-specific DNA binding proteins that function as context-dependent transcription factors, unable to work on their own but requiring the cooperative effort of adjacent DNA binding transcription proteins or non-DNA binding cofactors (Carlsson *et al* 1993, Giese and Grosschedl 1993). *Tcf* proteins are 'architectural' transcription factors that activate transcription by inducing binding of DNA; binding of β-catenin to *Lef-1* has been shown to substantially alter the ability of this transcription factor to bend DNA (Behrens *et al* 1996). β-Catenin associates with several proteins, but the direct target of β-catenin is thought to be *Tcf-1* and *Lef-1*. Moreover, others have shown that β-catenin contains importin-like sequence that mediate nuclear localisation independently of Lef-1/Tcf proteins (Kussel and Frasch 1996). In the nucleus, the β-catenin-transcription factor complex regulates transcription of target genes including *c-myc* (Ben-Ze'ev and Geiger 1998, He *et al* 1998). Recently, evidence has been produced showing that β-catenin is imported into the nucleus independently of Lef/Tcf binding and also exported from nuclei (Prieve *et al* 1998).

c) The consequence of β-catenin mutation

Elevation of cytoplasmic β-catenin occurs following either activation of the *Wnt* signalling pathway or inactivation of *APC*. It has recently been shown that mutations in

β-catenin which delete the N-terminal region also stabilise the protein and result in cytoplasmic accumulation of β-catenin in a manner that appeared to be independent of regulation by *Wnt* or *APC* (Yost *et al* 1996, Munemitsu *et al* 1996, Rubinfeld *et al* 1997, Barth *et al* 1997). Several reports have emphasised that the tumour suppressor adenomatous polyposis coli (*APC*) function to affect intestinal tumorigenesis through its regulation of β-catenin signalling. Additional evidence for the importance of β-catenin signalling in tumorigenesis has come from the observation that some human colorectal neoplasms with wild type *APC* genes have mutations in β–catenin (Ilyas *et al* 1997, Morin *et al* 1997). Mutations in the N-terminal regulatory domain of β-catenin were found in 48% of colorectal tumours lacking *APC* mutations and were associated with the early adenomatous stage of colorectal cancer (Sparks *et al* 1998). β-Catenin mutations were also observed more frequently in small colorectal adenomas than in larger adenomas and invasive carcinomas (Samowitz *et al* 1999). Somatic mutations of the catenin gene were found in approximately 50% of transgenic mouse lines of hepatocellular carcinoma and 36% of human hepatocellular carcinomas (de la Coste *et al* 1998). Increased expression of β-catenin was also identified as an early event in colorectal carcinogenesis and was often associated with a subsequent inactivation of the *p53* tumour suppressor gene in human cell line (Damalas *et al* 1999).

β-Catenin immunoreactivity is normally detected exclusively in the cell membrane and cytoplasm of morphologically normal intestinal epithelial cells with predominant distribution in the differentiated non-proliferative cell population. In contrast, β-catenin was seen to be localised predominantly in the nucleus of adenomas from *Min/+* mice and transgenic mice expressing a mutant truncated form of the *APC* gene (Sheng *et al* 1998). β-Catenin was expressed predominant at the cell membrane and cytoplasm of the nontransformed rat intestinal epithelial (RIE-1) cells in culture, whereas predominantly nuclear localisation of β-catenin was observed in the human colon cancer cell line SW480. In azoxymethane (AOM) treated rats, overexpression and localisation of -- β-catenin was observed in all adenomas (Sheng *et al* 1998).

β-Catenin also functions in cell-adhesion by linking cadherin to the actin cytoskeleton (Aberle *et al* 1994), it binds directly to the cytoplasmic domain of cadherin molecules, and simultaneously bind to the unrelated protein α-catenin, which is in turn linked to actin filaments. Catenin-mediated linkage to the cytoskeleton appears to be crucial to the function of adherins junctions; cadherin is unable to mediate cell adhesion in cells lacking either α- or β-catenin. Both catenins therefore regulate cadherin function in adhesion and are key mediators between the cadherins, APC and the Wnt signal transduction pathway. The evidence is summarised as follows:

1. β-Catenin is a target of tyrosine kinases and phosphatases that regulate cell adhesion.
2. β-Catenin is a major component of the *Wnt/Wingless* signal transduction pathway that is important in cell-fate divisions and pattern formation during development.
3. β-Catenin mediated signals between cadherins and the *Wnt/Wingless* signalling pathway.
4. Mutations in Apc protein and β-catenin resulted in constitutive activation of β-catenin signalling and were correlated with cancer formation.
5. β-Catenin might regulate role of *Apc* protein in organising microtubules.

1.4.3. E-cadherin

Cell-cell adhesion plays an important role in tissue morphogenesis and homeostasis (Gumbiner 1996, Huber *et al* 1996a), and is commonly mediated by the cadherins, a family of calcium-dependent transmembrane adhesion receptors (Geiger and Ayaton 1992, Kemler 1992, Takeichi 1991 and 1995).

a) Structure

The cadherin gene (*HSECAD*) is located on human chromosome 16q22.1 and consists of 6 exons. It codes for a transmembrane protein with a molecular mass of 120 kDa, which exists as a homodimer (Nagar *et al* 1996, Shapiro *et al* 1995). The extracellular N-terminal end contains five repeat domains which each contain a histidine-arginine-valine (HAV) motif (Overduin *et al* 1995) and is essential for the mature molecule to exert its role in cell-cell adhesion. The extracellular domain also possesses a flexible hinge region. The cytoplasmic domain is a highly conserved

region that is common to all members of the cadherin family. The two parts of the molecule are connected by a single, 32 amino acid, hydrophobic, membrane spanning domain.

b) Function

In epithelial cells, cell-cell adhesion is mediated primarily by epithelial (E)-cadherin, a 120 kDa transmembrane glycoprotein, localised at the adherens junctions (Takeichi 1991). The cadherins and catenin, however, are more than just intercellular glue. β-Catenin seems to participate in signal transduction pathways independently from its role in cell-cell adhesion and thus linked the cell surface to downstream cytoplasmic and nuclear events. E-cadherin is essential for the formation and maintenance of epithelium. Cadherin-mediated adhesion is a highly dynamic process that is regulated by several signal transduction pathways. Cadherin receptors exist as dimers at the cell surface. The receptors interact with the same type of molecules in neighbouring cells (homophilic binding). This interaction occurs in an antiparallel fashion and results in the lateral clustering or zipping up of cadherin complexes at sites of cell-cell contact. Functional adhesion requires calcium ions, to stabilise the extracellular domain, and association of the receptors with actin cytoskeleton, which is indirectly mediated by the actin binding protein α-catenin and α-actinin. The cytoplasmic domain of E-cadherin binds to the catenins (β-catenin and γ-catenin). β-Catenin links E-cadherin to α-cadherin and the actin cytoskeleton and the linkage to the actin cytoskeleton is essential for the adhesion function of cadherins at the zonula adherens junction. Binding of the cadherin-catenin complex to transmembrane tyrosine kinases and phosphatases juxtaposes adhesion and signalling complexes such that cells can respond to extracellular signals with rapid and local changes in adhesion. Activation of tyrosine kinases leads to tyrosine phosphorylation of catenins and downregulation of cadherin-mediated adhesion, which result in the dissociation of the cadherin-catenin complex from the actin cytoskeleton and a concomitant decrease in intercellular adhesion.

The importance of E-cadherin in the control of cell motility has led to speculation about its role as an 'invasion suppressor'. During tumorigenesis in epithelial cells,

E-cadherin adhesiveness is frequently reduced or abolished in a variety of different ways. Transfection of invasive E-cadherin-negative cell lines with fully functional E-cadherin expression vectors, resulted in loss of invasive features (Vleminckx *et al* 1991). Loss of E-cadherin mediated adhesion results in increased dedifferentiation of tumour cells (transition from adenoma to carcinoma) (Perl *et al* 1998). Loss of expression of E-cadherin is thought to occur late in carcinogenesis and although few mutations of *HSECAD* have yet been described in colorectal cancer, mutations in other cancers occur along the whole length of the *HSECAD* gene without an obvious 'hot spot'. However, loss of E-cadherin function can also occur in the absence of *HSECAD* gene mutation. Mutation of other members of the E-cadherin-catenin-unit (ECCU), such as α- and β-catenin, abolish E-cadherin-mediated adhesion (Oyama *et al* 1994, Morton *et al* 1993). It has been shown that phosphorylation of β-catenin renders it useless for ECCU (and thereby E-cadherin) function, the epidermal growth factor receptor (Shiozaki *et al* 1995), c-erb-B-2 (Ochiai *et al* 1994), hepatocyte growth factor receptor (Shibamoto *et al* 1994) c-met, and the oncoprotein ppbO $^{v\text{-}src}$ (Behrens *et al* 1993) are all able to phosphorylate β-catenin. Finally, and possibly most importantly for tumour development, functional control was also dependent partially on APC, since both E-cadherin and APC compete for β-catenin binding (Hulsken *et al* 1994). E-cadherin has been postulated as a mediator of contact inhibition in cells. Finally, when the actin filaments of the cytoskeleton polymerise, they released DNAses and because of its association with the actin cytoskeleton, -- E-cadherin has been implicated in the control of apoptosis (Salomon and Diaz-Cano 1995). Recent evidence suggests that the E-cadherin gene is regulated by the interplay between Myc and AP-2. AP-2 was the transcription factor that has been shown to bind to the bHLHZip domain of c-myc (Batsche *et al* 1998)

1.4.4. Members of the Wnt signalling pathway

1.4.4.1. Frizzled

In *Drosophila melanogaster*, *Frizzled* encoded an integral membrane protein with seven potential transmembrane domains. The homologues *frizzled-1* and *frizzled-2*

(*fz-1, fz-2*) have been cloned from rat and human, by Northern analysis revealed expression in a wide variety of tissues including kidney, liver, heart, uterus and ovary (Chan *et al* 1992, Zhao *et al* 1995). Six novel mammalian *frizzled* homologues have been identified recently, each of them seemed to be expressed in a distinctive set of tissues during development or postnatally (Wang *et al* 1996).

The frizzled proteins have been identified as receptors for the Wnt pathway. The prototypic member of frizzled family, Frzb, was cloned and protein was purified from bovine cartilage (Hoang *et al* 1996). Members of the Frzb family seem to be surprisingly similar in their specificity for inhibiting Wnt signalling. Frzb-1, originally discovered by primary protein sequencing of highly purified cartilage-derived protein preparations, contains an N-terminal domain with 50% identity to the cysteine-rich domain of Drosophila Frizzled (Hoang *et al* 1996). The open reading frame revealed the presence of a signal peptide and a hydrophobic domain followed by multiple potential serine/threonine phosphorylation sites and a serine-rich C-terminus

Frzb-1 prevented Wnt-1 induced cytosolic accumulation of β-catenin in human embryonic kidney cells (Lin *et al* 1997). Moreover, they also studied structure and function, which showed that complete removal of the frizzled domain of Frzb-1 abolished the Wnt-1/Frzb-1 protein interaction and the inhibition of Wnt-1 mediated axis duplication in *Xenopus* embryos (Lin *et al* 1997). In contrast, removal of the C-terminal portion of the molecule preserved both Frzb-Wnt binding and inhibitory function of Wnt signalling (Lin *et al* 1997). Partial deletion of the Frzb-1 cysteine-rich domain maintained Wnt-1 interaction, but inhibitory function was lost (Lin *et al* 1997). Thus, the frizzled domain was necessary and sufficient for both activities (Lin *et al* 1997).

Frizzled (fze3) is a human homologue of *Drosophila*, *fzd7*, mapping to human chromosome 2q33. *Fze3* was specifically expressed in oesophageal carcinoma tissue compared with the adjacent normal mucosa (Tanaka *et al* 1998). They found that fze3 protein contained an N-terminal signal sequence, 10 cysteine residues typical of the cysteine-rich extracellular domain of *Fz* family members, 7 putative transmembrane

domains and an intracellular C-terminal domain. They suggested that *fze3* gene expression might downregulate APC function and enhanced β-catenin-mediated signals in poorly differentiated human oesophageal carcinomas.

1.4.4.2. Axin

The human *Axin* gene maps to chromosome 16p13.3 and encodes a 900 amino acid polypeptide with 87% identity to the mouse protein (Zeng *et al* 1997). The sequence also contains a regulator of G protein signalling domain terminus of *Drosophila* and vertebrate "dishevelled" proteins (Zeng *et al* 1997).

The amino-terminal domain of human Axin, which contains the regulator of G-protein signalling (RGS) domain, binds directly to the APC tumour suppressor protein at a site in the APC protein that is often deleted in neoplasia (Hart *et al* 1998). Human Axin (hAxin) contains independent binding sites for APC, β-catenin and GSK-3β and overexpression of hAxin strongly promotes the downregulation of wild type β-catenin in colon cancer cells whereas mutant oncogenic β-catenin is unaffected (Hart *et al* 1998). Moreover, the downregulation was increased by deletion of the APC-binding domain from Axin, suggesting that APC might function to depress Axin activity and hAxin dramatically facilitated the phosphorylation of APC and β-catenin by GSK-3β *in vitro* (Hart *et al* 1998). Thus, Axin provided the missing link for the connection of APC and GSK-3β.

Mutations in mouse *Axin* gene caused axis duplication in homozygous mouse embryo. A recent study in *Xenopus* identified *Axin* as a new potential component of the regulation of β-catenin signalling (Zeng *et al* 1997). It was shown that murine Axin inhibited the dorsal axis formation in *Xenopus* that was normally observed on expression of Wnt-1.

Rat Axin (rAxin) consists of 832 amino acids and possesses Regulators of G protein Signalling (RGS) in its N-terminal and C-terminal regions which is dishevelled (Dsh) mouse homologous domains (Ikeda *et al* 1998). rAxin and Axil contained GSK-3β and β-catenin binding sites in the central region at amino acids 298-506. rAxin showed 94% identity with mouse Axin and interacted directly with

the armadillo repeats of β-catenin (Ikeda *et al* 1998). Axil was identified, which showed 44% amino acids identity with Axin (Yamamoto *et al* 1998). rAxin and Axil were directly phosphorylated by GSK-3β and formed complex with β-catenin by binding to the N-terminal of β-catenin (Ikeda *et al* 1998). The binding site of both rAxin and Axil for GSK-3β was distinct from the β-catenin-binding site and they both promoted GSK-3β-dependent phosphorylation of β-catenin (Ikeda *et al* 1998, Yamamoto *et al* 1998). The regulators of G-protein signalling (RGS) domain of rAxin was demonstrated to form a complex with full-length APC but not a truncated APC in vitro (Kishida *et al* 1998). Moreover, they also demonstrated that the down regulation activity of APC on β-catenin required the binding of rAxin (Ikeda *et al* 1998). Therefore, Axin, rAxin and Axil negatively regulated the Wnt signalling pathway by directly interacting with GSK-3β and β-catenin and mediated the signal from GSK-3β to phosphorylate β-catenin. These results indicated that Axin or rAxin or Axil, APC, GSK-3β, and β-catenin formed a tetrameric complex which resulting in the regulation of the stabilisation of β-catenin, subsequently, leading to negatively regulation of the Wnt signalling pathway.

1.4.4.3. Glycogen synthase kinase 3β (GSK-3β)

Glycogen synthase kinase 3β (GSK-3β) is an isoform of GSK-3, and was originally characterised as a serine/threonine kinase that phosphorylates and inactivates glycogen synthase, and subsequently was demonstrated to be identical to protein kinase F_A that activates ATP-Mg-dependent type-1 protein phosphatase (Plyte *et al* 1992). GSK-3β was implicated in the regulation of several physiological responses in mammalian cells by virtue of its activity phosphorylating many substrates including neuronal cell adhesion molecule, neurofilament, synapsin I, tau, transcription factors and *APC* (Mandelkow *et al* 1992, Plyte *et al* 1992, Yang *et al* 1992, Rubinfeld *et al* 1996). The cDNAs of GSK-3β in mammals have been isolated and they encoded the protein kinases with M_rs of 51 and 47 kDa, respectively (Woodgett 1990).

Both structure and function of mammalian GSK-3β were homologous to the *Drosophila zeste-white3/shaggy* gene product (Ruel *et al* 1993). Furthermore, it has been shown that GSK-3β phosphorylated APC and that the phosphorylation enhanced the binding of APC to β-catenin (Rubinfeld *et al* 1996). The wild type GSK-3β phosphorylates β-catenin at a conserved N-terminal site (Rubinfeld *et al* 1996). It was well known that APC was required for the degradation of β-catenin, although the role of APC was not well understood (Polakis 1997). It has been shown recently that the ubiquitination-proteasome pathway was involved in the degradation of β-catenin and that mutations in the GSK-3β consensus phosphorylation site of β-catenin prevented ubiquitination (Aberle *et al* 1997). Thus, it appeared that GSK-3β phosphorylated -- β-catenin and that the phosphorylation of β-catenin was essential for its degradation.

1.4.4.4. Transcription factors: Tcf family

There are four known members of the transcription factors *Tcf* and *Lef* family in mammals: the lymphoid-specific factors *Tcf-1* and *Lef-1* (van de Wetering *et al* 1991, Travis *et al* 1991) and the less well characterised *Tcf-3* and *Tcf-4* (Castrop *et al* 1992). *Tcf-1* and *Lef-1* are the two members of a small subfamily of vertebrate high-mobility-group (HMG) box transcription factor genes (van de Wetering *et al* 1991, Waterman *et al* 1991, Travis *et al* 1991).

In mammalian cells, Lymphoid enhancer-binding factor (*Lef-1*) interacted with -- β-catenin and coexpressed *Lef-1* and β-catenin formed complex that was localised to the nucleus and was detected by immunoprecipitation (Behrens *et al* 1996). The N-terminal domain of *Lef-1* was necessary and sufficient for the interaction with -- β-catenin (Behrens *et al* 1996). *Lef-1* was closely related to *Tcf-1*, which has a similar expression pattern in the mouse (Oosterwegel *et al* 1993, van de Wetering 1991) and to *Tcf-3* and *Tcf–4* (Korinek *et al* 1997, Molenaar *et al* 1996). Functional and biochemical characterisation of *Lef-1* has indicated that this protein has no transcriptional activation potential by itself and was unable to stimulate transcription from a synthetic enhancer containing multimerised *Lef-1* binding sites (Travis *et al* 1991, Waterman *et al* 1991). *Lef-1* stimulated the function of the T-cell receptor α

(TCR α) enhancer in collaboration with other DNA-binding proteins (Travis *et al* 1991, Waterman *et al* 1991). *Lef-1* acted as an architectural transcription factor that introduced a sharp bend in the DNA (Giese *et al* 1992, Love *et al* 1995) and contained a context-dependent activation domain, which functioned only in a specific context of other transcription factors (Carlsson *et al* 1993, Giese and Grosschedl 1993). The amino-terminal 76 residues of *Lef-1* could be associated directly with -- β-catenin (Behrens *et al* 1996, Huber *et al* 1996). A similar β-catenin interaction domain has been identified in the Lef-1-related proteins Tcf-1, Tcf-3 and Tcf-4, which in combination with overexpressed β-catenin stimulated transcription from multimerised Lef/Tcf binding sites (Korinek *et al* 1997, Molenaar *et al* 1996). Other reported that the association of β-catenin with Lef-1 in the nucleus suggested the DNA-binding or regulatory properties of the transcription factor might be altered and Lef-1-induced DNA bending could affect gene regulation (Giese *et al* 1995). The architectural transcription factor Lef-1 was shown to be a strong candidate as a downstream target of β-catenin, was given the observations that: Lef-1 bound directly to β-catenin, β-catenin modulated the DNA-binding properties of Lef-1 and Lef-1, like β-catenin and members of the Wnt pathway, induced axis duplication of *Xenopus* embryo (Behrens *et al* 1996). Tcf/Lef transcriptional activation and upregulation of cytosolic β-catenin in a mammalian system were induced by Wnt-1 (Young *et al* 1998).

In the absence of Wnt signalling, Lef-1/Tcf proteins suppressed transcription in association with Groucho and the cyclic AMP response element binding protein (Eastman and Grosschedl 1999). Recent work has established genetic and biochemical interactions between Lef-1/Tcf proteins and Groucho, a transcriptional corepressor that interacted with several DNA-binding proteins such as Hairy, Engrailed and Dorsal (Cavallo *et al* 1998, Roose *et al* 1998, Fisher and Caudy 1998, Levanon *et al* 1998). In addition, Lef-1 and Tcf-1 had different nuclear localisation properties (Prieve *et al* 1998) and might differ in their binding of various Groucho family members (Roose *et al* 1998, Levanon *et al* 1998).

1.4.4.5. Groucho

Groucho (Gro) is a broadly expressed *Drosophila* corepressor involved in segmentation, sex determination and neurogenesis (Hartley *et al* 1988, Paroush *et al* 1994, Parkhurst 1998, Fisher and Caudy 1998). Stifani *et al* (1992) described human homologues of *Drosophila* groucho protein, which were designated as transducin-like enhancer of split (*TLE*). In mammals, multiple homologues with a similar overall domain structure have been identified. These were termed *TLE1-4* in man (Stifani *et al* 1992) and *mGrg-1*, *-3*, *-4* and *–5* in mouse (Mallo *et al* 1993). Liu *et al* (1996) demonstrated *TLE1* and *TLE2* genes map to 19p 13.3 by *in situ* hybridization. Groucho expressed nuclear proteins that do not bind to DNA. Groucho acted as a corepressor that mediates repression by a variety of specific DNA binding protein (Parkhurst 1998). Groucho interacts with AML1 and AML2 (AML genes are members of gene family of heterodimeric transcription factors) on T cell receptor regulation and Wnt signalling (Levanon *et al* 1998). Corepressors are defined as proteins that are required for the repressor activity of a specific transcription factor but did not have the ability to bind DNA alone. *TLE*/Gro interacted with *LEF-1*, and inhibited *LEF-1*:β-catenin-dependent transcription (Levanon *et al* 1998). Groucho binds a region of human Tcf-1 that is separated from the β-catenin binding domain. The mechanism by which Groucho represses transcription could involve recruitment of repressive chromatin through interactions with histone H3 (Palaparti *et al* 1997).

1.4.4.6 Dishevellled

Dishevelled (*Dsh*) encodes a cytoplasmic protein (Dsh) with no known biochemical function and little homology to other proteins (Klingensmith *et al* 1994). In the mouse, three *dsh* genes (*Dvl-1*, *Dvl-2* and *Dvl-3*) have been cloned by homology (Sussman *et al* 1994).

Amino acid sequence comparison of all known *dsh* genes reveals regions of high homology in the amino-terminus and in the central domain while the carboxy-terminus is highly divergent (Klingensmith *et al* 1994). The N-terminal conserved domain shares homology to Axin, which also plays an important role in Wnt signalling (Zeng *et al* 1997, Ikeda *et al* 1998, Behrens *et al* 1998). This N-terminal

domain is referred to as the DIX (Dishevelled and Axin) domain. The central region of Dsh contains a domain referred to as *discs-large* homology region (Dhr) or PDZ (Klingensmith *et al* 1994, Ponting 1995), which is found in several other proteins such as PSD-95, ZO-1 and Discs-large (Ponting 1995). Structural analysis demonstrated that a carboxy-terminal four-residue motif (X-Thr/Ser-X-Val) binds to the PDZ domain of PSD-95 (Doyle *et al* 1996) and to the PDZ domain of the human homologue of the *Drosophila discs-large* tumour suppressor gene product, DlgA (Morais Cabral *et al* 1996). The carboxy-terminal is recently described domain referred to as the DEP (Dsh/egl-10/Pleckstin) domain (Ponting 1996).

Dsh proteins are localised predominantly in the cytoplasm of the cells (Yanakawa *et al* 1995). Studying in vitro showed a fraction of Dsh protein localised to the cell membrane (Yanakawa *et al* 1995), which suggested that the membrane fraction of protein is active in signalling. The molecular mechanism by which Dsh/Dvl is involved in signal transduction of Wnt is largely unclear, especially in mammalian system.

Siamois, is a *Xenopus* zygotic homeobox gene, was specifically activated by -- β-catenin, which appeared to mediate the effects of the Wnt pathway on axis formation (Carnac *et al* 1996, Fagotto *et al* 1997). Siamois was a mediator of the Wnt signalling pathway and that the synergy between the Wnt and mesoderm induction pathways occurred downstream of the early target genes of these two pathways (Carnac *et al* 1996).

1.5. β-Catenin downstream target genes

1.5.1. c-Myc

c-Myc was one of the first cellular oncogenes to be discovered (Bishop 1983), it has been shown to play a role in growth control, differentiation and apoptosis and abnormal expression has been associated with many naturally occurring neoplasms (Askew *et al* 1991, Evan and Littlewood 1993, Evan *et al* 1992). Takahashi *et al* (1991) refined the assignment of *c-Myc* to chromosome 8q24.12-q24.13. The gene product encoded by the *c-myc* oncogene is a transcription factor. A molecular weight

of 65,000, which is located predominantly in the nucleus and binds to DNA (Persson and Leder 1984).

The carboxy terminus of c-myc is composed of 90 amino acids, contained three structural domains that are homologous to domains found in other transcription factors, including the leucine zipper, a helix-loop-helix motif (HLH) and an adjacent domain rich in basic amino acids (Blackwell *et al* 1990, Murre *et al* 1989). There are two nuclear localisation signals in the carboxy terminus (Henriksson and Luschher 1996). The transcription activation domain has been mapped to the amino terminus, has short 'acidic' proline-rich and glutamine-rich clusters similar to those associated with some transactivation domains (Kato *et al* 1990), which contained multiple phosphorylation sites.

c-Myc is expressed in almost all proliferating normal cells where its expression was strictly dependent on mitogenic stimuli. It is downregulated in many kinds of cells when they are induced to terminally differentiate (Evan and Littlewood 1993). The expression of the *c-myc* gene is closely correlated with growth and removal of growth factors at any point in the cell cycle results in its immediate downregulation (Dean *et al* 1986, Waters *et al* 1991). *c-Myc* expression is absent in quiescent cells (Waters *et al* 1991). Overexpression of *c-myc* in growing cells led to reduce growth factor requirements and a shortened G_1 phase (Karn *et al* 1989) while reduced expression caused lengthening of the cell cycle (Shichiri *et al* 1993). It has been reported that *c-myc* was able to increase the expression levels of cyclins E and A and suppressed the expression of cyclin D1 (Hanson *et al* 1994, Perez-Roger *et al* 1997, Philipp *et al* 1994, Solomon *et al* 1995). Recently, it has been reported that *c-myc* affected the cell cycle at multiple independent points (Mateyak *et al* 1999). *c-Myc* mediated apoptosis was dependent on *p53* in some cell types (Hermeking and Eick 1994, Hsu *et al* 1995). Deregulated myc expression resulted in more tumorigenesis when expressed in mice with a *p53* null background (Evan and Littlewood 1998, McCormack *et al* 1998). A molecular framework was provided by He *et al* (1998) for understanding of the overexpression of *c-myc* in colorectal cancers. They showed that expression of *c-myc* was suppressed by wild type *APC* and activated by β-catenin and

that effects were mediated through Tcf-4 binding sites in the *c-myc* promoter (He *et al* 1998). In colorectal cancers with APC mutations or activating β-catenin mutations, increased β-catenin/Tcf-4 activity led to overexpression of *c-myc*, which then promoted neoplastic growth (He *et al* 1998). Thus *c-myc* was a target gene in the Wnt signalling pathway.

1.5.2. Cyclin D1

CCND1 gene map to chromosome 11q12-q13 (Hinds *et al* 1994). *Cyclin D1* gene encodes a regulatory subunit of a multiprotein cyclin D1-dependent kinase holoenzyme complex, which phosphorylates and inactivates the tumour suppressor protein pRB (retinoblastoma protein) (Goodrich *et al* 1991, Weinberg 1995). N-terminal contains the sequence Leu-X-Cys-X-Glu, which is shared by DNA viral oncoproteins (SV40 T antigen, adenovirus E1A, and human papillomavirus E7).

Cyclin D1 is degraded by the ubiquitin pathway and its degradation is enhanced by phosphorylation on threonine 286 by glycogen synthase kinase 3β (Diehl *et al* 1998). Cyclin D1 is one of the key regulators of Cdk4 and Cdk6 and is thought to have an important role in G_1 progression (Resnitzky *et al* 1994, Resnitzky and Reed 1995). Cyclin D1 was amplified and overexpressed in a number of breast and prostate tumours, pancreatic cancer, colon adenocarcinomas and squamous cell carcinomas of the head and neck (Lammie and Peters 1991, Buckley *et al* 1993, Tam *et al* 1994, Gausauge *et al* 1997, Han *et al* 1998, Maeda *et al* 1998). This circumstantial evidence for the involvement of cyclin D1 in oncogenesis was substantiated when it was shown that cyclin D1 cooperated with *Myc* family members in the induction of tumours in transgenic mice (Bodrug *et al* 1994, Lovec *et al* 1994, Wang *et al* 1994). It has been reported that cyclin D1 is a target gene for repression by *c-myc* (Philipp *et al* 1994). Moreover, they also reported that the repression occurred at the level of transcription and was mediated by core elements of the cyclin D1 promoter (Philipp *et al* 1994).

1.5.3. AP-1

AP1 was mapped to human chromosome 1p32-p31 (Hattori *et al* 1988), and to mouse chromosome 4 (Bahary *et al* 1991). *AP-1* is one of the genes affected by -- β-catenin overexpression (Mann *et al* 1999). The direct interaction of the β-catenin-Tcf/Lef complex with the promoter regions of both components of the AP-1 complex was also reported (Mann *et al* 1999). AP-1 has been shown to increase the expression of urokinase-type plasminogen activator receptor (uPAR) in the colorectal cancer cell line RKO (Lengyel 1996).

1.5.4. Integrin-linked kinase (ILK)

The integrin-linked kinase (ILK) was identified from a yeast two-hybrid genetic screen by using as bait the cytoplasmic domain of the β_1 integrin subunit (Hannigan *et al* 1996). ILK can interact with β_1 and β_3 integrins. The kinase activity of ILK was modulated by interaction of cells with components of the extracellular matrix (Hannigan *et al* 1996) or by integrin clustering. Overexpression of ILK in epithelial cells resulted in the stimulation of anchorage-independent cell growth (Hannigan *et al* 1996) and cell cycle progression (Radeva *et al* 1997). In the cell cycle progression was caused by the constitutive upregulation of expression of cyclin D1 and cyclin A, resulting in the hyperphosphorylation of the retinoblastoma protein (Radeva *et al* 1997). Overexpression of ILK in epithelial cells also resulted in the induction of tumorigenicity in nude mice (Wu *et al* 1998), indicating that *ILK* was a protooncogene. Overexpression of ILK in intestinal epithelial cells as well as in mammary epithelial cells resulted in an invasive phenotype concomitant with a down-regulation of E-cadherin expression, translocation of β-catenin to the nucleus, formation of a complex between β-catenin and the high mobility group transcription factor, LEF-1, and transcriptional activation by this LEF-1/β-catenin complex (Novak *et al* 1998). They demonstrated that the oncogenic properties of ILK involve activation of the LEF-1/β-catenin signalling pathway (Novak *et al* 1998).

Chapter 2

Comprehensive study of Apc, β-catenin and E-cadherin expression in mutant mice

The previous chapter introduced APC as a multifunctional protein with major but tissue-specific oncosuppressor activity. While one of its roles is to bind and facilitate the destructive proteolysis of the signalling molecule β-catenin, other roles include regulation of microtubule dynamics in cell movement and cytokinesis and perhaps the organisation of receptor arrays at cell-to-cell junctions. It is far from obvious why these different functions should be associated with a single protein, why this protein should be critical for prevention of carcinogenesis in certain epithelia, or why deficiency of its function should be an early rather than later manifestation of the carcinogenesis process. This thesis presents data that relate to these questions. In this chapter the distribution of Apc is studied in a variety of normal murine tissues, with special reference to epithelia. By immunohistochemistry, the localisation of Apc is compared with that of other molecules concerned with Wnt signalling (β-catenin and E-cadherin which is an integral membrane protein binding to β-catenin). The data show patterns of distribution, particularly prominent within the hierarchy of cells in complex epithelial tissues such as the intestinal tract, that indicate that the association of Apc and β-catenin is a dynamic one. While in some cells, E-cadherin, Apc and -- β-catenin appear in a similar, membrane related position, in others they are clearly demonstrated colocalisation. In particular, in animals genetically modified to have deficient Apc expression, the quantity and location of intracellular β-catenin in certain cells of some tissues is modified dramatically. These cells may be the founders of neoplastic clones and their detailed study is the subject of the next chapter.

From the above, it is clear that Apc, β-catenin, and E-cadherin are involved with each other both in normal circumstances and in carcinogenesis. The Apc protein is an important protein in regulation of β-catenin levels in the Wnt signalling pathway. Here, I decided to focus on the pattern of Apc expression in epithelial cells from each organ in *Apc* ^{Min}, (*Apc* ^{Min}*/p53* $^{-/-}$) and (*Apc* ^{Min}*/Msh2* $^{-/-}$) mice. In addition, β-catenin and E-cadherin expression was also investigated in the same specimens in *Apc* ^{Min}, (*Apc* ^{Min}*/p53* $^{-/-}$) and (*Apc* ^{Min}*/Msh2* $^{-/-}$) mice, so that the relationship between Apc and either β-catenin or E-cadherin protein could be demonstrated.

2.1 Materials and Methods

2.1.1. Mice

Mice mutant for *Msh2* (de Wind *et al* 1995), *p53* (Clarke *et al* 1993) and *Apc* ^{Min} (Moser *et al* 1992) were maintained as out-bred colonies segregating for Ola/129, Balb C, SWR and C57Bl/6 genomes. Mice were monitored on a daily basis for signs of ill health and were killed when they showed overt signs of neoplastic disease.

2.1.2. Tissue processing

Each organ was removed from mice immediately after killing by cervical dislocation. Intestinal contents were cleaned out by gently flushing with phosphate buffered saline. The whole piece of intestine was placed on Whatman filter paper number 1. The intestine was opened longitudinally along the anti-mesenteric surface from one end to the other, spread out flat and fixed in methacarn (see appendix B) at room temperature overnight. Other organs were cut longitudinally into 0.5 mm thick slices so that the fixative could penetrate through the specimen and fixed in 10% buffered formalin overnight at room temperature. "Swiss roll" preparation of the intestine was made by holding one end of a piece of intestine with tissue forceps and rolling to the other end. The rolls of intestine were fixed in position with disposable needles 25 gauge. All the specimens were dehydrated through graded ethanol solutions (70%, 85%, and 90%, two changes every 20 minutes and absolute ethanol for 40 minutes, 3 times). The specimens were cleared in xylene (every 40 minutes, 3 times) and blocked in paraffin wax at 60 ^{0}C. The specimens were in paraffin wax for 40 minutes, 3 changes of paraffin wax.

2.1.3. Optimisation of the immunohistochemistry technique

The core method was immunohistochemistry with monoclonal or polyclonal antibodies, detection by a commercial avidin-biotin immunoperoxidase complex method, after application of an appropriate secondary antibody.

2.1.3.1. Primary antibodies

All primary antibodies in this study were optimised to find the correct working concentration, using 3 to 4 serial dilutions as follows:

Rabbit polyclonal APC, 3161 (Midgley *et al* 1997, purified rabbit antiserum to human APC C-terminal peptide, corresponding to codons 2813-2827; contained protein 0.116 μg/μl) 0.0232, 0.00232 and 0.000232 μg/μl;

Mouse monoclonal Ki67 (Novocastra, UK, 100 μg/ml) 0.05, 0.1, 0.2 and 0.3 μg/μl;

Rabbit polyclonal p53 (CM5, Novocastra, UK, 100 μg/ml) 0.001, 0.002, 0.003 and 0.004 μg/μl;

Mouse monoclonal β-catenin (IgG_1, clone 14, Transduction Laboratory, UK, 250 μg/ml) 0.0025, 0.005, 0.0075 and 0.10 μg/μl;

Mouse monoclonal E-cadherin (Transduction Laboratory, UK, 250 μg/ml) 0.00125, 0.0025 and 0.050 μg/μl;

Rat monoclonal BrdU (Harlan SeraLab, UK, 500 μg/ml) 0.0025, 0.005, 0.0075 and 0.01 μg/μl

Primary antibody was diluted in 20% normal serum in Tris buffered saline and 0.1%Tween 20 (see appendix B). The normal serum was from the species corresponding to the secondary antibody used in the staining. Activity of the diluted primary antibody was first confirmed on frozen tissue sections from tissues with known expression since frozen tissue sections do not require any antigen retrieval technique. Incubation was for either an hour at room temperature or overnight at 4 ^{0}C. Optimisation on paraffin embedded tissues was then performed for both incubation times and with the same concentration of primary antibodies used in frozen sections. The optimum working condition for each primary antibody obtained from the optimisation reactions was as follows:

Primary antibody	Working concentration (μg/ml)	Incubation time	Temperature
APC	0.00232	Overnight	4 ^{0}C
Ki67	0.1	1 hour	Room temperature
β-catenin	0.005	1 hour	Room temperature
E-cadherin	0.0025	Overnight	4 ^{0}C
BrdU	0.005	1 hour	Room temperature
p53	0.002	Overnight	4 ^{0}C

2.1.3.2. Secondary antibodies

Secondary antibodies used in this study were swine anti-rabbit biotin-conjugated secondary antibody (SAR) (Dako, Denmark), rabbit anti-mouse biotin-conjugated secondary antibody (RAM) (Dako, Denmark) and rabbit anti-rat biotin-conjugated secondary antibody (RAR) (Pierce, USA). Secondary antibody was diluted in to 2 to 3 dilutions in 20% normal serum in Tris buffered saline and 0.1% Tween 20 (see appendix B) and incubated as follows;

Swine anti-rabbit biotin-conjugated secondary antibody (SAR) (Dako, Denmark, 1.07g/l) 0.05, 0.027 and 0.014 μg/μl

Rabbit anti-mouse biotin-conjugated secondary antibody (RAM) (Dako, Denmark, 0.85 g/l) 0.04, 0.021 and 0.015 μg/μl

Rabbit anti-rat biotin-conjugated secondary antibody (RAR) (Pierce, USA, 0.5 mg/ml) 0.05, 0.01 and 0.002 μg/μl

The optimum concentration of secondary antibodies for this immunohistochemistry staining was shown in the table below

Secondary antibody	Working concentration (μg/μl)	Primary antibody
Swine anti-rabbit/Biotin	0.027	APC and p53
Rabbit anti-mouse/Biotin	0.021	Ki67, β-catenin and E-cadherin
Rabbit anti-rat/Biotin	0.01	BrdU

2.1.3.3. Antigen retrieval technique

Each primary antibody required different techniques of antigen retrieval in formalin-fixed paraffin-embedded tissue sections to reveal antigenic sites altered or obscured by fixation. To define the optimum conditions, paraffin tissue sections were subjected to following conditions:

(a) No pretreatment;

(b) Pretreatment by trypsin digestion: after sections were dewaxed and rehydrated, incubation in 0.1% trypsin solution (see appendix B) for 30 minutes at 37 ^{0}C;

(c) High temperature pretreatment: dewaxed and rehydrated sections were immersed in either 0.05 M citrate buffer (see appendix B) or 0.1 M EDTA buffer (see appendix B), followed by microwaving at 700 watts for 5 minutes, 3 times;

(d) DNA denaturation: dewaxed and rehydrated sections were exposed to 1 N HCl at 60 ^{0}C for 10 minutes or 2 N HCl at 27 ^{0}C for 25 minutes (this method was used exclusively for BrdU antibody staining)

From the above conditions we found that the optimum condition for each primary antibody was as follows:

Primary antibody	**Pretreatment condition**
APC	None
Ki67	High temperature, in citrate buffer
p53	High temperature, in citrate buffer
β-catenin	High temperature, in citrate buffer
E-cadherin	High temperature, in citrate buffer
BrdU	2 N HCl at 27 ^{0}C, 25 minutes

2.1.3.4. Blocking endogenous peroxidase activity

Because horseradish peroxidase was used as the detection system in these reactions, it was necessary to block endogenous non-specific peroxidase in the tissues by pretreatment with hydrogen peroxide. In a series of optimising trials, the conditions suited to each antibody were determined as shown in the following table.

Primary antibody	Hydrogen peroxide concentration	Incubation time (minutes)	Temperature
Ki67	1.5% in distilled water	15	Room temperature
β-catenin	1.5% in distilled water	15	Room temperature
BrdU	1.5% in distilled water	15	Room temperature
APC	3.0% in distilled water	20	Room temperature
p53	0.5 % in methanol	15	Room temperature
E-cadherin	0.5 % in methanol	15	Room temperature

2.1.3.5. Permeabilisation of the sections

In some conditions, permeabilisation prior to antibody exposure was found to improve the ultimate antigen visualisation. Saponin and TritonX-100 methods were tested and the final conditions used were; permeated the sections with 0.1% saponin (saponin 10 mg dissolved in 100 ml of distilled water) for 30 minutes.

2.1.3.6. Double labelling immunohistochemistry of β-catenin and BrdU

Additional optimisation was required for double immunostaining of β-catenin and BrdU. The final conditions were high temperature pretreatment, followed by immersion in 2 N HCl at 27 ^{0}C for 25 minutes, and finally blocking of endogenous peroxidase in 1.5% hydrogen peroxide for 15 minutes. BrdU staining was visualised with horseradish peroxidase and β-catenin staining was visualised with alkaline phosphatase. Alkaline phosphatase is an intestinal isoenzyme. Endogenous alkaline phosphatase can be inhibited by the addition of levamisole to the Tris buffer pH 8.2 prior to the preparation of the working solution. After optimisation of each step of the immunohistochemistry technique in this study I outline the protocol for the techniques used in this study in the following table 2.1.

Table 2.1. Immunohistochemistry techniques

Primary antibody	Concentration (μg/μl)	Incubation conditions	Pretreatment	Endogenous peroxidase blocking	Secondary antibody, concentration (μg/μl)	Detection system
β-catenin, mouse monoclonal	0.005	1 hour at RT	High temperature	1.5%H_2O_2, in distilled water	Rabbit anti-mouse, 0.021	ABComplex/ HRP
E-cadherin, mouse monoclonal	0.0025	1 hour at RT	High temperature	0.5% H_2O_2, in methanol	Rabbit anti-mouse, 0.021	ABComplex/ HRP
APC, rabbit polyclonal	0.00232	Overnight at 4 ^{0}C	None	3.0%H_2O_2, in distilled water	Swine anti-rabbit, 0.027	ABComplex/ HRP
p53, rabbit polyclonal	0.002	Overnight at 4 ^{0}C	High temperature	0.5% H_2O_2, in methanol	Swine anti-rabbit, 0.027	ABComplex/ HRP
Ki67, mouse monoclonal	0.1	1 hour at RT	High temperature	1.5%H_2O_2, in distilled water	Rabbit anti-mouse, 0.021	ABComplex/ HRP
BrdU, rat monoclonal	0.005	1 hour at RT	HCl 2N at 27 ^{0}C	1.5%H_2O_2, in distilled water	Rabbit anti-rat, 0.01	ABComplex/ HRP
β-catenin and BrdU	0.005 β-catenin, 0.005 BrdU	Overnight at 4 ^{0}C	High temperature and HCl 2N at 27 ^{0}C	1.5%H_2O_2, in distilled water	Rabbit anti-mouse, 0.021, Rabbit anti-rat, 0.01	ABComplex/ HRP for BrdU, ABComplex/ AP for β-catenin

2.1.4. Purification of rabbit polyclonal APC antibody

Protein A Sepharose beads (Pharmacia, Sweden) 0.5 g were swelled by suspension in 2.0 ml of distilled water for 3 hours, centrifuged at 13,000 rpm, for 20 seconds, and washed by multiple resuspensions and centrifugation in distilled water. The washed beads were loaded into a 1 cm diameter column equilibrated in 20 mM sodium phosphate buffer pH 7.0 (see appendix B). Five hundred microliters of crude APC antiserum was applied to the protein A column followed by 3 column volume of 20 mM sodium phosphate buffer. For elution of the immunoglobulin bound to the Sepharose, 1.5 ml of 0.1 M. glycine buffer pH 3.0 (see appendix B) was applied and 3 drops of each fraction was collected into 2 drops of 0.5 M. Tris/HCl pH 9.0 (see appendix B) to give 20 fractions in total. 1 μl of each fraction was spotted onto nitrocellulose membrane and allowed to air dry for 1 minute. The nitrocellulose membrane was stained in 0.25% Coomassie brilliant blue, in 10% methanol and 7% acetic acid (see appendix B) for 30 seconds, washed in 10% methanol and 7% acetic acid for 5 minutes and air-dried at room temperature. Positivity staining (immunoglobulin enriched) fractions were aliquoted, 0.02% sodium azide (see appendix B) added to each aliquot, and stored at -20^{0}C. The protein A column was stored in 20% ethanol in 0.1 M sodium phosphate buffer pH 7.0 (see appendix B), at 4 ^{0}C, and could be re-used (for further purifications of the same antiserum).

2.1.5. Immunohistochemistry

Immunohistochemistry was performed on 3 micron paraffin sections, mounted on poly-l-lysine coated, cleaned glass slides. Following antigen retrieval (as required) and hydrogen peroxide treatment, the sections were exposed sequentially to 20% normal serum in 0.1%Tween 20/TBS (see appendix B) to block non-specific antibody-binding sites, to primary antibody in the same buffer, 3 buffer washes, secondary antibody and ABComplex/HRP detection system, all in 0.1%Tween 20/TBS buffer. The complex was developed with diaminobenzidine 0.5 mg/ml (DAB, see appendix B) for 5-8 minutes at room temperature, lightly counterstained with Harris haematoxylin (see appendix B) 20 to 25 seconds. Details of the protocol are in the appendix A.

2.2. Results

2.2.1. Immunohistochemistry pattern of APC antibody staining

The expression pattern of Apc was studied in the epithelial cells of normal mice and animals bearing germline alterations in the *Apc*, *Msh2* and *p53* genes by antibody staining. In normal animals Apc protein staining was found positive in cytoplasm in columnar epithelium in the intestine whereas in the lower third of the crypts was almost always negative. In addition, the intestinal columnar epithelium of the luminal surface showed strong staining along their apical surfaces, this apical polarity pattern continued up to the villi, where the cells also showed accentuation of staining on their lateral margins. Diffuse cytoplasmic positive Apc staining was found in columnar epithelial lining in bronchiole of the lung. Similarity diffuse cytoplasmic Apc expression was found in hepatocytes, in cuboidal epithelium of the fallopian tube, uterine gland, proximal and distal renal tubules, epididymis, mammary gland and salivary gland. This pattern of Apc staining also found in the endothelial lining cells in lymphatic vessels in the spleen, lymph node and uterine body. The stratified squamous epithelium in epidermis showed cytoplasmic staining of Apc protein. Muscle and brain tissue showed diffuse cytoplasmic staining whereas neurons and pancreatic acinar cells showed negative staining, although pancreatic ductal epithelium showed cytoplasmic positive staining. The Apc positivity also was observed in the podocyte in renal glomerulus, chondrocyte, and inner nuclear layer of retina and in nucleus of sertoli cell in the testes. The cardiac muscle showed negative Apc staining.

The staining intensity of Apc was weak or absent in intestinal lesions arising in $Apc^{Min+/-}$, ($Apc^{Min+/-}/p53^{-/-}$) and ($Apc^{Min+/-}/Msh2^{-/-}$) mice.

2.2.2. Immunohistochemistry pattern of E-cadherin staining

The pattern of E-cadherin expression was investigated in the epithelial cells of various tissues in $Apc^{Min+/-}$, ($Apc^{Min+/-}/p53^{-/-}$) and $Msh2^{-/-}$ mice as above. The pattern of E-cadherin expression within morphologically normal epithelium: columnar, cuboid, endothelial lining and stratified squamous epithelium was at the lateral cell membrane in

all types of epithelium with the exception of the proximal renal tubule which showed strong E-cadherin staining at the basement membrane and diffuse staining in cytoplasm. E-cadherin staining was also noted in non-epithelium cells such as pancreatic acinar cells and in the zona pellucida. No E-cadherin expression was seen in brain, retina, cardiac and skeletal muscle. Thus, although Apc and E-cadherin was found to be colocalised in intestinal epithelial, there are many circumstances in which this expression differed substantially. In particular in endothelial lining cells, stratified squamous epithelium, muscle, brain, retina and in zona pellucida.

E-cadherin expression was found to be positive by immunostaining in large adenomas but reduced or absent in small lesions. This pattern of E-cadherin staining in the lesions was true for all genotype combination.

2.2.3. Immunohistochemistry pattern of β-catenin staining

The expression pattern of β-catenin in the epithelial cells of various organs in *Apc* $^{Min+/-}$, (*Apc* $^{Min+/-}$*/p53* $^{-/-}$) and *Msh2* $^{-/-}$ mice was investigated. In normal animals, β-catenin immunopositivity was found at the lateral cell membrane of normal epithelial cells. β-Catenin expression was also observed in the nucleus of the Paneth cell. β-Catenin expression was observed at the lateral cell membrane of the columnar epithelium in the intestine, with immunoreactivity of epithelial cells increased gradually from the bases of the crypts to the luminal surfaces. A similar pattern of β-catenin expression was found at the lateral cell membrane of bronchiolar epithelium in the lung, including endothelial lining cells in the alveoli, uterine body, choroid plexus in the brain, ventricle in the brain, lymphatic vessel in the spleen and the lymph node. β-Catenin positivity was found at the lateral cell membrane of pancreatic acinar cells, hepatic bile duct, Graaffian follicle, fallopian tube, uterine gland and epididymis. Whereas diffuse cytoplasmic including basolateral positive staining of β-catenin was observed in the cuboidal epithelium in renal tubule of the renal cortex, mammary gland and salivary gland.

β-Catenin stained strongly in the cytoplasm of the stratified squamous epithelium of the epidermis. In non-epithelial cells such as chondrocytes, β-catenin showed positive

staining at the cell membrane of chondrocytes. In the cardiac muscle β-catenin expression was found strongly expressed at the intercalated disc. There was β-catenin expression observed at the cell membrane of sertoli cell in the testes, and in the cytoplasm of granulosa lutian cell. β-Catenin staining was found to be diffusely positive in outer and inner plexiform layers of retina, hippocampus, cytoplasmic of granular layer and pyramidal layer of the cerebrum including molecular layer and granular layer of the cerebellum. β-Catenin showed negative staining in muscle and Purkinje cell in the brain.

Thus, although β-catenin and E-cadherin frequently co-localised in epithelial cell type, there are some circumstances in which their expression differs. In particular, in cardiac muscle, chondrocytes and neurons.

Overexpression of β-catenin was found in dysplastic and neoplastic cells in the intestine and pancreas in *Apc* $^{Min+/-}$ and (*Apc* $^{Min+/-}$*/p53* $^{-/-}$) mice, in comparison with adjacent morphologically normal cells. They showed both nuclear and cytoplasmic staining of β-catenin, which will be studied in detail in the next chapter.

Example of tissues stained with Apc, β-catenin and E-cadherin are shown in the figure 2.1 to 2.5. Summaries of the patterns of immunohistochemistry staining are presented in the following tables:

Table 2.3. Immunohistochemistry staining pattern in (*Apc* $^{Min+/-}$/*p53* $^{-/-}$) mice

Organs	β-catenin	Apc	E-cadherin
Intestine, normal	(+) at lateral cell membrane of epithelium	(+) in cytoplasm and apical surface of epithelium	(+) at lateral cell membrane of epithelium
Intestinal adenoma	(++++) in nuclei and cytoplasm	(+) range from weak to unstained	Negative/positive
Pancreas	(+) at lateral cell membrane of pancreatic acinar cell	(+) in cytoplasm of ductal epithelium	(+) at lateral cell membrane of pancreatic acinar cell
Pancreatic lesion	(++++) in nuclei and cytoplasm of lesions	(+) in cytoplasm of ductal epithelium	(+) at periphery of pancreatic tumour cells
Uterus	(+) in uterine epithelium	(+) in cytoplasm of epithelium	(+) at border of epithelium
Ovary	(+) in corpus luteum and epithelium of Fallopian tube	Epithelium of Fallopian tube	(+) in corpus luteum and epithelium of Fallopian tube
Testes	(+) at membrane of sertoli cell	(+) in nucleus of sertoli cell	Negative
Epididymis	(+) at lateral cell membrane of epithelium	(+) in cytoplasm of epithelium	Negative
Spleen	(+) membrane of endothelial cells	(+) cytoplasm of endothelial lining cells	(+) membrane of endothelial lining cells
Kidney	(+) in cytoplasm of renal cortex tubules, granular pattern	(+) in cytoplasm and nuclei of proximal and distal tubules, podocyte	(+) in cytoplasm of proximal and distal renal tubules
Liver	(+) at periphery of hepatocytes and cytoplasm (granular pattern), membrane of bile duct	(+) in cytoplasm of hepatocytes	(+) membrane of hepatocytes

Table 2.3. Immunohistochemistry staining pattern in (*Apc* $^{Min+/}$*p53* $^{-/-}$) mice (cont.)

Organs	β-catenin	Apc	E-cadherin
Lung	(+) at lateral cell membrane of bronchiolar epithelium	(+) in cytoplasm of bronchiolar and alveolar epithelium	(+) at lateral cell membrane of bronchiolar epithelium
Heart	(+) at intercalated disc of cardiac muscle	(+) in cytoplasm of cardiac muscle	Negative
Brain	Positive	Positive	Negative
Retina	(+) in outer and inner plexiform layers	(+) in inner nuclear layers	Negative
Lymph node	(+) membrane of endothelial lining cells	(+) cytoplasm of endothelial lining cells	(+) membrane of endothelial lining cells
Mammary gland	(+) at base of epithelium	(+) in cytoplasm of alveolar epithelium	(+) at lateral of epithelium
Salivary gland	(+) at lateral cell membrane of glandular and ductal epithelium	(+) in cytoplasm of glandular epithelium	(+) at lateral cell membrane of glandular and ductal epithelium
Muscle	Negative	(+) in cytoplasm of muscle fibre	Negative
Bone	(+) in chondrocyte	(+) in chondrocytes	Negative
Skin	(+) at lateral cell membrane of epithelium	(+) in cytoplasm of epithelium	(+) in cytoplasm and lateral cell membrane of epithelium

Table 2.4. Immunohistochemistry staining in (*Apc* $^{Min+/-}$/*Msh2* $^{-/-}$) mice

Organs	β-catenin	Apc	E-cadherin
Intestine, normal	(+) at lateral border of epithelium	(+) in cytoplasm and apical surface of epithelium	(+) at lateral surface of epithelium
Intestinal adenoma	(++++) in cytoplasm and nuclei	Weak staining	(+) in small lesions but negative in large lesions
Pancreas	(+) at lateral cell membrane of pancreatic acinar cell	(+) in ductal epithelium	(+) at lateral cell membrane of pancreatic acinar cell
Pancreatic lesion	(++++) in nuclei and cytoplasm of lesions	(+) in ductal epithelium	Negative
Uterus	(+) at lateral cell membrane of endothelium	(+) in cytoplasm of endothelium	(+) at lateral cell membrane of endothelium
Ovary	(+) in corpus luteum and epithelium of Fallopian tube	Epithelium of Fallopian tube	(+) in corpus luteum and epithelium of Fallopian tube
Testes	(+) at membrane of sertoli cell	(+) in nucleus of sertoli cell	Negative
Epididymis	(+) at lateral cell membrane of epithelium	(+) in cytoplasm of epithelium	Negative
Spleen	(+) membrane of endothelial lining cells	(+) cytoplasm of endothelial lining cells	(+) membrane of endothelial lining cells
Kidney	(+) in cytoplasm of renal cortex tubules	(+) in cytoplasm of proximal and distal renal tubules, podocyte	(+) in cytoplasm of proximal renal tubules
Liver	(+) in cytoplasm of hepatocytes (granular pattern), epithelium of	(+) in cytoplasm of hepatocytes	(+) at periphery of hepatocytes

	bile duct		

Table 2.4. Immunohistochemistry staining in (*Apc* $^{Min+/}$*/Msh2* $^{-/-}$) mice (cont.)

Organs	β-catenin	Apc	E-cadherin
Lung	(+) at lateral cell membrane of bronchiolar epithelium	(+) in cytoplasm and apical surface of bronchiolar epithelium	(+) at lateral cell membrane of bronchiolar epithelium
Heart	(+) at intercalated disc	(+) in cytoplasm of heart muscle	Negative
Brain	Positive	Positive	Negative
Retina	(+) in outer and inner plexiform layers	(+) in inner nuclear layers	Negative
Lymph node	(+) at lateral cell membrane of lymphatic endothelial lining	(+) cytoplasm of endothelial lining cells	(+) lateral cell membrane of endothelial lining cells
Mammary gland	(+) at the base of epithelium	(+) in cytoplasm of alveolar epithelium	(+) at periphery of alveolar epithelium
Salivary gland	(+) at lateral border of glandular and ductal epithelium	(+) in cytoplasm of glandular and ductal epithelium	Negative
Muscle	Negative	(+) in cytoplasm of muscle fibre	Negative
Bone	(+) in chondrocyte	(+) in chondrocytes	Negative
Skin	(+) at lateral cell membrane of stratified epithelium of epidermis	(+) in cytoplasm and nuclei of epithelium	(+) at lateral cell membrane of stratified epithelium of epidermis

Table 2.5. Immunohistochemistry staining in *Apc* $^{Min+/-}$ mice

Organs	β-catenin	Apc	E-cadherin
Intestine, normal	(+) at lateral border of epithelium	(+) in cytoplasm and apical surface of epithelium	(+) at lateral surface of epithelium
Intestinal adenoma	(++++) in cytoplasm and nuclei	(+) range from weak to unstained	Negative/positive
Pancreas	(+) at lateral cell membrane of pancreatic acinar cell	(+) in cytoplasm of ductal epithelium	(+) at lateral cell membrane of pancreatic cell
Pancreatic lesion	(++++) in cytoplasm and nuclei of pancreatic lesions	(+) in cytoplasm of ductal epithelium	Negative in pancreatic lesions
Uterus	(+) at lateral cell membrane of endothelium	(+) in cytoplasm of endothelium	(+) at lateral cell membrane of endothelium
Ovary	(+) in corpus luteum and epithelium of Fallopian tube	Epithelium of Fallopian tube	(+) in corpus luteum and epithelium of Fallopian tube
Testes	(+) at membrane of sertoli cell	(+) in nucleus of sertoli cell	Negative
Epididymis	(+) at lateral cell membrane of epithelium	(+) in cytoplasm and nuclei of epithelium	(+) at periphery of epithelium
Spleen	(+) membrane of endothelial lining cell	(+) cytoplasm of endothelial lining cells	(+) membrane of endothelial lining cells
Kidney	(+) in cytoplasm of renal cortex tubules	(+) in cytoplasm of proximal and distal renal tubules, podocyte	(+) in cytoplasm of proximal renal tubules
Liver	(+) in cytoplasm of hepatocytes (granular pattern), epithelium of bile duct	Negative	(+) endothelial lining
Lung	(+) at lateral border of	(+) in cytoplasm of	(+) at lateral border of

	bronchiolar epithelium	bronchiolar epithelium	bronchiolar epithelium

Table 2.5. Immunohistochemistry staining in *Apc* $^{Min+/-}$ mice (continued)

Organs	β-catenin	Apc	E-cadherin
Heart	(+) at intercalated disc of cardiac muscle	Negative	Negative
Brain	Positive	Positive	Negative
Retina	(+) in outer and inner plexiform layers	(+) in inner nuclear layers	Negative
Lymph node	(+) membrane of endothelial lining cell	(+) cytoplasm of endothelial lining cells	(+) membrane of endothelial lining cells
Mammary gland	(+) at base of glandular epithelium	(+) in cytoplasm of epithelium	(+) at lateral cell membrane of epithelium
Salivary gland	(+) at lateral, base of epithelium and in cytoplasm (granular pattern)	(+) in cytoplasm of epithelium	(+) at periphery of epithelium
Muscle	Negative	(+) in cytoplasm of muscle fibre	Negative
Bone	chondrocyte	chondrocyte	Negative
Skin	(+) at lateral cell membrane of stratified epithelium of epidermis	(+) in cytoplasm of epithelium	(+) in cytoplasm at lateral cell membrane of epithelium

Table 2.6. Immunohistochemistry staining in *Msh2* $^{-/-}$ mice

Organs	β-catenin	Apc	E-cadherin
Intestine, normal	(+) at lateral cell membrane of epithelium	(+) in cytoplasm and apical surface of epithelium	(+) at lateral cell membrane of epithelium
Intestinal adenoma	Negative in small lesions but (+++) in large lesions	Weak	Negative
Pancreas	(+) at lateral cell membrane of pancreatic acinar cell	(+) in cytoplasm of ductal epithelium	(+) at lateral cell membrane of pancreatic cell
Pancreas lesion	No lesion	No lesion	No lesion
Uterus	(+) at lateral cell membrane of epithelium	(+) in cytoplasm of epithelium	(+) at lateral cell membrane of epithelium
Ovary	(+) in corpus lutia and epithelium of Fallopian tube	Negative	Negative
Testes	(+) at membrane of sertoli cell	(+) in nucleus of sertoli cell	Negative
Epididymis	(+) at lateral cell membrane of epithelium	(+) in cytoplasm and nuclei of epithelium	(+) at periphery of epithelium
Spleen	(+) membrane of endothelial lining cells	(+) cytoplasm of endothelial lining cells	(+) membrane of endothelial lining cells
Kidney	(+) in cytoplasm of renal cortex tubules	(+) in cytoplasm of proximal and distal renal tubules, podocyte	(+) in cytoplasm of proximal renal tubules
Liver	(+) in cytoplasm of hepatocytes (granular pattern), epithelium of bile duct	Negative	(+) endothelial lining
Lung	(+) at lateral border of bronchiolar epithelium	(+) in cytoplasm of bronchiolar epithelium	(+) at lateral border of bronchiolar epithelium

Table 2.6. Immunohistochemistry staining in *Msh2* $^{-/-}$ mice (continued)

Organs	β-catenin	Apc	E-cadherin
Heart	(+) at intercalated disc	(+) in cytoplasm of muscle fibre	Negative
Brain	Positive	Positive	Negative
Retina	(+) in outer and inner plexiform layers	(+) in inner nuclear layers	Negative
Lymph node	(+) membrane of endothelial lining cells	(+) cytoplasm of endothelial lining cells	(+) membrane of endothelial lining cells
Mammary gland	(+) at base of glandular epithelium	(+) in cytoplasm of epithelium	(+) at lateral cell membrane of epithelium
Salivary gland	(+) at lateral, base of epithelium and in cytoplasm (granular pattern)	(+) in cytoplasm of epithelium	(+) at periphery of epithelium
Muscle	Negative	(+) in cytoplasm of muscle fibre	Negative
Bone	chondrocyte	chondrocyte	Negative
Skin	(+) at lateral cell membrane of stratified epithelium of epidermis	(+) in cytoplasm of stratified epithelium of epidermis	(+) in cytoplasm at lateral cell membrane of stratified epithelium of epidermis

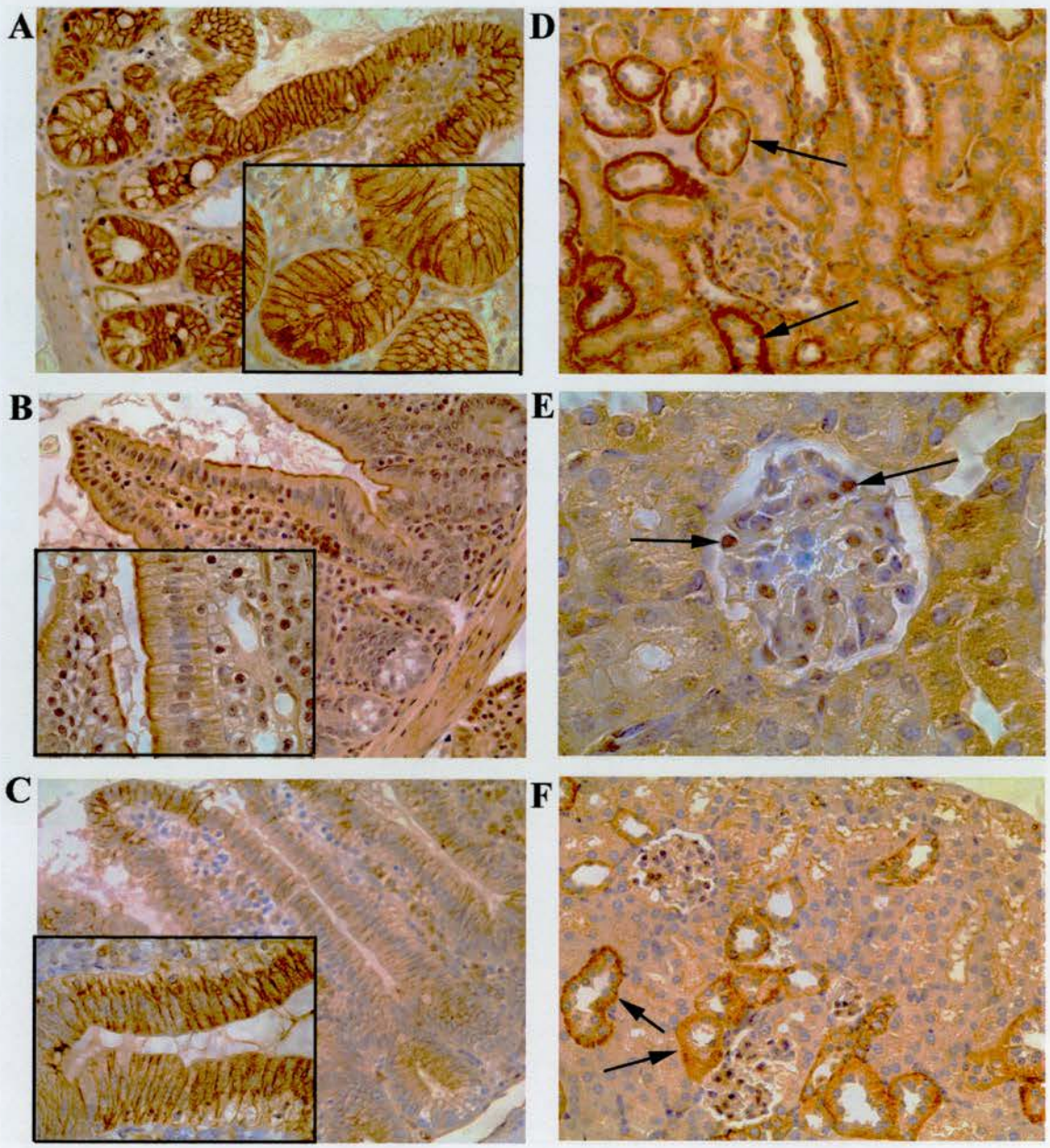

Figure 2.1 The pattern of β-catenin, Apc and E-cadherin staining in the normal intestine and kidney in *Apc*^{Min}, *p53* and *Msh2*$^{-/-}$ mice

A-C Photographs demonstrating the staining in normal intestine: (A) Photograph showing normal pattern of β-catenin in intestinal epithelium (magnification x400, inset x1000), (B) Photograph showing normal pattern of Apc staining (magnification x400, inset x1000) and (C) Photograph showing normal pattern of E-cadherin staining (magnification x400, inset x1000). D-F Photographs demonstrating the staining in the kidney: (D) and (F) Photographs showing normal pattern of β-catenin and E-cadherin staining in proximal renal tubules (arrows) (magnification x400), (E) Photograph showing pattern of Apc staining in podocytes (x1000).

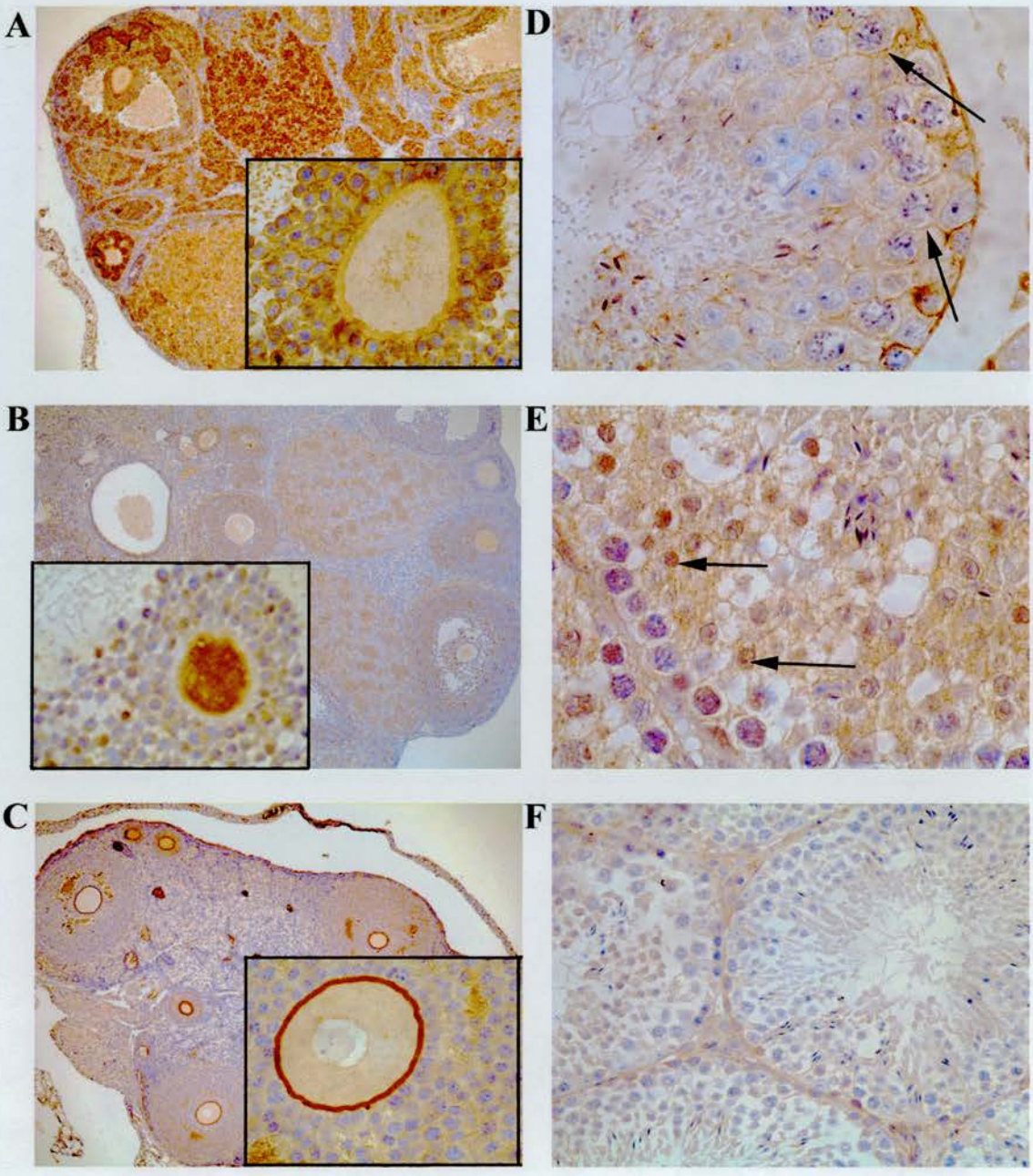

Figure 2.2 The pattern of β-catenin, Apc and E-cadherin staining in the ovary and testes in *Apc^{Min}*, *p53* and *Msh2$^{-/-}$* mice

A-C Photographs demonstrating the staining in ovary: (A) Photograph showing β-catenin expression in Graaffian follicle (inset mag. x1000), (B) Photograph showing Apc negativity in ovarian follicle (inset mag. x1000), and (C) Photograph showing E-cadherin positive staining in zona pellucida (inset x1000). D-F Photographs demonstrating the staining in the testes: (D) Photograph showing β-catenin positive staining at cellular membrane of sertoli cells (arrows, mag. x1000), (E) Photograph showing Apc positivity in the nuclei of sertoli cells (arrows, mag. x1000) and (F) Photograph showing E-cadherin negative staining.

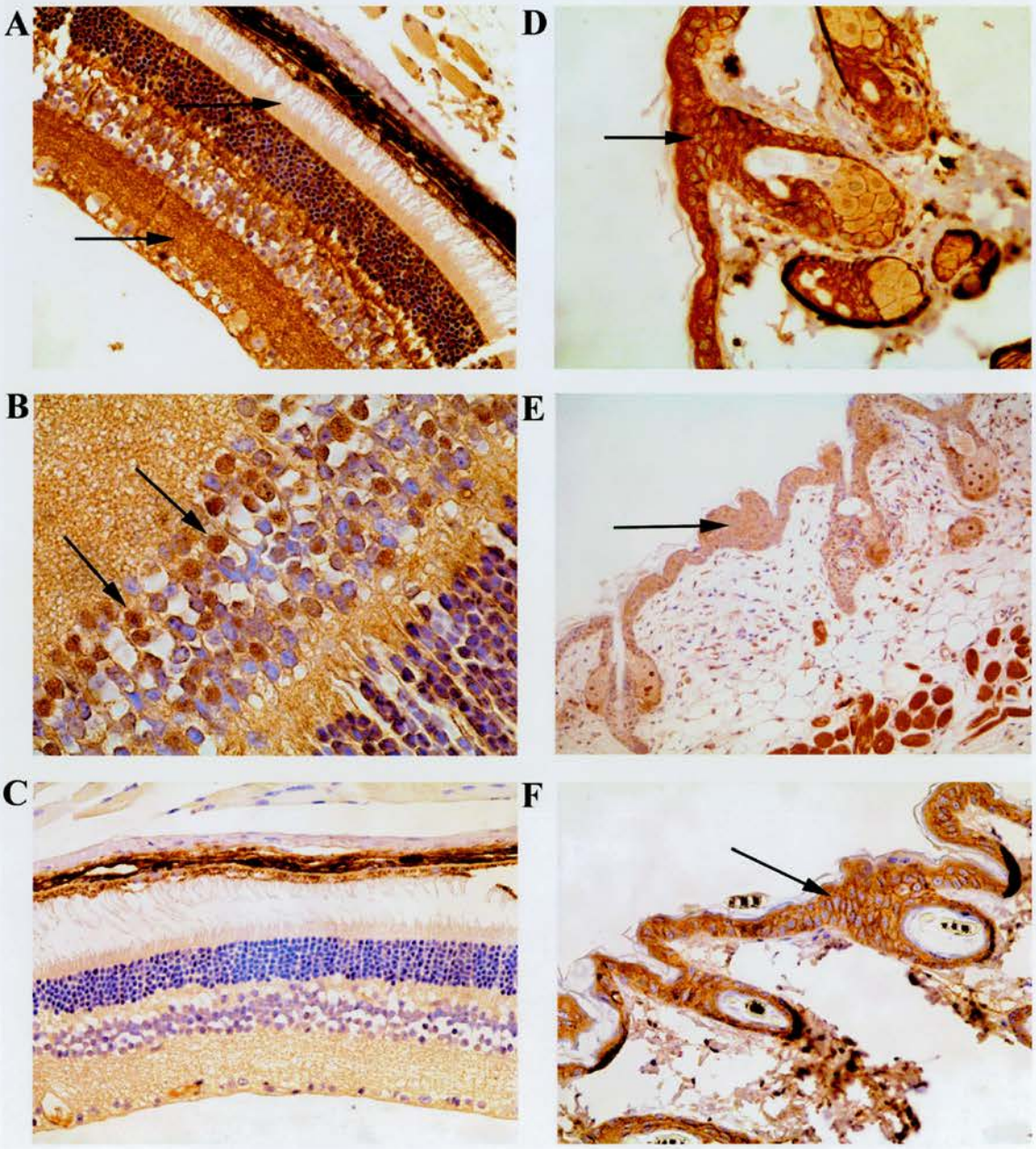

Figure 2.3 Photographs showing the pattern of immunohistochemistry of β-catenin, Apc and E-cadherin in retina and skin

A-C Photographs showing pattern of staining in retina: (A) β-catenin positive staining in plexiform layers (arrows, mag. x400), (B) Apc positive staining in outer nuclear layer (arrows, mag. x 1000) and (C) E-cadherin failed to show positivity in the retina. D-F Photographs showing positive staining of β-catenin (D), Apc (E) and E-cadherin (F) in the epidermis (arrows, mag. x400).

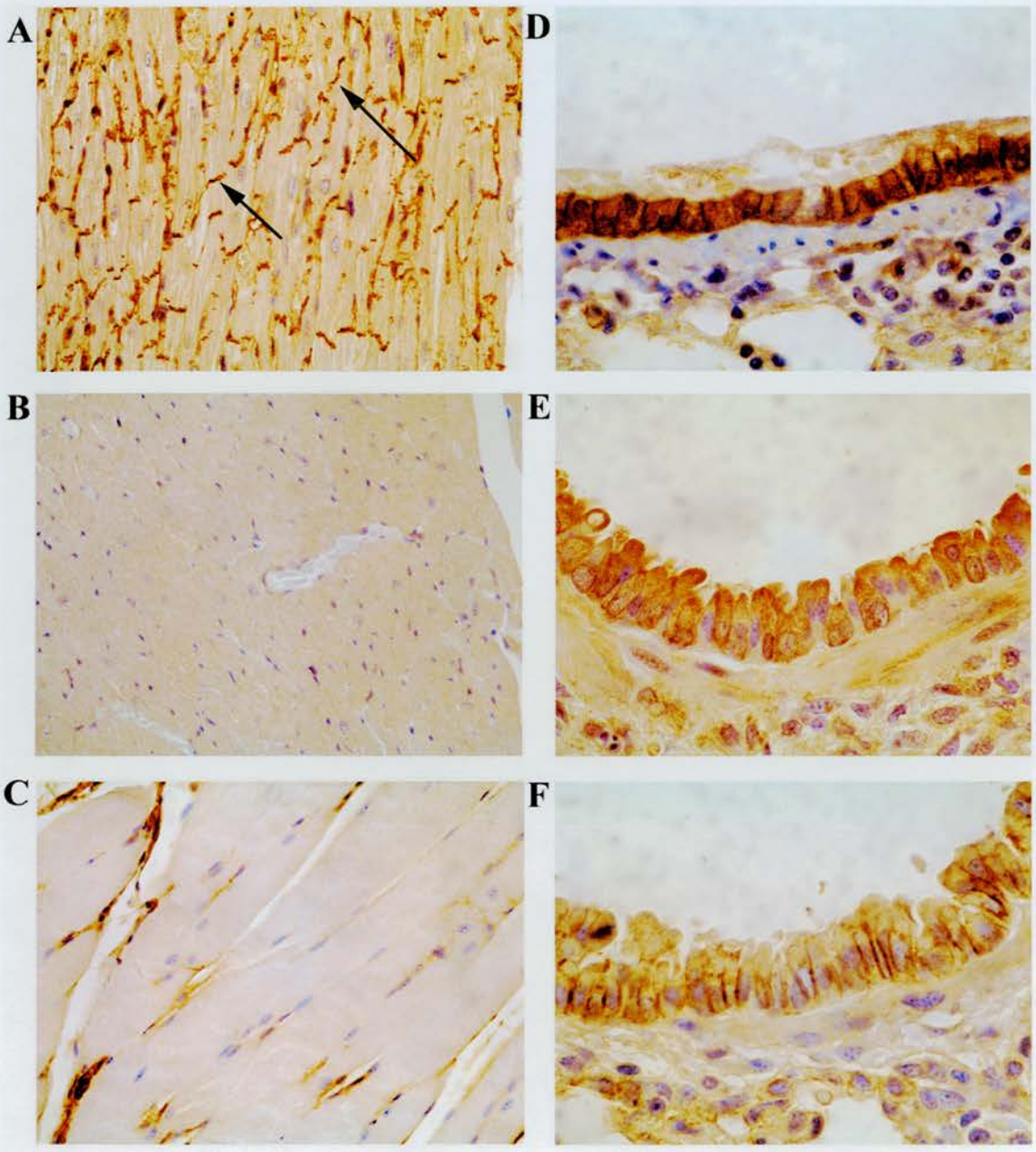

Figure 2.4 The pattern of β-catenin, Apc and E-cadherin staining in the heart and lung in *Apc*^{Min}, *p53* and *Msh2*$^{-/-}$ mice

A-C Photographs demonstrating the staining in the heart: (A) Photograph showing β-catenin expression at intercalated disc in cardiac muscle (arrows, mag. x400). (B) and (C) Photographs showing negative staining of Apc and E-cadherin (mag. x400). D-F Photographs demonstrating the staining in the lung: (D) and (F) Photographs showing β-catenin and E-cadherin positivity at lateral cell membrane of columnar epithelium(mag. x1000). (E) Photograph showing Apc staining in cytoplasm of columnar epithelium (mag. x1000).

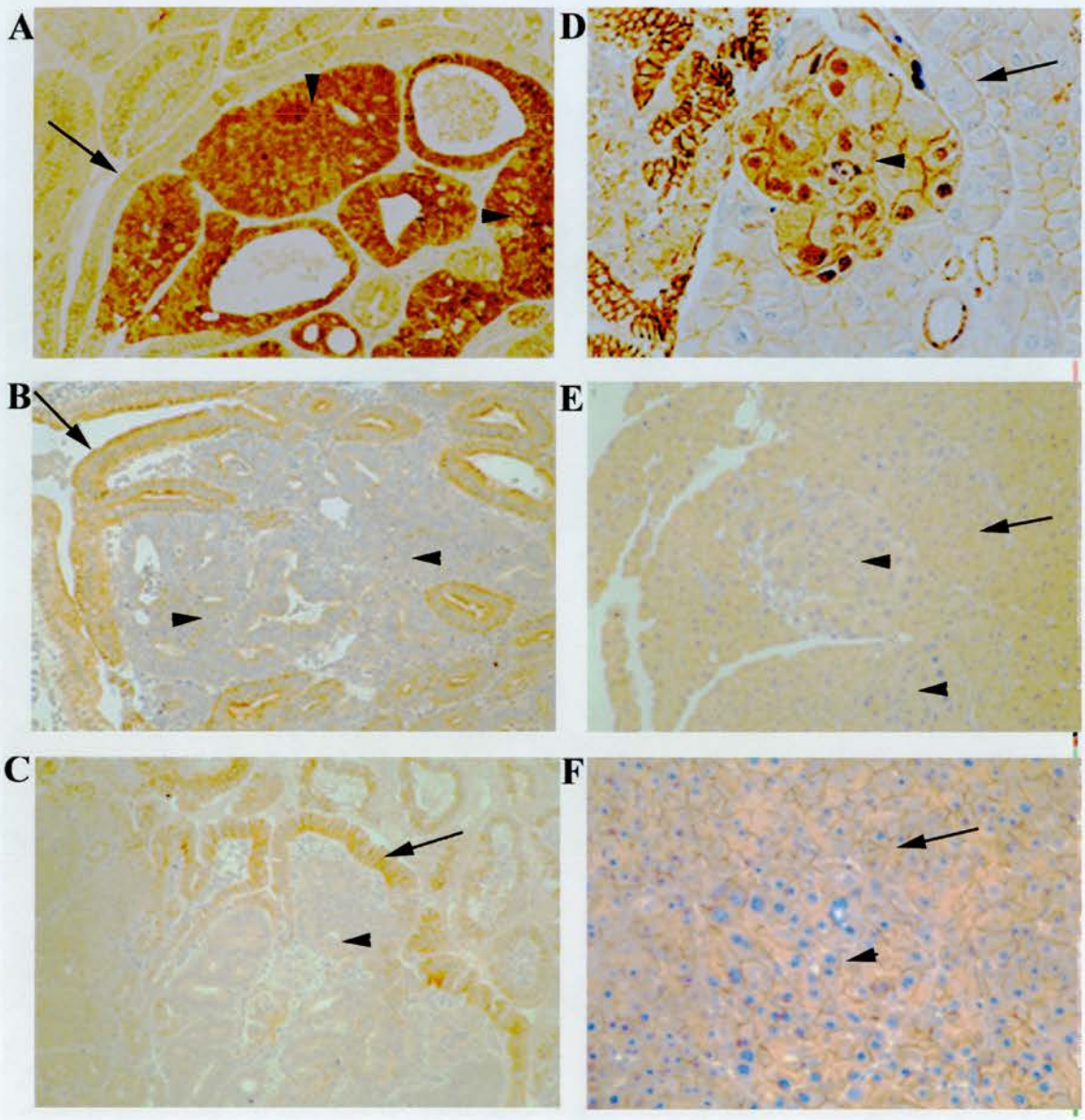

Figure 2.5 The pattern of β-catenin, Apc and E-cadherin immunohistochemical staining in intestinal and pancreatic lesions arising in *Apc*$^{+/-}$ and *Apc*$^{+/-}$/*p53*$^{-/-}$ mice

Photographs A-C showing intestinal lesions, photographs D-F showing pancreatic lesions at magnification x400. (A) Photograph showing overexpression of β-catenin in intestinal lesion (arrow head) normal pattern in epithelium covering lesion (arrow) (B) Photograph showing Apc negative staining in intestinal lesions (arrow head) and normal pattern of staining in the epithelium (arrow) (C) Photograph showing normal E-cadherin staining in epithelial (arrow) and no staining in the intestinal lesions (arrow head). Both B and C showed some area of positive staining of Apc and E-cadherin respectively. (D) Photograph showing β-catenin overexpression in pancreatic lesion (arrow head) compared with normal pancreatic acinar cells (arrow) (E) Photograph showing absence of Apc staining in pancreatic lesion (arrow head) compared with normal pancreatic acinar cells (arrow) (E) Photograph showing normal E-cadherin staining at pancreatic cell membrane in normal (arrow) and pancreatic lesion (arrow head).

2.3. Discussion

The data showed that the distribution of Apc is widespread, including epithelial, mesenchymal and central nervous system tissues. It shows cytoplasmic, membrane-related and nuclear patterns, which is similar to the pattern of staining in normal human tissues (Midgley *et al* 1997). Of interest, strong positive Apc nuclear staining was noted in the inner nuclear layer of retina and sertoli cell, which are present in the seminiferous tubules and functions in releasing an androgen-binding protein. These results were supported by Neufeld and White (1997) who demonstrated nuclear localisation of Apc in non-migrating cells whereas cytoplasmic localisation of Apc was found in migrating cells (Neufeld and White 1997). In *Apc* $^{Min+/-}$ mice, mutation of a wild type *Apc* allele to produce the Min allele does not affect the expression pattern of Apc protein.

The pattern of β-catenin and E-cadherin expression in normal tissues in *Apc* $^{Min+/-}$, (*Apc* $^{Min+/-}$ */p53* $^{-/-}$) and (*Apc* $^{Min+/-}$ */Msh2* $^{-/-}$) mice showed frequent co-localisation in epithelial cells at the zonula adherens junction. E-cadherin staining was found positive in epithelial cell types except in the epididymis. In non-epithelial cell types including cardiac muscle, skeletal muscle, chondrocyte, neuron and inner nuclear layer of the retina E-cadherin staining was negative. This is due to in the neuron, chondrocyte, skeletal muscle and cardiac muscle consisting of N-cadherin (Takeichi 1987), OB-cadherin (Okazaki *et al* 1994), M-cadherin (Donalies *et al* 1991) and H-cadherin (Lee 1996). These family members do not cross react with the antibody against E-cadherin used in this study.

β-Catenin expression was found positive in all epithelial cell types and in non-epithelial cell type including nervous tissue, cardiac muscle, connective tissue such as chondrocyte whereas β-catenin was negative in skeletal muscle. Intense staining of -- β-catenin was observed at the intercalated disc in the cardiac muscle in which -- E-cadherin was found negative. The intercalated disc represents the boundaries between individual cardiac muscle cells. It covers the ends of adjacent contiguous cardiac muscle cells at the level of the Z line. This specialised attachment is called a fascia adherens, which is similar to the zonula adherens of an epithelial cell (Kessel 1998). In the fascia

adherens of cardiac muscle cells a different member of the cadherin family is present other than E-cadherin as mentioned above. There is no fascia adherens in the structure of the smooth and skeletal muscle cells. In the kidney, β-catenin expression was demonstrated in cytoplasm and at basolateral cell membrane in renal tubule, in particular in proximal and distal renal tubule, which showed colocalisation with E-cadherin. Normally, E-cadherin expression is restricted to the distal renal tubule and collecting duct in human (Vestweber *et al* 1985). There is evidence of the expression of -- cadherin-6, which is a fetal kidney cadherin, expressed in 32 primary renal cell cancer and in the proximal renal tubule epithelium in human normal kidney (Paul *et al* 1997). In addition, they also found cadherin-6 coprecipitated with β-catenin antibody in primary renal cell cancer, which indicated the tendency of these types of renal tubules to give rise to the majority of neoplasm of this organ. In my study E-cadherin was found colocalised with β-catenin in proximal and distal tubules in mouse which is due to species difference as previously observed (Piepenhagen and Nelson 1995). Nuclear positive of β-catenin was found occasionally in renal proximal tubule could be the resulting of proliferation in these epithelial cells.

In the normal mouse intestinal epithelium, Apc protein expression at the apical surface of epithelium does not colocalise with β-catenin or E-cadherin but they show colocalisation at the lateral cellular membrane of epithelial cell type. Miyashiro *et al* (1995) reported the pattern of APC and α-catenin (a member of catenin family) immunostaining in human osteosarcoma cell line using both microscopic and electron microscopic studies. In this study they showed colocalisation of APC and α-catenin at the lateral cell membrane. These studies support the concept that APC or Apc function in regulation of cell adhesion with catenins and cadherins in the epithelium whereas the APC or Apc in the microvilli in the apical surface has other functions independent of catenins or cadherins.

The pattern of Apc, β-catenin and E-cadherin protein staining in normal tissues in different genotype background of animal was not different, at least at the level of immunohistochemistry. Interestingly, the expression of Apc and E-cadherin in the

intestinal and pancreatic lesions showed absence of positivity to weak staining whereas β-catenin was found very intense in the lesions arising in mutant animals. This observation suggests a relationship between Apc, E-cadherin and β-catenin in the Wnt signalling pathway in carcinogenesis which needs to be further investigated in detail.

Chapter 3

β-Catenin dysregulation in murine intestinal and pancreatic lesions

In the previous chapter, the expression of Apc and related molecules was described in the normal tissues of wild type mice and genetic variants with germline deficiency of *Apc*, *p53* and *Msh2*. These mice are susceptible to neoplasia in various organs, however, the opportunity to analyse and to examine the expression of these molecules and -- β-catenin in particular, in such neoplasms, from their earliest origin through to more advanced lesions. *Apc* $^{Min+/-}$ mice develop large and small intestinal adenomas, a small proportion of which become malignant (Moser *et al* 1992, 1993). *p53* deficient mice develop predominantly lymphomas and sarcomas (Clarke *et al* 1993). In -- (*Apc* $^{Min+/-}$*/p53* $^{-/-}$) mice, cooperativity between these mutations has been demonstrated, dysplasia and preneoplastic foci were seen in 61% of these animals and pancreatic acinar cell adenocarcinoma in 22% and also were characterised by sarcoma and lymphoma, both thymic and extra-thymic. (*Apc* $^{Min+/-}$*/Msh2* $^{-/-}$) mice are characterised by accelerated intestinal tumorigenesis as well as reduced survival of the mice (Reitmair *et al* 1996). It is of interest to focus on β-catenin expression in particular because of its functional relationship to Apc. Therefore, I decided to focus on intestinal epithelial cells and pancreatic acinar cells, which show dysregulation of β-catenin.

In light of the known development of intestinal adenomas in animals mutant for *Msh2* but wild type *Apc*, and the dependence of pancreatic adenoma predisposition in *p53* null on *Apc* ^{Min} background, it was of particular interest to study early events in tumour development in the intestine and pancreas in these animals.

3.1. Materials and Methods

3.1.1. Mice

Mice mutant for *Msh2* (de Wind *et al* 1998), *p53* (Clarke *et al* 1993) and *Apc* ^{Min} (Moser *et al* 1992) were maintained as out-bred colonies segregating for Ola/129, Balb C, SWR and C57Bl/6 genomes. Mice were monitored on a daily basis for signs of ill health and were killed when they clearly showed signs of neoplastic disease.

3.1.2. Immunohistochemistry

Swiss rolls of the intestines were made as previously described (see 2.1.2). All tissues were processed and paraffin-embedded (see 2.1.2). Three-micron sections were subjected to high temperature antigen retrieval as required for β-catenin immunostaining, followed by blocking in 1.5% H_2O_2 solution and non-specific binding by incubation in 20% normal rabbit serum. Sections were then incubated with a 1:50 dilution of mouse monoclonal antibody raised against β-catenin (IgG_1, clone 14, Transduction Laboratories, UK) and subsequently with 1:400 dilution of rabbit anti-mouse biotinylated secondary antibody (Dako, Denmark). The ABComplex/HRP (Dako, Denmark) was used as the detection system and the labelled complex was developed with diaminobenzidine 0.5 mg/ml (see appendix B). Details of the immunohistochemistry protocol are in appendix A.

3.1.3. Histological Microdissection

This was performed as previously described (Going and Lamb 1996). Paraffin-embedded tissues were cut at 7 microns, collected on clean plain glass slides and dried in a 37 ^{0}C oven, overnight. They were subsequently dewaxed in xylene for 10 minutes and re-hydrated in graded alcohol and distilled water. The sections were then stained in 0.05% aqueous toluidine blue (see appendix B) for 20 seconds, washed and stored in distilled water until dissection. Excess water was blotted from the slide, which was then placed on the stage of a stereo microscope. Proteinase K buffer solution (see appendix B) was dropped onto the section. Dissection was performed with an electrolytically

sharpened 25 mm length tungsten wire needle using a Leica mechanical micromanipulator. Detail of the protocol for microdissection is in appendix A.

3.1.4. PCR analysis of *Apc* locus

Samples from the microdissection were digested overnight in buffer containing proteinase K 1mg/ml and 1% Tween 20 (see appendix B). The proteinase K was subsequently heat-inactivated at 95 ^{0}C, for 10 minutes in a PCR thermal cycler. PCR amplification of *Apc* (*Min* PCR) was then performed as previously described (Luongo *et al* 1994) using the primers

5' TCTCGTTCTGAGAAAGACAGAAGCT 3' and

5' TGATACTTCTTCCAAAGCTTTGGCTAT 3'

Each 50 µl reaction contained; 0.05 µM of *Apc* PCR primers (Oswel, UK), 0.2 mM of each dNTP, 5% DMSO, 10 mM Tris/HCl, 25 mM KCl, 50 mM $MgCl_2$, 2.5 units *Taq* DNA Polymerase (PCR reagents were supplied by GIBCO/BRL), and 2 µl of DNA template. Samples were amplified under the following conditions: 1 cycle at 94 ^{0}C for 2 minutes followed by 30 cycles at 94 ^{0}C for 1 minute, 60 ^{0}C for 1 minute, and 72 ^{0}C for 1 minute followed by 1 cycle at 72 ^{0}C for 10 minutes. One microliter of each PCR reaction was then subjected to a second round of amplification using the nested primers

5' AGTAAGCAGAGACACAAGCA 3' and

5' CGGTGGTAGAAGCAGAACTT 3'

Each 50 µl reaction used 0.05 µM of nested primers, 65 mM $MgCl_2$ and the same concentration of other PCR reagents and subjected under the same parameters as in *Min* PCR. Sixteen microlitres of each final PCR product was cleaved with the *Hind*III restriction enzyme (GIBCO/BRL); puc19 was included as a cleavage control. The PCR products were analysed on 4% agarose gel stained with ethidium bromide 10 mg/ml (see appendix B) viewed under UV light and photographed.

3.2. Results

3.2.1. Expression of β-catenin in intestinal lesions

(A) *Apc* ^{Min} and *p53/ Apc* ^{Min} mutants

The pattern of β-catenin staining in intestinal lesions developing within *Apc* heterozygotes was investigated. To control for staining variability between sections, changes in the intensity of expression were always scored relative to normal epithelium within the same section. The lesions were subclassified as: (I) single dysplastic crypts, showing nuclear pleomorphism and stratification; (II) complex lesions, comprising several architecturally distorted crypts in the lamina propia with virtually normal overlying surface epithelium; (III) small adenomas, identified by the overall disturbance of architecture including the surface and distinguished from the previous category on the basis of increased size and surface involvement; and (IV) large adenomas (Figure 3.1).

There was a striking difference in β-catenin staining intensity and distribution in dysplastic crypts and small adenomas as compared with morphologically normal epithelium. Whereas membrane staining was observed in the lower crypt epithelium of normal mucosa, and nuclear staining was almost completely restricted to cells at the crypt base, the dysplastic crypts, complex lesions and small adenomas showed intense staining. This staining extended throughout the cytosol and included the nucleus in a high proportion of cells. In some cells strong nuclear staining without concomitant cytoplasmic staining was observed. These patterns of β-catenin staining in the dysplastic crypts and small adenomas of both *Apc* ^{Min} and (*Apc* ^{Min}/*p53* $^{-/-}$) mice were more intense. The pattern of β-catenin staining is summarised in Table 3.1 and Figure 3.3, it was essentially identical in *Apc* ^{Min} and (*Apc* ^{Min}/*p53* $^{-/-}$) mice, with all features described below noted in both groups.

A substantial proportion of all lesion types showed heterogeneous staining of -- β-catenin even where only single crypts were involved (type I lesions, Figure 3.2B, 3.2E, Figure 3.3). The term 'heterogeneous or mosaic' was used to describe lesions in which only a proportion of cells was characterised by increased intensity of β-catenin staining. Thus, although the predominant pattern was as described, some cells retained

the membrane restricted pattern characterised of normal cells. However, no lesions were observed in which the cytosol and nuclear pattern were absent from all the cells. The proportion of cells overexpressing β-catenin was highest in type I, II and type III lesions. Mosaic type IV lesions showed the lowest proportion of cells staining positive for -- β-catenin (Figure 3.2F). Large areas of weak staining were observed in some late stage lesions, including those categorised both as type IV (large adenomas) lesions (Figure 3.2G). Lesions in *Apc* ^{Min} and (*Apc* ^{Min}/*p53* $^{-/-}$) mice are identical as described in table 3.1.

In all categories of lesion, the predominant pattern of increased β-catenin staining was within the nucleus and in cytoplasm. Any specific increase in the localisation of β-catenin to the cell membrane was not observed. However a pattern of strong nuclear localisation without concomitant cytoplasmic staining was also observed within some lesions. This pattern of staining was observed following fixation by both methacarn and neutral buffered formalin.

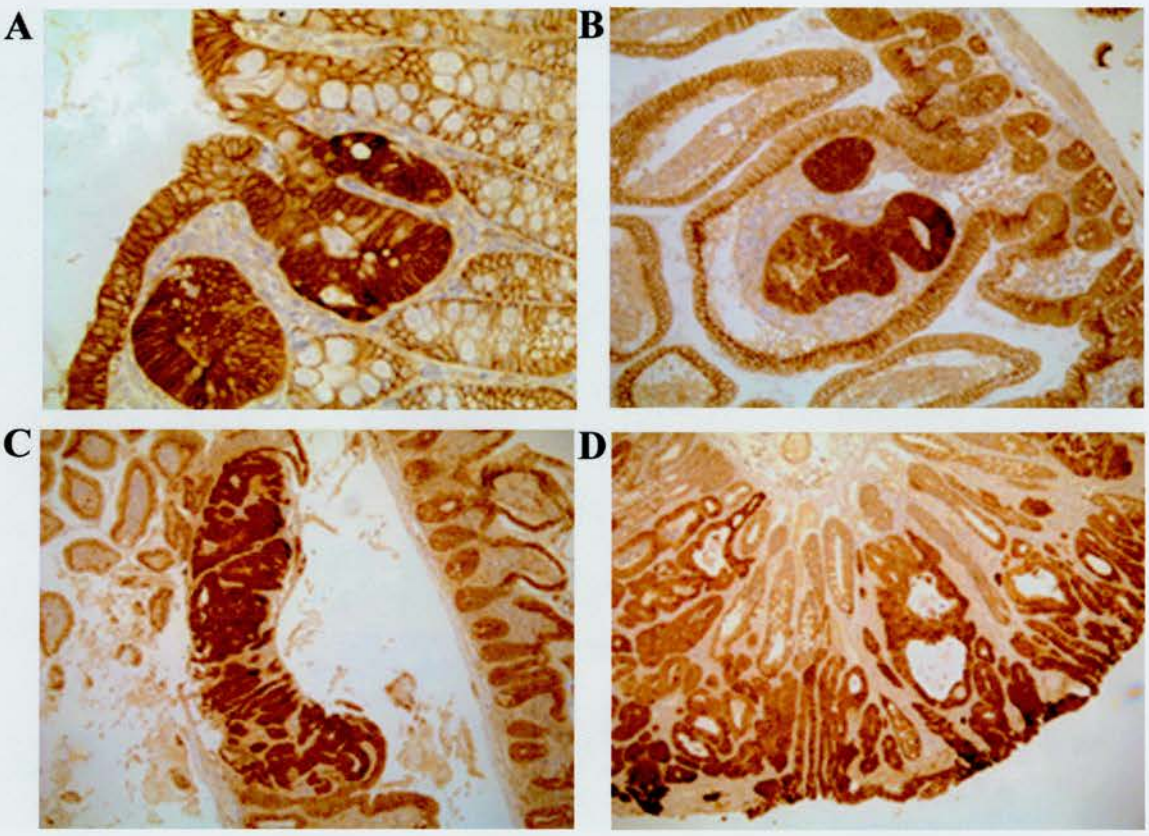

Figure 3.1 Photographs showing classification of the intestinal lesions

The intestinal lesions are classified as (A) a single dysplastic crypt (mag. X400), (B) a complex lesion (mag. X400), (C) a small adenoma (mag. X200) and (D) a large adenoma (mag. X200) as described in the text.

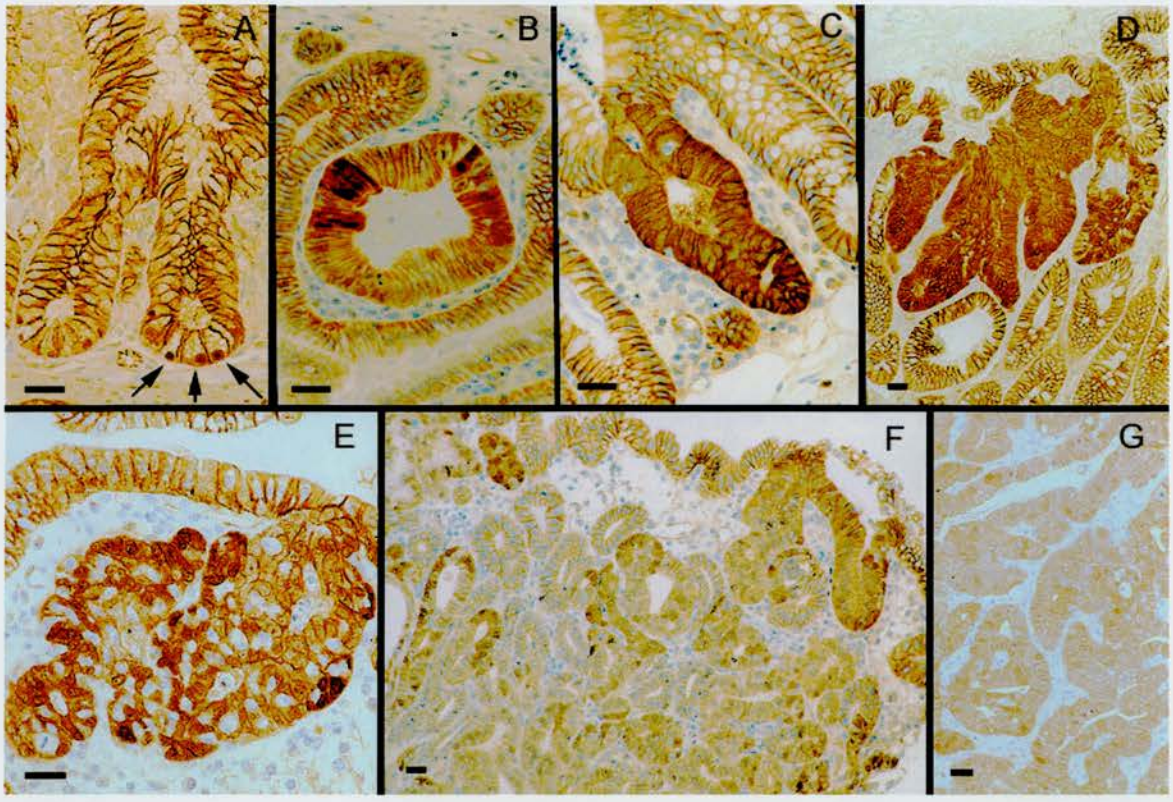

Figure 3.2 The pattern of β-catenin staining in the intestine of $Apc^{Min+/-}$ and $Apc^{Min+/-}/p53^{-/-}$ animals

(A-G) Photographs demonstrating the various features observed in animals with these genotypes. All the features illustrated here were observed irrespective of *p53* status. All scale bars represent 10 uM A) β-catenin staining in morphologically normal crypts of the small intestine. β-catenin was detected throughout the cytoplasm of epithelial cells but was strongly localised to the lateral borders. Strong nuclear localisation was observed in cells at the crypt base (arrows) B) Heterogeneous expression in a type I lesion. The majority of cells show the normal pattern of staining, with localisation to the lateral borders. A subset of cells show increased cytoplasmic and nuclear staining. C) Uniformly increased β-catenin staining within a type 1 lesion. D) Increased β-catenin staining in a type II lesion. E) Heterogeneous expression in a type II lesion. Cells showing increased β-catenin showed cytoplasmic localised and in some instances nuclear localisation. F) Heterogeneous expression of β-catenin within a type III lesion. G) Reduced expression within a type IV lesion. Where expression of β-catenin was retained this was often localised to the nucleus.

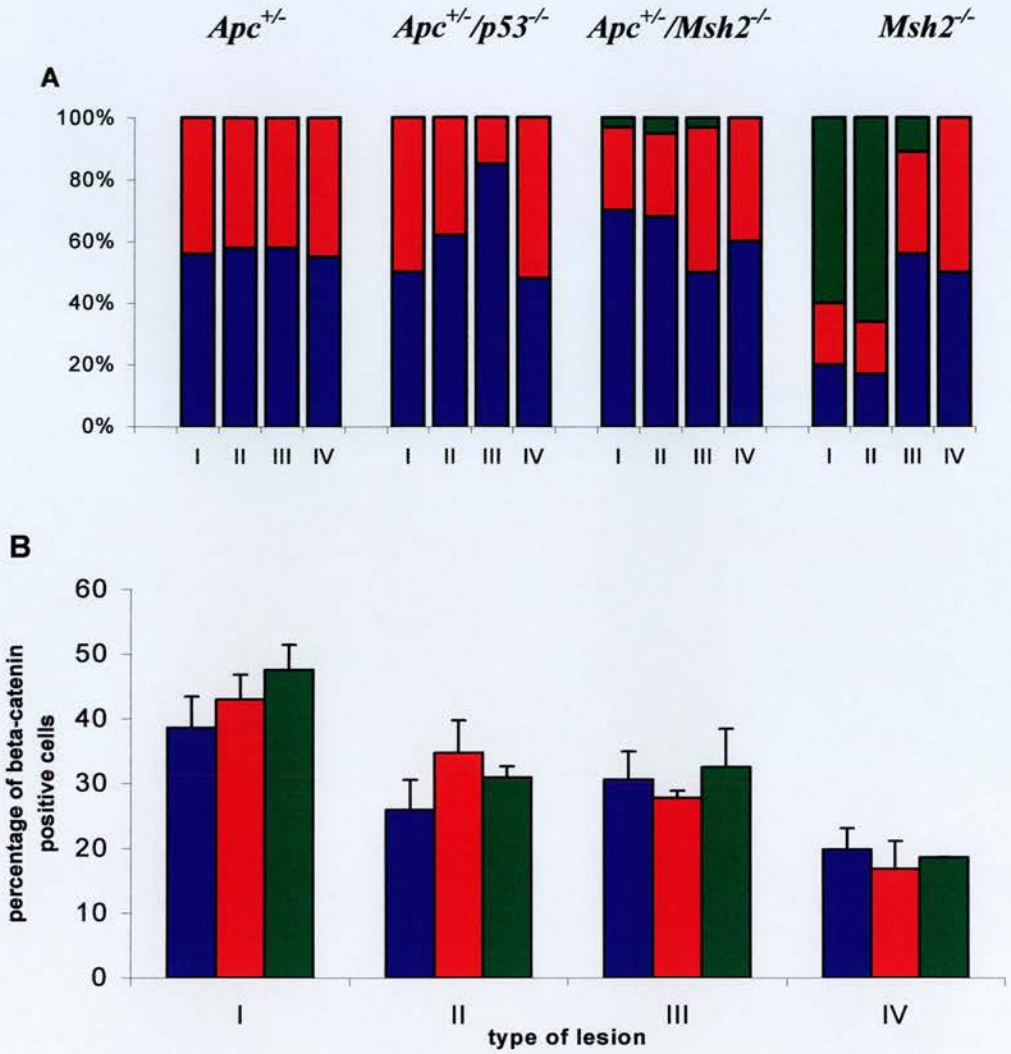

Figure 3.3 β-catenin expression patterns within each class of intestinal lesion.
A) Percentage of each lesion type showing either upregulation of β-catenin in all cells (blue bars); a mosaic or heterogeneous pattern of upregulation as defined in the text (red bars); or no upregulation (green bars). B) Histogram showing the percentage of cells expressing high levels of β-catenin within lesions characterised by mosaic expression of β-Catenin. Blue bars, $Apc^{Min+/-}$; Red bars, $Apc^{Min+/-}$/ $p5^{-/-}$; Green bars, $Apc^{Min+/-}/Msh2^{-/-}$. Mean values are given for each lesion category, as defined in the text. Error bars represent SEM. Insufficient numbers of mosaic lesions were identified in $Msh2^{-/-}$ mice to permit analysis.

Table 3.1 β-catenin expression patterns within intestinal lesions

	Lesion Type											
	I			**II**			**III**			**IV**		
	(+)	**M**	**(-)**	**(+)**	**M**	**(-)**	**(+)**	**M**	**(-)**	**(+)**	**M**	**(-)**
$Apc^{Min+/-}$	56	44	0	58	42	0	58	42	0	55	45	0
	N=41			**N=96**			**N=36**			**N=20**		
$Apc^{Min+/-}/p53^{-/-}$	50	50	0	62	38	0	85	15	0	48	52	0
	N=52			**N=63**			**N=20**			**N=27**		
$Msh2^{-/-}$	39	0	61	40	0	60	86	0	14	100	0	0
	N=13			**N=5**			**N=7**			**N=2**		
$Apc^{Min+/-}/Msh2^{-/-}$	36	55	9	67	28	5	27	73	0	0	100	0
	N=57			**N=114**			**N=11**			**N=6**		

Percentage of each lesion type showing either 100% upregulation of β-catenin **[(+)]**; or no upregulation **[(-)]**; a mosaic or heterogeneous pattern of upregulation as defined in the text **(M). N** indicates the number of lesions scored.

(B) *Msh2* $^{-/-}$ and (*Apc* $^{Min+/-}$/*Msh2* $^{-/-}$) mice

The same spectrum of morphological changes, from type I to type IV was observed in *Msh2* $^{-/-}$ and (*Apc* $^{Min+/-}$/*Msh2* $^{-/-}$) animals, although fewer of type IV lesions were found in the mice with *Msh2* $^{-/-}$ background. However, the pattern of β-catenin staining in lesions differed from those in animals, which were *Apc* ^{Min} or (*Apc* $^{Min+/-}$/*p53* $^{-/-}$) mice. Significantly in *Msh2* $^{-/-}$ animals, type I, II and III lesions were identified which showed normal β-catenin staining in all the cells (Figure 3.4B), a pattern which was never observed in *Apc* ^{Min} or (*Apc* $^{Min+/-}$/*p53* $^{-/-}$) mice (Figure 3.4A). All type IV adenomas however were characterised by increased intensity of β-catenin staining.

In (*Apc* $^{Min+/-}$/*Msh2* $^{-/-}$) mice, the majority of these lesions stained strongly for -- β-catenin (Figure 3.4C) but again a small number of type I and II lesions (5%) with the normal pattern of β-catenin expression were identified (Figure 3.4D). All type IV lesions arising in either *Msh2* $^{-/-}$ or (*Apc* $^{Min+/-}$/*Msh2* $^{-/-}$) mice analysed showed increased intensity of β-catenin staining with an almost identical pattern to that observed in -- *Apc* $^{Min+/-}$ mice.

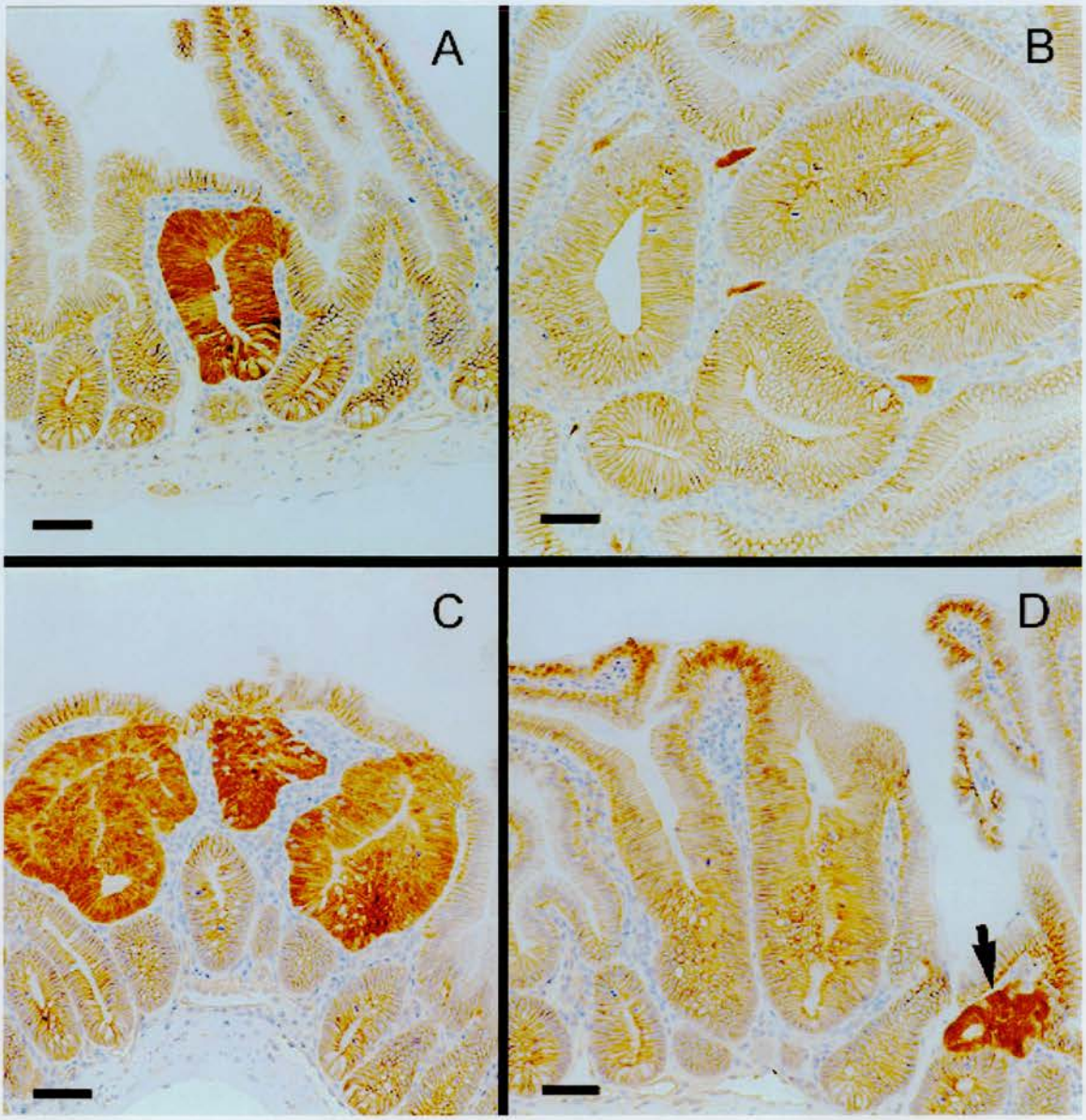

Figure 3.4 The pattern of β-catenin expression in the intestine of *Msh2* $^{-/-}$ mice (A-B) and (*Msh2* $^{-/-}$, *Apc*$^{Min+/-}$) mice (C-D)

(A) Increased β-catenin staining in a type I lesion. (B) Normal pattern of β-catenin expression in a type II lesion, with β-catenin strongly localised to the lateral borders. (C) Increased β-catenin expression in a type II lesion. (D) Normal β-catenin expression in a type II lesion, with retained localisation to the lateral borders. A type I lesion showing β-catenin dysregulation is indicated for comparison (arrow). All scale bars represent 10μm.

3.2.2. Expression pattern of β-catenin within the pancreas

(A) *Apc* $^{Min+/-}$ and (*Apc* $^{Min+/-}$/*p53* $^{-/-}$) mice

Eighty three percent of mice mutant for both *p53* and *Apc* developed pancreatic tumours in this series. The tumours were adenomas or adenocarcinomas, predominantly of acinar cell type, although foci of ductal differentiation were also observed. The pattern of β-catenin staining was abnormal both within these lesions and also in areas that appeared more normal morphologically. Within morphologically normal pancreatic cells, β-catenin was usually observed at the cell membrane, without obvious nuclear localisation. In (*Apc* $^{Min+/-}$/*p53* $^{-/-}$) mice, all foci showing histological abnormality, both adenoma and adenocarcinoma were characterised by high intensity of β-catenin staining (Figure 3.5). In formalin fixed tissues (Figure 3.5C), the β-catenin distribution in these lesions was membrane-associated, cytosolic and nuclear, as in the intestinal tumours of these animals. However, following methacarn fixation, nuclear staining remained prominent in the adenomas and adenocarcinomas, cytosolic staining was often absent. In general, methacarn-fixed material showed less intense β-catenin staining at the cell membrane of morphologically normal cells, making the contrast with the β-catenin overexpression cells of the lesions more easily appreciated. The cell type observed in these lesions was predominantly acinar, although some foci showed ductal differentiation (Figure 3.5F, 3.5H).

The most remarkable feature in the pancreas of the *Apc* $^{Min+/-}$ animals, however, was the presence of intense β-catenin staining in cell clusters that did not show the morphological features of adenoma or carcinoma. The size of these clusters varied from single cells (Figure 3.5A), through small aggregates of 2-10 cells (Figure 3.5B), to large foci (Figure 3.5E). The presence of these β-catenin overexpression cell clusters gave the pancreas a vivid patchwork appearance that had not been evident from inspection of the haematoxylin and eosin stained sections. On closer examination and careful comparison of adjacent sections stained by haematoxylin and eosin, and β-catenin immunohistochemistry, it became clear that many of the clusters contained dysplastic cells with enlarged, irregular nuclei. Such cells were never seen outside of β-catenin

staining regions. It was also true, however, that a high proportion of β-catenin staining cells in these preneoplastic foci showed no morphologically detectable change.

In view of these changes in preneoplastic foci in (*Apc* $^{Min+/-}$/*p53* $^{-/-}$) mice, the pancreas of *Apc* $^{Min+/-}$ mice with wild type *p53* was studied with particular interest. Unlike the (*Apc* $^{Min+/-}$/*p53* $^{-/-}$) mice, these animals do not develop pancreatic neoplasia (Clarke *et al* 1995). β-Catenin dysregulated foci were also seen in the pancreas of these mice, in approximately the same numbers as in the mice with abnormal *p53*, although it was technically difficult to develop this observation into a more quantitative score. The dysregulated cells showed the same nuclear localisation of β-catenin as described above. While many had apparently normal morphology, others showed dysplastic features.

In contrast, β-catenin dysregulated cells were never observed in normal animals (wild type for *Apc*) or in *p53* null mice on a wild type *Apc* background.

(B) *Msh2* $^{-/-}$ and (*Apc* $^{Min+/-}$/*Msh2* $^{-/-}$) mice

The pancreatic tissue derived from *Msh2* $^{-/-}$ mice and (*Apc* $^{Min+/-}$/*Msh2* $^{-/-}$) mice were analysed. No abnormal expression of β-catenin or histological atypia was observed in *Msh2* $^{-/-}$ mice. However, in (*Apc* $^{Min+/-}$/*Msh2* $^{-/-}$) mice again are identified foci of -- β-catenin dysregulation, these did not differ in morphological appearance from those seen in *Apc* $^{Min+/-}$ animals. (*Apc* $^{Min+/-}$/*Msh2* $^{-/-}$) mice developed spontaneous pancreatic neoplasms, whereas *Msh2* $^{-/-}$ mice on a wild type *Apc* background did not.

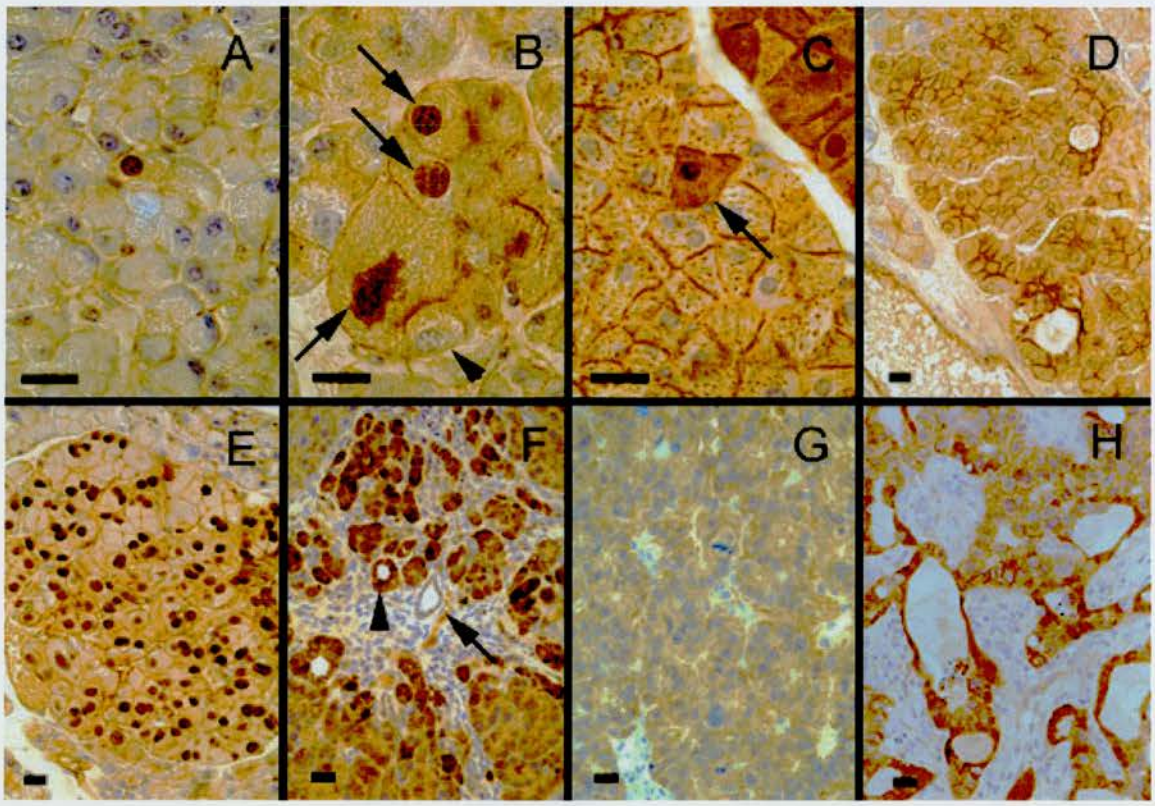

Figure 3.5 The pattern of β-catenin staining in the pancreas of *Apc*$^{Min+/-}$ and *Apc*$^{Min+/-}$/*p53*$^{-/-}$ mice

(A-E) are representative of the patterns of β-catenin staining and histological atypia observed in the pancreas of both *Apc*$^{Min+/-}$mice and *Apc*$^{Min+/-}$/*p53*$^{-/-}$ mice. (F-H) are representative of these patterns in pancreatic adenomas and adenocarcinomas arising in *Apc*$^{Min+/-}$/*p53*$^{-/-}$ mice. All scale bars represent 10uM A) A single pancreatic acinar cell characterised by increased nuclear and cytoplasmic expression. The surrounding acinar cells are representative of the normal pattern of β-catenin staining, with localisation to the cell borders. B) Small focus of acinar cells with increased expression. These foci were often composed of cells with increased nuclear size, prominent examples of which are indicated by arrows. This focus also contains a cell (arrow head) with no increase in nuclear expression of β-catenin. C) This picture demonstrates the pattern of staining observed in formalin fixed tissues. Cells (arrowed or restricted to the upper right hand portion of this photograph) showing increased nuclear and cytoplasmic staining of β-catenin. D) A dysplastic adenoma showing increased β-catenin expression, but with no apparent nuclear localisation. E) Increased β-catenin staining in a pancreatic focus, showing strong nuclear localisation. Again, these foci were often composed of cells with increased nuclear size. F) Heterogeneous β-catenin expression in an adenoma containing areas of acinar-ductal transdifferentiation (arrow head). No β-catenin staining was detectable in normal ducts (arrow). G) Weak staining of β-catenin within an acinar adenocarcinoma. H) Areas of ductal differentiation within an acinar adenocarcinoma which retained high intensity of β-catenin expression.

3.2.3. Loss of *Apc* within intestinal and pancreatic lesions

To characterise the status of the remaining *Apc* allele in intestinal and the pancreatic lesions arising in *Apc* $^{Min+/-}$ mice, PCR analysis on microdissected foci (Figure 3.6A and 3.6B) was performed. Lesions of various sizes were microdissected as described (see appendix A) using serial sections were identified areas of increased β-catenin staining as a guide for microdissection. In this way it proved possible to analyse the status of the *Apc* alleles in lesions as small as 50 cells. All lesions showing β-catenin dysregulation, including the smallest were analysed by this method. Loss of the remaining wild type *Apc* allele in both the intestinal and pancreatic lesions was found in *Apc* $^{Min+/-}$ and (*Apc* $^{Min+/-}$*/p53* $^{-/-}$) mice whereas in (*Apc* $^{Min+/-}$*/Msh2* $^{-/-}$) mice the wild type *Apc* allele was still intact (Figure 3.7).

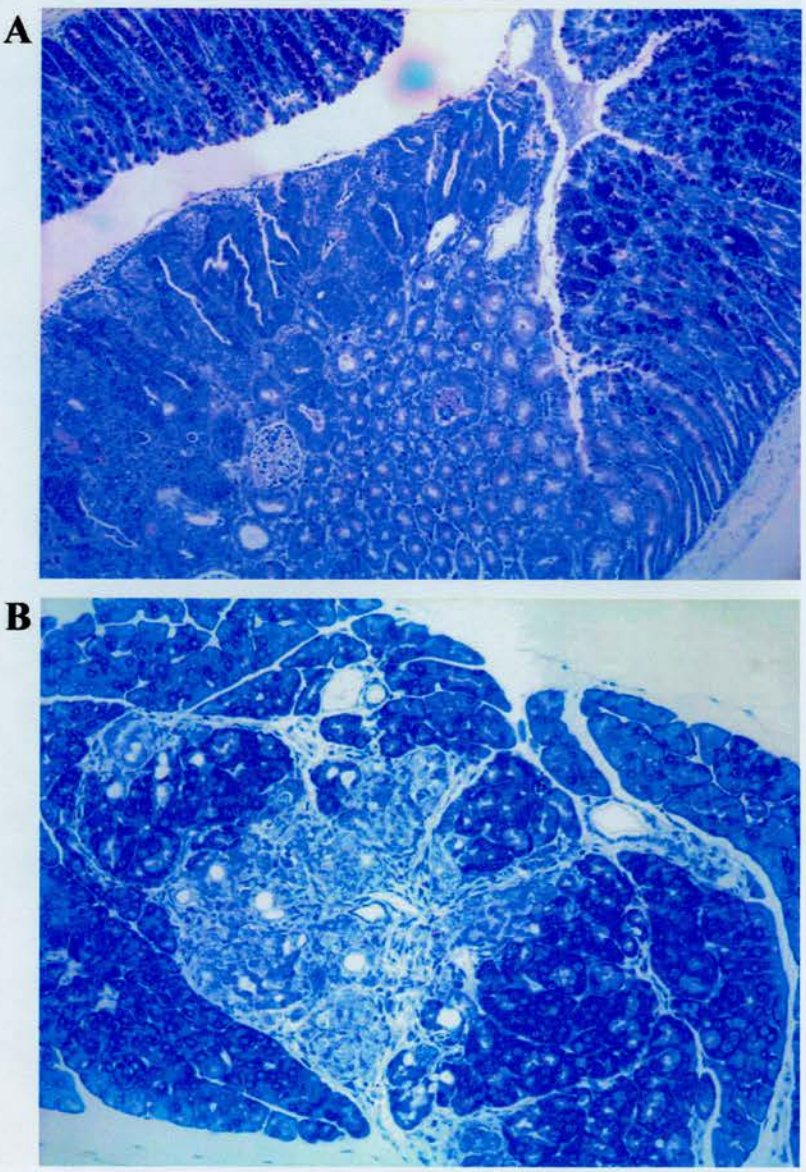

Figure 3.6 Photographs showing histopathological microdissected lesions

Photographs showing pale areas of intestinal lesion (A) and pancreatic lesion (B) stained with toluidine blue, before microdissection. All photographs obtained at x400 of magnification.

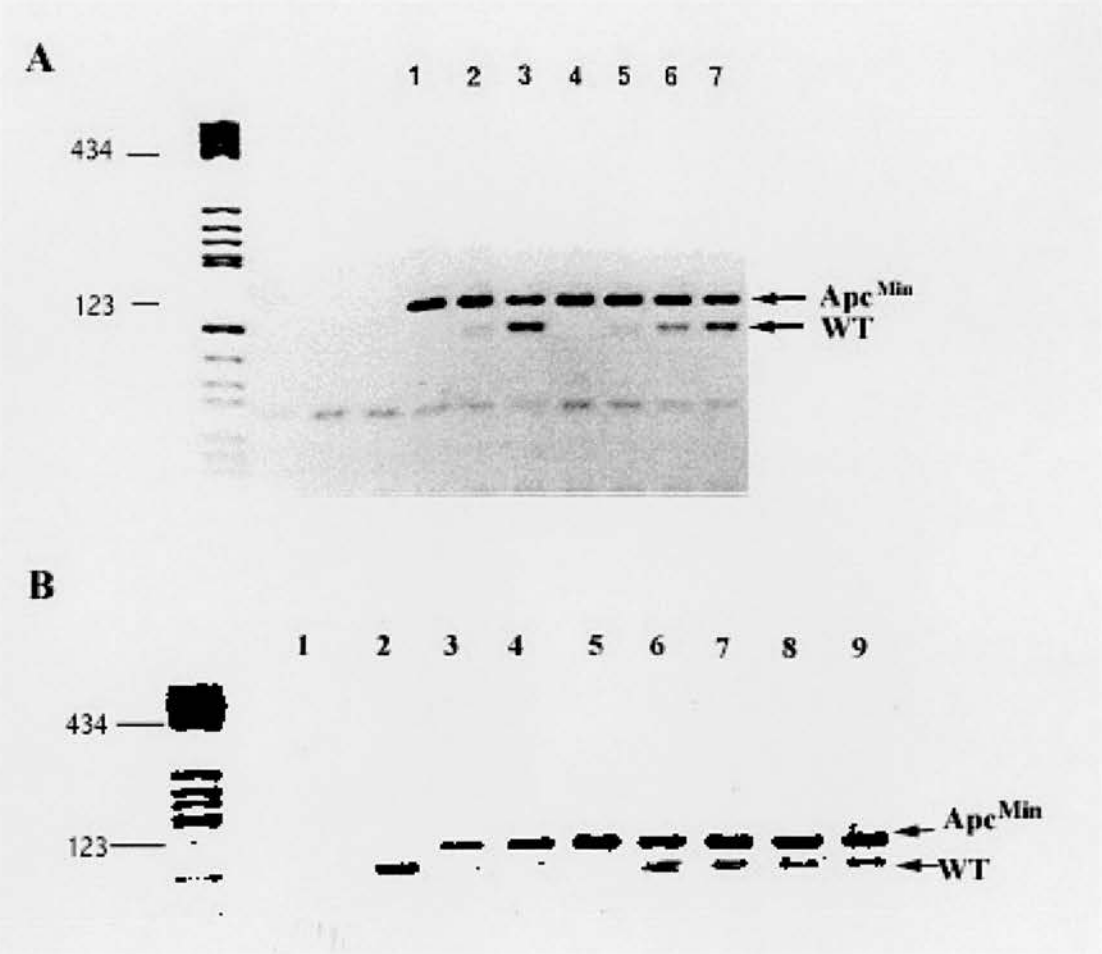

Figure 3.7 PCR analysis of *Apc* alleles from microdissected tissues from Apc^{Min} and $Msh2^{-/-}$ mice

Photographs representative results from PCR analysis of microdissected lesions. WT, the amplification products from the wild type *Apc* allele (111 bp). $Apc^{Min,}$, the amplification product from the mutant allele (123 bp). (A) Samples were all derived from lesions arising within Apc^{Min} mutant mice and were as follow: lane1 and 2, pancreatic foci showing β-catenin dysregulation; lane 3, normal pancreas; lane 4 and 5, small intestinal lesions; lane 6 and 7, normal intestinal epithelium. (B) Samples were all derived from lesions arising within Apc^{Min} and *Msh2* mutant mice and were as follows: lane 1 is negative control, lane 2 is *HindIII* restriction enzyme control, lane 3, 4 and lane 5 are intestinal lesions, lane 6 is normal intestinal tissue from Apc^{Min} mice. Lane7 and lane 8 are pancreatic lesions, lane 9 is normal pancreatic tissue from $Msh2^{-/-}$ mice. All results were obtained using microdissected areas containing approximately 50 cells.

3.3. Discussion

This chapter shows that β-catenin dysregulation is a feature of early neoplasia in both intestine and pancreatic epithelium of *Apc* $^{Min+/-}$ mice. It appears in the earliest single crypt lesions in the intestine and also in lesions that are as small as single cells, which is frequently seen as small cell clusters in the exocrine pancreas. In both sites, β-catenin is distributed with a striking nuclear localisation, as well as being generally overexpression. The significance of the cytosolic localisation is less certain, as this was often absent from methacarn-fixed tissues. It was prominent, however after formalin fixation, and may reflect the true distribution of β-catenin in the cytosol, but in a form soluble by the glacial acetic acid/methanol/chloroform in methacarn.

The data also show that, as these abnormal foci progress to morphologically identifiable adenomas and carcinomas, they also tend to lose the earlier overexpression of β-catenin. Similar observations of the loss of β-catenin expression in late lesions have been made from azoxymethane treated rat to induce intestinal adenomas (Sheng *et al* 1998).

Three additional findings are particularly significant in the interpretation of these observations. First, even in the smallest β-catenin dysregulation lesions in *Apc* $^{Min+/-}$ mice, the normal *Apc* allele is lost. By microdissection, I analysed β-catenin overexpression lesions of approximately 50 cells in size, which is equivalent to about 4-5 cell divisions. The clarity of these results make it clear that these early lesions are clonal derivatives of founder cells that have lost *Apc*, since a mixture of even a small proportion of cells with a retained normal allele would have produced an obviously different ratio of normal to mutant alleles from the pattern consistently observed. Second, β-catenin dysregulation was never seen in the pancreas of animals with a wild type *Apc* background. Third, in animals with wild type *Apc* but *Msh2* null germline, β-catenin dysregulation was observed in most intestinal adenomas but was absent from some of the earliest lesions.

Inactivation of the remaining allele of the murine *Apc* was demonstrated in 100% of tumour arising in *Min* mice (Levy *et al* 1994). Moreover, they observed inactivation in

the earliest recognisable phase of tumours, including some lesions containing as few as two dysplastic crypts. The conclusion from my study is that β-catenin dysregulation occurs as a direct consequence of loss of Apc-dependent proteolysis. In lesions within both tissue types, β-catenin was predominantly localised to the nucleus, in agreement with the report by Sheng *et al* (1998) that β-catenin was localised predominantly in the nucleus of adenomas from *Min/+* mice and transgenic mice expressing a mutant truncated form of the *APC* gene. β-Catenin interaction with the transcription factor *Lef-1* is known to activate transcription of the downstream target gene such as *c-myc* and -- *AP-1*, in the nucleus (He *et al* 1998, Mann *et al* 1999). The pattern of dysregulation was not consistent in all the categories of lesions analysed. Thus, high intensity of β-catenin staining were most consistently observed in early (type I and type II) lesions. Lower degree of β-catenin staining was seen in larger lesions with only focal areas of weak staining within some larger adenomas and adenocarcinomas. These findings suggested that the genetic changes, which led to elevated β-catenin, were most relevant to the very early stages of neoplasia. This concept was supported by observation of localised areas of reduced or absent β-catenin staining within some adenomas and by studies of human tumorigenesis in which down-regulation of both β-catenin and E-cadherin has been reported in a range of carcinomas (Takayama *et al* 1996). In human colon cancer, about 48% of mutations in the NH_2-terminal regulatory domain of *CTNNB1* gene were found in the early adenomatous stage of colorectal neoplasia (Sparks *et al* 1998). This study was supported by the study of Samowitz *et al* (1999) whom demonstrated that the percentage of β-catenin mutations in small adenomas (12.5%) was significantly greater than that in large adenomas (2.4%) and invasive cancers (1.4%). Furthermore, mutations of the β-catenin gene were also found in tumours derived from other organs both in human and animals (de la Coste *et al* 1998). They found 26% of human hepatocellular carcinoma had β-catenin mutations, and β-catenin mutations were found in 50% of hepatic tumours in transgenic mice (de la Coste *et al* 1998).

Loss of β-catenin overexpression in late lesions is not absolute. In those lesions, which no longer overexpressed β-catenin, further maintenance of the neoplastic state

may be sustained by mutations in other genes. β-Catenin itself may be subject to inactivation, or be down regulated by other signals emanating from altered gene expression.

The absence of β-catenin overexpression in some intestinal type II lesions from (*Apc* $^{Min+/-}$*/Msh2* $^{-/-}$) mice suggests that upregulation of β-catenin is not obligatory at this stage. However, as the large lesions uniformly do overexpress β-catenin, it is clear that inactivation of *Apc* is still selected for during adenoma growth. β-Catenin dysregulation was shown as a common event observed in early lesions except in both *Msh2* $^{-/-}$ and (*Apc* $^{Min+/-}$*/Msh2* $^{-/-}$) mice, which show the normal pattern of staining and distribution of β-catenin in the lesions identified as type II. Thus, β-catenin overexpression was not absolutely associated with early neoplastic change. These findings show that dysregulated β-catenin is not an obligate event in early lesion formation. Furthermore, it suggests *Msh2* deficiency predisposes to such apparent β-catenin-independent events, possibly through mutations in other components of the Wnt signalling pathway which do not affect β-catenin levels or through mutations in other pathways. This data suggests there are at least two pathways that permit the development of very small lesions. These pathways appeared to converge as the proportion of lesions showing normal β-catenin staining decreased with lesion size. The simplest interpretation of these results was that the *Msh2* $^{-/-}$ background revealed the existence of a pathway to early lesion formation, but further development of adenomas was still dependent on total loss of Apc function. The data suggest there is an alternative genetic route to adenoma formation, independent of *Apc* knockout, but ineffective in generating further progressive lesions. It could be of significance in understanding the earliest stages of adenoma formation. The genetic instability associated with *Msh2* null status alone could not make the larger lesions thus it is dependent on *Apc* knockout.

β-Catenin dysregulation was observed in clones within the pancreas of *Min* animals, but these only progressed in the absence of wild type *p53*. This shows that functional *p53* stops preventing the development of neoplasia in this tissue, either by stopping cell growth or initiating cell death.

Nuclear size variation within even very small pancreatic lesions was noted, which raising the possibility that loss of *Apc* function may promote genetic instability. Similar nuclear abnormalities were identified in intestinal lesions. The roles played by both tissue specificity and *p53* in determining nuclear atypia were characterised in greater detail (see detail in Chapter 4).

Chapter 4

Nuclear volume analysis

Studies in this chapter pursued the initial observation of nuclear polymorphism in pancreatic lesions. Nuclear size is determined by the relative quantities of DNA, histone, acidic proteins, RNA and enzymes present within the nucleus. Genetic instability is often reflected by changes in the nuclear volume. However, nuclear volume also changes through the cell cycle in normal euploid cells as a consequence of the normal replicative cycle. This chapter is focused upon changes in the nuclear volume in the intestinal and pancreatic lesions arising in mice bearing defects in *p53*, *Apc* and the mismatch repair gene, *Msh2*.

Mitotic nondisjunction can be a phenomenon of malignant cells, resulting in chromosomal abnormalities. The term polyploidy is used to describe the situation where more than two multiples of the haploid chromosome set are found. The naming of polyploids is based on the number of sets of chromosomes found: a triploid has 3n chromosomes; a tetraploid has 4n; a pentaploid has 5n and so forth. This condition is relatively infrequent in most animal species although well known in lizards and amphibians but much more common in plant species. In man, polyploidy is seen in both the liver and in the pancreas. Odd numbers of chromosome sets are not usually maintained reliably from generation to generation because a polyploid organism with an odd number of homologues usually does not produce genetically balanced gametes. Polyploidisation can originate in two ways: (1) the addition of one or more extra sets of chromosomes which is identical to the normal haploid chromosome of the same species, termed autopolyploidy; and (2) the combination of chromosome sets from different species which may occur as a consequence of interspecific matings, termed allopolyploidy.

Cell division involves both nuclear (mitosis) and cytoplasmic (cytokinesis) phases giving rise to two new cells. The period between two mitotic divisions is defined as the

somatic cell cycle and usually requires between 2-4 days. The time from the end of one interval to the beginning of the next is called interphase. Interphase is divided into G_1, S and G_2 periods. The period of actual division, corresponding to the somatic mitosis, is called M phase. G_1 phase is the gap between mitosis and the onset of DNA replication. During G_1 phase RNAs and proteins are synthesised, but there is no DNA replication. The initiation of DNA replication marks the transition from G_1 phase to the period of S phase. S phase is defined as a duration in which all DNA has been replicated and the total DNA content increases from the diploid value of 2n to the fully replicated value of 4n. The period from the end of S phase until mitosis is called the G_2 phase. During this period, the cell has two complete diploid sets of chromosomes. Observations made in the study of yeast fission showed that as cells grow during G_2 phase, mRNA and protein increase until mitosis is triggered, after which there is a sharp drop in both mRNA and protein (reviewed in Lew and Kornbluth 1996). In labile cell such as haematopoietic cells, cells undergo division without any stimuli. In permanent cell types such as neurons and muscle cells, mature cells are considered to be withdrawn from the cell cycle into another state that is called G_0. In G_0, they are unable to proceed into S phase. In stable cell types such as the hepatocyte, fully differentiated cells can be stimulated to leave G_0 and re-enter the cell cycle.

Circuits that respond to features such as completion of replication or cell mass are called checkpoints. Genetic studies have identified many of the components of checkpoints in the yeasts *Saccharomyces cerevisiae* (Murray 1995) and *Schizosaccharomyces pombe* (D'Urso and Nurse 1995). The checkpoints play a role in preventing the cycle from proceeding until a particular condition has been satisfied. There are at least two points in the cycle at which a decision is taken on whether to proceed; first is the commitment to chromosome replication, which occurs in G_1. Second is the commitment to mitotic division, which occurs at the end of G_2 phase. This provides an opportunity for the cells to check that nuclear mass has increased to a level adequate for division. In addition, there are systems to ensure that the fidelity of replication is maintained, these are DNA damage checkpoints. The DNA damage checkpoints act at three stages in the cell cycle, one at the G_1/S transition, one that

monitors progression through S and one at the G_2/M boundary (Iatropoulos and Willium 1996). Arrest in G_1 prevents copying of damaged bases, which would fix mutations in the genome. Arrest in G_2 allows DNA double-strand breaks to be repaired before mitosis. Blocking cells with double-stranded DNA breaks from entering mitosis prevents segregation of broken chromosomes, which would cause missegregation of genes distal to the break. The other checkpoint prevents entry into S phase until DNA damage is repaired this prevents the replication of DNA from damaged templates, which would lead to DNA rearrangements.

Regulation of cell division is critical for the normal development of multicellular organisms. The molecular processes, which regulate chromosome replication and cell division, are fundamentally similar in all eukaryotic cells.

The cell cycle can be viewed as a kinase cycle with down-stream events such as DNA replication occurring as a function of the activity of a particular cyclin-dependent kinase (Cdk). The discovery that degradation of mitotic cyclins is necessary for cells to exit mitosis showed that the proteolytic process is critical in the control of Cdk activity and in driving the progression of the cell through the cell cycle. The ubiquitination pathway has been found to trigger anaphase independently of Cdk activity, which indicates that proteolysis directly controls a step in the chromosome cycle and is not only used to drive the cell cycle.

The three cellular components involved in nuclear division are the DNA, the spindle and the spindle pole or centrosome. Any defects that happen to any of these components will result in genetic instability, which is characteristic of precancerous and cancerous cells. Defects in the DNA could be responsible for chromosomal rearrangements such as deletions, amplifications and translocations. Defects in the spindle could lead to mitotic nondisjunction, producing loss or gain of whole chromosomes. Defects in the centrosome could lead to changes in the ploidy of the genome. These three categories of genomic change, chromosomal rearrangements, aneuploidy and polyploidy are all common during cancer cell development.

The protein encoded by the *p53* tumour suppressor gene, functions in the checkpoint control that arrests cells with damaged DNA in G_1. Cells with functional *p53* arrest in G_1

when exposed to γ-irradiation whereas cells lacking functional *p53* do not. Although p53 protein normally has an extremely short half-life, DNA damage leads to the stabilisation of p53, which then stimulates transcription of a number of genes including *ATM* (Ataxia Telangiectasia Mutated) and *p21*. The *ATM* gene has been implicated in regulation of *p53*. p21 (Dulic *et al* 1994, El-Deiry *et al* 1994), is a protein that binds to and inactivates the cyclin-dependent kinases (Cdk) necessary for initiating DNA synthesis. As a result cells are arrested in G_1 until DNA damage is repaired. One report has even suggested that p21 induction caused irreversible cell cycle arrest in both G_1 and G_2/M (Fang *et al* 1999).

p53 has also been implicated in the G_2/M arrest and resulting in delayed DNA replication. *p53* regulates a mitotic spindle checkpoint that prevents DNA synthesis before chromosomal segregation, which is a control of a G_2/M checkpoint (Cross *et al* 1995, Guillouf *et al* 1995). Furthermore, *p53* appears to be an integral part of the process that regulates the number of centrosomes in a cell (Fukasawa *et al* 1996). These functions of *p53* in controlling the G_2/M checkpoint may account for the phenotype of genomic instability that is commonly associated with *p53* mutation.

It has been reported that the APC protein inhibits cell cycle transition from the G_1 to S phase and that overexpression of the Cdk-cyclin proteins abrogate the cell cycle blocking activity of *APC* (Baeg *et al* 1995, Heinen and Groden 1999). Recently, EB1, which is a component of the microtubule cytoskeleton in mammalian cells, was demonstrated to be colocalised both to cytoplasmic microtubules in interphase cells and to spindle microtubules during mitosis *in vitro* (Berrueta *et al* 1998, Morrison *et al* 1998). Taken together with a study by Neufeld and White (1997) which showed nuclear and cytoplasmic localisation of APC in human tumour cell lines, these findings are consistent with a role for APC in both G_1 and mitotic checkpoint control.

The mismatch repair system has been found to interact with the G_2 checkpoint (Hawn *et al* 1995) in response to methylating agent induced DNA damage. High levels of hMSH2 protein were detected in the crypts of Lieberkuhn (Wilson *et al* 1995, Leach *et al* 1996) which undergo rapid proliferation and are involved in the continuous production of differentiated cells. The mismatch repair machinery has also been

associated with apoptosis, which probably reflects the consequences of a mismatch repair protein dependent checkpoint. Overexpression of hMSH2 and hMLH1 has been shown to lead to apoptosis in cells exposed to methylating agent (Zhang *et al* 1999), although the mechanism by which hMSH2 and hMLH1 may control apoptosis is still unclear. Recently, a *Msh2*-dependent apoptotic response (mediated through a *p53*-dependent pathway) was demonstrated in the mouse small intestine (Toft *et al* 1999). Those previous studies suggested that mismatch repair gene is critical in the surveillance of cells with damaged DNA.

In summary, there is a significant body of work implicating *p53*, *Apc* and the mismatch repair proteins in control of cell cycle checkpoints in the cell cycle and deficiency in these genes is associated with genetic instability.

DNA-aneuploidy and genetic instability is a feature of tumorigenesis which can be scored by DNA ploidy analysis using image cytometry either by a two dimensional or a three dimensional method. Image cytometry (ICM) is widely used to measure DNA ploidy and has a number of advantages and limitations. ICM requires small numbers of nuclei, 250 or more, and is usually applied to the disaggregated cells of solid tumours. DNA content measured by image cytometry (ICM-DNA) has been used successfully to identify aneuploid DNA content in a variety of malignancies and has enabled correlation of ploidy with prognosis (Forsslund and Zetterberg 1990, Lukes *et al* 1994, Mir *et al* 1992). However, it should always be remembered that the DNA ploidy measured by cytometry is only an estimate of the genetic material and can not reflect single events in the genome nor the functional state of a tumour cell.

Earlier studies of DNA ploidy measurement in histological sections used a two-dimensional (2D) approach (Moberger *et al* 1984, Greene *et al* 1991). However the information obtained by 2D analysis was often subject to inaccuracy (Uyterlinde *et al* 1989, Mairinger *et al* 1994, Sperb *et al* 1993, Sapi *et al* 1993). The principal reason for this was that in conventional 4 μ thick histologic sections, incomplete nuclear segments occur as parts are cut off from nuclei with a diameter exceeding the section thickness. This phenomenon is called capping (Bins and Takens 1985, Haroske *et al* 1984). In thicker sections (8-10 μ), capping is reduced but overlapping nuclei are still a major

problem. Moreover, measurement of non-overlapping nuclei can be very time-consuming and not always accurately reproducible. These problems can be overcome by means of three-dimensional (3D) imaging, using a confocal laser scanning microscope (CLSM) and thick histological sections. The basic principle of any scanning microscope is that the sample is scanned with a probe that illuminates discrete points in the sample. The signal from the interaction of the radiation probe with the sample is collected and used to reconstruct an image. Both the lateral (x, y) and depth (z) resolution of a CLSM is better than that of conventional microscopes, giving higher resolution images. With CLSM, it is possible to optically section a thick histological section, without interference from out-of-focus signals. Moreover, small samples can provide an adequate number of nuclei for this method (Lajoie *et al* 1993). One problem with this technology is that the stain used can affect the accuracy of the 3D measurement. The nuclear fluorescent stain for routine two-dimensional and 3D CLSM morphometric and cytometric assessments should have the following properties: (a) high specificity, proportionality, and sensitivity for DNA; (b) stability (no or little bleaching); (c) simplicity of the staining procedure; and (d) is inexpensive. Recently, two new cyanine fluorochromes, TOTO-1 iodide and YOYO-1 iodide with DNA and RNA specificity have become commercially available (Molecular Probes Inc., Eugene, OR). TOTO-1 iodide and YOYO-1 iodide bind to DNA by intercalation. The relative fluorescence intensities of these dyes when bound to the DNA bands obtained by gel electrophoresis indicate that dye-binding depends on DNA content rather than base composition (Glazer *et al* 1990, Rye *et al* 1992). Moreover, integrated TOTO-1 iodide and YOYO-1 iodide fluorescence showed good linearity with the DNA content of diploid, tetraploid and octaploid liver nuclei (Tekola *et al* 1994).

Conventional two-dimensional studies of DNA ploidy can be performed using the Highly Optimised Microscope Environment (HOME) which provides a simple facility combining a microscope, electronic display and stage to enable location and relocation of individual cells in pathological specimens. The system permits a variety of morphological measurements to be taken on typical histological specimens.

From the observations made in the previous chapter it was noted that nuclear pleomorphism was apparent in the pancreatic lesions arising in the mice mutant in *Apc*

and *p53*. Two hypotheses for these observations were proposed; (a) that nuclear change is an early event in the pancreatic lesions but not in the intestinal lesions; (b) that the genotypes of the mutant mice were influencing the genetic instability in the lesions. To test these hypotheses, a study was designed (a) to study nuclear change in small populations of preneoplastic cells in mutant mice; (b) to determine the influence of a range of genotypes of mice on the nuclear content seen in preneoplastic and neoplastic lesions in the pancreas and in the intestine; and (c) to evaluate two dimensional analysis using the HOME in comparison with three dimensional analysis performed using the confocal laser scanning microscope.

The cell turnover rate was also measured by BrdU to clarify if any differences observed in nuclear volume were related to cell turnover or if the change in the nuclear volume could be directly attributed to genetic instability.

4.1 Materials and Methods

4.1.1 Mice

Mice mutant for *Apc* ^{Min} (Moser *et al* 1992) and *Msh2* (de Wind *et al* 1998) were maintained as out-bred colonies. Mice were monitored on a daily basis for signs of ill health and prior to killing were injected intraperitoneally with BrdU (Boehringer Mannheim, Germany) 250 mg per kg of body weight to permit cell turnover to be scored in histological sections. Mice were killed by cervical dislocation 2 hours after BrdU injection. The intestine and pancreas were removed immediately and immersed in methacarn solution (see appendix B), left overnight at room temperature and processed and embedded as previously described (see section 2.1.2)

4.1.2. Double labelling of β-catenin and BrdU

Immunohistochemical staining of β-catenin and BrdU was optimised as previously described in session 2.1.3.

Three micron thick paraffin embedded sections were exposed to high temperature antigen retrieval followed by incubation in 2.0 N HCl at 27 ^{0}C for 25 minutes to denature the DNA. Sections were permeabilised in 0.1% Saponin/TBS, subsequently blocked in 1.5% hydrogen peroxide solution and incubated with 20% normal rabbit serum in 0.1% Saponin/TBS (see appendix B) to block non-specific binding. Sections were incubated with primary antibodies; mouse monoclonal anti-β-catenin (Transduction Laboratories, UK) and rat monoclonal anti-BrdU (Harlan Sera lab, UK) overnight at 4 ^{0}C, followed by incubation with secondary antibody rabbit anti-rat/biotinylated (Immunopure, Pierce, USA) for 30 minutes at room temperature followed by incubation in ABComplex/HRP for 30 minutes. The staining was visualised with diaminobenzidine 0.5 mg/ml (see appendix B). The sections were next incubated with secondary antibody rabbit anti-mouse/biotinylated (Dako, Germany), here ABComplex/AP was used as a detection system. The labelled complex was visualised with Vector Red (Vector Laboratory, UK). Details of the protocol are in appendix A.

4.1.3. Triple labelling of immunofluorescence on 15 micron thick paraffin sections

Immunofluorescent triple labelling was initially optimised on three micron thick sections. After dewaxing and rehydrating the sections, YOYO-1 iodide (Molecular Probes, The Netherlands) was diluted in Tris/HCl, pH 7.6 in serial concentrations of; 0.1, 0.05, 0.025 μmol/μl to optimise the staining. The sections were dewaxed, rehydrated, pretreatment in high temperature condition and HCl as previously described in section 4.1.2. Subsequently, section were permeabilised in 0.1% Saponin/TBS for 15 minutes on the shaking plate, followed by incubating with serial concentration of YOYO-1 diluted in 20% normal goat serum, 0.025, 0.05, 0.075 and 0.01 μmol/μl, overnight, in the dark at 4 ^{0}C and finally, washed well in 0.01% Saponin/TBS for 60 minutes at room temperature on the shaking plate. The optimum concentration of YOYO-1 was 0.05 μmol/μl.

However, non-specific cytoplasmic fluorescence was observed in the stained sections, which was thought to reflect RNA staining. The sections were incubated with RNAse at a concentration of 7 μg/ml at 37 ^{0}C for 15, 30 and 45 minutes. Using this approach, specific DNA staining in the nuclei was obtained after treatment with RNAse at 37 ^{0}C for 45 minutes.

The next step was to optimise the use of the secondary antibodies for indirect immunofluorescence. They were goat anti-mouse conjugated to rhodamine (Chemicon-International, Inc.) and goat anti-rat Cy5 conjugate (Chemicon-International, Inc.). These two secondary antibodies were diluted in serial concentrations of 0.5, 0.25, 0.125, 0.005, 0.0025 and 0.00125 μg/μl. The optimum concentration for goat anti-mouse rhodamine was 0.25 μg/μl and goat anti-rat Cy5 was 0.0025 μg/μl.

Triple labelling immunofluorescence was first tried on three micron thick sections. The sections underwent antigen retrieval in citrate buffer pH 6.0 and microwaved at 700 watts for 5 minutes, 3 times. After the sections were cool, they were immersed in 2 N HCl and incubated at 27 ^{0}C for 25 minutes. The sections were then washed well in water and permeabilised with 0.1% saponin in TBS for 30 minutes at room temperature, on a shaking platform. Then, sections were treated with RNAse 7 μg/ml at 37 ^{0}C for 45

minutes, followed by incubation with 20% normal goat serum for 30 minutes. The sections were incubated with primary antibodies: β-catenin and BrdU, diluted in 20% normal goat serum overnight at 4 ^{0}C. Next day, the sections were washed with 0.1% saponin in TBS for 15 minutes, 3 times. Secondary antibodies and YOYO-1 were diluted and added to the sections and incubated in the dark, overnight at 4 ^{0}C. On the third day, the sections were washed 3 times with 0.1% saponin in TBS in the dark, for 15 minutes, and observed under a fluorescence microscope. This protocol was also used for triple labelling immunofluorescence on fifteen micron thick sections although the protocol had to be modified for the thick sections.

Fifteen micron thick paraffin embedded sections were cut and mounted on poly-L-lysine coated slides (see 2.1.5). Sections were dewaxed and rehydrated in graded alcohols (see 2.1.5). High temperature antigen retrieval was performed as previously described (see 2.1.5). Sections were then incubated at 27 ^{0}C for 25 minutes in 2.0 N HCl to denature the DNA, followed by a rinse in running tap water. Sections were placed in a slide rack and immersed in 0.1% Saponin/TBS (see appendix B) to permeabilise the cell membrane for 2 hours. The sections were then placed in a moist chamber and covered with 20% normal goat serum in 0.1% Saponin/TBS to block non-specific binding and left overnight at 4 ^{0}C. Then, sections were incubated with primary antibodies: 1:50 mouse monoclonal anti-β-catenin (Transduction Laboratories, UK) and 1:100 rat monoclonal anti-BrdU (Harlan Sera Lab, UK) in 20% normal goat serum for 24 hours at 4 ^{0}C. The sections were washed with 0.1% saponin/TBS for 8 periods of 15 minutes on a shaking platform. Then the sections were incubated with secondary antibodies: 1:200 (0.25 μg/μl) goat anti-mouse/Rhodamine (Chemicon-International, Inc., UK), 1:800 (0.0025 μg/μl) goat anti-rat/Cy5 (Chemicon-International, Inc., UK) and 0.05% (0.05 μM/μl) YOYO-1 (Molecular Probes, The Netherlands) for 24 hours in the dark at 4 ^{0}C. The sections were washed with 0.1% Saponin/TBS for 2 hours in the dark on a shaking platform. The stained sections were immersed in PBS and examined under CLSM.

4.1.4. Method for nuclear volume analysis (2D)

Sections were double labelled with β-catenin and BrdU and examined using the Highly Optimised Microscope Environment (HOME). Lesions were identified on the basis of altered β-catenin staining in both the pancreas and the intestine. BrdU positive and BrdU negative nuclei in the lesions were randomly chosen and assessed for nuclear volume analysis (see appendix A).

4.1.5. Method of nuclear content analysis (3D)

Triple labelled sections were examined under a confocal laser scanning microscope (CLSM). Individual sections were placed in a petri dish and immersed in phosphate buffered saline. The lesions were identified as areas of high intensity of β-catenin staining. Each lesion was scanned with wavelengths of 488 nm, 514 nm and 647 nm to avoid cross talk between channels. Each section was scanned at 1micron steps. Images were analysed with Imaris software and VoxelShopPro.

A subregion of the area of interest was selected and the complete nuclei of BrdU positive and BrdU negative nuclei were randomly chosen. The nuclear mass and nuclear volume was analysed. The threshold level of threshold segmentation had to be determined, it was set at 40% of the maximum threshold. This threshold value was obtained from a calibration test using Fluorescent latex microspheres (Polyscience Inc., excitation 488 nm) that were 10.16 μm in diameter. The fluorescent latex microspheres were immersed in PBS identical to that used for the histological section and scanned with CLSM, magnification of 630 immersion-objective lens. These microspheres autofluorescence so that they can be examined under CLSM without any staining. The images of the microspheres were transferred to Imaris software and VoxelShopPro. It was then necessary to calibrate the programme by defining what level of fluorescence represent a true image. This was performed using "threshold segmentation". The threshold was initially set to the maximum value and subsequently reduced by 5% until the images of the microspheres were cleared from the background. The threshold value was found to be at 40% of the maximum. After threshold segmentation had been performed, the objects were extracted and figures for nuclear mass and volume obtained.

The optimisation of the latex bead volume was performed by Dr. Peter G. Bush and the expected volume (πr^3) of latex bead is 558 μm^3.

VoxelShopPro volume determination of latex beads (10.16 μm diameter) using different threshold values

Threshold	25%	30%	35%	40%	45%	50%	55%
Volume	781	692	623	569	528	485	442
	758	668	609	552	507	456	363
	756	674	608	554	514	468	422
	761	675	602	553	511	468	446
	764	682	613	557	514	468	412
	755	658	606	554	502	452	422
	742	655	621	566	521	473	423
	744	731	616	561	516	472	380
	740	670	601	547	502	462	424
	825	688	593	541	499	457	379
		663	592	539	498	464	401
			661	602	551	452	430
						455	429
						493	414
							420
							405
							415
							364
							433
							416
Mean	762	678	612	558	514	466	412
N	10	12	12	12	12	14	20
SEM	7.95	5.87	5.26	4.79	4.32	3.24	5.30

NB. N = number of samples

SEM = standard error of the mean

4.2. Results

4.2.1. Three dimensional analysis of nuclear volume

The intestinal tumour lesions were classified as in section 3.2.1: (I) single dysplastic crypts, showing nuclear pleomorphism and stratification; (II) complex lesions, comprising several architecturally distorted crypts in the lamina propia with virtually normal overlying surface epithelium; (III) small adenoma, identified by the overall disturbance of architecture including the surface and distinguished from the previous category on the basis of increased size and surface involvement; and (IV) large adenomas. The pancreatic lesions were classified according to the area of the lesion: type I is less than 1 mm^2; type II is 1-25 mm^2; type III is 25-50 mm^2; type IV is 50-100 mm^2; type V is 100-400 mm^2 and type VI is 400-1600 mm^2.

Triple labelling was performed on 15 micron thick sections from (*Apc* $^{Min+/-}$/*Msh2* $^{-/-}$) mice to analyse the nuclear content in lesions from both in the intestine and pancreas. The lesions were identified by their high intensity of β-catenin staining, labelled with rhodamine (Figure 4.1C, top right), DNA in all nuclei was labelled by YOYO-1 (Figure 4.1C, top left), and those cells in S-phase were demonstrated by BrdU incorporation, (Cy5 labelled, Figure 4.1C, lower left). For comparison an intestinal crypt from a wild type mouse is shown in Figure 4.1A. Overlaid pictures of the three immunofluorescence label are shown in Figures 4.1B and 4.1D. The images were analysed using the Imaris software program for DNA content. With the Imaris software program, the S phase nuclei in the tumour lesions were identified by the blue channel (Cy5 staining) and the nuclear mass was obtained with threshold segmentation in the green channel that showed the DNA content by YOYO-1 (Figure 4.2). The results obtained show that in wild type cells and type I and II intestinal lesions, the nuclear mass obtained from S phase nuclei was no different from that obtained from BrdU negative nuclei in the same specimen (Figure 4.3A). Whereas in type III and IV lesions the nuclear mass obtained from S phase nuclei was larger than that obtained from BrdU negative cells. Similarly data obtained for nuclear volume from the same nuclei showed an increase in the nuclear volume of S phase cells only in type III and type IV intestinal lesions (Figure 4.3B). However, the number of cell scored in this study was only 50 nuclei in total, which

limited the power of this analysis. The crypt nuclei in both the lesion and in normal crypt were packed together very densely making it very difficult to isolate individual nuclei and measure the nuclear content (compared Figure 4.1 and 4.4). One advantage of this approach is that the nuclear content value obtained should reflect the absolute nuclear content of the three dimensional structure and so should be more accurate than the data obtained from a two- dimensional study (HOME) which is a relative value.

In the pancreas, only a few S phase nuclei were observed in lesions, on average 0.05% of cells showed BrdU positivity, and no S phase nuclei were observed in the normal pancreas (Figure 4.5). In pancreatic sections individual nuclei could be clearly isolated so that the nuclear content analysis using pancreas was more accurate than in the intestine (Figure 4.6). The result showed the pancreatic nuclear volume obtained from wild type animals is in the range of 50-250 μm^3 and its mode is at 100 μm^3. Whereas the nuclear mass of pancreatic acinar cells obtained from wild type mice varied in range from 150,000 to 650,000 and its mode is at 150,000-250,000. However, this approach was again hindered by the presence of overlapping cells and the presence of some bi-nucleated cells. The most serious drawback was simply the time required to analyse each nucleus. I spent 3 months analysing a total of 50 nuclei obtained from the three- dimensional study, which is very time-consuming. I therefore decided to halt the three-dimensional analysis of the nuclear content of the intestinal and pancreatic lesions.

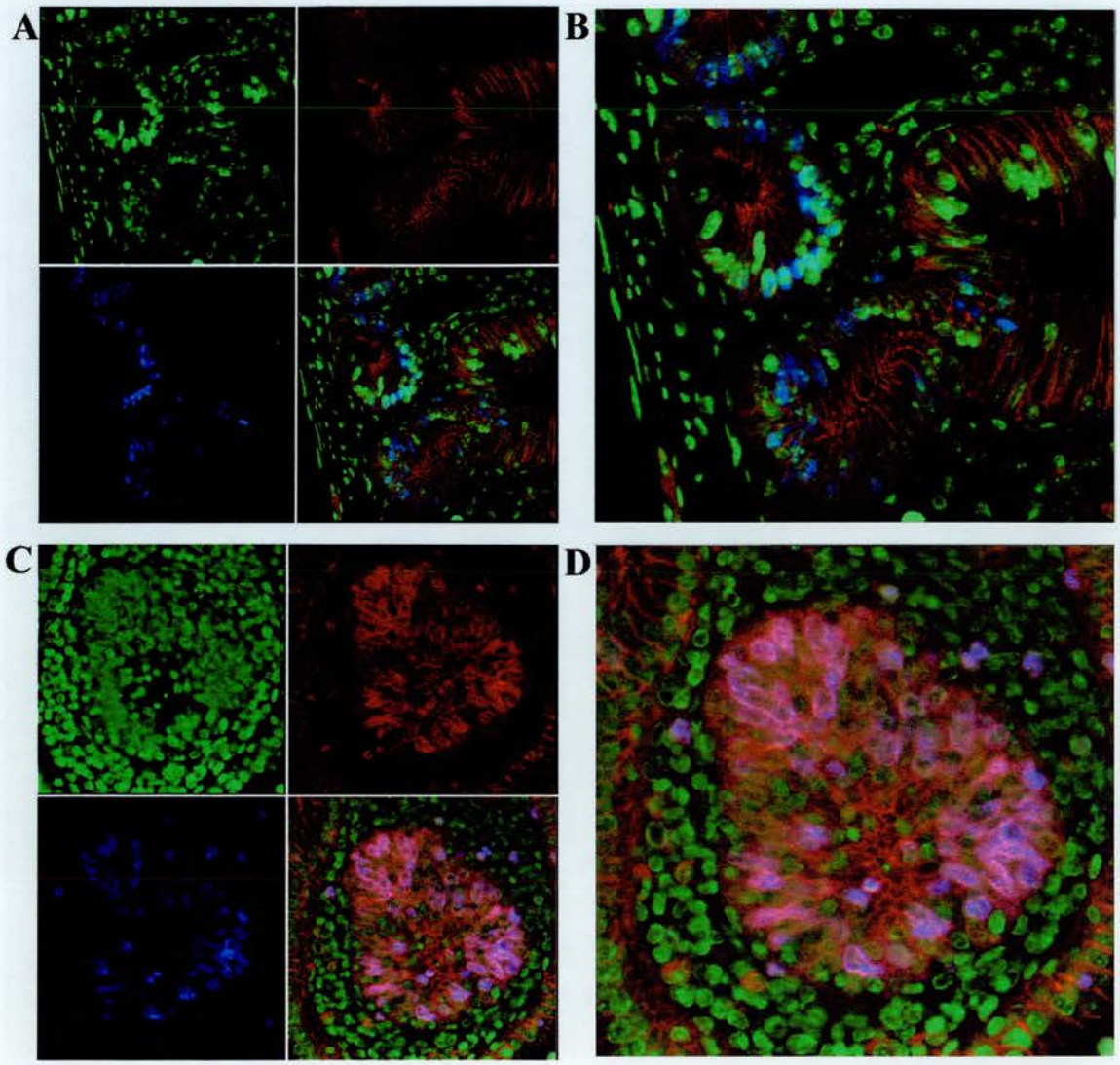

Figure 4.1 Triple labelling fluorescence of β-catenin, BrdU and DNA in the small intestine in wild type mouse (A-B) and in the intestinal tumour lesion in *Apc*$^{Min+/-}$, *Apc*$^{Min+/-}$/*p53*$^{-/-}$ mice (C-D)

Photographs showing triple labelling immunofluorescence in mouse intestine: DNA staining with YOYO-1 is shown in green (top left in A and C), β-catenin staining is shown in red (top right in A and C), BrdU staining is shown in blue (lower left in A and C) and an overlay of all three stainings is shown in lower right in A and C. A and B photographs showing triple labelling immunofluorescence of wild type intestine. C and D photographs showing the intestinal lesion type I. All the figures were obtained at magnification x630.

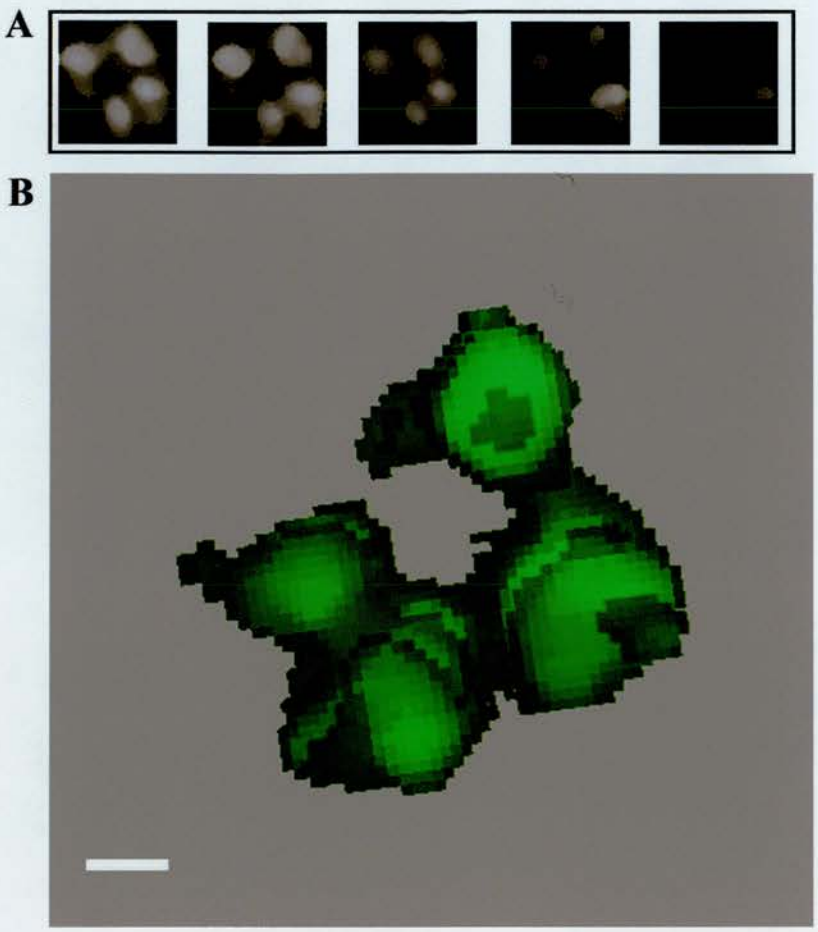

Figure 4.2 Photographs showing three dimensional structure of a single pancreatic acinar nuclei within histological normal cell in a wild type animal

Photograph A and B are of a single pancreatic acinar nuclei in a wild type animal obtained using the confocal laser scanning microscope. Photograph (A) shows a series of images of DNA content following staining with YOYO-1 in a single pancreatic acinar nuclei obtained using threshold segmentation. Photograph (B) shows a two dimensional representation of the three dimensional reconstruction of these images. A scale bar represents 1μm.

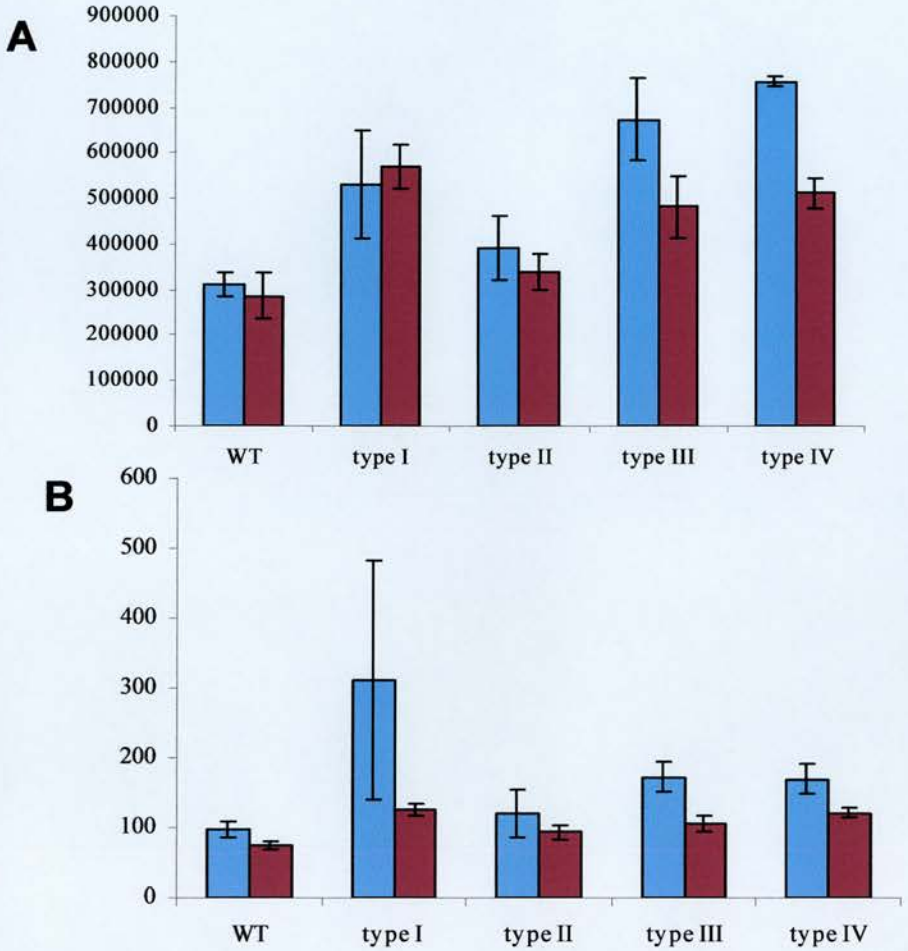

Figure 4.3 Histogram showing 3D data of nuclear mass and nuclear volume obtained from intestinal lesions arising in *Apc*$^{+/-}$*/Msh2*$^{-/-}$ mice

A) Data is presented as the average nuclear mass (indicated on the Y axis) of cells within wild type (WT) mice and in lesion types I-IV. The nuclear mass obtained from BrdU positive nuclei is shown in blue and the nuclear mass obtained from BrdU negative nuclei is shown in red. B) Data is presented as the average nuclear volume (μm^3) (indicated on Y axis) of cells within wild type (WT) mice and in intestinal lesion type I-IV. The nuclear volume obtained from BrdU positive nuclei is shown in blue and the nuclear volume obtained from BrdU negative nuclei is shown in red. Error bar is represented range of the mean.

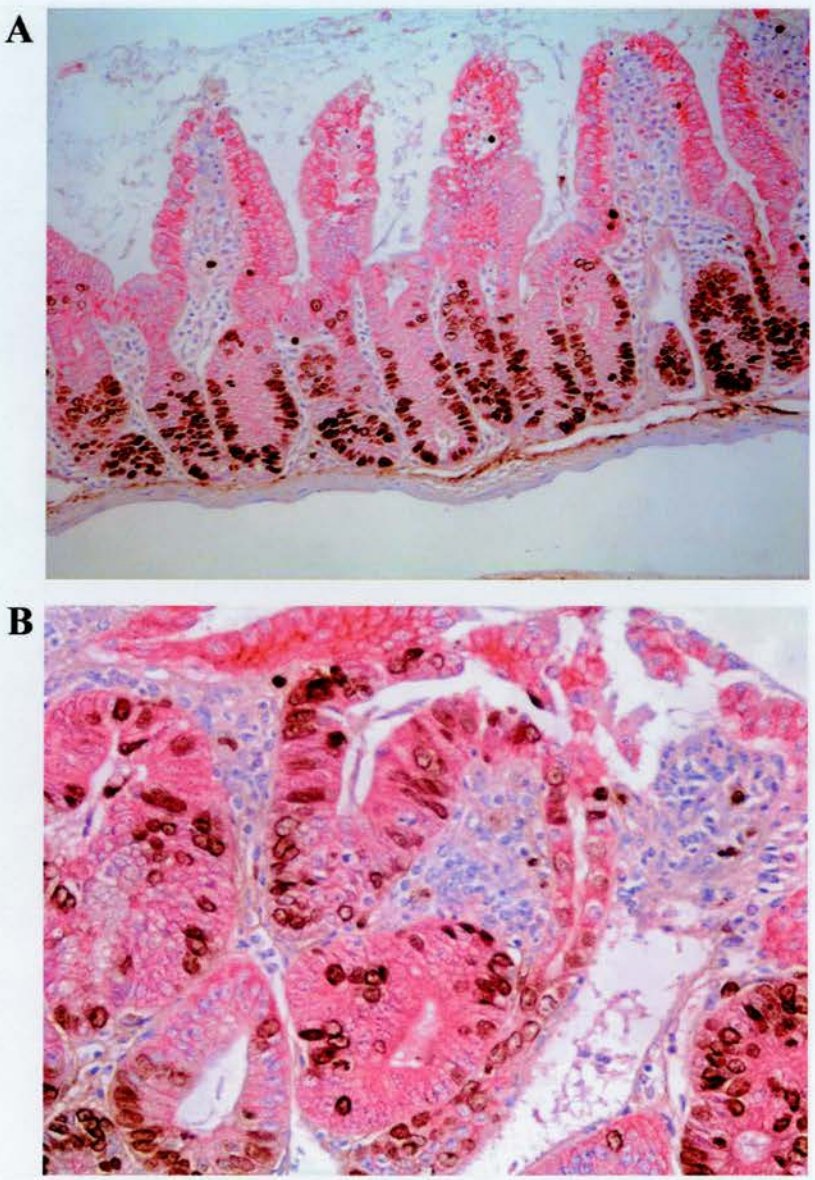

Figure 4.4 Double labelling of β-catenin and BrdU in small intestine in wild type mice and intestinal tumour lesions in *Apc*$^{Min+/-}$, *Apc*$^{Min+/-}$/*p53*$^{-/-}$ mice

(A) Photograph showing double labelling of β-catenin and BrdU in normal intestine (mag. x200), β-catenin expressed at the epithelial cell membrane is shown in red and BrdU positive nuclei in the intestinal crypt is shown in brown colour. (B) Photograph showing double labelling of β-catenin and BrdU in the intestinal lesion (mag. x400), high intensity of β-catenin staining in the nuclei and cytoplasm of the intestinal lesion is shown in red and BrdU positive nuclei in the intestinal crypt are shown in brown colour.

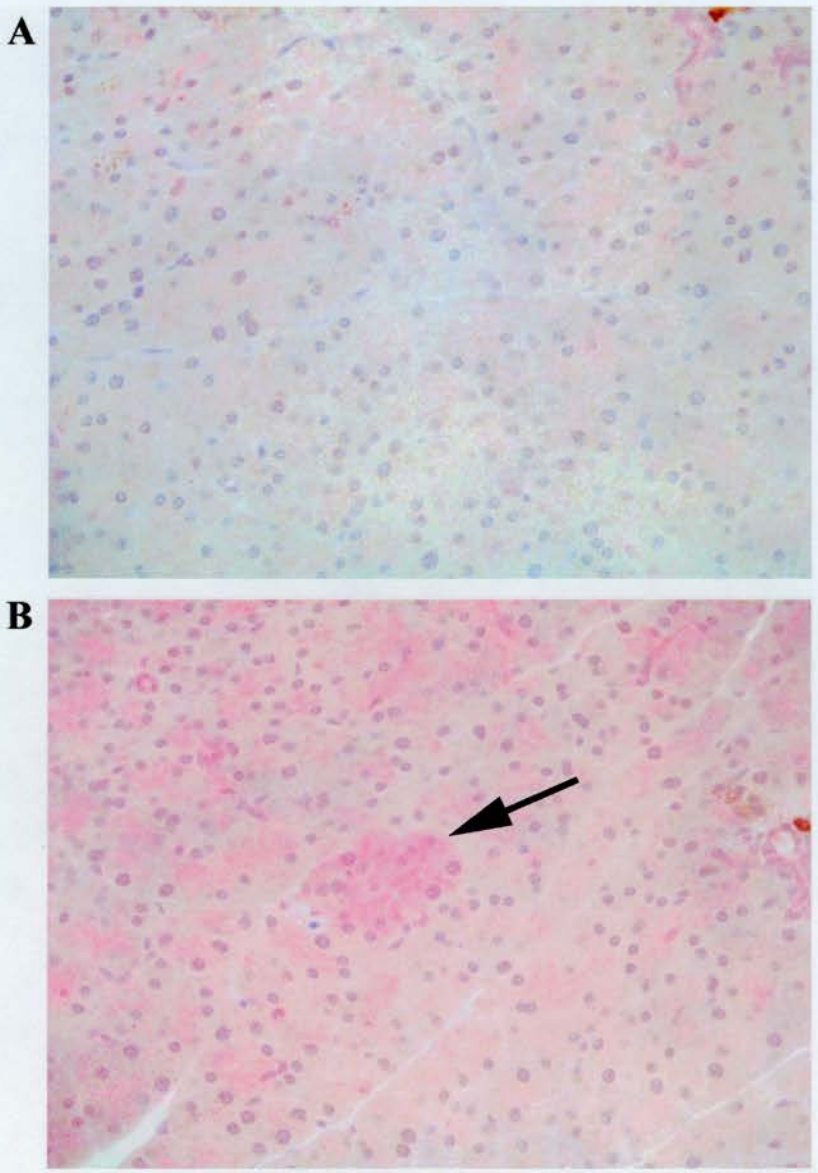

Figure 4.5 Double labelling of β-catenin and BrdU in pancreas in wild type mice and pancreatic lesions in *Apc*$^{Min+/-}$, *Apc*$^{Min+/-}$/*p53*$^{-/-}$ mice

(A) Photograph showing double labelling of β-catenin and BrdU in normal pancreas (mag. x400), β-catenin localisation at the cell membrane is shown in red. (B) Photograph showing double labelling of β-catenin and BrdU in the pancreatic lesion (mag. x400), β-catenin localisation in the nuclei and cytoplasm of pancreatic lesion is shown in red (arrow) no BrdU positive cell found in these histological sections.

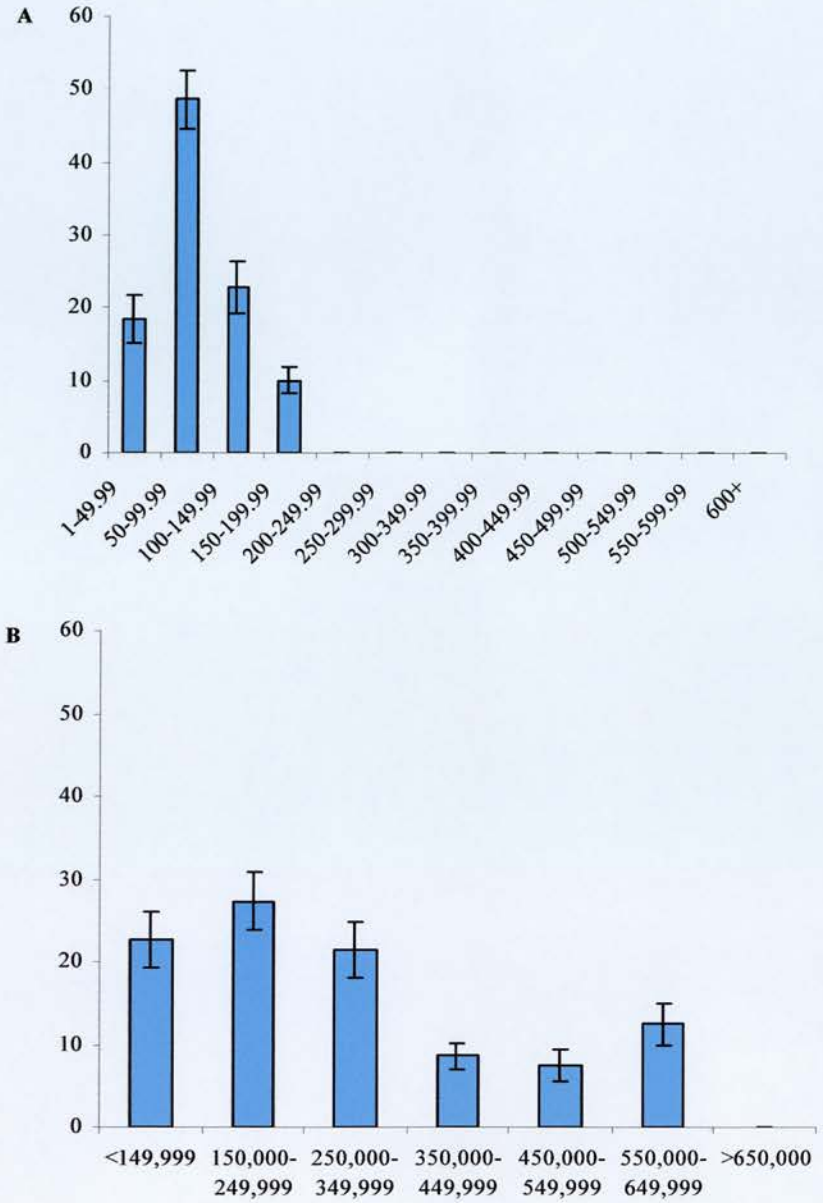

Figure 4.6 Histogram showing 3D data of pancreatic nuclear mass obtained from wild type mice

(A) Data is presented as percentage of cells having nuclear volume (μm^3) indicated on the X axis. (B) Data is presented as percentage of cells having nuclear mass indicated on the X axis. Error bar represents standard error of mean (SEM). The data was obtained from pancreatic acinar cells from wild type mice.

4.2.2.Two dimensional analysis of nuclear volume

(A) Analysis of nuclear volume in spontaneous intestinal lesions in *Apc* $^{Min+/-}$, (*Apc* $^{Min+/-}$*/p53* $^{-/-}$) and *Msh2* $^{-/-}$

My first aim was to compare the data obtained from three-dimensional analysis (see previous section) of nuclear content with a two-dimensional analysis of nuclear volume of the intestinal and pancreatic lesions arising in mice mutant in *Apc*, *p53* and *Msh2*.

Immunohistochemistry was performed on three micron sections to identify the lesions showing high intensity of β-catenin staining. The area of the nuclei in the intestinal lesions from *Apc* $^{Min+/-}$, (*Apc* $^{Min+/-}$*/p53* $^{-/-}$) and *Msh2* $^{-/-}$ were measured with the HOME microscope together with normal crypt nuclei from each genotype and in the wild type animals. The Kolmogorov-Smirnov statistical test was used to assess the significance of differences in the nuclear volume between the different types of lesions in each genotype of mice. Control data was obtained from normal intestine in wild type mice and from morphologically normal intestinal crypts in each genotype. The nuclear volume obtained from intestinal lesions in all lesion types in each genotype of mice were greater than control data obtained from morphologically normal tissue in mutant mice ($p<0.05$) as shown in Figure 4.7 and tables of statistic (see appendix D). The distribution of nuclear volume (Figure 4.8) and the cumulative percentage of cells having a given nuclear volume showed that the nuclear volume obtained from tumour lesions was larger than the nuclear volume in wild type mice and morphologically normal intestinal crypt cells ($p< 0.05$) as shown in Figure 4.9, 4.10, 4.11 and 4.12.

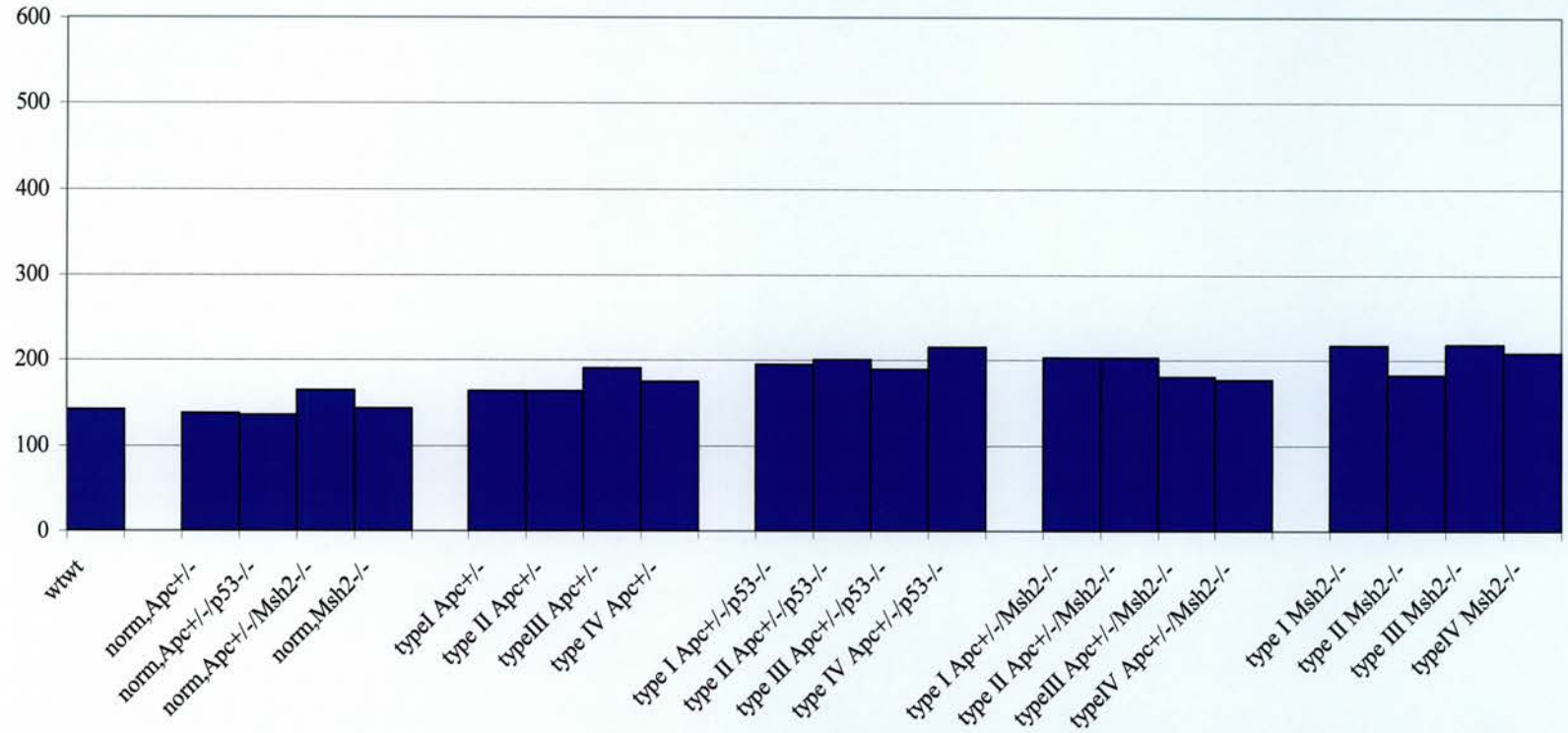

Figure 4.7 Histogram showing average of the nuclear volume in spontaneous intestinal lesions arising in singly and doubly mutant mice in the *Apc*, *p53* and *Msh2* alleles

Data is presented as the average of nuclear volume indicated on the Y axis. Data is presented for each lesion category (type I, II, III and IV as described in the text) in each genotype indicated on the X axis. Data obtained from at least 3 mice, the age of these mice is between 3 to 5 months old. Control data for normal intestine was obtained from wild type mice and from morphologically normal intestinal crypts from each genotype.

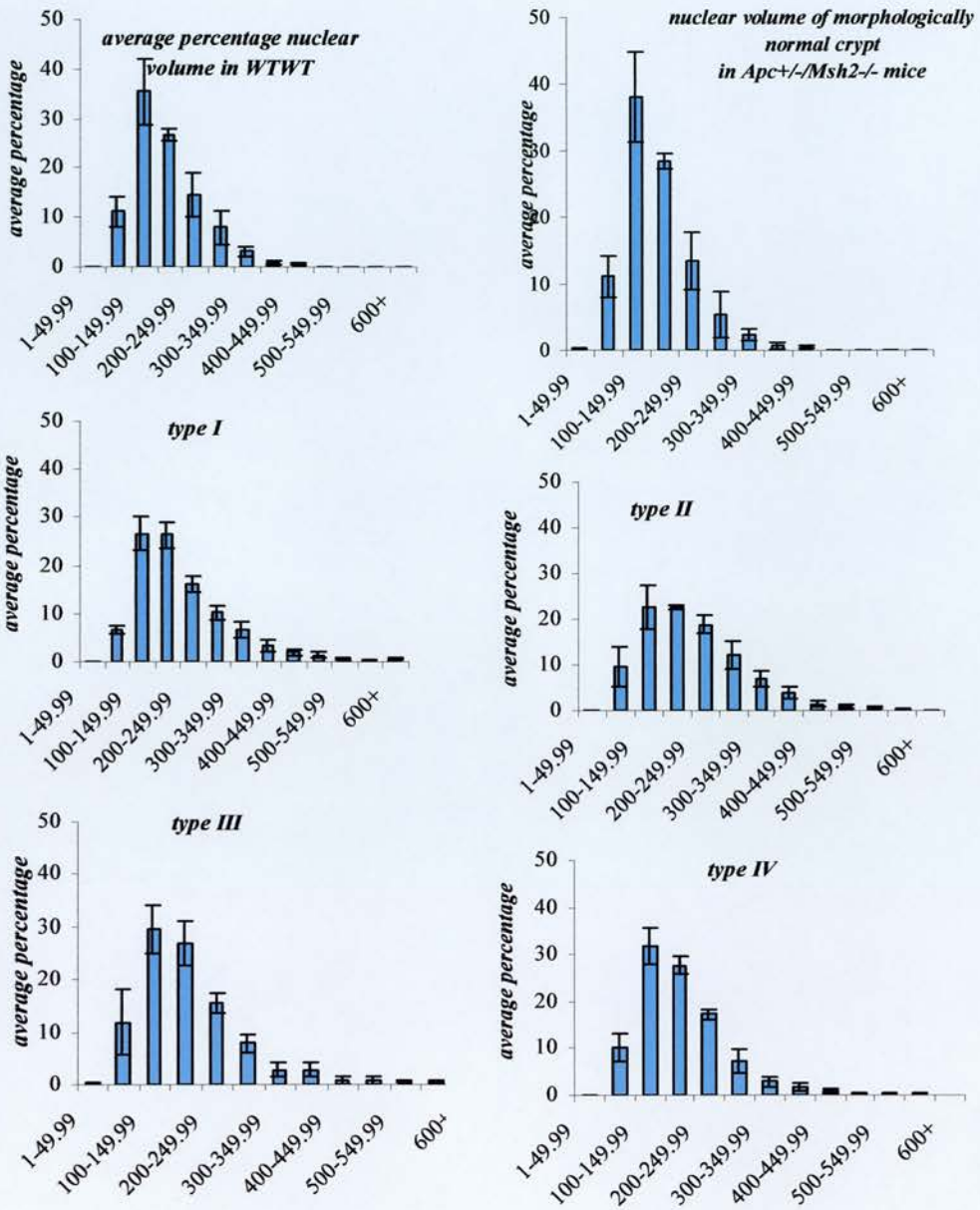

Figure 4.8 Histogram showing distribution of nuclear volume in intestinal lesions arising in *Apc*$^{+/-}$*/Msh2*$^{-/-}$ mice

Data is presented as the average percentage of cells having nuclear volume equal or greater than the size categories (nuclear volume ranged from 1 to 600+ μm^3) indicated on the X axis. Data is presented for each lesion category (type I, II, III and IV as described in the text). Error bars indicate standard error of the mean (SEM) obtained from at least 3 mice. Control data is indicated for wild type intestine obtained from wild type mice (top left) and for morphologically normal intestinal crypts from *Apc*$^{+/-}$*/Msh2*$^{-/-}$ mice (top right).

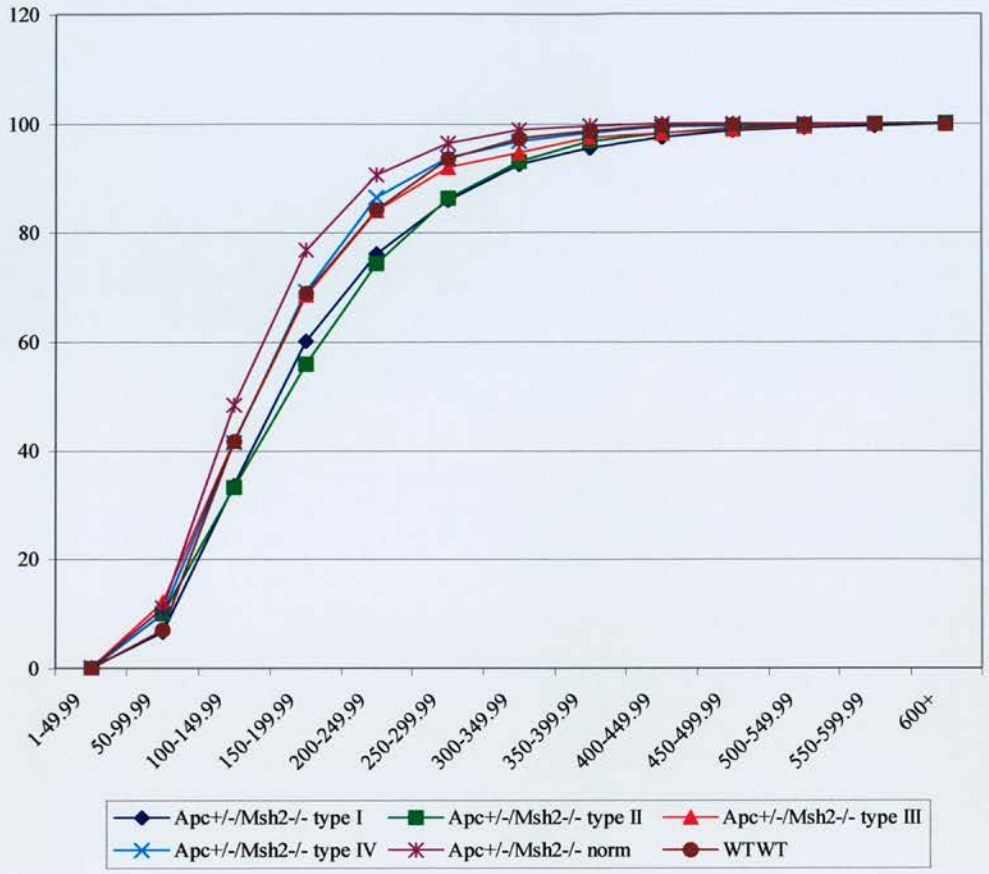

Figure 4.9 Graph showing the distribution of nuclear volume in intestinal lesions arising in mice which were *Apc*$^{+/-}$/*Msh2*$^{-/-}$

Data is presented as a cumulative percentage of cells having nuclear volumes equal or greater than the size categories indicated on the X axis (nuclear volume ranged from 1 to 600+ μm^3). Data is presented for each lesion category (type I, II, III and IV as described in the text). Control data is given, for normal obtained from morphologically normal intestinal crypts in *Apc*$^{+/-}$/*Msh2*$^{-/-}$ mice and wild type mice.

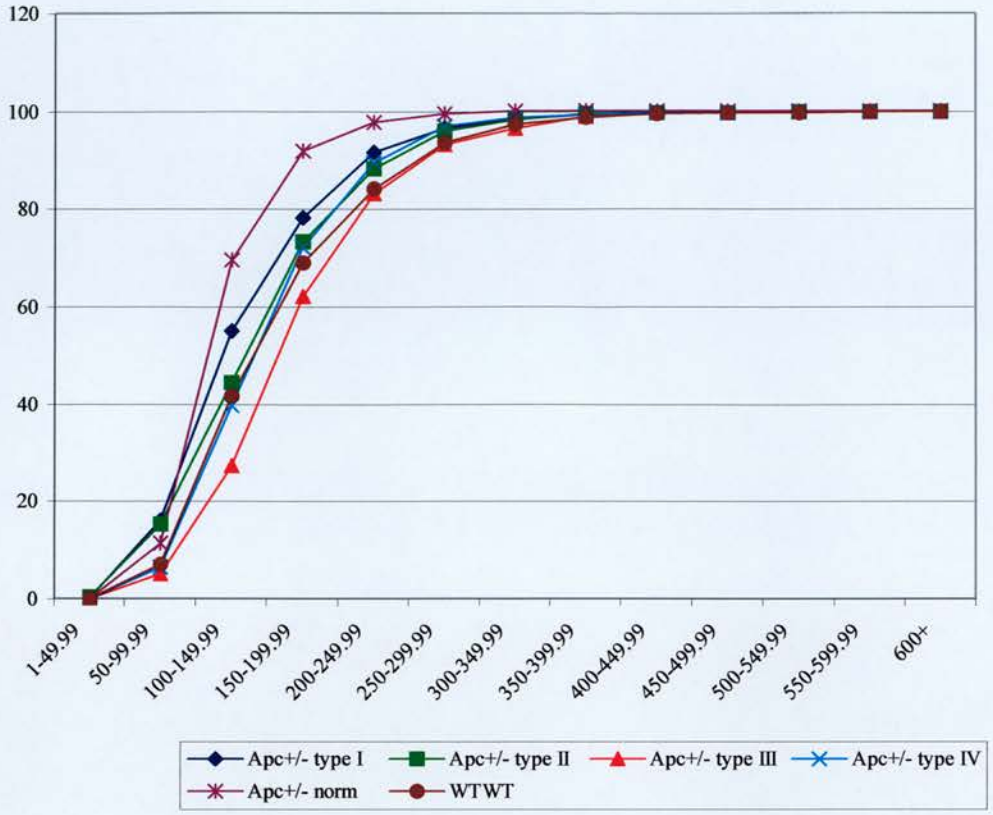

Figure 4.10 Graph showing the distribution of nuclear volume in intestinal lesions arising in mice which were *Apc*$^{+/-}$

Data is presented as a cumulative percentage of cells having nuclear volumes equal or greater than the size categories (nuclear volume ranged from 1 to 600+ μm^3) indicated on the X axis. Data is presented for each lesion category (type I, II, III and IV). Control data is given obtained from morphologically normal intestinal crypts from *Apc*$^{+/-}$ mice and wild type mice.

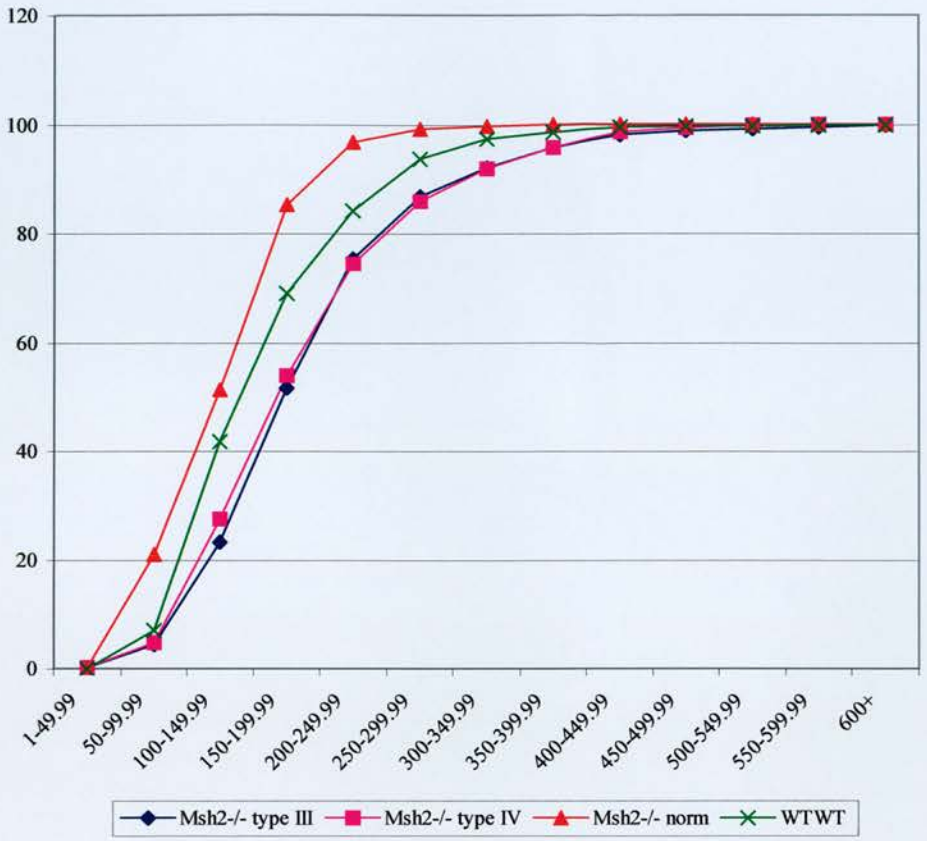

Figure 4.11 Graph showing the distribution of nuclear volume in intestinal lesions arising in mice which were *Msh2*$^{-/-}$

Data is presented as a cumulative percentage of cells having nuclear volumes equal or greater than the size categories (nuclear volume ranged from 1 to 600+ μm^3) indicated on the X axis. Data is presented for lesion category (type III and IV). Control data was obtained from morphologically normal intestinal crypts in *Msh2*$^{-/-}$mice and wild type mice.

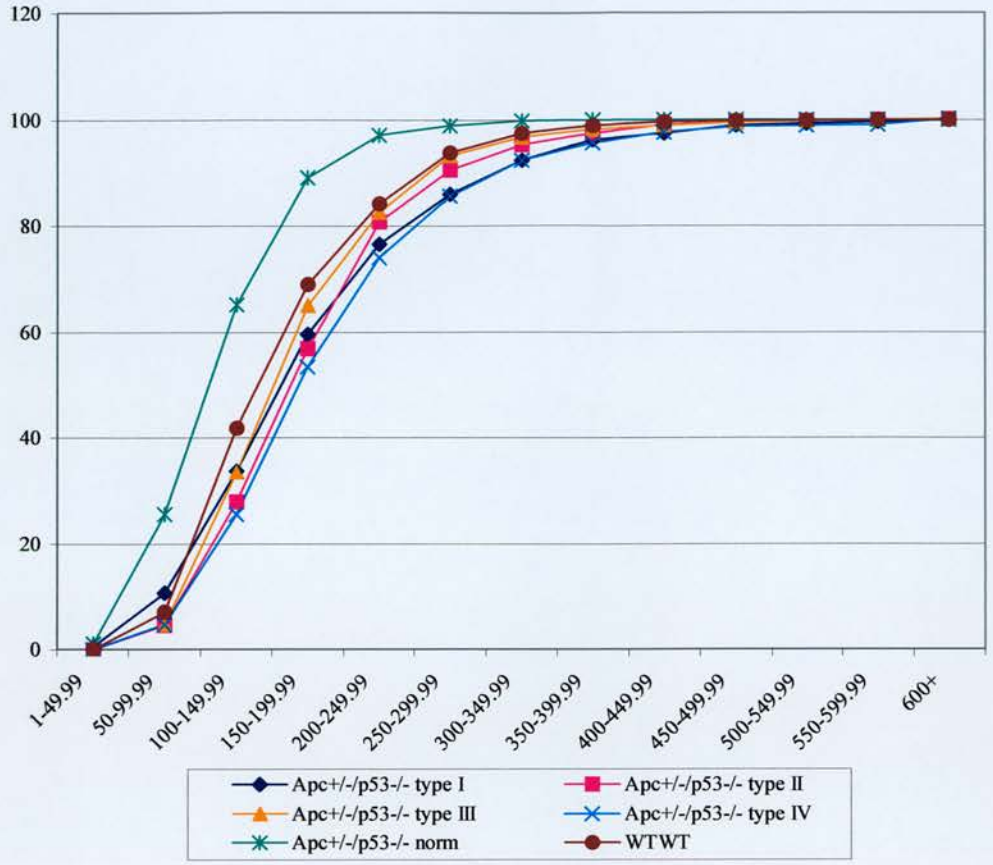

Figure 4.12 Graph showing the distribution of nuclear volume in intestinal lesions arising in mice which were *Apc*$^{+/-}$/*p53*$^{-/-}$

Data is presented as a cumulative percentage of cells having nuclear volumes equal or greater than the size categories (nuclear volume ranged from 1 to 600+ μm^3) indicated on the X axis. Data is presented for each lesion category (type I, II, III and IV). Control data was obtained from morphologically normal intestinal crypts in *Apc*$^{+/-}$/*p53*$^{-/-}$ mice and wild type mice.

(B) Analysis of nuclear volume in spontaneous pancreatic lesions in *Apc* $^{Min+/-}$, (*Apc* $^{Min+/-}$*/p53* $^{-/-}$) and *Msh2* $^{-/-}$

As nuclear pleomorphism was observed in small pancreatic lesions, I wished to characterise this increase in the nuclear volume of cells within these lesions. Lesions in the pancreas were identified by high intensity staining of β-catenin. The nuclear area of cells within the pancreatic lesions, of normal pancreatic acinar cells in mutant mice and of pancreatic acinar cells in wild type animals were measured by using the HOME microscope. The Kolmogorov-Smirnov statistical test was used to compare differences in the profiles of nuclear volume. Statistical data is summarised in appendix D. The nuclear volume of morphologically normal cells in *Apc* $^{Min+/-}$, (*Apc* $^{Min+/-}$*/p53* $^{-/-}$) and (*Apc* $^{Min+/-}$*/Msh2* $^{-/-}$) showed significant increases ($p<0.05$) compared to control data from wild type pancreas (Figure 4.13).

Nuclear volume was markedly increased in all lesion types arising in *Apc* $^{Min+/-}$, (*Apc* $^{Min+/-}$*/Msh2* $^{-/-}$) and (*Apc* $^{Min+/-}$*/ p53* $^{-/-}$) mice compared to morphologically normal cells of the same genotype. For (*Apc* $^{Min+/-}$*/Msh2* $^{-/-}$) and *Apc* $^{Min+/-}$ genotype the most extreme difference were observed in type I lesions with larger lesion types (IV and V) approaching normality (Figure 4.14, and 4.15). Mice, which were (*Apc* $^{Min+/-}$*/p53* $^{-/-}$), showed the most extreme changes in nuclear volume (Figure 4.16). Here again, type I lesions showed the highest degree of change. However, in contrast to the results obtained with the other two genotypes, similar gross changes were observed in the largest (type V) lesions (compared Figure 4.16 with 4.14 and 4.15).

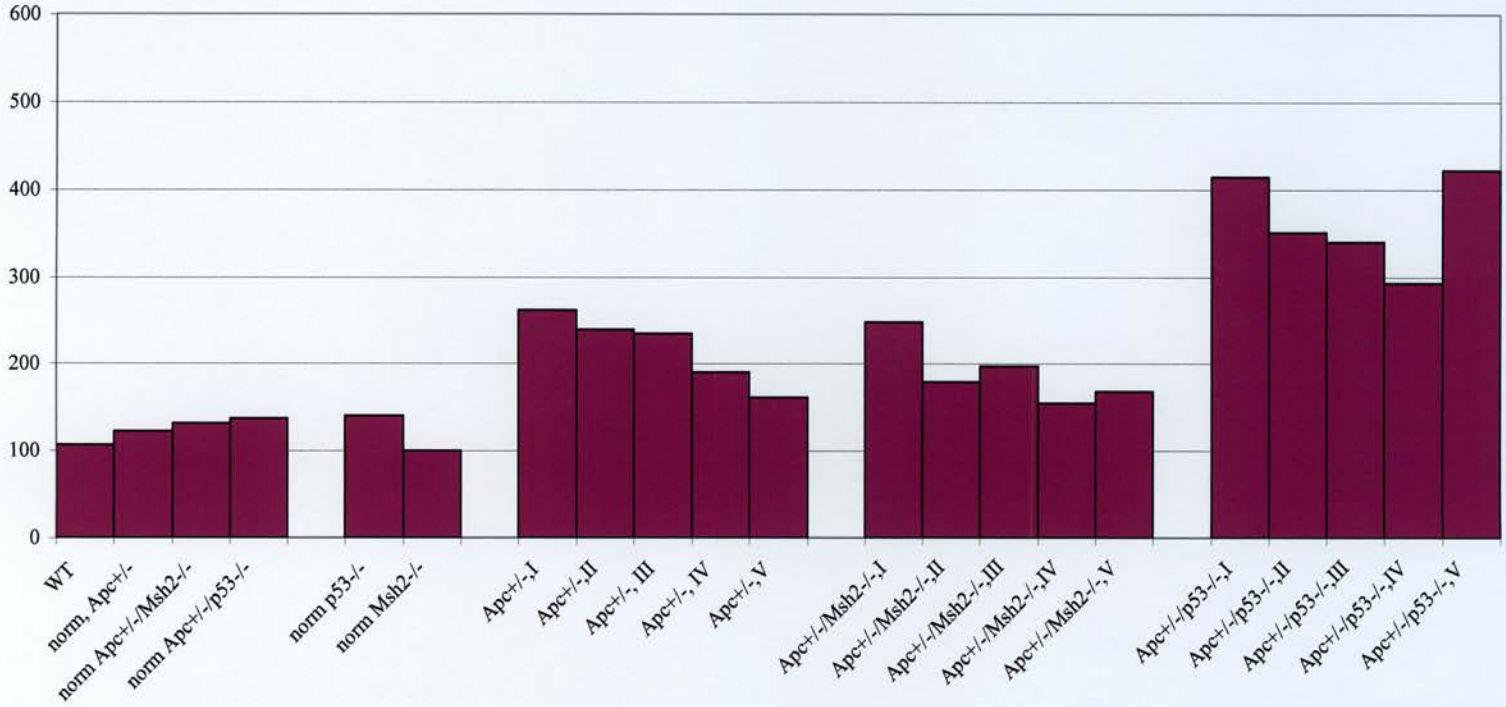

Figure 4.13 Histogram showing the average nuclear volume in spontaneous pancreatic lesions arising in singly and doubly mutant mice at *Apc*, *p53* and *Msh2* alleles

Data are presented as the average of nuclear volume indicated on the Y axis. Data is presented for each lesion category (type I, II, III, IV and V) from each genotype (X axis). Data were obtained from at least 3 mice, which were between 3 to 5 months old. Control data is obtained from morphologically normal pancreatic acinar cells in each genotype and wild type mice.

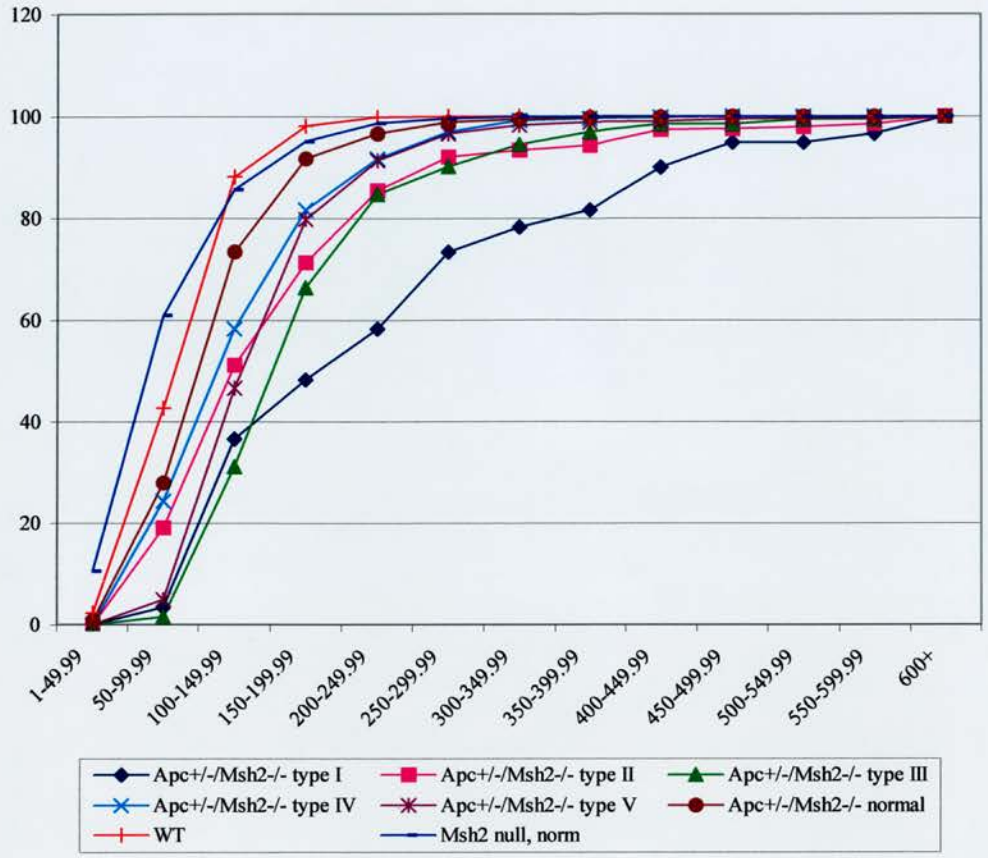

Figure 4.14 Graph showing the distribution of nuclear volume in pancreatic lesions arising in mice which were *Apc*$^{+/-}$/*Msh2*$^{-/-}$

Data is presented as a cumulative percentage of cells having nuclear volumes equal or greater than the size categories (nuclear volume ranged from 1 to 600+ μm^3) indicated on the X axis. Data is presented for each lesion category (type I, II, III, IV and V). Control data was obtained from morphologically normal pancreatic acinar cells in *Apc*$^{+/-}$/*Msh2*$^{-/-}$ mice and wild type animals.

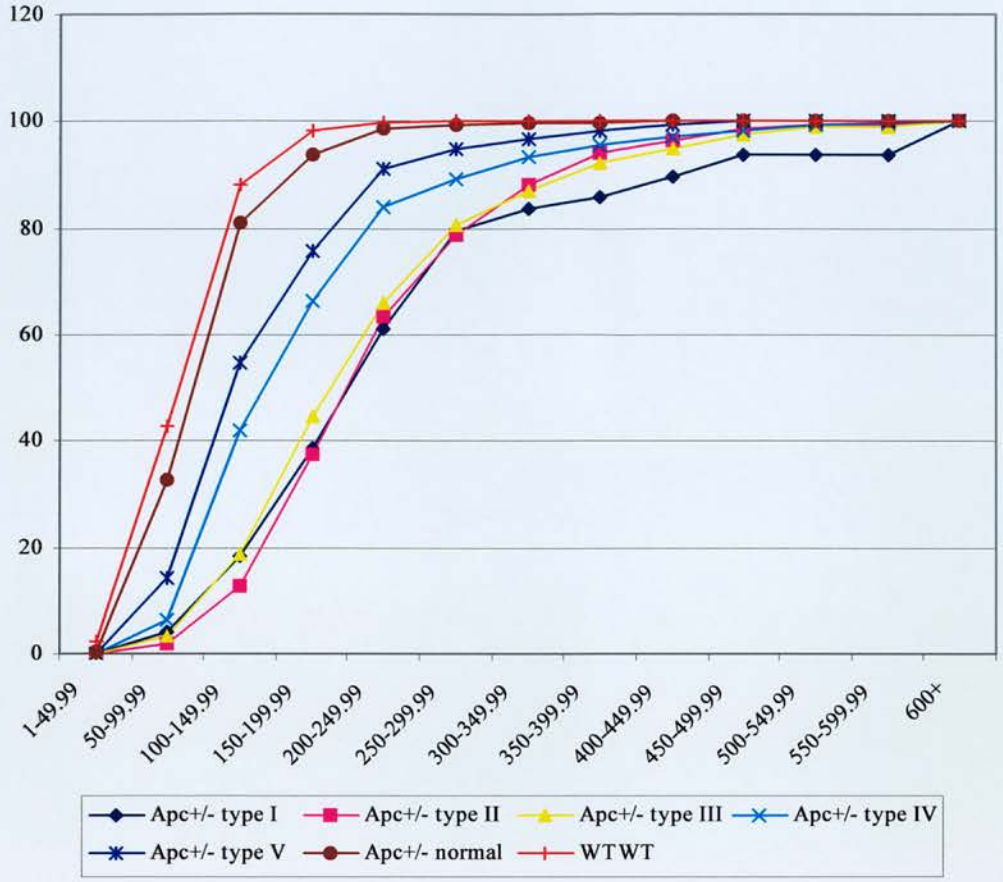

Figure 4.15 Graph showing the distribution of nuclear volume in pancreatic lesions arising in mice which were *Apc*$^{+/-}$

Data is presented as a cumulative percentage of cells having nuclear volumes equal or greater than the size categories (nuclear volume ranged from 1 to 600+ μm^3) indicated on the X axis. Data is presented for each lesion category (type I, II, III, IV and V). Control data was obtained from morphologically normal pancreatic acinar cells in the *Apc*$^{+/-}$ mice and wild type mice.

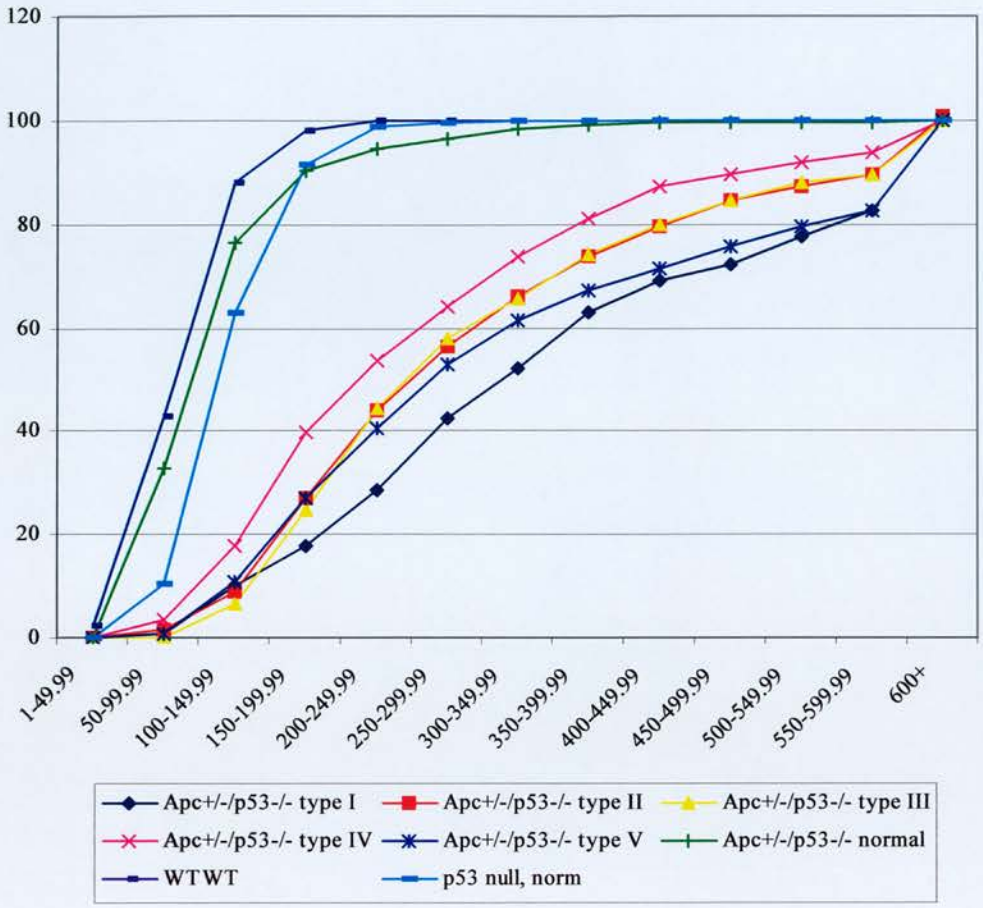

Figure 4.16 Graph showing the distribution of nuclear volume in pancreatic lesions arising in mice which were *Apc*$^{+/-}$/*p53*$^{-/-}$

Data is presented as a cumulative percentage of cells having nuclear volumes equal or greater than the size categories (nuclear volume ranged from 1 to 600+ μm^3) indicated on the X axis. Data is presented for each lesion category (type I, II, III, IV and V). Control data was obtained from morphologically normal pancreatic acinar cells in *Apc*$^{+/-}$/*p53*$^{-/-}$ mice and wild type mice.

(C) Analysis of BrdU incorporation in spontaneous intestinal lesions arising in (*Apc* $^{Min+/-}$*/Msh2* $^{-/-}$) and *Msh2* $^{-/-}$

By using BrdU incorporation it was possible to (a) determine the number of cycling cells in lesions compared with morphologically normal cells in wild type animals; and (b) to address whether any observed increase in nuclear volume was occurring solely because of an increase in the cell turnover or because of an underlying genetic instability.

Mice singly or doubly mutant for *Apc* and *Msh2* were injected with BrdU 2 hours prior to killing to identify those cells in S phase in the intestinal lesions and compared with wild type mice. BrdU index was calculated from the number of BrdU positive cells in the total number of cells obtained from each lesion type in each genotype of animals. Preliminary studies were performed, because there were constraints on the availability of mice. This study therefore remains to be completed for all lesion types.

Preliminary data presented here suggest that, in morphologically normal cells, *Msh2* mutant and *Apc* mutant mice have an elevated BrdU index (Figure 4.17) compared to cells in a wild type background. Surprisingly, (*Apc* $^{Min+/-}$*/Msh2* $^{-/-}$) cells did not differ from those in a wild type background.

In *Apc* $^{Min+/-}$ mice, the BrdU index was seen to rise in lesions of through categories I to III (Figure 4.17). In *Msh2* null mice a similar increase was seen with larger category size with a reduction in the index in category IV lesions. In (*Apc* $^{Min+/-}$*/Msh2* $^{-/-}$) lesions the pattern was again similar, although the increase in index was less marked through lesions I to III and there was no reduction in index in category IV lesions (Figure 4.17).

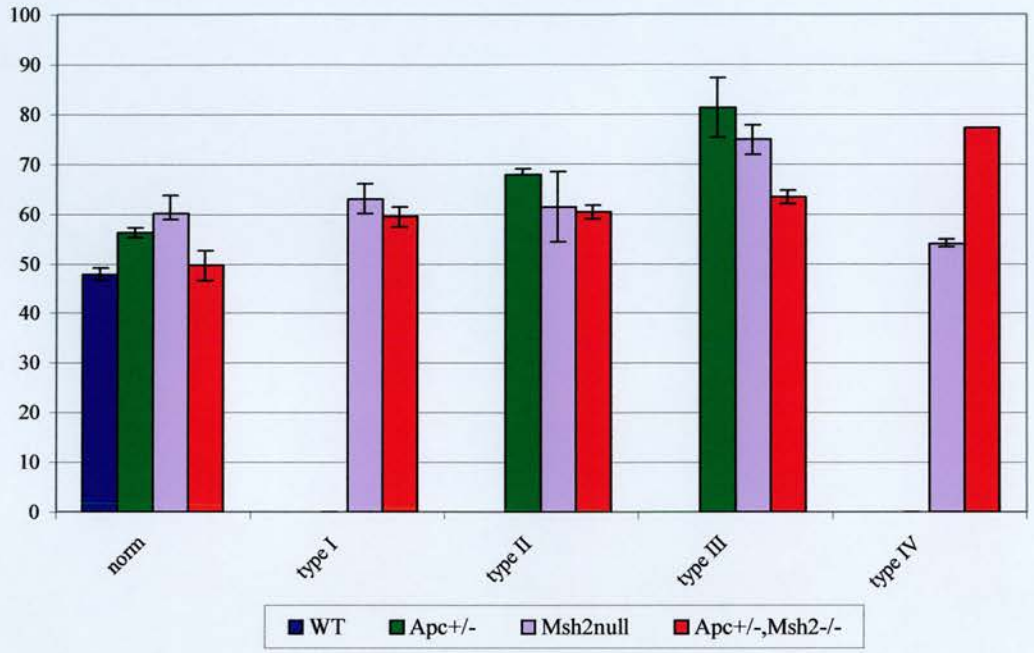

Figure 4.17 Histogram showing BrdU index in the intestinal lesions arising in *Apc*$^{+/-}$, *Msh2*$^{-/-}$ and *Apc*$^{+/-}$/*Msh2*$^{-/-}$ mice

Data is presented as percentage of BrdU index, indicated on the Y axis, of BrdU positive cells, observed in each lesion type (type I, II, III, and IV) indicated on the X axis. Control data was obtained from the wild type animals and morphologically normal intestinal crypt cells. Bar indicates range of mean average.

I finally analysed nuclear volume in relation to the BrdU index. Cumulative nuclear volume from both BrdU positive and negative cells within each lesion type was compared to comparable data from morphologically normal tissue for that genotype. Across all genotype analysed, the BrdU positive cells showed the largest nuclear volume, as predicted ($p<0.05$). Actual differences in nuclear volume irrespective of cell cycle status may be inferred from a comparison of the distributions obtained for BrdU positive cells between cells within lesions and cells with morphologically normal epithelium. Such comparisons suggest that in some lesion categories there is a clear difference in ploidy (for example in *Apc* $^{Min+/-}$ type II and III lesions as shown in Figure 4.18). Alternatively, other lesions show almost identical distributions (the majority of lesions arising in either *Msh2* $^{-/-}$ as shown in Figure 4.19 or (*Apc* $^{Min+/-}$*/Msh2* $^{-/-}$) mice as shown in Figure 4.20).

Such comparisons of course assume that BrdU positive cell populations are at an equivalent stage in the cell cycle, which has not formally been proven for the cells analysed here.

Only a few BrdU positive cells was observed in the pancreatic lesions [within type II lesions arising in (*Apc* $^{Min+/-}$*/Msh2* $^{-/-}$) mice] and no BrdU positive cell was observed in morphologically normal pancreatic acini. Therefore, a comparison in the pancreas was not possible.

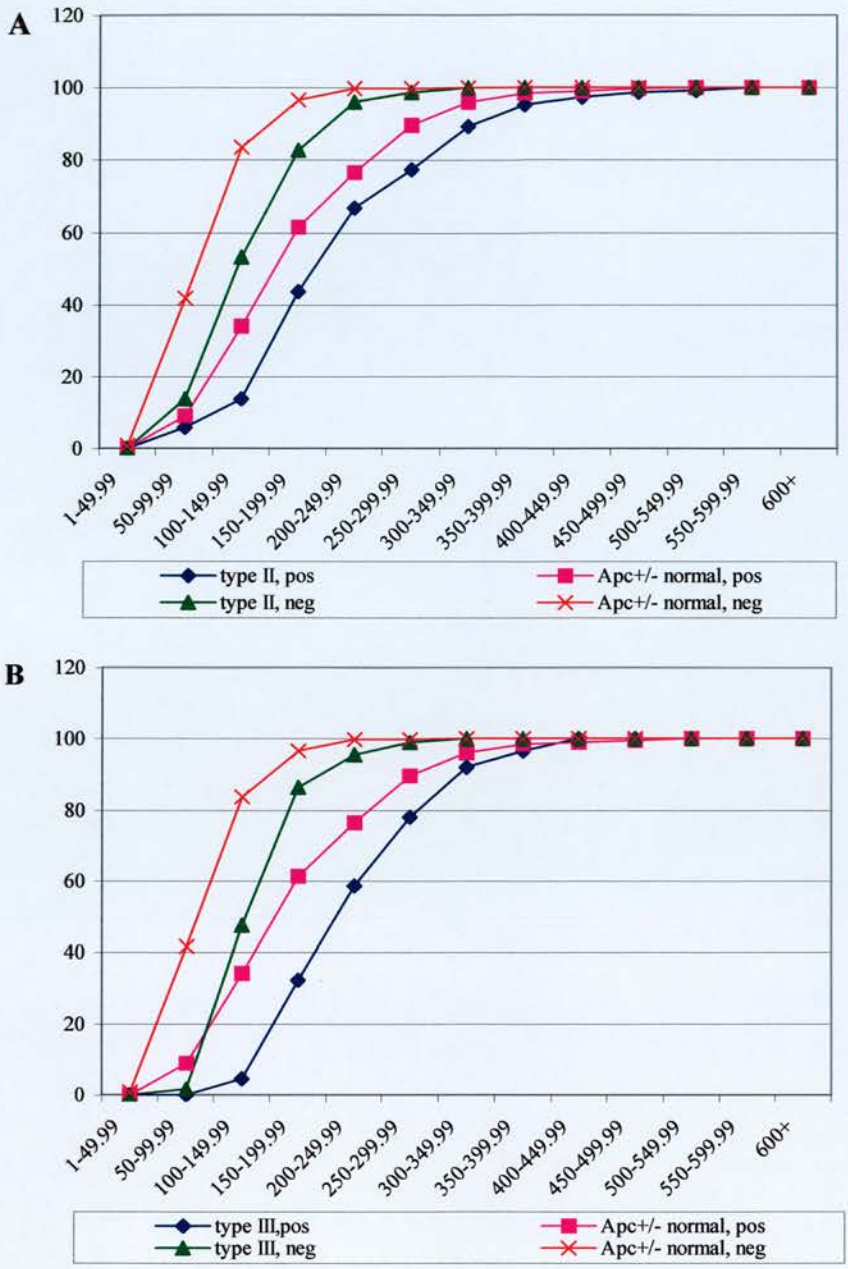

Figure 4.18 Graph showing the distribution of nuclear volume in intestinal lesions arising in *Apc*$^{+/-}$ mice

Data is presented as the cumulative percentage of cells having nuclear volume equal or greater than the size categories indicated on the X axis. Data is presented for each lesion categories (type I, II, III and IV). Control data was obtained from wild type mice and morphologically normal intestinal crypt cells. Graph A is represented a cumulative percentage of nuclear volume in type II lesion; Graph B is represented a cumulative percentage of nuclear volume in type III lesion compared with nuclear volume obtained from morphologically normal crypts.

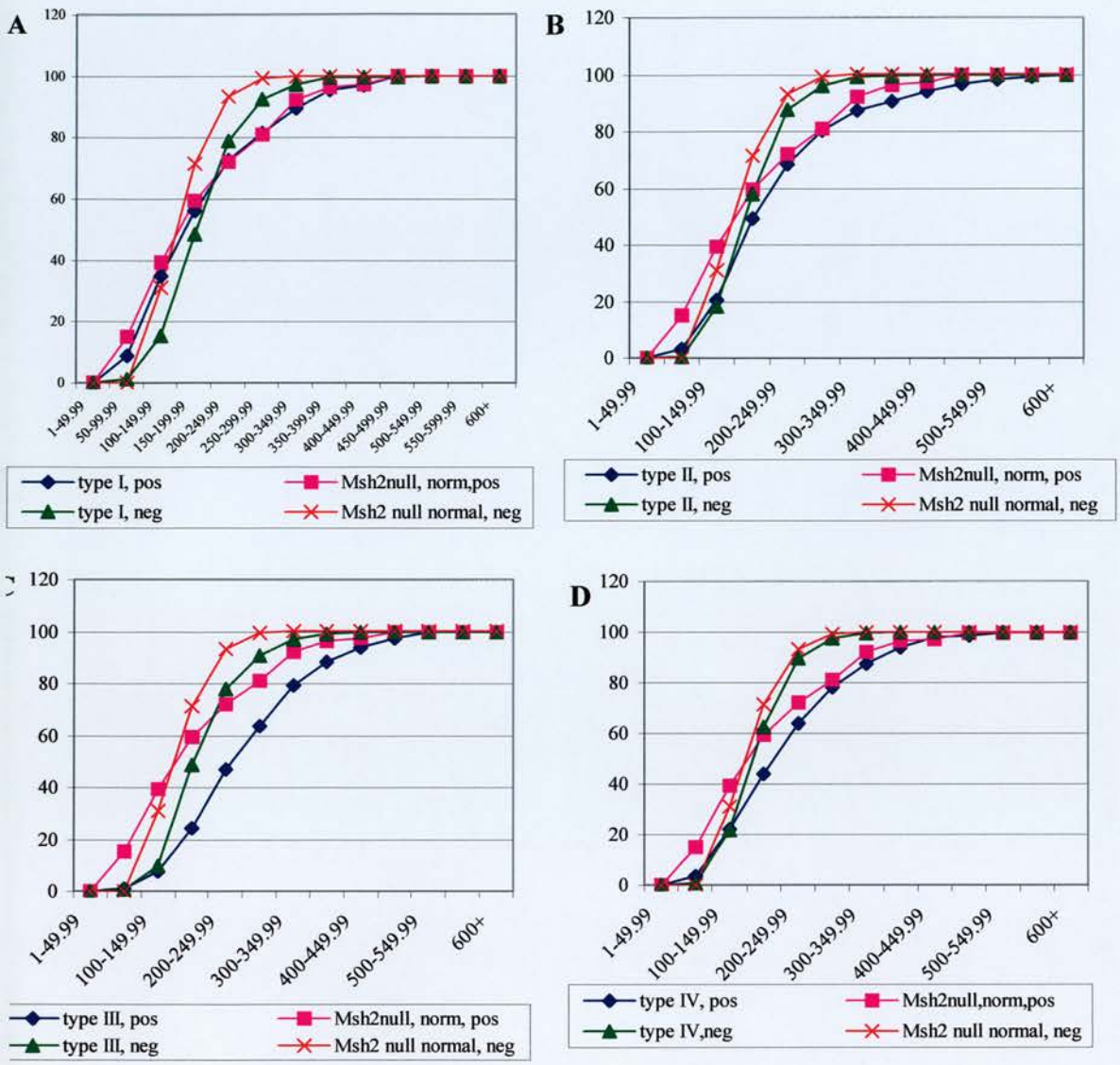

Figure 4.19 Graphs showing the distribution of nuclear volume in intestinal lesions arising in *Msh2*$^{-/-}$ mice with BrdU incorporation

Data is presented as the cumulative percentage of cells having nuclear volume equal or greater than the size indicated on the X axis. Data is presented for each lesion category (type I, II, III and IV) which showed BrdU positive and BrdU negative cells. Control data was obtained from wild type mice and morphologically normal intestinal crypt cells from *Msh2*$^{-/-}$ mice. Graph A presents the cumulative percentage in type I lesion; Graph B represents cumulative percentage in type II lesion; Graph C represents cumulative percentage in type III lesion and Graph D represents cumulative percentage in type IV lesion, compared with the nuclear volume obtained from morphologically normal crypt cells.

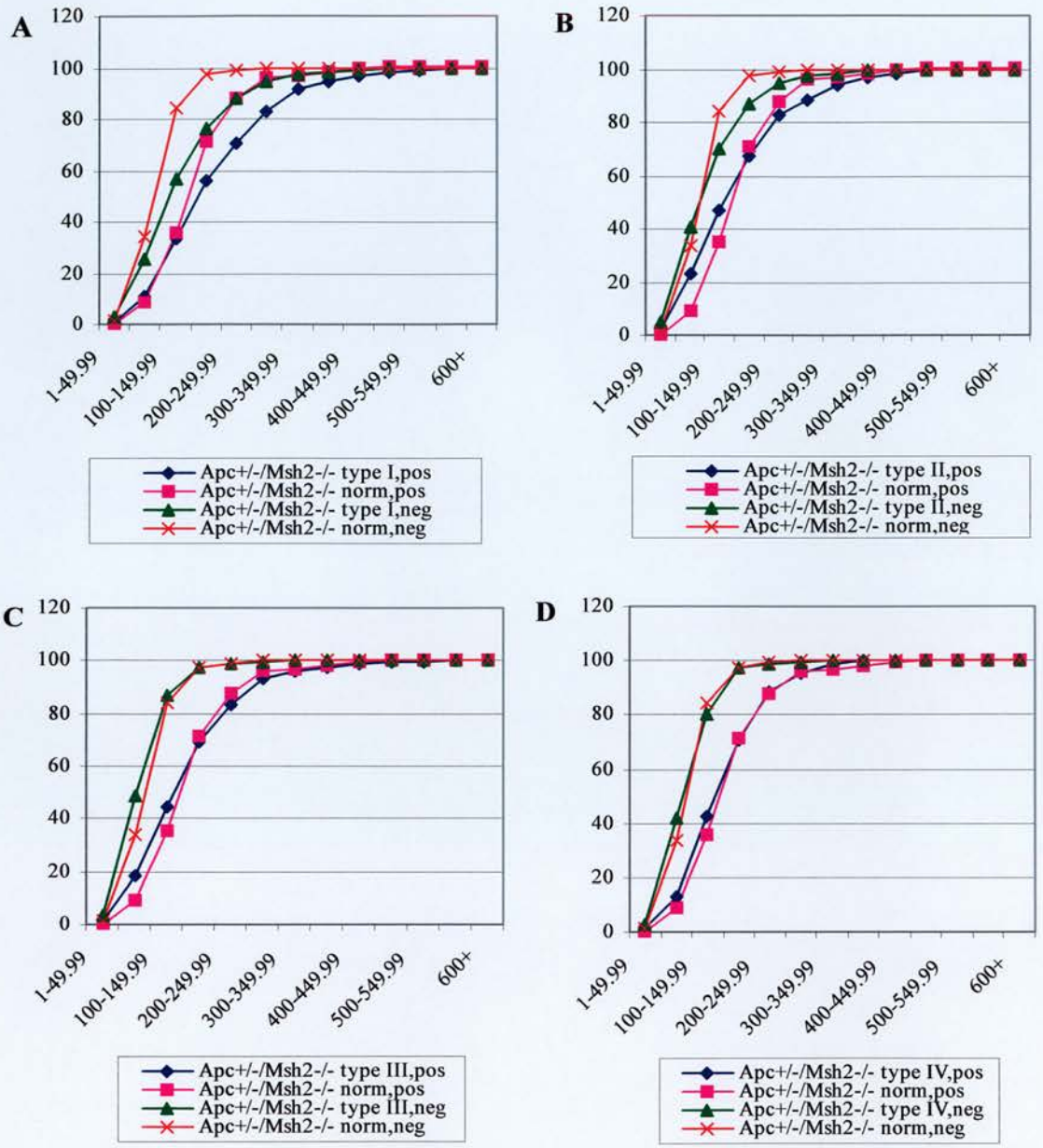

Figure 4.20 Graphs showing the distribution of nuclear volume in intestinal lesions arising in *Apc*$^{+/-}$*/Msh2*$^{-/-}$ mice with BrdU incorporation

Data is presented as the cumulative percentage of cells having nuclear volume equal or greater than the size categories indicated on the X axis. Data is presented for each lesion category (type I, II, III and IV). Control data was obtained from wild type mice and morphologically normal intestinal crypt cells from *Apc*$^{+/-}$*/Msh2*$^{-/-}$ mice. Graph A presents the cumulative percentage of the nuclear volume in type I lesion; Graph B presents cumulative percentage of the nuclear volume in type II lesion; Graph C presents cumulative percentage of the nuclear volume in type III lesion and Graph D presents cumulative percentage of the nuclear volume in type IV lesion compared with the nuclear volume obtained from morphologically normal crypt cells.

4.3. Discussion

4.3.1. Three dimensional study

The three-dimensional study of nuclear content in both intestinal and pancreatic lesions was hindered by the density of the cells within lesions, which made it extremely difficult to isolate individual nuclei and accurately measure DNA content. In addition, three-dimensional analysis is an extremely time-consuming procedure. The distributions of nuclear volume obtained from the intestinal lesions arising in (*Apc* $^{Min+/-}$*/Msh2* $^{-/-}$) mice obtained by 3D study analysis were approximately comparable to those obtained using 2D analysis, however the quality of data obtained from 3D analysis was surprisingly poor. This could have occurred as a consequence of the analysis of fewer cells, a factor that clearly limits the power of the 3D study. Thus, although theoretically the 3D analysis should be a more powerful approach, I found that in practice the 2D approach yielded more data and was in fact used for all subsequent analysis. I would conclude that in the tissue samples analysed here the 3D method is not a suitable practical method to determine nuclear content.

4.3.2. Two dimensional study

Nuclear volume analysis in the intestinal tumour lesions arising in mutant mice showed that there was an increase in nuclear size when compared to wild type mice and normal intestinal crypts from each genotype of mice. The change in nuclear volume in intestinal tumour lesions was only small but still significant. This difference probably arose from either from a real change in ploidy or from an increase in cell turnover rate. In fact the BrdU index (Figure 4.17) suggested that in the larger lesions, the difference in the nuclear volume is due to an increase in the cell turnover. In a more detailed analysis of volume only with BrdU positive cells, I obtained evidence that in at least some lesions the increase in volume was occurring due to increased turnover. However, notably this did not seem to be the case for type II and III lesions in *Apc* $^{Min+/-}$ mice. In BrdU negative cells from all genotypes in all lesions, the nuclear volume is larger than the nuclear volume obtained from morphologically normal crypt cells. This either

reflects very subtle changes in DNA ploidy, or suggests there was an increase in the number of cells in compartments of the cell cycle other than S phase that showed relatively increased nuclear volume (i.e. such as an increase in cells at the G_2 checkpoint).

Nuclear volume analysis in the pancreatic lesions showed a marked increased in nuclear size when compared with pancreatic acinar cells from wild type mice and with morphologically normal pancreatic nuclei in mutant mice. A greater increase in the nuclear volume was observed in early lesions (type I, II and III) than in the late lesions (type IV, V and VI) in every genotype of mice. In the late lesion stage it appears that the size of the nuclei is again approaching normality. This suggests that there is an increase in genomic instability in small lesions but that the cells which predominant in the large lesions show less divergence from normality. Interestingly, a *p53* deficient background resulted in much more extreme changes in nuclear volume in all lesion types when compared to lesions arising in either (*Apc* $^{Min+/-}$*/Msh2*$^{-/-}$) or (*Apc* $^{Min+/-}$*/p53*$^{+/+}$) mice. These results support the notion that *p53* mutations contribute to tumour progression by promoting genetic instability (Gualberto *et al* 1998). Gualberto *et al* showed that absence of wild type *p53* in knockout mice permits the generation of polyploid cells. Fukasawa *et al* (1997) also demonstrated that loss of the p53 tumour suppressor functions results in genetic instability, associated with changes in chromosome ploidy and gene amplification. My findings of an increase in nuclear volume in pancreatic lesions arising in a *p53* deficient background are supported by these studies. The resulting genetic instability caused by *p53* deficiency could be due to a number of mechanisms, including p53's role in the regulation of centrosome duplication, a loss of p53-dependent apoptosis for eliminating cells with genetic damage (Clarke *et al* 1993). Or loss of the *p53* controlled G_2 checkpoint that prevents entry into mitosis after DNA damage (Bunz *et al* 1998) and arrested cells with damaged DNA in G_1 checkpoint. Lack of G_1 checkpoint control is an early event in the process of carcinogenesis where it is associated with the malignant transformation of individual cells (Syljuasen *et al* 1999, Venkatachalam *et al* 1998). Many groups have reported that inactivation of *p53* renders cells more susceptible to gene amplification and the development of aneuploidy (Levine

et al 1991, Livingstone *et al* 1992, Hartwell and Kastan 1994, Jacks and Weinberg 1996, Ko and Prives 1996).

Within pancreatic acinar cell lesions, nuclear volume was markedly increased in comparison to that of normal cells and this difference was not due to cell turnover as only a few cycling cells were observed. The extent of difference in nuclear volume was found to be influenced by both losses of *Apc* and *p53*. These genotypes had little effect on the nuclear volume of cells in intestinal lesions, suggesting that the genetic basis for controlling genetic stability is markedly different between these two tissue types.

Overexpression of β-catenin in wild type mice has previously been shown to promote the accumulation of functionally competent *p53* (Damalas *et al* 1999). Subsequently, activation of *p53* is known to be capable of promoting apoptosis, which may represent a mechanism of controlling genetic instability and be reflected in the small differences in nuclear volume observed in the pancreatic lesions arising in ($Apc^{Min+/-}/Msh2^{-/-}$) and ($Apc^{Min+/-}/p53^{+/+}$) mice. Overexpression of β-catenin has also recently been demonstrated to correlate with decreased cell proliferation and apoptosis (Mahmoud *et al* 1997) which support my observation that in the pancreas mitotic figures could only be observed in very large lesions.

In $Apc^{Min+/-}$ mice, the changes in nuclear volume obtained within cells in pancreatic lesions were greater than those observed (figure 4.15) in the intestinal lesions (Figure 4.10). However taken together this increase in the nuclear volume of cells in $Apc^{Min+/-}$ mice, provides *in vivo* evidence in support of the concept that *Apc* may function to negatively regulates cell growth by inhibiting cell cycle transition from the G_1 phase to S phase at the middle to late G_1 phase (Baeg *et al* 1995, Heinen and Groden 1999). Therefore, mutations or loss of Apc could lead to an increased number of cells moving from G_1 to S phase and result in an increased BrdU index as was observed in the intestinal lesions in the preliminary study presented here (Figure 4.17). It has been reported that EB1, a partner of Apc, is localised both to cytoplasmic microtubules in interphase cells and to spindle microtubules during mitosis (Berrueta *et al* 1998, Morrison *et al* 1998). The association between EB1 and APC suggests a possible role for Apc in cellular division and the control of normal growth and differentiation of epithelial

cells. EB1 has been shown to function as a cytokinesis checkpoint in yeast (see detail in chapter1). Thus, Apc may indirectly regulate cytokinesis via EB1. Thus, the absence or mutation of Apc could lead to genomic instability.

In vitro experiments suggested that β-catenin may function as an oncogene by promoting the G_1 to S phase transition and protecting cells from suspension-induced apoptosis (Orford *et al* 1999). One mechanism by which this could occur is by activation of the *c-myc* promoter, which has been suggested as one target of the Wnt pathway. Interestingly, diploid cells have shown to be highly susceptible to the development of tetraploid when c-myc overexpression is coupled to p53 deficiency (Yin *et al* 1999). In fact, synergy between p53 and c-myc overexpression has been observed in many systems including the promotion of genomic instability in a mouse model of mammary neoplasia (McCormack et al 1998). It has been suggested that activation of c-myc would result in an increase in cyclin D1 protein (Rosenwald *et al* 1993, He *et al* 1998). Alternatively, overexpression of β-catenin has been demonstrated to directly activate the cyclin D1 (Zhang *et al* 1997) and result in an increase expression of cyclin D1 (Tetsu and McCormick 1999). Overexpression of cyclin D1 is known to shorten the G_1 to S transition and thus promote cell progression (Sherr 1994). Other genes have been implicated as downstream targets of β-catenin, these may also influence neoplastic development and include Cdk4 (Zhang *et al* 1997) and AP-1 (Mann *et al* 1999).

In ($Apc^{Min+/-}/Msh2^{-/-}$) mice, the average nuclear volume obtained from morphologically normal pancreatic acinar cells and cells within lesions was again greater than that obtained from normal cells in ($Apc^{+/+}/Msh2^{-/-}$) mice, supporting the concept that changes in nuclear volume was caused by loss of Apc function. In contrast, *Msh2* deficiency appeared to have no effect upon nuclear volume, as comparison of the nuclear volume of the cells from pancreatic lesions in $Apc^{Min+/-}$ and ($Apc^{Min+/-}/Msh2^{-/-}$) mice it showed no marked difference. This is as predicted from studies of hereditary non-polyposis colon cancer in human where tumour predominantly retains their diploid status. *Msh2* primarily functions in the initial recognition of mismatched nucleotides generated during DNA replication (Fishel *et al* 1993, Leach *et al* 1993). Thus, the absence of *Msh2* leads to the loss of function of this repair pathway and the induction of

microsatellite instability and replication error positivity (RER^+). It has been reported that *Msh2* also functions in mediating the deletion of cells with DNA damaged (Toft *et al* 1999). These two roles show that *Msh2* is critical in the surveillance of cells with DNA damaged and the absence of *Msh2* may lead to genetic instability at the sequence level and predisposes to tumour development.

By analysing the level of BrdU incorporation, the data showed that the number of S phase cells in the intestinal lesions was increased compared to the number of S phase cells observed in wild type mice and morphologically normal tissue as shown in figure 4.17. In addition, the BrdU index increased when the lesion was larger. This suggested that in late stage lesions there was an increase in the S phase component. There are two possible explanations for this increase in the number of S phase cells; first, an increase in cell turnover rate and second, an increase in S phase duration (Bleiberg *et al* 1985). From my data, the BrdU index showed an increase in intestinal lesions but BrdU was extremely low in pancreatic lesions. From this data it is not possible to determine which of these possibilities was the most likely. It is possible that the failure to detect many BrdU positive cell in the pancreas occurred because of a failure of BrdU to incorporate within cells in this tissue or because this truly reflects a very slow turnover rate. To independently determine the proliferation rate in pancreatic tissue, immunostaining with the cell proliferation marker Ki67 was performed but unfortunately the pattern of staining obtained was inconsistent and there was high background, which made it difficult to interpret the results. Moreover, the specimen material was of limited supply so I was unable to satisfactorily complete this section of the experiment. However, an estimation of the mitotic index, which is another method to detect cellular proliferation, was performed. A scorable mitotic index was only identified within very large lesions (type VI lesion). Therefore, this would suggest that the cell turnover rate in the pancreas is very low both in morphologically normal cells and during tumour development.

The nuclear volume of BrdU positive cells was larger than the nuclear volume of BrdU negative cells. This is not surprising as it is well recognised that cells in S phase have an increased DNA content due to synthesis. A similar pattern of cumulative distribution in nuclear volume was observed in each type of lesion in all genotype of

mice. In *Apc* $^{Min+/-}$ mice the BrdU index was observed to rise through lesion categories I to III and a similar increase was seen in *Msh2* $^{-/-}$ mice but in *Msh2* null mice type IV lesions showed a reduction in the BrdU index. In (*Apc* $^{Min+/-}$/*Msh2* $^{-/-}$) mice, the BrdU index was observed to rise through lesion categories I to III. These data suggested that differences in nuclear volume are influenced by *Apc* mutations, which may be responsible for later progression of intestinal tumorigenesis. The data obtained on the *Apc* ^{Min} background contrasts with that on the *Apc* $^{Min+/-}$ and *Msh2* $^{-/-}$ background, where the volume of S phase cells is, overall, similar between morphologically normal cells and cells within lesions. These observations again suggest that Msh2 deficiency is not driving marked ploidy change in contrast to the situation with *Apc* ^{Min}.

Taken together, the results showed that in a *p53* deficient background there was an extreme change in nuclear volume in the pancreatic lesions. These changes were initiated by loss of Apc function but were not influenced by loss of *Msh2*. Intestinal lesions showed much smaller differences in nuclear volume. Preliminary data analysing BrdU incorporation suggests that an increase in the nuclear volume in intestinal lesions could be accounted for both by an increase in cell turnover and also by changes in DNA ploidy. The former of these was associated with loss of *Msh2*, the later with loss of *Apc*. Where these mutations were combined it was of interest to note that the prevailing pattern resembled that seen in *Msh2* null mice rather than in the *Apc* ^{Min} mice.

Chapter 5

3D image analysis of the apoptotic response in normal murine small intestine

Small intestinal epithelial crypts have been used as a model for studying the cellular response to various stresses. Most studies have been undertaken in two dimensions and are unable to demonstrate dynamic changes in response to injury in the intestinal crypt. This study was designed to investigate early and delayed apoptotic response induced by γ-irradiation in the murine model by using three-dimensional reconstruction. In this chapter, the p53 tumour suppressor gene protein, Apc protein and Ki67 protein expression patterns are analysed and three dimensional reconstruction attempted of normal small intestinal crypts in *p53* wild type and in a specific *p53* genetic defect mouse with immunohistochemistry staining on serial tissue sections.

γ-Irradiation is an extrinsic source that causes DNA damage whilst intrinsic damage is generated by the cell itself, either as a result of DNA metabolism or as a result of spontaneous chemical reactivity of DNA such as DNA alkylation (e.g. etoposide treatment), reactive oxygen species, or defects in mitosis. Apoptosis possesses two major morphological features: cell shrinkage and nuclear condensation (Kerr *et al* 1972). The microscopically visible part of the process depends upon:

(1) The characteristics of the tissue or cell system being studied,

(2) The degree of fragmentation that occurs during the apoptotic process,

(3) The removal mechanisms of the apoptotic fragments and

(4) Sensitivity of the detection procedures (Potten 1996).

Apoptosis characteristically affects scattered single cells not groups of cells, as is the case with necrosis. Apoptosis is manifested histologically by the formation of small, roughly spherical or ovoid cytoplasmic fragments, some of which contain

pyknotic remnants of nuclei (Kerr *et al* 1972). Apoptotic bodies arising in tissues are quickly ingested by nearby cells and degraded within their lysosomes. There is no inflammatory response such as occurs in necrosis (Kerr *et al* 1994). During apoptosis, ultrastructural alterations in of the cytoplasm are rather non-specific whereas the nuclear characteristics are relatively drastic changes. These include chromatin condensation and nuclear fragmentation. Cells undergoing apoptosis show morphological changes, including plasma and nuclear membrane blebbing, cell shrinkage, and chromatin condensation and fragmentation. These changes distinguish apoptosis from necrosis (Wyllie *et al* 1980). Necrosis is caused by physical, chemical or osmotic damage that results in disruption of internal and external membranes of cells and cell organelles. The cytoplasm of the necrotic cell becomes grossly swollen, the cell membrane and organelle membrane progressively disintegrate. Lytic necrosis produces the release of denatured proteins and DNA fragments into the intercellular space as well as local inflammatory responses. Therefore, cells undergoing apoptosis exhibit intact external membranes until late phases of the metabolic suicide. The adjacent cells engulf the dying cell and eliminate it before its contents are released and thus avoid triggering local inflammatory reactions.

In 1980, Wyllie showed that apoptosis was associated with a unique change in the nuclear DNA. There was double-stranded cleavage at the linker regions between nucleosomes, leading to the formation of fragments that were multiples of 180-200 base pairs. These fragments could be detected by agarose gel electrophoresis. The cleavage affected nuclear but not mitochondrial DNA and was indicative of apoptotic cell death (Kroemer *et al* 1995).

Apoptosis is both a genetically controlled response to injury (White 1996) and also has a major role in normal development. It is believed that cells can activate an intrinsic death program and thus actively contributed to their own death. The duration of the apoptotic process is largely unclear (Potten 1996). Apoptotic processes involve the active participation of endogenous cellular enzymes well before membranes loose their integrity. The resulting DNA damage is 'sensed' by the cell, via activation of *p53* or other molecules, and the cell either arrests in the cycle or undergoes apoptosis

(Green and Martin 1995). Signal transduction pathways leading from receptors, such as Fas and the TNF receptor, to the activation of effectors of cell death, such as the Caspase protease family, have been elucidated (Nagata 1997).

5.1. Materials and Methods

5.1.1. Mice

Out-bred wild type male mice and out-bred *p53* genetic defects mice (Clarke *et al* 1993), aged between 8-10 weeks were used in this study. *p53* mutant animals were from an outbred colony segregating for Ola/129 and SWR genomes. All animals were kept in an animal house in conditions that include good ventilation, food and water *ad libitum*, 3-4 mice per cage. Groups of 3 mice were exposed in plastic cages to -- γ-irradiation from a ^{137}Cs source at 5 Gray (Gy) for 15 minutes (Clarke *et al* 1994). Wild type *p53* animals were killed by cervical dislocation at the following time points, 2 and 4 hours after irradiation for observation of the early apoptotic response. *p53* null animals were sacrificed at 23, 24, and 25 hours after irradiation for observation of the delayed apoptotic response (Clarke *et al* 1997, Merrit *et al* 1997). Non-exposed mice were transported to the radiation unit together with the treated mice and subjected to a similar routine for control of the apoptotic response induced by stress.

5.1.2. Tissue processing

The whole ilea were selected for analysis because the apoptotic index is higher here than for other regions of the small intestine (Toft, unpublished data). Intestines were removed immediately from mice after cervical dislocation and were fixed in 10% formal buffered saline. One centimetre tail tips of each mouse were taken for reconfirmation of the mouse genotype. The specimens were processed manually to minimise damage to the antigenicity. The swiss rolls of intestine (see appendix A) were dehydrated in a series of ethanols at concentration of 50%, 70%, 85%, and 90% for 20 minutes twice and absolute ethanol for 40 minutes, repeated 3 times. The specimens were cleared in xylene changed three times, every 40 minutes, subsequently blocked in paraffin wax at 56 ^{0}C. The specimens underwent 3 changes of paraffin wax, every 40 minutes. Finally, the specimens were embedded in paraffin wax.

5.1.3. Immunohistochemistry

The number of three micron serial sections was determined (to give the complete intestinal crypt), three micron thick sections were cut longitudinally serially for 40 sections. Immunohistochemistry technique was performed as previously described (see appendix A). High temperature antigen retrieval technique was performed (see appendix A) as required for p53 and Ki67 antigens (see table 2.1), followed by endogenous peroxidase blocking for 15-20 minutes. Non-specific binding blocking was blocked by incubation in 20% normal serum corresponding to the secondary antibodies used for 20 minutes. The first section was incubated with Ki67 antibody (NCL-Ki67-MM1, Novocastra, UK) which detected cell proliferation in every phase of cell cycle except G_0, the second section was incubated with APC antibody (Midgley *et al* 1997), the third section was incubated with p53 antibody (NCL-p53-CM5p, Novocastra, UK) and the fourth section was stained with haematoxylin and eosin. Immunohistochemistry was performed as described in appendix A.

5.1.5. PCR analysis of *p53* locus

Genomic DNA was extracted from the tail tip of the mice by phenol method. PCR amplification was performed as previously described (Clarke *et al* 1993, Purdie *et al* 1994) (see appendix A).

5.1.6. Methods for 3 dimensional reconstruction from 2 dimensional serial sections

The whole series of serial sections were previewed to identify intestinal crypts, which express p53, Ki67 and Apc protein and were complete within the sectioned volume. Slides were placed on the stage of the microscope and the appropriate magnification was selected. The surrounding structures of the crypt were used as markers to carry out the orientation. The **Roche Manager system** was used to capture the images utilising **Image Manager 2.3 software**. Images were carefully focused in the **live** window, the light of the microscope adjusted until there was a small level of **artificial colour** of the images. Images were balanced by selecting where the artificial colour was white, **white balance parameter** and black, **black balance parameter** box. Images were then captured.

Sequential histological images were stored. Each image in the series was then recalled from the hard drive and aligned together using the **3dfi** program.

The **3dfi** programme was the alignment program used to align the serial images captured in the Roche manager system. The first image slice was selected and a **Region of Interest** selected by dragging the mouse in the currently displayed image. The principle underlying alignment is that a sequence of pairs of images is processed. One of each pair (reference slice) is kept fixed while the other image (working slice) is rotated and translated as needed to set optimum registration. The **working slice** was shown in green, the **reference slice** was shown in red and the regions that overlap were a yellow colour. The speed of translation and image update is directly related to the chosen image size. The next image slice is then selected by clicking on up or down arrow markers and the new image slice aligned. There is correlation window that shows the correlation value between working slice and reference slice. This number can be used as an aid to alignment though ultimately the user must decide which is the correct position to choose. Now, the serial paraffin sections should be in the 3D-volume data set and are ready for 3D analysis with the Imaris software program.

Imaris software program can visualise and analyse three dimensional volume data. The **Imaris** window contains the following menus: **File**, **Restoration**, **Visualisation** and **Modules**. The **tiff** files were connected to the **Imaris file** format because it is more effective for the **Imaris software program** to work with **Imaris file**. The **Depthview** option displays the images automatically through the whole series. The **Subregion** option from **Visualisation menu** saves the defined area of interested. The **Sections** option from the **Visualisation menu** allows the images to be visualised in the X-Z and in the Y-Z planes. All possible X-Z and Y-Z planes can be showed simply by moving the cursor and the accuracy of the alignment can be assessed with this function. The **Perspective projection** option from **Visualisation menu** is divided into three parts: **Transformation**, **Render mode** and **Animation**. **Transformation** contains the tools to change the viewing parameters: the distance of the object from the eye, the view angle, the near and the far clipping planes and the field of view (focal length of objective). **Render modes**, a particular algorithm that creates a projection of the three-dimensional

image, which has been recorded. There are two principal render modes: projection mode and ray tracing mode. An **Animation** sequence is a series of images computed from different viewpoints that are gradually changed from one frame to the next. With **Perspective projection** function the 3D images will be shown on the window and the object can be visualised and analysed.

5.2. Results

Expression of p53 protein in the intestinal crypt of irradiated *p53* wild type mice (Figure 5.1) at the different time points was evaluated by immunohistochemistry. Non-irradiated *p53* wild type and *p53* null mice showed no p53 protein positivity. Numerous nuclei positive for p53 protein were detected in *p53* wild type mice exposed to -- γ-irradiation at 4 hours after irradiation. This p53 nuclear protein was found in the intestinal crypt cells, which appeared histologically normal, near the base of the crypt in the region above the Paneth cells in the small intestine (Figure 5.3A). No positive staining of p53 protein was seen in the nuclear fragments of apoptotic bodies in irradiated *p53* mice (Figure 5.3A). The numbers of p53 protein positive cells was highest in *p53* wild type mice at 4 hours after irradiation, approximately 12-15 nuclei per crypt, compared to the number of p53 protein positive nuclei, approximately 5-6 nuclei per crypt, observed in *p53* wild type mice at 2 hours after irradiation. In γ-irradiated *p53* deficient mice and non-irradiated mice no positive staining for p53 protein was observed at any time point.

Apc immunohistochemistry staining of wild type non-irradiated mice showed Apc protein staining strongly at the apical surface of the intestinal epithelial villi and diffuse staining of the cytoplasm whereas there was slightly expression of Apc protein at the luminal surface of the intestinal crypt (Figure 5.2A). Similar pattern of Apc staining was observed in γ-irradiated and non-irradiated mice both *p53* wild type and *p53* deficient mice. The positive staining of Apc was also noted in apoptotic bodies in irradiated *p53* wild type mice, irradiated *p53* deficient mice and also in spontaneous apoptotic bodies in control animals. However, when I tried to confirm the Apc protein immunostaining on apoptotic bodies by using rabbit polyclonal Apc, C-20 (Santa Cruz Biotechnology, UK) which is raised against a peptide corresponding to amino acids 2824-2843 mapping at the carboxy-terminal, no Apc positivity was observed of any apoptotic bodies.

γ-Irradiated and non-irradiated ilea in both *p53* wild type and *p53* deficient mice showed the positive staining of nuclear Ki67 protein in the upper 2/3 portion of the intestinal crypt cells (Figure 5.2B). This pattern of nuclear Ki67 protein was found

positive in the whole piece of the intestinal specimen. No positive staining of Ki67 protein was observed in the intestinal villi.

Apoptotic bodies were found scattered, approximately 18-20 apoptotic bodies per crypt, in the intestinal crypt in wild type *p53* mice at 4 hours after exposure to γ-radiation (Figure 5.3B). Whereas lower numbers of apoptotic bodies, approximately 5-8 apoptotic bodies per crypt, was observed in *p53* wild type mice 2 hours after γ-irradiation and approximately 3-5 apoptotic bodies per crypt was observed in *p53* null mice at 23 and 24 hours after irradiation. There were very few apoptotic bodies found in non-irradiated *p53* wild type and *p53* deficient mice. Apoptotic bodies were clearly demonstrated with a routine haematoxylin and eosin stain. In addition, the morphological appearance of many of the apoptotic bodies observed in late response was larger than the morphological appearance of apoptotic bodies observed in the early response. However, both sizes of apoptotic bodies were found in late response but the large apoptotic bodies were more frequently observed.

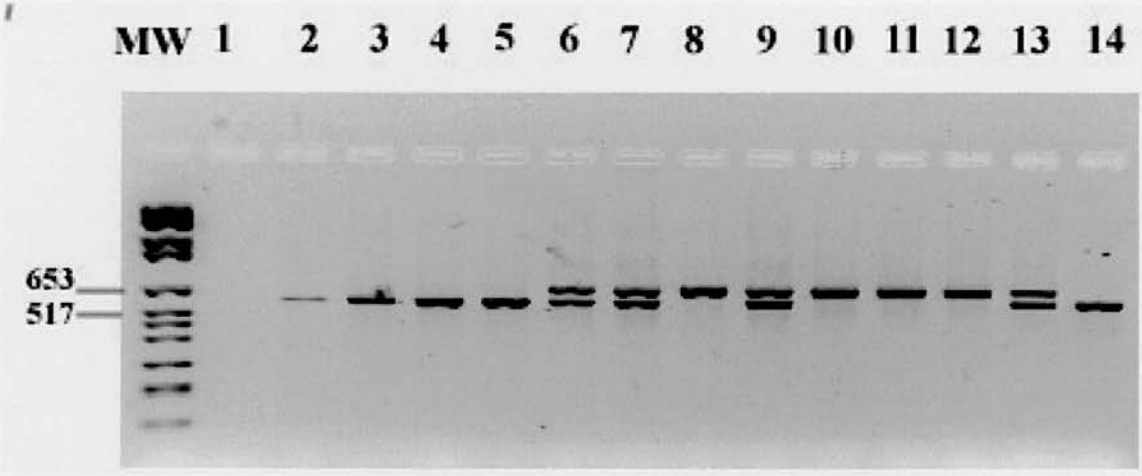

Figure 5.1 PCR analysis of *p53* locus

Representative results from PCR analysis of *p53* genotyping. Samples were all derived from the tail tips of *p53* mice and were as follows: lane 1 is negative control, lanes 2, 3, 4, 5, and lane 14 are *p53* null mice. Lanes 6, 7, 9 and lane 13 are *p53* heterozygous mice. Lanes 8, 10, 11 and lane 12 are *p53* wild type mice.

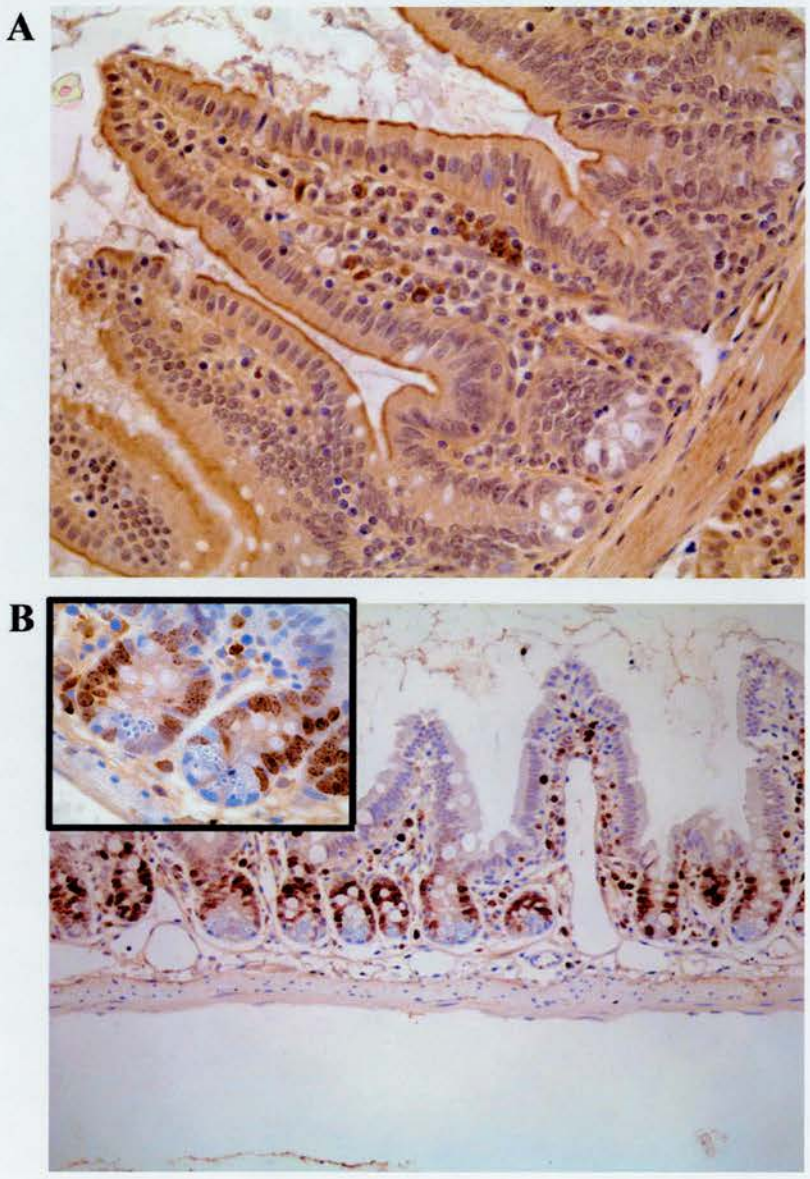

Figure 5.2 Photographs showing the pattern of immunohistochemical staining of Apc and Ki67 protein in the mouse intestine

(A) Photograph showing Apc protein staining in the intestinal epithelium (mag. x400). (B) Photograph showing nuclear Ki67 protein staining in the intestinal crypt cells (mag. x400, inset mag. x1000).

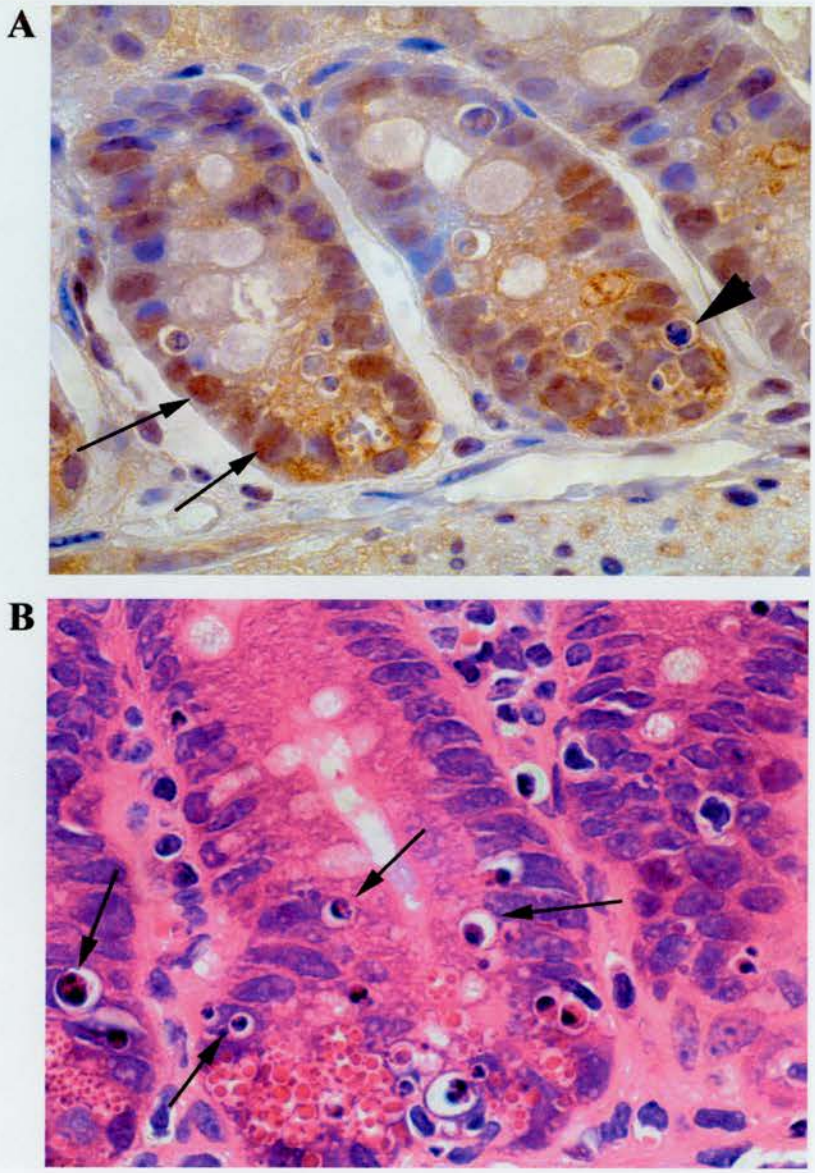

Figure 5.3 Photographs showing the pattern of immunohistochemical staining of p53 protein and haematoxylin-eosin staining of apoptotic bodies in the mouse intestinal crypts in *p53* wild type mice 4 hours post γ-irradiation

(A) Photograph showing nuclear p53 staining in the intestinal crypt (arrows and arrow head indicates apoptotic body, mag. x1000). (B) Photograph showing apoptotic bodies in the intestinal crypts (arrows, mag. x1000).

5.3. Discussion

My analysis of apoptosis in *p53* mice largely confirms others' observations (Kerr *et al* 1972, Clarke *et al* 1994, Merrit *et al* 1994, Arai *et al* 1996). In this study, a large number of apoptotic bodies were found in *p53* wild type mice at 4 hours after exposure to -- γ-radiation. Moderate numbers of apoptotic bodies was observed in the intestine of *p53* deficient mice at 24 and 25 hours after exposure to γ-radiation. The morphological appearance of the apoptotic bodies observed in late response were larger than the morphological appearance of apoptotic bodies in the early response, which is supported an observation by evidence from others using electron microscopy in which the unusual morphology of late, *p53*-independent death, apoptotic cells in comparison with classical apoptotic bodies (Merrit *et al* 1997) was demonstrated. Many of the apoptotic cells they found contained marginated and condensed chromatin in nuclei that were large and in some cases appeared to be attempting mitosis and thus multinucleated whereas classical apoptotic bodies showed chromatin condensation and nuclear fragmentation (Kerr *et al* 1972).

The pattern of Ki67 nuclear protein staining in irradiated and non-irradiated *p53* wild type and *p53* deficient mice was similar. Potten demonstrated a reduction in proliferation at the crypt base in mice within 3 hours after exposure to 8 Gray of γ-radiation. Proliferation was at a minimum by 15 hours post-irradiation and repopulation began at about 15 hours and reached a peak at 22-32 hours post-irradiation (Potten *et al* 1990). This study was not designed to analyse in detail the proliferation index, however, the difference in Ki67 expression pattern could not be observed. This may be probably due to the dose of γ-irradiation used in the studies, 8 Gray of γ-radiation was used in Potten's work whereas 5 Gray of γ-radiation was used in my study.

p53 nuclear positivity was found only in irradiated *p53* wild type mice demonstrating the induction of *p53* gene in response to DNA damage from γ-radiation, which confirms the observations of others (Merrit *et al* 1994, Midgley *et al* 1995, Arai *et al* 1996). p53 nuclear protein was found expression in the intestinal crypt cells, which appeared histologically normal, near the base of the crypt in the region above the Paneth cells in

the small intestine, and peak levels of p53 positive nuclei were seen at position 4-5, which is the stem cell position ((Merrit *et al* 1994, Arai *et al* 1996). The maximum peak of p53 expression was 4 hours after exposure to 5 Gray of γ-radiation.

The pattern of Apc protein staining observed in irradiated *p53* wild type and *p53* deficient mice was the same as the Apc staining pattern in the normal mouse intestinal villi and intestinal crypt cells described in chapter 2. Apc protein staining showed no alteration after γ-irradiation exposure even at late response. This could mean that *Apc* gene regulation is not responsive to DNA damage from γ-radiation or there might be alterations in the *Apc* after γ-irradiation exposure, which is unable to be detected by immunohistochemistry. Moreover, this study was designed to look at acute effects caused by γ-irradiation so the period analysed might not be enough to detect any alteration that could be observed with immunohistochemical staining. However, others have reported that the level of *APC* mRNA and protein were increased after exposure to the methylating agent, N-methyl-N-nitro-N-nitrosoguanidine, and this response required *p53* (Narayan and Jaiswal 1997). Thus, an alteration in Apc can be detected in response to injury by a different mechanism to the DNA damage caused by γ-radiation leading to DNA strand breakage of phosphodiester bonds whereas DNA damage caused by methylating agents leads to adduct formation in DNA base. The Apc positivity of apoptotic bodies was found in all apoptotic bodies. Cleavage of APC during the apoptotic process has been demonstrated (Browne *et al* 1995, 1998, Webb *et al* 1999). They detected a 90 kDa protein cleavage fragment, which is highly conserved in human, rat and mouse, in apoptotic cells of all cell line investigated, which was not present in attached cells. However, the Apc positivity of apoptotic bodies which I saw was not observed with the other antibody (rabbit polyclonal APC, C-20, Santa Cruz Biotechnology, UK) which is raised against a peptide corresponding to amino acids 2824-2843 mapping at the carboxy-terminal whereas rabbit polyclonal APC 3161 is raised against amino acids 2817-2827 at the carboxy-terminal. This could be due to two different APC antibodies recognise different epitopes of APC or Apc protein fragment in apoptotic bodies.

The images obtained from the serial sections were captured, aligned and stored in the *tiff* file format. The image files were transferred to the Imaris software program to reconstruct the three-dimensional images (3D). When the images were opened in Imaris software, we found that the images were not aligned properly. Despite trying several times the image files could not be aligned. After consultation with the programmer and the company who supplied the alignment program, it was modified several times. However, I was unable to align this series of images, therefore rendering and reconstruction of the image series into three-dimensional crypts was impossible. The other factor that may affect reconstruction of the intestinal crypt was the use of immunoperoxidase staining on the serial sections. The intensity of the signal from immunoperoxidase staining was too weak to be detected by the Imaris software.

From this study I may suggest (1) to solve the problem of the alignment, the program requires further modification so that it is suitable for use with the paraffin serial sections (2) to study and work with the Imaris software program should use other staining such as fluorescence or haematoxylin and eosin that yield strong intensity of signal so that the signal is able to be detected by the Imaris software program.

Discussion

This thesis focused on the early events in tumorigenesis using various mouse models. I first determined the pattern of Apc protein expression in normal epithelium in animals, which were wild type and in animals bearing genetic defects in *p53*, *Apc* and the mismatch repair gene, *Msh2*. I choose to use immunohistochemical analysis to demonstrate the pattern of Apc protein expression in various mouse organs. This expression pattern was compared to the pattern of β-catenin and E-cadherin expression within the same tissues. This is the first report comparing the pattern of Apc expression in mouse tissues with the pattern of β-catenin and E-cadherin protein expression in wild type mice and in mice bearing genetic defects. When APC and β-catenin localisation was compared, two patterns were seen; (1) co-localisation at the lateral cell membrane and (2) no co-ordinated expression, with APC found in the cytoplasm and β-catenin found at the basolateral cell membrane. The first pattern was seen in the intestinal epithelium. The second pattern was seen in the other epithelial types examined such as renal tubule or alveolar epithelium of mammary glands. β-Catenin and E-cadherin were always found colocalised in all types of epithelium at the lateral cell membrane. This implies that β-catenin always interacts with E-cadherin but that Apc does not always interact with β-catenin. Hemizygosity for *Apc* did not affect the pattern of Apc protein expression in normal epithelium in *Apc* $^{Min+/-}$ mice. Nuclear localisation of Apc was observed in the inner nuclear layer of the retina and in sertoli cells, which are non-migrating cells. Cytoplasmic localisation of Apc was also observed in all epithelium cell types, which are migrating cells, such as intestinal epithelium and renal tubular epithelium. These observations are supported by the findings of Neufeld and White (1997). The pattern of Apc expression is similar to the previously reported pattern of APC expression in human tissues (Midgley *et al* 1997) which implies that *Apc* $^{Min+/-}$ mice may indeed be appropriate models in which to study Apc protein function and that the findings obtained may relate well to human colorectal cancer. Interestingly, the results showed that in morphologically normal intestinal epithelium, Apc and β-catenin

expression colocalised at the lateral cell membrane a similar co-localisation of Apc and β-catenin in the retinal pigment epithelium of the rat has been noted by others (Bubb, VJ. personal communication), in this case at the basal cell membrane. This suggests that in these tissues Apc and β-catenin function together. The observed co-localisation of these proteins also suggests that both Apc and β-catenin may interact with each other in the development of colorectal cancer and congenital hypertrophy of the retinal pigment epithelium (CHRPE). It is interesting to note that although APC expression is ubiquitous in all epithelium types such as the intestine, lung and kidney, the spectrum of disease associated with inherited lose of APC (FAP) is limited to specific organs and manifest as colorectal cancer, osteomas, CHRPE and desmoid tumours. This suggests that the observed co-localisation may reflect novel functions for these proteins in certain tissues. Unfortunately, when analysing the pattern of β-catenin staining of osteoblasts the staining pattern was difficult to interpret because of distortion of the tissue, and therefore in this tissue it was not possible to absolutely establish if these proteins co-localise. Future studies should include a repeat analysis of this tissue, given the predisposition to osteomas in FAP patients. In addition, it would be interesting to compare staining patterns with those found in human specimens obtained from affected FAP patients. In general the precise biological role of these proteins remain unclear, but several groups have produced data suggesting a role in regulating cellular progression from G_1 to S phase. *In vitro* studies have shown that Apc functions in regulation of cell progression from G_1 to S phase (Heinen and Groden, 1999), and that β-catenin can promote the G1 to S phase transition (Orford *et al* 1999).

I next addressed whether the pattern of β-catenin expression was dysregulated in the intestinal and pancreatic lesions arising in mice bearing germ line defects in *Apc*, *p53* and *Msh2*. Immunohistochemistry was used to analyse these lesions. As scored immunohistochemically, levels of β-catenin in *Apc* $^{Min+/-}$, *p53* $^{-/-}$ and *p53* $^{+/+}$ mice were very high in small lesions in both the intestine and pancreas. Nuclear localisation of β-catenin was observed in small lesions in both the intestinal and pancreatic acinar cells. This nuclear localisation is consistent with the findings of Sheng *et al* (1998) in which

intestinal adenomas were induced by carcinogen exposure in *Apc* $^{Min+/-}$ mice. This increase is assumed to arise as a consequence of increased levels of cytoplasmic β-catenin, which is subsequently translocated into the nucleus. It then complexes with a transcription factor such as Tcf/Lef-1, thereby activating transcription of downstream target genes (Korinek *et al* 1997, Morin *et al* 1997, Hsu *et al* 1998, He *et al* 1998). The observed overexpression of β-catenin in small lesions of the intestine is consistent with the findings of Samowitz *et al* (1999). These results suggest that mutation of β-catenin is important in the early stages of adenoma formation but is less important for subsequent neoplastic progression. This data agrees very well with my findings that β-catenin is preferentially upregulated in small lesions and showed a heterogeneous pattern of staining in the larger lesions. A widespread role for β-catenin in tumour progression is suggested by other data including identification of mutations in β-catenin in mouse and human hepatocellular carcinomas (de la Coste *et al* 1998). Others have shown that mutation of β-catenin was an early event in chemically induced mouse hepatocellular carcinogenesis (Devereux *et al* 1999). This evidence supports the hypothesis that -- β-catenin overexpression is an early event in tumorigenesis in cases where the Wnt signalling pathway is disrupted, presumably shortly after Apc inactivation. Inactivation of Apc results in accumulation of cytoplasmic β-catenin and excess β-catenin is translocated into the nucleus, leading to upregulation of transcription. Therefore, it would be interesting to perform β-catenin staining in the various stages of human colorectal cancer specimens to prove this hypothesis.

The upregulation of β-catenin was not always evident in lesions arising in *Msh2* mutant mice. This result suggests either that mutations may occur downstream of -- β-catenin in the Wnt pathway, or that dysregulation of Wnt pathway is not important in all early lesions on a *Msh2* null background and that an alternative pathway is involved in tumorigenesis in *Msh2* null background mice.

Msh2 is a key component of the mismatch repair machinery, defects of which are known to be important in the development of hereditary non-polyposis colon cancer in humans. Loss of function of the mismatch repair genes is associated with microsatellite

instability and predisposes to the promotion of neoplasia following hits at other genes such as *APC*. From my data, β-catenin was not always seen to be upregulated in intestinal lesions arising in the (*Apc* $^{Min+/-}$*/Msh2* $^{-/-}$) mice. This implies that in a mismatch repair deficient environment, lesions are arising as a consequence of mutations in genes either downstream of β-catenin or in an entirely different pathway. One set of candidate targets downstream of β-catenin is the Tcf family of transcription factors, which are the direct targets of β-catenin in the Wnt pathway. Indeed mutations in the *Tcf* genes have recently been reported in HNPCC (Duval *et al* 1999). Therefore, an analysis of the status of these transcription factors in those lesions not upregulating β-catenin would be one logical next target for study.

During the above analysis of β-catenin dysregulation in the intestinal and pancreatic lesions arising in the mutant mice, extensive changes in nuclear size/volume were observed in pancreatic lesions but not in intestinal lesions. This clearly demonstrated a highly tissue specific difference in the roles played by β-catenin and Apc in the early stages of carcinogenesis. Nuclear pleomorphism was observed in pancreatic lesions showing β-catenin dysregulation. To prove that the observed change in nuclear size reflects changes in ploidy or aneuploidy an analysis of nuclear volume in both the intestinal and pancreatic lesions was performed in conjunction with a determination of the cell turnover rate. Nuclear volume analysis was performed using both two-dimensional techniques and three-dimensional methods, the latter giving an absolute value for volume rather than a relative value. Many problems were encountered using the three dimensional method. I found the most important confounding factor to be the density of tissue structure, which made determination of individual nuclear content a difficult and time-consuming task. In contrast, large amount of data concerning relative nuclear volume was obtained without difficulty using the two dimensional technique.

Two-dimensional analysis of relative nuclear volumes showed that there were small but significant changes in nuclear volume in the intestinal lesions arising in each genotype studied. In contrast, there was a large, statistically significant difference in nuclear volume obtained from pancreatic lesions compared to control tissue, in

particular in lesions arising in (*Apc* $^{Min+/-}$/*p53* $^{-/-}$) mice. Two major findings are (a) that nuclear volume was increased in the absence of *Apc* and (b) that this increase was accelerated in the absence of *p53*.

Apc has been reported to have a role in the regulation of the G_1 phase of the cell cycle by negatively modulating the activity of cyclin-CDK complexes (Baeg *et al* 1995). Additionally, APC has been found to localise to the nucleus with foci in the nucleoli (Neufeld and White 1997) which may suggest a regulatory role for APC in mitosis and ribosomal RNA synthesis. It has also been shown that the EB1 protein, which is a partner of APC, is located at the centrosome during mitosis. By association this suggests that APC may be located at the centrosome; and, although EB1 binding to microtubules has been shown to be APC-independent (Berrueta *et al* 1998), APC could still function in fine-tuning of EB1 function. Implications are that loss of function or mutations in *Apc* could result in misalignment of the mitotic spindle and resulting changes in ploidy or genomic instability ultimately leading to carcinogenesis.

Possible explanations for the accelerated changes in nuclear volume in the absence of p53 include the loss of function of *p53* as a cell cycle checkpoint allowing cells with damaged DNA to replicate and progression to a malignant phenotype. There is evidence supporting the involvement of *p53* in control of G_1 arrest (Martinez *et al* 1991) which prevents the cells from replicating damaged DNA, apoptosis (Clarke *et al* 1993) and regulation of the G_2 phase of the cell cycle (Guillouf *et al* 1995) which prevents chromosome segregation if the chromosome is not intact. p53 was also reported to be important in spindle checkpoint function (Cross *et al* 1995, Lanni and Jacks 1998) which ensures the maintenance of diploidy. Other studies performed in human colorectal cell lines have shown that p53 can mediate an upregulation of APC in response to DNA damage (Narayan and Jaiswal 1997) which may indicate synergy between mutations in Apc and p53 in increasing genetic instability and tumour development.

Determination of nuclear volume in pancreatic lesions arising in *Msh2* null mice did not reveal any significant changes. The mismatch repair system recognises inappropriate base-pairing resulting either from DNA damage or from DNA replication slippage. Defects in the mismatch repair system lead to microsatellite instability, which is not

predicted to result in a change in the nuclear volume in the *Msh2* null animals. In man this genetic instability can occur in colorectal lesions, which retain *APC* (Heinen *et al* 1995), which suggests that *APC* mutations do not promote microsatellite instability neither is it preferred target for mutagenesis in all types of colorectal cancer.

The preliminary cell turnover data suggested that the differences observed in nuclear volume in the intestinal lesions were probably explained by differences in cell turnover rather than by the genotypes of the affected animals. In the majority of lesion types the BrdU index was elevated corresponding to a small but significant increase in nuclear volume. It is possible that the observed increases in nuclear volume and cell turnover rate in the lesions occurred independently, and there are at least two possible mechanisms underlying the increase in the number of S phase cells. One is an increase in cell turnover rate and the other is an increase in S phase duration in the cancer cell cycle (Baserga 1965).

The differences in nuclear volume in pancreatic lesions could not be explained by alterations in the cell turnover rate as the number of S phase cells observed within normal pancreatic acinar cells and pancreatic acinar cell lesions was only 0.05% by the methodology employed in this study analysing BrdU incorporation. This is a very surprising finding, as logically cells should be turning over in these lesions. However, a survey analysis of mitotic index supports this notion, as mitotic figures were only observed in carcinomas of the pancreas (lesions beyond the type V scored here).

In summary: (a) Apc is widely expressed in mouse tissues in all epithelial cell types, connective tissue, bone and nerve tissues. In the epithelia, Apc and β-catenin are not always co-localised but β-catenin and E-cadherin always co-localise; (b) increased β-catenin staining by immunohistochemical method is a marker of early murine pancreatic and intestinal lesions and this suggests it may be a useful marker of human tumorigenesis; (c) lesions arising in a *Msh2* deficient background do not always show dysregulation of β-catenin, suggesting the presence of an alternative pathway to tumour development; (d) marked changes in nuclear volume are seen within small pancreatic lesions. These reflected aneuploidy or polyploidy in the pancreas but surprisingly no

marked change was seen in the intestine; and (e) the observed genetic instability in the pancreas was driven by loss of both *Apc* and *p53*.

Appendix A Protocols

1. Immunohistochemistry

Glass slides were cleaned, by immersion in detergent (Decon, Decon Laboratory, UK) for 1 hour, at room temperature before placing in 74% ethanol for 5 minutes. The slides were air dried at room temperature. Poly-L-lysine (Sigma, Germany) was used to coat the glass slides so that the tissue section adheres to the slides throughout the whole process of immunohistochemistry. Cleaned glass slides were immersed in poly-L-lysine solution (see appendix B) for 5 seconds. The slides were allowed to drain, air-dried and then oven dried at 50 ^{0}C, overnight. All antibodies used in the experiment were optimised (as previously described in section 2.1.3 and table 2.1) to find the optimum dilution for staining before performing the experiment.

Three micron thick sections were cut with a microtome. Each section was gently picked up with a brush and placed in 56 ^{0}C water bath to stretch the section. A glass slide was immersed underneath the tissue section in the water bath to collect the section and the section was left to dry for a few minutes before placing the sections in a slide rack and transferring to 37 ^{0}C oven. The sections were dried in a 37 ^{0}C oven, overnight. The sections were dewaxed in xylene for 10 minutes, re-hydrated by passing through in a standard series of graded alcohol; absolute, 74%, 64% ethanol for 2 minutes each before rinsed in running tap water for 5 minutes. The antigen retrieval technique was performed for β-catenin and E-cadherin staining as these antigens needed to be unmasked for successful staining (see 2.1.3). Briefly, the sections were placed in a plastic slide rack and immersed in 0.05 M citrate buffer, pH6.0 (see appendix B) and placed in the microwave oven. The slides were microwaved at 700 watts, for 5 minutes, repeated 3 times. The sections were cooled down to room temperature before being rinsed in running tap water for 5 minutes. The sections were immersed in H_2O_2 solution to block endogenous peroxidase for 15-20 minutes (as described in table 2.1), followed by a rinse in running tap water for 5 minutes. The slides were washed in 0.1%Tween 20/TBS (see appendix B) and placed against cover plates (Shandon, UK) and hold in Sequenza rack

(Shandon, UK) which is the apparatus used to hold the slides in routine immunohistochemistry technique. Non-specific blocking was carried out by adding 100 µl of 20% normal serum in 0.1%Tween 20/TBS (see appendix B) corresponding to secondary antibodies used on each section and left to incubate at room temperature for 20 minutes. The sections were incubated with volume primary antibody (as described in table 2.1). Sections were then washed three times with 3 ml of 0.1%Tween 20/TBS (see appendix B). Sections were incubated with secondary antibody: biotinylated rabbit anti-mouse for β-catenin and E-cadherin and biotinylated swine anti-rabbit for APC antibody, for 30 minutes at room temperature. Both primary and secondary antibodies were diluted in 20% normal serum in 0.1%Tween 20/TBS. Sections were washed with 0.1%Tween 20/TBS for 5 minutes, 3 times. Avidin biotin complex (ABComplex) horseradish peroxidase is based on the non-covalent bond reaction between avidin, which is a glycoprotein and biotin, which is a water-soluble vitamin. Four hydrophobic pockets on the surface of the tertiary structure of avidin behave as specific binding sites for four biotin residues. Biotin may be conjugated with a variety of molecules such as the enzyme horseradish peroxidase, which is a chemical procedure, biotinylation. ABComplex method is used to enhance the signal of antigen-antibody complex labelled with a biotinylated secondary antibody, which was detected by horseradish peroxidase. ABComplex/HRP (Dako, Denmark) was made by dropping one drop each of Strep/avidin and biotinylated horseradish peroxidase (Dako, Denmark) into 5 ml of 0.1 M Tris buffer pH 7.6 (see appendix B). The solution was mixed well and left for 30 minutes at room temperature to complete the reaction. Sections were incubated with ABComplex/HRP for 30 minutes at room temperature, followed by 3 washes with 0.1%Tween 20/TBS. The labelled complex was developed with diaminobenzidine 0.5mg/ml (DAB, see appendix B) for 5-8 minutes at room temperature and rinsed in running tap water to stop the reaction. Subsequently the slides were lightly counterstained with Harris haematoxylin (see appendix B) by dipping the section in haematoxylin for 20-25 seconds, followed by a rinse in tap water to wash off excess stain and dipping in Scott's tap water (see appendix B) for 25 seconds and a final rinse in tap water. The sections were dehydrated in a series of alcohol: 64%, 74%, absolute alcohol

for 2 minutes each and in xylene for 10-15 minutes. Finally, sections were coverslip mounted with DPX by dropping few drops of DPX on coverslip and gently placing the section onto coverslip avoiding trapping air bubbles.

2. Immunohistochemistry double staining of β-catenin and BrdU

Three microns of paraffin embedded sections were cut and mounted on poly-L-lysine coated slides. Sections were de-waxed and re-hydrated in graded alcohol. High temperature antigen retrieving was performed as previously described. The sections were incubated in 2.0 N. HCl at 27 ^{0}C for 25 minutes to denature the DNA, followed by a rinse in running tap water. Sections were incubated in 0.1% Saponin in TBS to permeate cell membrane for 30 minutes. Endogenous peroxidase blocking was performed by quenching in 1.5% H_2O_2 in distilled water for 15 minutes on shaking platform, followed by a rinse in running tap water. The sections were placed against cover plates and held in the Sequenza rack (Shandon, UK). Sections were incubated with 20% normal rabbit serum in 0.1% Saponin/TBS (see appendix B) to block non-specific binding for 30 minutes at room temperature. Sections were incubated with primary antibodies; 1:50 mouse monoclonal anti-β-catenin (Transduction laboratories, UK) and 1:100 rat monoclonal anti-BrdU (Harlan Sera lab, UK) in 20% normal rabbit serum overnight at 4 ^{0}C. The sections were washed with 0.1% saponin/TBS three periods of 5 minutes. The sections were incubated with secondary antibody, rabbit anti-rat/biotinylated (Immunopure, Pierce, USA) 1:900 for 30 minutes at room temperature followed by three times washing with 0.1% saponin/TBS. Then, the sections were incubated with ABComplex/HRP for 30 minutes (see 2.1.5) washed three times with 0.1% saponin/TBS. The sections were visualised with diaminobenzidine 0.5 mg/ml (see appendix B) for 5-8 minutes, the slides were taken off the cover plates and placed in a slide rack, then rinsed in running tap water to stop the reaction. The slides were placed back into new cover plates and held in the Sequenza rack. The sections were incubated with secondary antibody rabbit anti-mouse/biotinylated 1:400 (Dako, Denmark) for 30 minutes at room temperature. The sections were washed three times with 0.1% saponin/TBS. This time ABComplex/AP was used as a detection system. The sections were incubated with ABComplex/AP for 30 minutes at room temperature.

ABComplex/AP must be made up 30 minutes before use by adding one drop of each avidin and biotin-phosphatase conjugate into 0.1 M Tris/HCl buffer pH 7.6 (see appendix B). Vector Red (Vector Laboratory, USA) was used as the visualised system. Immediately before used, 2 drops of reagent1 were added to 5 ml of 0.1 M Tris/HCl buffer pH 8.2 and mixed well. Two drops of reagent 2 were added, mixed well and finally addition of 2 drops of reagent 3 and it was mixed well. The sections were incubated in the dark for 20-30 minutes, followed by rinsing of the sections in running tap water. The tissue was counter stained with haematoxylin, dehydrated and coverslip mounted in DPX.

3. Haematoxylin and Eosin staining

Three micron thick sections were cut longitudinally serially with a microtome for 40 sections. Each section was gently picked up with a brush and floated on 56 ^{0}C water bath to stretch the piece of tissue. Clean glass slides were prepared. Then labelled with the number corresponding to the number of the serial section and immersed underneath the tissue section in water bath to collect the section. The sections were dried for a few minutes before being placed in a slide rack and transferred to a 37 ^{0}C oven. The sections were dried in a 37 ^{0}C oven, overnight. Next day, the sections were soaked in water and immersed in Harris's Haematoxylin (Shandon, UK)(see appendix B) for 5 minutes, then washed in water to get rid off excess stain. Subsequently, the sections were place in 1% acid alcohol (see appendix B) for 5-10 seconds, followed by immersion in Scott's Tap water (see appendix B) for 1-2 minutes and washed in water. The sections were stained in 0.5% aqueous Eosin (Shandon, UK)(see appendix B) for 1 minute, washed in water. The sections were dehydrated, mounted and cover slipped.

4. Histological microdissection of β-catenin overexpressed lesions

Histological microdissection was performed as described by Going and Lamb (1996). Paraffin-embedded tissues were cut at 7 micron thickness with a microtome. Each tissue section was floated on water at 56 ^{0}C to stretch the tissue section. A clean plain glass slide was inserted underneath the section in warm water to collect the tissue section and dried at 37 ^{0}C overnight. The tissue section was subsequently de-waxed in xylene for 10 minutes and re-hydrated in graded alcohol (see 2.1.2) and distilled water. The sections

were then stained in 0.05% aqueous toluidine blue (see appendix B) for 20 seconds, washed in distilled water for 5 minutes and stored in distilled water until dissection. Excess water was blotted from the slide and placed on the stage of a stereo microscope. Proteinase K buffer solution (pH 8.3: Tris HCl 18 mM, Tris Base 36 mM, EDTA 1mM) was dropped onto the section to cover the section. Dissection was performed with an electrolytically sharpened 25 mm length tungsten wire needle (diameter 0.5 mm, tip radius 2.5 microns) in a needle holder mounted in the tool holder of a Leica mechanical micromanipulator. The section stained with toluidine blue showed pale blue stained in the areas of tumour lesions compared to dark blue stained in the area of normal tissue in the same section. The serial 3 micron section stained with β-catenin was used to compare with the 7 micron section stained with toluidine blue. Under the microscope, dissection began by moving the needle until the tip attached to the edge of the lesion. The tip of the needle was slowly traced around the lesion until the lesion peeled off from the glass slide and the whole area of lesion was removed in buffer with a micropipette that was set up at 65 µl and transferred to an eppendorf tube and kept at 4 ^{0}C until further analysis.

5. PCR analysis of *Apc* locus

Samples from the microdissection were digested overnight in proteinase K 1 mg/ml buffer and 1% Tween 20 (see appendix B) in a final volume of 130 µl buffer and left overnight at 4 ^{0}C. The proteinase K was subsequently heat-inactivated at 95 ^{0}C, for 10 minutes in a PCR thermal cycler. PCR amplification of *Apc* was then performed as previously described (Luongo *et al* 1994) using the primers

5'TCTCGTTCTGAGAAAGACAGAAGCT 3' and

5' TGATACTTCTTCCAAAGCTTTGGCTAT 3'.

Each 50 µl reaction contained; 0.05 µM of *Apc* PCR primers (Oswel, UK), 0.2 mM of each dNTP, 5% DMSO, 10 mM Tris/HCl, 25 mM KCl, 50 mM $MgCl_2$, 2.5 units *Taq* DNA Polymerase (PCR reagents were supplied by GIBCO/BRL), and 2 µl of DNA template sample, overlaid with one drop of paraffin oil. Samples were amplified under the following conditions: 1 cycle at 94 ^{0}C for 2 minutes followed by 30 cycles at 94 ^{0}C for 1 minute, 60 ^{0}C for 1 minute, and 72 ^{0}C for 1 minute followed by 1 cycle at 72 ^{0}C for

10 minutes. One microliter of each PCR reaction was then subjected to a second round of amplification for single cell PCR using the nested primers
5' AGTAAGCAGAGACACAAGCA 3' and 5' CGGTGGTAGAAGCAGAACTT 3' (Audrey Peter, personal communication). Nested PCR was used in order to improve the sensitivity and specificity of the reaction, the second round of amplification contained two nested primers that are internal to the first primer pair. Each 50 µl reaction contained 0.05 µM of nested primers, 500 µM $MgCl_2$ and the same concentration of other PCR reagents and subjected to the same parameters as in *Min* PCR. Sixteen microlitres of the final PCR product was cleaved with the *Hind*III restriction enzyme (GIBCO/BRL) by incubation at 37 ^{0}C, 4 hours or overnight in a 20 µl reaction containing: 2 units of *Hind*III restriction enzyme and 2 µl of reaction buffer (see appendix B), puc19 was included as a cleavage control. The PCR product was digested by *Hind*III to a 123 base pair fragment, which is *Min* allele. Fifteen microlitres of each *Hind*III digested product and digested puc19 were loaded into 4% agarose gel by mixed with 20 µl of loading buffer containing ethidium bromide (see appendix B). Four microlitres of molecular weight marker V (Boehringer Mannheim, Germany) was loaded so that the molecular weight of PCR product could be calculated. Electrophoresis conditions were 5 volt/cm for an hour in TBE buffer. Samples were examined under UV light and photographed.

6. PCR analysis of *p53* locus

PCR amplification was performed as previously described (Clarke *et al* 1993, Purdie *et al* 1994). Three primers were added to the reaction mixture, a pair specific to wild type allele and a third specific to targeted allele. The first upstream primer is in exon 6,
5' GTGGTGGTACCTTATGAGCC 3' and the second, which is specific for targeted DNA is 5' CATCGCCTTCTATCGCCTTC 3'. The downstream primer is in intron 7,
5' CAAAGAGCGTTGGGCATGTG 3'. Each 50µl reaction contained: 0.5 µM each primer, dNTPs 200µM, DMSO 5%, $MgCl_2$ 1.0 µM, KCl 200 mM, Tris/HCl 200 mM, detergent (W-1) 5%, *Taq* DNA polymerase 2 units and 2 µl of DNA sample (PCR reagents were supplied from GIBCO/BRL). One drop of paraffin oil was overlaid onto the surface of the mixture. Sample were amplified under the following conditions: 1cycle

at 94 ^{0}C for 2 minutes followed by 30 cycles at 94 ^{0}C for 1 minute, 62 ^{0}C for 1 minute and 72 ^{0}C for 1 minute and followed by 1 cycle at 72 ^{0}C for 10 minutes. Four microlitres of molecular weight marker VI (Boehringer Mannheim, Germany) and 15 µl of each PCR product were loaded into 2%gel after mixing with 20 µl loading buffer containing ethidium bromide (see appendix B). Electrophoresis was run in TBE buffered under conditions of 5 volts/cm, for an hour. Samples were analysed on 2% agarose gel under UV light and photographed.

7. DNA extraction by phenol method

Genomic DNA was extracted from the tail tip of the wild type *p53* and *p53* deficient mice by a phenol method. TE9: SDS (see appendix B) 0.5 ml was added to the tail sample in an eppendorf tube, followed by 25 µl proteinase K (20 mg/ml) and incubated overnight at 37 ^{0}C in the orbital shaker. Next day, TE saturated phenol (see appendix B) 0.5 ml was added to the sample, mixed thoroughly and microfuged for 2 minutes. The top layer of aqueous supernatant was carefully removed to a clean tube and an equal volume of PC-9 added (see appendix B), mixed and microfuged for 2 minutes. The aqueous supernatant was removed to a clean tube and an equal volume of chloroform: iso-amyl alcohol added (see appendix B), mixed thoroughly and microfuged for 2 minutes. The aqueous supernatant was removed to a clean tube and 0.25 ml of 7.5 M ammonium acetate (see appendix B) and 3.75 ml of cold absolute ethanol added to precipitate the DNA, mixed well and centrifuges at 10000 rpm for 5 minutes. The supernatant was discarded and the tube was inverted over a clean paper towel for 20 minutes to allow the DNA pellet to dry. DNA was resuspended in 250 µl of TE and stored at 4 ^{0}C. The optical density was measured at 260 nm and 280 nm; the ratio of which should be 1.8 for DNA. The concentration of the DNA was calculated by using the following equation: DNA concentration (µg/ml) = OD 260 nm x 50 x 1000/10. Where 10 µl is the quantity of DNA measured and 1000 µl is the volume into which it was diluted. An OD of 1 = 50 µg/ml for double stranded DNA.

8. Method for nuclear volume analysis with HOME

For nuclear volume analysis the Applications program is used. If this is the first time the system has been used, it has to calibrate the stage and the objectives have to be calibrated. To ensure correct measurements with the microscope, the relative height and width of the screen has to be checked. In addition, the stage has to be checked for rotation. If this is problem the stage will have to be re-balanced. To calibrate the stage a grid will appear on the screen, this grid is superimposed onto the grid located on the calibration slide (10x). The two grids should overlap almost perfectly. Normally when entering the application the next screen you are presented with is the **zero calibration screen**. Place the calibration slide on the microscope. Match the centre of the screen cross (green overlay) with the centre of the calibration slide; the centre of the slide calibration cross occurs within the 100x ellipse, the correct Y axis on the calibration slide is the black line showing the objective sizes, the X and Y lines on the calibration slide should be straight. Now, in the AxioHOME measurement environment. The application menu, **General Morphometry** is used. A typical **General Morphometry** sessions consists of the following stages; Entry of Slide Reference Number, Selection of toolbox type i.e. object or structure, Creation or Selection of a protocol, Measurement, Display of results and Saving the file. Briefly one selects the appropriate protocol, then draws around the nucleus according to the marker selected, either the positive or negative nucleus of interest. This step must be done under oil immersion objective lens. The nuclei were only considered for sampling if the nuclear membrane was sharp and intact over 75% of its circumference. At least five hundred nuclei were measured from each type of lesions for each genotype. For assessment of nuclear volume, the individual radius was calculated from nuclear intercept length and multiplied by $4/3\ \pi r^3$. Furthermore, the running means of nuclear volume of each lesion types in different genotypes were assessed and graphically compared. The advantage of using AxioHOME is that all the cell positions are recorded on the hard drive if there is any uncertainty a nucleus is able to be re-scored by the original observer or by an independent observer.

9. Method for three dimensional analysis of the nuclear volume

Triple labelled sections were examined using the confocal laser scanning microscope (CLSM). The section was placed in a petri dish and immersed in phosphate buffered saline. The lesions were identified by the presence of excessive rhodamine staining at the wavelength 514 nm, indicating areas of β-catenin overexpression. Immersion objective lens (magnification of x630) was used during laser scanning. The lesion was scanned through with each wavelength of laser (488 nm, 514 nm and 647 nm respectively) to avoid cross-talk between channels. The section was scanned through at 1micron steps. The scanned images from the three channels were overlaid afterward to build up the whole volume of sections and saved in the **tiff** file format. Images of 1.0 micron thick were transferred from CLSM and stored in CDROM and analysed with **Imaris software** and **VoxelShop Pro program**.

The images were opened in the Imaris program and the **Subregion of interest** was selected. This subregion was screened through the whole series and opened with shadow projection. With **perspective projection** images were seen in three dimensions so that it was possible to ascertain if images were of complete whole nuclei or not. The images were analysed in VoxelShop Pro, **threshold segmentation** option was used to select the BrdU positive cells (642 nm) and BrdU negative cells (488 nm) from the tumour lesions in intestine and pancreas. The threshold was set at 40% of the maximum threshold. This threshold was obtained from calibration with Fluorescent latex microspheres (Polyscience Inc., excitation 488 nm) that were 10.16 μm diameter. The images of the microspheres were used to calibrate threshold segmentation. The threshold was set to the maximum and decreased increments by 5% until the images of the microspheres were cleared from the background. That threshold was 40% from the maximum. After threshold segmentation, the objects were extracted by setting the minimum volume at 50 μm. to screen out the debris, and the **object statistic** option used to yield values for the nuclear mass and volume.

Appendix B Solutions

10% bufferred formalin

40% formalin 25 ml

Buffered saline 75 ml

Methacarn fixative

Methanol 40 ml

Chloroform 20 ml

Acetic acid 10 ml

0.05M Citrate buffer

Citric acid 1.05 g

Distilled water 500 ml, adjust pH 6.0

0.1M EDTA buffer

EDTA 1.86 g

Distilled water 500 ml, adjust pH 8.0

Tris/HCl pH 7.6

0.2 M. Tris 24 ml

0.1 N. HCl 38 ml

Make up to 100 ml with distilled water, adjust pH 7.6.

x10 Tris bufferred saline (TBS)

Tris 30.25 g

Distilled water 500 ml

Adjust pH 7.6

Make up to 2000 ml with distilled water and recheck pH

Hydrogen peroxide solution

1.5% H_2O_2: 15 ml of 30% H_2O_2 in 285 ml of distilled water

3.0% H_2O_2: 30 ml of 30% H_2O_2 in 270 ml of distilled water

0.5% H_2O_2 in methanol: 5 ml of 30% H_2O_2 in 295 ml of methanol

0.1% Trypsin solution

Trypsin 10 mg

$CaCl_2$ 10 mg

Distilled water 100 ml, adjust pH 7.8

Tris/HCl buffer for DAB solution

0.2 M. Tris 24 ml

0.1 M HCl 38 ml

Imidazole 0.0681 g

Make up to 100 ml with distilled water, adjust pH 7.6

0.2M. Tris base

Tris 12.1 g

Distilled water 500 ml

0.1M Sodium phosphate buffer pH 7.0

Sodium phosphate 14.2 g

Distilled water 1000 ml, pH7.0

20mM sodium phosphate buffer pH 7.0

0.1M Sodium phosphate pH 7.0 20 ml
Distilled water 80 ml, adjust pH 7.0

0.1M Glycine buffer pH 3.0
Glycine 7.507 g
Distilled water 1000 ml
Adjust pH 3.0

DAB solution
X50 DAB solution;
Dimethylaminobenzidine 125 mg
Distilled water 5 ml
Working DAB solution (0.5 mg/ml);
X50 DAB solution 100 µl
Tris/HCl buffer pH 7.6 4.8 ml Immediately before use, add 0.1 ml of 1% H_2O_2 in distilled water

Poly-L-Lysine
Poly-L-lysine 0.1% (w/v) 1ml
Distilled water 40 ml

0.1% Tween 20/TBS
TBS 1000 ml
Tween 20 1000 µl

Acid alcohol
70% alcohol 99 ml
Concentrated HCl 1 ml

Scott's Tap water
Potassium bicarbonate 2.0 g
Magnesium sulphate 20.0 g
Distilled water 1000 ml

0.5% Eosin (Shandon, UK)
Eosin 0.5 g in 100 ml distilled water

Harris'haematoxylin (Shandon Harris's haematoxylin Acidified, UK)

0.05% aqueous toluidine blue
1% toluidine blue 1ml
Distilled water 19 ml

0.5 M. Tris/HCl pH 9.0
Tris 60.55 g
Distilled water 1000 ml adjust pH 9.0 with HCl

0.25% Coomassie brilliant blue (Sigma, Germany)
Coomassie brilliant blue 250 mg
Dissolve in 100 ml 50% methanol, 10% acetic acid
50% methanol: methanol 50 ml and distilled water 50 ml
10% acetic acid: acetic acid 10 ml and distilled water 90 ml

Destaining solution
10% ethanol: ethanol 10 ml and distilled water 90 ml
7% acetic acid: acetic acid 7 ml and distilled water 93 ml

20% ethanol

ethanol 20 ml

distilled water 80 ml

0.02% Sodium azide

Sodium azide 0.02 mg

Distilled water 100 ml

Taq DNA Polymerase (GIBCO/BRL) Catalog Number 18038-026, Lot No. JPE421 UK

***Hind*III Restriction Enzyme** (GIBCO/BRL) Catalogue Number 15207-020, Lot No. JNS402

x1 Agarose gel buffer (TBE)

Tris 10.8 g

Boric acid 5.5 g

EDTA 3.72 g

Add distilled water to 800 ml and adjust pH 8.0, make up to a final volume 1000 ml with distilled water

TE saturated phenol

Mix equal parts of phenol and TE

Allow to separate and discard top aqueous layer. Store at 4 ^{0}C.

TE

10 mM Tris pH 8.0

1 mM EDTA

Store at 4 ^{0}C

3% Agarose gel

Agarose gel 3.0 g

TBE 100 ml

Blue gel loading buffer (TBE)

30% Glycerol

0.25% Bromphenol blue

in 1x TBE buffer

Digestion buffer for microdissected tissue

Tris/HCl pH 8.3

0.25 M EDTA, pH8.0

Proteinase K 1 mg/ml

Tween 20 1%

Ethidium bromide

Ethidium bromide 100 mg

Distilled water 10 ml

Final working concentration is 5 µl of ethidium bromide (10 mg/ml) volume in agarose buffer

Phenol

Phenol crystals 1 kg was melted at 65 ^{0}C

TE 1000 ml

Mix, allow to separate and discard TE

Add a further 1000 ml of 0.1%

8-Hydroxyquiniline in TE Store at 4 ^{0}C

7.5 M. Ammonium acetate

Ammonium acetate 607.89 g

Dissolve in distilled water 1000 ml. Store at 4 ^{0}C

TE-9

500 mM Tris pH 8.0

20 mM EDTA

10 mM NaCl

TE-9: SDS

TE-9 + 1% SDS

PC-9 (Phenol- Chloroform)

Phenol 480 ml

TE-9 320 ml

Chloroform 640 ml

Mix and leave to settle at 4 ^{0}C for 2 hours.

Repeat twice and discard top layer.

10x PCR Buffer

200 mM Tris/HCl pH 8.4

500 mM KCl

1x *Hind*III reaction Buffer

500 mM Tris/HCl pH 8.0

100 mM $MgCl_2$

500 mM NaCl

Appendix C Antibodies and visualisation system kits

Ki67 (NCL-KI67-MM1, Novocastra, UK); mouse monoclonal antibody. Product number: NCL-Ki67-MM1

p53 (NCL-p53-CM5p, Novocastra, UK); rabbit polyclonal antibody Product number: NCL-p53 CM5

APC; rabbit polyclonal antibody 3161, Midgley *et al* 1997

β-catenin (Mouse IgG_1, Clone 14,Transduction Laboratories, UK); mouse monoclonal antibody. Product number: C 19220

β-catenin, mouse monoclonal antibody, clone number 5H10. Catalog number MAB2081. Lot number 18040942. Chemicon International Inc, USA

E-cadherin (Anti-mouse E-Cadherin, Clone ECCD-2, R&D System, UK); rat monoclonal antibody. Product number: BTA 2

E-Cadherin, mouse IgG2a clone 36. Catalog number C20820. Transduction Laboratories, UK

Monoclonal Rat anti-Bromodeoxyuridine (BrdU), clone BU1/75 (ICR1). Product code MAS 250p. Harlan Sera-Lab Limited, UK

Donkey Anti-Rabbit IgG (ImmunoPure, Pierce, USA) peroxidase conjugated. Product number: 31458

Swine Anti-Rabbit- Biotinylated HRP-conjugated, F_{ab} fragment. Dako, Denmark product number: E043

Rabbit Anti-Mouse-Biotinylated HRP-conjugated, F_{ab} fragment. Dako, Denmark Product number: E0413

Rabbit anti-Rat IgG, (H+L) Biotin conjugated. Lot number 881209023. Product number 31836. Pierce, USA.

Goat anti-Rat Cy5 conjugated secondary antibody. Chemicon International Inc, USA

Goat anti-Mouse Rhodamine conjugated secondary antibody. Catalog number AP181R. Chemicon International Inc, USA

YOYO1 Iodide (491/509). Catalog number Y-3601. Molecular Probes, Inc. The Netherlands.

StrepABComplex/HRP. Product number: K0377, Dako, Denmark

ABComplex/AP Product number: K0376, Dako, Denmark

Vector Red, Alkaline phosphatase substrate Kit I. Catalog number SK-5100. Vector Laboratories, Inc, USA.

Protein A Sepharose 4 Fast Flow Code number 17-0974-01 Lot number 254140 Pharmacia Biotech AB Uppasala Sweden

Cell proliferation labelling reagent bromodeoxyuridine (BrdU) Catalog number RPN 201 Amersham Life Science

Nitrocellulose membrane Amersham Life Science

Appendix D Tables of statistics

Nuclear volume	N:WT	N:I	N:II	N:III	N:IV	WT:I	WT:II	WT:III	WT:IV	I:II	I:III	I:IV	II:III	II:IV	III:IV
1-49.99	1.052	0.556	1.052	1.052	0.989	-0.5	0	0	-0.06	-0.5	-0.5	0.433	0	-0.06	-0.06
50-99.99	18.32	14.77	20.82	20.65	20.76	-3.56	2.501	2.327	2.441	-6.06	-5.88	5.996	0.174	-0.06	0.114
100-149.99	23.43	31.48	37.25	31.68	39.63	8.054	13.82	8.254	16.21	-5.77	-0.2	8.152	5.566	2.385	7.952
150-199.99	20.07	29.54	32.33	24.18	35.79	9.477	12.26	4.114	15.73	-2.78	5.363	6.249	8.147	3.466	11.61
200-249.99	12.81	20.39	16.38	14.45	23.02	7.577	3.572	1.639	10.21	4.006	5.938	2.633	1.933	6.638	8.571
250-299.99	5.182	12.92	8.406	5.697	13.23	7.734	3.224	0.515	8.048	4.51	7.218	0.314	2.709	4.824	7.533
300-349.99	2.438	7.437	4.563	3.08	7.542	4.999	2.125	0.642	5.104	2.874	4.356	0.105	1.483	2.979	4.462
350-399.99	1.266	3.951	2.698	1.812	4.363	2.685	1.432	0.546	3.097	1.253	2.139	0.413	0.886	1.665	2.551
400-449.99	0.389	2.568	1.078	1.158	2.503	2.178	0.688	0.768	2.114	1.49	1.41	-0.06	-0.08	1.426	1.346
450-499.99	0.292	1.212	0.52	0.654	1.403	0.92	0.228	0.362	1.111	0.692	0.558	0.191	-0.13	0.883	0.749
500-549.99	0.195	0.874	0.266	0.302	1.101	0.679	0.071	0.107	0.906	0.608	0.572	0.227	-0.04	0.835	0.799
550-599.99	1E-06	0.448	0.072	0.151	1.041	0.448	0.072	0.151	1.041	0.376	0.297	0.592	-0.08	0.969	0.89
600+	1E-06	-0	-0	-0	-0	-0	-0	-0	-0	-0	-0	9E-06	3E-06	-0	-0
C	**0.053**	**0.047**	**0.047**	**0.045**	**0.047**	**0.05**	**0.05**	**0.047**	**0.05**	**0.043**	**0.04**	**0.042**	**0.04**	**0.043**	**0.04**

Table 4.1 Table showing the difference in spontaneous intestinal lesions arising in *Apc*$^{Min+/-}$/*p53*$^{-/-}$ mice

The data presented shows the difference in nuclear volume between each lesion type (type I, II, III and IV as described in the text), wild type mice (WT) and normal (N) intestinal crypt cells. The nuclear volume size categories are shown in the first column and the critical value (C) was calculated at p=0.05, with Kolmogorov Smirnov test, are shown in the bottom row. Values of p in excess of the critical value indicate a significant difference at the $p< 0.05$ level.

Nuclear volume	N:WT	N:I	N:II	N:III	N:IV	WT:I	WT:II	WT:III	WT:IV	I:II	I:III	I:IV	II:III	II:IV	III:IV
1-49.99	0	-0.23	-0.34	0	0	0.234	0.345	0	0	-0.11	0.234	0.234	0.345	0.345	0
50-99.99	4.273	-4.78	-3.89	6.196	4.813	9.051	8.167	1.924	0.54	0.884	10.97	9.591	10.09	8.707	1.383
100-149.99	27.88	14.5	25.11	42.22	29.97	13.38	2.769	14.34	2.087	10.61	27.72	15.47	17.11	4.856	12.25
150-199.99	22.77	13.59	18.43	29.7	19.65	9.184	4.341	6.929	-3.12	4.843	16.11	6.065	11.27	1.222	10.05
200-249.99	13.35	5.886	9.212	14.33	8.025	7.46	4.134	0.982	-5.32	3.326	8.443	2.139	5.116	-1.19	6.303
250-299.99	5.722	2.789	3.319	6.203	2.446	2.933	2.403	0.481	-3.28	0.53	3.414	-0.34	2.885	-0.87	3.758
300-349.99	2.629	1.405	1.653	3.376	1.295	1.224	0.976	0.747	-1.33	0.248	1.971	-0.11	1.723	-0.36	2.081
350-399.99	1.266	0.703	0.413	1.062	0.648	0.563	0.853	-0.2	-0.62	-0.29	0.359	-0.06	0.649	0.234	0.414
400-449.99	0.389	0.117	0.207	0.357	0.185	0.272	0.183	-0.03	-0.2	0.089	0.239	0.068	0.15	-0.02	0.172
450-499.99	0.292	0.117	0.207	0.182	0.185	0.175	0.086	-0.11	-0.11	0.089	0.065	0.068	-0.02	-0.02	-0
500-549.99	0.195	0.117	-0	-0	0.093	0.077	0.195	-0.19	-0.1	-0.12	-0.12	-0.02	-0	0.093	-0.09
550-599.99	1E-06	0.117	0	0	-0	-0.12	1E-06	-0	-0	-0.12	-0.12	-0.12	0	-0	7E-06
600+	1E-06	2E-04	-0	0	-0	-0	9E-06	-0	-0	-0	-0	-0	8E-06	1E-06	7E-06
C	**0.06**	**0.06**	**0.068**	**0.067**	**0.058**	**0.056**	**0.064**	**0.063**	**0.053**	**0.064**	**0.063**	**0.053**	**0.071**	**0.062**	**0.061**

Table 4.2 Table showing the difference of nuclear volume in spontaneous intestinal lesions arising in *Apc*$^{Min+/-}$ mice

The data presented shows the difference in the nuclear volume between each lesion type (type I, II, III and IV as described in the text), wild type (WT) mice and normal (N) intestinal crypt cells. The nuclear volume size categories are shown in the first column and the critical value (C) was calculated at p=0.05, with Kolmogorov Smirnov test, are shown in the bottom row. Values of p in excess of the critical value indicate a significant difference at the $p< 0.05$ level.

Nuclear volume	N:WT	N:I	N:II	N:III	N:IV	WT:I	WT: II	WT:III	WT:IV	I:II	I:III	I:IV	II:III	II:IV	III:IV
1-49.99	0.24	0.15	0.24	0.022	0.149	-0.09	0	-0.22	-0.09	-0.09	0.128	0.001	0.219	0.092	-0.13
50-99.99	3.936	4.288	1.096	-1.05	0.971	0.351	-2.84	-4.98	-2.97	3.192	5.336	3.317	2.144	0.125	-2.02
100-149.99	6.607	14.69	15.05	6.66	6.804	8.078	8.439	0.053	0.197	-0.36	8.026	7.881	8.386	8.242	-0.14
150-199.99	7.795	16.65	20.93	8.294	7.508	8.856	13.14	0.499	-0.29	-4.28	8.356	9.142	12.64	13.42	0.786
200-249.99	6.41	14.51	16.17	6.514	4.098	8.1	9.764	0.104	-2.31	-1.66	7.996	10.41	9.66	12.08	2.417
250-299.99	2.728	10.27	10.04	4.455	2.626	7.545	7.312	1.727	-0.1	0.233	5.817	7.647	5.585	7.414	1.829
300-349.99	1.429	6.277	5.774	4.15	2.096	4.848	4.345	2.722	0.668	0.503	2.127	4.181	1.624	3.678	2.054
350-399.99	0.786	3.934	2.802	2.084	1.077	3.149	2.016	1.298	0.291	1.132	1.85	2.858	0.718	1.725	1.007
400-449.99	0.389	2.523	1.846	1.86	0.641	2.133	1.457	1.47	0.252	0.676	0.663	1.881	-0.01	1.205	1.219
450-499.99	0.292	1.261	0.923	1.156	0.367	0.969	0.631	0.863	0.075	0.338	0.106	0.894	-0.23	0.556	0.789
500-549.99	0.195	0.721	0.308	0.571	0.184	0.526	0.113	0.376	-0.01	0.413	0.15	0.537	-0.26	0.124	0.387
550-599.99	1E-06	0.45	0.103	-0	5E-04	0.45	0.103	-0	5E-04	0.348	0.45	0.45	0.103	0.102	-0
600+	1E-06	-0	-0	0	5E-04	-0	-0	-0	5E-04	1E-05	-0	-0	-0	-0	-0
C	**0.057**	**0.053**	**0.055**	**0.057**	**0.054**	**0.053**	**0.054**	**0.056**	**0.053**	**0.051**	**0.053**	**0.05**	**0.055**	**0.051**	**0.053**

Table 4.3 Table showing the difference of nuclear volume in spontaneous intestinal lesions arising in *Apc*$^{Min+/-}$/*Msh2*$^{-/-}$ mice

The data presented shows the difference in the nuclear volume between each lesion type (type I, II, III and IV as described in the text), wild type (WT) mice and normal (N) intestinal crypt cells. The nuclear volume size categories are shown in the first column and the critical value was calculated at p=0.05, with Kolmogorov Smirnov test, are shown in the bottom row. Values of p in excess of the critical value indicate a significant difference at the $p< 0.05$ level.

Nuclear volume	N:WT	N:III	N:IV	WT:III	WT:IV	III:IV
1-49.99	0.256	0.163	0.132	-0.09	-0.12	0.031
50-99.99	13.86	16.65	16.15	2.783	2.282	0.501
100-149.99	9.507	28.07	23.87	18.56	14.36	4.204
150-199.99	16.26	33.62	31.41	17.36	15.15	2.212
200-249.99	12.45	21.26	22.06	8.813	9.615	-0.8
250-299.99	5.562	12.34	13.17	6.776	7.604	-0.83
300-349.99	2.373	7.52	7.698	5.147	5.325	-0.18
350-399.99	1.266	4.124	4.228	2.859	2.962	-0.1
400-449.99	0.389	1.789	1.369	1.4	0.98	0.42
450-499.99	0.292	1.071	0.621	0.779	0.329	0.45
500-549.99	0.195	0.714	0.123	0.52	-0.07	0.591
550-599.99	5E-06	0.446	-0	0.446	-0	0.446
600+	5E-06	1E-05	-0	1E-05	-0	2E-05
C	**0.057**	**0.057**	**0.059**	**0.056**	**0.057**	**0.057**

Table 4.4 Table showing the difference of nuclear volume in spontaneous intestinal lesions arising in *Msh2*$^{-/-}$ mice

The data presented shows the difference in nuclear volume between each lesion type (type I, II, III and IV as described in the text), wild type (WT) mice and normal (N) intestinal crypt cells. The nuclear volume size categories are shown in the first column. The critical value (C) was calculated at p=0.05, with Kolmogorov Smirnov test, are shown in the bottom row. Values of p in excess of the critical value indicate a significant difference at the $p< 0.05$ level.

Nuclear volume	I	II	III	IV	normal		I	II	III	IV	normal		III	IV	normal
1-49.99	0.262	-0.34	0	0.063	1.052		0.406	0	-0.22	-0.03	0.812		-0.09	-0.06	0.796
50-99.99	-5.5	-10.7	-0.4	-1.9	14.05		3.907	-5.34	-7.31	-5.41	14.39		0.456	-0.16	4.458
100-149.99	-21.4	-16.6	6.085	-14.1	-4.45		0.024	-5.38	-8.2	-16	16.82		10.31	-1.85	13.92
150-199.99	-18.7	-16.6	2.815	-18.8	-2.7		-0.62	0.878	-3.61	-16	12.27		13.25	-0.57	3.807
200-249.99	-15	-7.71	-0.66	-15.5	-0.54		0.522	6.193	-1.53	-12.5	6.4		7.174	-0.6	0.361
250-299.99	-10.7	-5.63	-0.03	-11.3	-0.54		-0.19	4.088	1.212	-8.15	2.454		6.26	-0.44	-0.38
300-349.99	-6.22	-3.1	0.105	-6.44	-0.19		-0.15	2.22	2.079	-4.44	1.009		4.505	0.221	0.065
350-399.99	-3.25	-2.28	-0.75	-3.72	-0		0.464	0.584	0.752	-2.81	0.48		2.313	-0.14	-0
400-449.99	-2.45	-0.87	-0.8	-2.32	0		-0.05	0.769	0.702	-1.86	-0		0.632	-1.13	-0
450-499.99	-1.09	-0.31	-0.47	-1.22	0		0.049	0.403	0.501	-1.04	0		0.417	-0.78	-0
500-549.99	-0.76	-0.27	-0.3	-1.01	0		-0.15	0.042	0.269	-0.92	0		0.412	-0.98	-0
550-599.99	-0.33	-0.07	-0.15	-1.04	0		0.002	0.031	-0.15	-1.04	0		0.295	-1.04	-0
600+	2E-04	0	1E-05	1E-05	0		2E-05	-0	1E-05	5E-04	0		2E-05	1E-05	-0
C	**0.05**	**0.059**	**0.056**	**0.046**	**0.058**		**0.046**	**0.048**	**0.048**	**0.046**	**0.054**		**0.047**	**0.051**	**0.054**

Table 4.4.1 Table showing the difference of nuclear volume in spontaneous intestinal lesions arising in *Apc$^{Min+/-}$*, *Apc$^{Min+/-}$/p53$^{-/-}$*, *Apc$^{Min+/-}$/Msh2$^{-/-}$* and *Msh2$^{-/-}$* mice

The data presented shows the difference in nuclear volume in each lesion type (type I, II, III and IV as described in the text) between each genotype mice and also in normal crypt cells. The nuclear volume size categories are shown in the first column. The 2nd - 6th column are *Apc$^{Min+/-}$/p53$^{-/-}$* compared with *Apc$^{Min+/-}$* mice, the 7th - 11th column are *Apc$^{Min+/-}$/p53$^{-/-}$* compared with *Apc$^{Min+/-}$/Msh2$^{-/-}$* mice and the 12th -14th column are *Apc$^{Min+/-}$/p53$^{-/-}$* compared with *Msh2$^{-/-}$* mice. The critical value (C) was calculated at p=0.05, with Kolmogorov Smirnov test, are shown in the bottom row. Values of p in excess of the critical value indicate a significant difference of the $p< 0.05$ level.

Nuclear volume	I	II	III	IV	normal		III	IV	normal		III	IV	normal
1-49.99	0.144	0.345	-0.22	-0.09	-0.24		-0.09	-0.12	-0.26		0.126	-0.03	-0.02
50-99.99	9.402	5.326	-6.91	-3.51	0.336		0.86	1.742	-9.59		7.768	5.247	-9.93
100-149.99	21.46	11.21	-14.3	-1.89	21.27		4.223	12.27	18.37		18.51	14.16	-2.9
150-199.99	18.04	17.48	-6.43	2.833	14.98		10.44	18.27	6.512		16.87	15.44	-8.46
200-249.99	15.56	13.9	-0.88	3.008	6.936		7.831	14.94	0.897		8.709	11.93	-6.04
250-299.99	10.48	9.715	1.246	3.174	2.994		6.294	10.88	0.16		5.048	7.706	-2.83
300-349.99	6.072	5.321	1.974	2.002	1.2		4.4	6.659	0.256		2.425	4.657	-0.94
350-399.99	3.712	2.869	1.502	0.909	0.48		3.063	3.58	-0		1.56	2.671	-0.48
400-449.99	2.405	1.64	1.503	0.456	-0		1.432	1.184	-0		-0.07	0.728	-0
450-499.99	1.144	0.716	0.973	0.182	0		0.889	0.436	-0		-0.08	0.254	-0
500-549.99	0.603	0.308	0.571	0.091	0		0.714	0.031	-0		0.144	-0.06	-0
550-599.99	0.333	0.103	-0	5E-04	0		0.446	0	-0		0.446	-0	-0
600+	-0	-0	0	5E-04	0		1E-05	0	-0		1E-05	-0	-0
C	**0.053**	**0.063**	**0.063**	**0.05**	**0.061**		**0.063**	**0.054**	**0.062**		**0.056**	**0.054**	**0.058**

Table 4.4.2 Table showing the difference of nuclear volume in spontaneous intestinal lesions arising in *Apc*$^{Min+/-}$, *Apc*$^{Min+/-}$/*Msh2*$^{-/-}$ and *Msh2*$^{-/-}$ mice

The data presented shows the difference in nuclear volume in each lesion type (type I, II, III and IV as described in the text) between each genotype mice and also in normal crypt cells. The nuclear volume size categories are shown in the first column. The 2nd-6th column are *Apc*$^{Min+/-}$ compared with *Apc*$^{Min+/-}$/*Msh2*$^{-/-}$ mice, the 7th-9th column are *Apc*$^{Min+/-}$ compared with *Msh2*$^{-/-}$ mice and the 10th-12th column are *Msh2*$^{-/-}$ compared with *Apc*$^{Min+/-}$/*Msh2*$^{-/-}$ mice. The critical value (C) was calculated at p=0.05, with Kolmogorov Smirnov test, are shown in the bottom row. Values of p in excess of the critical value indicate a significant difference at the $p< 0.05$ level.

Nuclear volume	N:I	N:II	N:III	N:IV	N:V	N:WT	WT:I	WT:II	WT: III	WT: IV	WT:V	I:V	I:IV	I:III	I:II	II:V	II:IV	II:III	III:V	III:IV	IV:V
1-49.99	0.253	0.253	0.253	0.253	0.253	1.944	2.198	2.198	2.198	2.198	2.198	0	0	0	0	0	0	0	0	0	0
50-99.99	28.49	30.87	29.07	26.32	18.29	10.1	38.59	40.97	39.18	36.42	28.39	10.2	2.168	-0.58	2.376	12.58	4.545	1.793	10.79	2.751	8.036
100-149.99	62.75	68.4	62.46	39.24	26.29	6.98	69.73	75.38	69.44	46.22	33.27	36.46	23.51	0.292	5.654	42.11	29.16	5.946	36.17	23.22	12.95
150-199.99	55.14	56.24	49.31	27.35	18.24	4.252	59.39	60.49	53.56	31.61	22.49	36.9	27.79	5.831	1.101	38	28.89	6.932	31.07	21.96	9.113
200-249.99	37.25	35.22	32.59	14.42	7.359	1.338	38.59	36.56	33.93	15.75	8.697	29.9	22.84	4.665	-2.03	27.86	20.81	2.633	25.23	18.17	7.057
250-299.99	19.65	20.48	18.77	9.865	4.259	0.76	20.41	21.24	19.53	10.63	5.019	15.39	9.783	0.875	0.832	16.22	10.62	1.707	14.51	8.909	5.606
300-349.99	16.07	11.68	12.87	6.465	2.835	0.253	16.33	11.94	13.12	6.719	3.089	13.24	9.608	3.207	-4.39	8.849	5.219	-1.18	10.03	6.401	3.63
350-399.99	14.16	5.61	7.453	4.405	1.804	0.127	14.29	5.736	7.58	4.531	1.931	12.36	9.754	6.706	-8.55	3.806	1.205	-1.84	5.65	3.049	2.601
400-449.99	10.2	3.566	5.248	2.969	0.772	0	10.2	3.566	5.248	2.969	0.772	9.432	7.235	4.956	-6.64	2.794	0.597	-1.68	4.476	2.279	2.197
450-499.99	6.122	1.395	2.332	1.563	1E-05	0	6.122	1.395	2.332	1.563	1E-05	6.122	4.56	3.79	-4.73	1.395	-0.17	-0.94	2.332	0.77	1.562
500-549.99	6.122	0.465	0.875	0.625	1E-05	0	6.122	0.465	0.875	0.625	1E-05	6.122	5.497	5.248	-5.66	0.465	-0.16	-0.41	0.875	0.25	0.625
550-599.99	6.122	0.465	0.875	0.313	1E-05	0	6.122	0.465	0.875	0.313	1E-05	6.122	5.81	5.248	-5.66	0.465	0.153	-0.41	0.875	0.562	0.312
600+	2E-05	0	1E-05	6E-06	2E-05	0	2E-05	0	1E-05	6E-06	2E-05	2E-06	1E-05	7E-06	-0	-0	-0	-0	-0	4E-06	-0
C	**0.172**	**0.062**	**0.075**	**0.062**	**0.084**	**0.163**	**0.174**	**0.068**	**0.08**	**0.068**	**0.088**	**0.174**	**0.173**	**0.178**	**0.173**	**0.086**	**0.065**	**0.078**	**0.096**	**0.078**	**0.086**

Table 4.6 Table showing the difference of nuclear volume in spontaneous pancreatic lesions arising in *Apc*$^{Min+/-}$ mice

The data presented shows the difference in nuclear volume between each lesion type (type I, II, III, IV, V and VI as described in the text), wild type (WT) and normal (N) pancreatic cells. The nuclear volume size categories are shown in the first column. The critical value (C) was calculated at p=0.05, with Kolmogorov Smirnov test, are shown in the bottom row. Values of p in excess of the critical value indicate a significant difference at the $p< 0.05$ level.

Nuclear volume	N:I	N:II	N:III	N:IV	N:V	N:VI	N: WT	WT:I	WT: II	WT: III	WT: IV	WT: V	WT: VI	I:VI	I:V	I:IV	I:III	I:II	II:VI	II:V	II:IV	II:III	III: VI	III:V	III: IV	IV:V
1-49.99	0	-0.06	0	0	0	0	2.2	2.2	2.13	2.2	2.2	2.2	2.2	0	0	0	0	0.06	-0.06	0.06	-0.06	-0.06	0	0	0	0
50-99.99	32	31.1	32.6	29.1	31.9	31.7	10	42	41.2	42.7	39.1	42	41.8	0.22	0.03	2.88	-0.68	0.83	-0.61	0.8	2.04	-1.51	0.9	-0.71	3.55	2.84
100-149.99	66.1	67.2	69.7	58.6	65.3	64	11.9	78	79.1	81.5	70.4	77.2	75.9	2.04	0.81	7.52	-3.59	-1.11	3.15	-1.92	8.63	-2.48	5.63	-4.4	11.1	6.71
150-199.99	72.8	63.5	65.9	50.7	63.4	54.6	7.76	80.6	71.2	73.6	58.4	71.1	62.4	18.2	9.48	22.2	6.98	9.38	8.83	-0.11	12.8	-2.4	11.2	-2.51	15.2	12.7
200-249.99	66.1	50.4	50.2	40.7	54.1	35.4	5.3	71.4	55.7	55.5	46	59.4	40.7	30.7	12	25.4	16	15.8	14.9	3.73	9.66	0.21	14.7	3.94	9.46	13.4
250-299.99	53.9	40	38.5	32.6	43.7	20.4	3.49	57.4	43.5	42	36.1	47.2	23.8	33.6	10.2	21.4	15.4	13.9	19.7	3.7	7.45	1.51	18.2	5.21	5.94	11.2
300-349.99	46.5	32.7	33.1	24.8	37.1	13.2	1.49	48	34.2	34.5	26.3	38.6	14.7	33.2	9.37	21.7	13.4	13.8	19.5	4.4	7.93	-0.35	19.8	4.06	8.28	12.3
350-399.99	36.2	25.3	25	17.9	31.9	7.72	1	37.2	26.3	26	18.9	32.9	8.72	28.4	4.23	18.2	11.2	10.9	17.6	6.63	7.35	0.3	17.3	6.93	7.05	14
400-449.99	30.5	19.8	19.4	12.1	27.9	4.51	0.62	31.1	20.4	20	12.7	28.6	5.13	26	2.51	18.4	11.1	10.7	15.3	8.18	7.69	0.39	14.9	8.57	7.3	15.9
450-499.99	27.2	15.1	15.1	9.94	23.8	1.68	0.5	27.7	15.6	15.6	10.4	24.3	2.18	25.5	3.39	17.3	12.1	12.1	13.4	8.74	5.13	-0.06	13.5	8.68	5.2	13.9
500-549.99	21.8	12.1	11.7	7.58	20.1	0.66	0.5	22.3	12.6	12.2	8.07	20.6	1.15	21.1	1.73	14.2	10.1	9.68	11.5	7.95	4.55	0.44	11	8.39	4.11	12.5
550-599.99	17.1	9.87	10	5.64	16.8	0.27	0.5	17.6	10.4	10.5	6.14	17.3	0.77	16.8	0.24	11.4	7.02	7.2	9.6	6.95	4.24	-0.17	9.78	6.78	4.41	11.2
600+	-0	-0.61	-0	-0	-0	0	0	-0	-0.61	-0	-0	-0	0	-0	0	0	0	0.61	-0.61	0.61	-0.61	-0.61	-0	0	0	0
C	**0.1**	**0.05**	**0.06**	**0.06**	**0.06**	**0.06**	**0.06**	**0.11**	**0.06**	**0.07**	**0.06**	**0.06**	**0.07**	**0.1**	**0.1**	**0.1**	**0.11**	**0.1**	**0.05**	**0.05**	**0.05**	**0.06**	**0.06**	**0.06**	**0.06**	**0.05**

Table 4.7 Table showing the difference of nuclear volume in spontaneous pancreatic lesions arising in *Apc$^{Min+/-}$/p53$^{-/-}$* mice

The data presented shows the difference in nuclear volume between each lesion type (type I, II, III, IV, V and VI as described in the text), wild type (WT) and normal (N) pancreatic cells. The nuclear volume size categories are shown in the first column. The critical value (C) was calculated at p=0.05, with Kolmogorov Smirnov test, are shown in the bottom row. Values of p in excess of the critical value indicate a significant difference at the $p< 0.05$ level.

Nuclear volume	N:WT	N:I	N:II	N:III	N:IV	N:V	WT: I	WT:II	WT: III	WT: IV	WT:V	I:V	I:IV	I:III	I:II	II:III	II:IV	II:V	III:IV	III:V	IV:V
1-49.99	1.448	0.75	0.75	0.75	0.75	0.75	2.198	2.198	2.198	2.198	2.198	0	0	0	0	0	0	0	0	0	0
50-99.99	14.8	24.54	8.842	26.39	3.516	23	39.34	23.64	41.19	18.32	37.8	1.54	21.03	-1.85	15.7	-17.5	5.326	-14.2	22.87	3.388	19.49
100-149.99	14.72	36.71	22.32	42.19	15.13	26.8	51.43	37.04	56.91	29.85	41.52	9.904	21.58	-5.48	14.39	-19.9	7.184	-4.49	27.05	15.38	11.67
150-199.99	6.544	43.29	20.33	25.29	9.94	11.84	49.84	26.87	31.83	16.48	18.39	31.45	33.35	18	22.97	-4.96	10.39	8.484	15.35	13.45	1.902
200-249.99	3.192	38.29	11.13	11.97	4.867	5.289	41.48	14.32	15.16	8.059	8.481	33	33.42	26.32	27.17	-0.85	6.26	5.837	7.105	6.682	0.422
250-299.99	1.125	25.54	6.73	8.776	1.805	2.305	26.67	7.855	9.901	2.93	3.43	23.24	23.74	16.77	18.81	-2.05	4.925	4.425	6.971	6.471	0.499
300-349.99	0.625	21.04	6.022	4.821	0.108	1	21.67	6.647	5.446	0.733	1.625	20.04	20.93	16.22	15.02	1.201	5.914	5.022	4.713	3.821	0.892
350-399.99	0.25	18.08	5.49	2.72	0.116	0.833	18.33	5.74	2.97	0.366	1.083	17.25	17.97	15.36	12.59	2.77	5.374	4.657	2.604	1.887	0.717
400-449.99	0.125	9.875	2.594	1.36	0.058	0.778	10	2.719	1.485	0.183	0.903	9.097	9.817	8.515	7.281	1.234	2.536	1.817	1.302	0.583	0.719
450-499.99	3E-06	5	2.417	1.485	1E-05	0.541	5	2.417	1.485	1E-05	0.542	4.459	5	3.515	2.583	0.932	2.417	1.875	1.485	0.944	0.541
500-549.99	3E-06	5	2.115	0.495	1E-05	0.361	5	2.115	0.495	1E-05	0.361	4.639	5	4.505	2.885	1.62	2.115	1.754	0.495	0.134	0.361
550-599.99	3E-06	3.333	1.511	0.495	1E-05	0.361	3.333	1.511	0.495	1E-05	0.361	2.972	3.333	2.838	1.823	1.016	1.511	1.15	0.495	0.134	0.361
600+	-0	3E-05	7E-06	1E-05	3E-05	0	1E-05	-0	-0	2E-05	-0	3E-05	-0	2E-05	2E-05	-0	-0	7E-06	-0	1E-05	-0
C	**0.065**	**0.156**	**0.076**	**0.092**	**0.065**	**0.064**	**0.159**	**0.081**	**0.096**	**0.071**	**0.07**	**0.158**	**0.159**	**0.171**	**0.164**	**0.104**	**0.081**	**0.081**	**0.096**	**0.096**	**0.07**

Table 4.8 Table showing difference of nuclear volume in spontaneous pancreatic lesions arising in *Apc$^{Min+/-}$/ Msh2$^{-/-}$* mice

The data presented shows the difference in nuclear volume between each lesion type (type I, II, III, IV, V and VI as described in the text), wild type (WT) and normal (N) pancreatic cells. The nuclear volume size categories are shown in the first column. The critical value (C) was calculated at p=0.05, with Kolmogorov Smirnov test, are shown in the bottom row. Values of p in excess of critical value indicate a significant difference of the $p< 0.05$ level.

Nuclear volume	I	II	III	IV	V	normal		I	II	III	IV	V	normal		I	II	III	IV	V	normal
1-49.99	0	-0.06	0	0	0	0.75		0	0	0	0	0	0.75		0	0.064	0	0	0	0
50-99.99	2.658	17.52	1.485	20.81	4.164	-4.75		3.333	19.03	1.485	24.36	4.874	27.62		0.676	1.511	0	3.552	0.709	32.37
100-149.99	26.53	42.03	24.64	40.59	35.63	-2.84		32.59	49.35	27.69	51.99	32.28	40.8		6.054	7.32	3.047	11.4	-3.34	43.64
150-199.99	30.77	44.35	41.79	41.96	52.73	1.214		29.97	58.59	47.68	39.81	24.96	10.51		-0.8	14.23	5.887	-2.15	-27.8	9.296
200-249.99	29.95	41.34	40.29	37.94	50.91	2.104		19.56	47.82	40.05	25.2	15.66	2.709		-10.4	6.482	-0.24	-12.7	-35.3	0.604
250-299.99	30.77	35.66	32.1	33.13	43.78	2.362		12.11	28.89	24.21	13.01	5.451	0.396		-18.7	-6.77	-7.89	-20.1	-38.3	-1.97
300-349.99	26.31	27.55	29.1	25.53	36.98	0.869		-1.26	14.59	14.09	9.892	3.395	0.135		-27.6	-13	-15	-15.6	-33.6	-0.73
350-399.99	18.83	20.56	23.03	18.58	31.85	0.746		-2.01	6.198	10.15	6.352	2.006	0.003		-20.8	-14.4	-12.9	-12.2	-29.8	-0.74
400-449.99	21.08	17.67	18.51	12.52	27.67	0.498		4.286	3.017	6.095	4.348	1.028	0.002		-16.8	-14.7	-12.4	-8.17	-26.6	-0.5
450-499.99	22.7	13.16	14.15	10.44	23.77	0.498		5.204	1.149	3.763	2.969	0.231	-0		-17.5	-12	-10.4	-7.47	-23.5	-0.5
500-549.99	17.3	10.5	11.69	8.073	20.21	0.498		1.122	-0.72	1.837	1.562	-0.36	-0		-16.2	-11.2	-9.85	-6.51	-20.6	-0.5
550-599.99	14.23	8.861	10.05	6.136	16.96	0.498		2.789	-1.05	0.38	0.625	-0.36	-0		-11.4	-9.91	-9.67	-5.51	-17.3	-0.5
600+	-0	-0.61	0	-0	1E-05	2E-05		6.122	0.465	0.875	0.312	3E-05	2E-05		6.122	1.077	0.875	0.313	2E-05	-0
C	**0.178**	**0.071**	**0.096**	**0.063**	**0.062**	**0.058**		**0.225**	**0.079**	**0.103**	**0.068**	**0.088**	**0.059**		**0.192**	**0.055**	**0.08**	**0.06**	**0.081**	**0.058**

Table 4.9 Table showing the difference of pancreatic nuclear volume in different mouse genotype.

The data presented shows the difference in nuclear volume in each lesion type (type I, II, III, IV, V and VI as described in the text) between each genotype of mice and also in normal pancreatic cells. The nuclear volume size categories are shown in the first column. The 2nd-7th column are *Apc*$^{Min+/-}$*/p53*$^{-/-}$ compared with *Apc*$^{Min+/-}$*/Msh2-/-* mice, the 8th-13th column are *Apc*$^{Min+/-}$*/Msh2*$^{-/-}$ compared with *Apc*$^{Min+/-}$ mice and the 14th-19th column are *Apc*$^{Min+/-}$*/p53*$^{-/-}$ compared with *Apc*$^{Min+/-}$ mice. The critical value (C) was calculated at p=0.05, with Kolmogorov Smirnov test, are shown in the bottom row. Values of p in excess of the critical value indicate a significant difference of the $p< 0.05$ level.

Bibliography

Aaltonen LA., Peltomaki P., Leach FS., Sistonen P., Pylkkanen L., Mecklin J-P., Jarvinen H., Powell SM., Jen J., Hamilton SR., Petersen GM., Kinzler KW., Vogelstein B. and de la Chapelle A. (1993). Clues to the pathogenesis of familial colorectal cancer. *Science* **260**: 812-826

Aaltonen LA., Peltomaki P., Mecklin J-P., Jarvinen H., Jass JR., Green JS., Lynch HT., Watson P., Tallqvist G., Juhola M., Sistonen P., Hamilton SR., Kinzler KW., Vogelstein B. and Delachapelle A. (1994). Replication errors in benign and malignant tumours from hereditary nonpolyposis colorectal cancer patients. *Cancer Res.* **54**: 1645-1648

Aberle H., Butz S., Stappert J., Weissig H., Kemler R. and Hoschuetzky H. (1994). Assembly of the cadherin-catenin complex in vitro with recombinant proteins. *J Cell Sci* **107**: 3655-3663

Aberle H., Bauer A., Stappert J., Kispert A. and Kemler R. (1997). β-catenin is a target for the ubiquitin-proteasome pathway. *EMBO J* **16**: 3797-3804

Alani E., Chi NW. and Kolodner R. (1995). The *Saccharomyces cerevisiae* MSH2 protein specifically binds to duplex oligonucleotides containing mismatched DNA base pair and insertions. *Gene Dev* **9**: 234-247

Arai T., Kida Y., Harmon BV. and Gobe GC. (1996). Comparative alterations in p53 expression and apoptosis in the irradiated rat small and large intestine. *Br J Cancer* **74**: 406-412

Armstrong JF., Kaufman MH., Harrison DJ. and Clarke AR. (1995). High-frequency developmental abnormalities in *p53*-deficient mice. *Curr Biol* **5**: 931-936

Askew DS., Ashmun RA., Simmons BC. and Cleveland JL. (1991). Constitutive c-myc expression in an IL-3 dependent myeloid cell line suppresses cell cycle arrest and accelerates apoptosis. *Oncogene* **6**: 1915-1922

Baeg GH., Matsumine A., Kuroda T., Bhattacharjee RN., Miyashiro I., Toyoshima K. and Akiyama T. (1995). The tumour suppressor gene product APC blocks cell cycle progression from G0/G1 to S phase. *EMBO J* **14**: 5618-5625

Bahary N., Zorich G., Pachter JE., Liebel RL. and Friedman JM. (1991). Molecular genetic linkage maps of mouse chromosome 4 and 6. *Genomics* **11**: 33-47

Baker SJ., Markowitz S., Fearon ER., Willson JKV. and Vogelstein B. (1990). Suppression of human colorectal carcinoma cell growth by wild type p53. *Science* **249**: 912-915

Barth A., Nathke IS. and Nelson WJ. (1997). Cadherins, catenins and APC protein: interplay between cytoskeletal complexes and signalling pathways. *Curr Opin Cell Biol* **9**:683-690

Baserga R. (1965). The relationship of the cell cycle to tumour growth and control of cell division: A Review. *Cancer Res* **25**: 581-595

Batsche E., Muchardt C., Behrens J., Hurst HC. and Cremisi C. (1998). RB and c-Myc activate expression of the E-cadherin gene in epithelial cells through interaction with transcription factor AP-2. *Mol Cell Biol* **18**: 3647-3658

Behrens J., Vakaet L., Friis R., Winterhager E., Roy FV., Mareel M. and Birchmeier W. (1993). Loss of

epithelial differentiation and gain of invasiveness correlates with tyrosine phosphorylation of the E-cadherin/β-catenin complex in cells transformed with atemperature-sensitive v-SRC gene. *J Cell Biol* **120**: 757-766

Behrens J., von Kris JP., Kuhl M., Bruhn L., Wedlich D., Grosschedl R. and Birchmeier W. (1996). Functional interaction of β-catenin with the transcription factor LEF-1. *Nature* **382**: 638-642

Behrens J., Jerchow B-A., Wuetele M., Grimm J., Asbrand C., Wirtz R., Kuhl M., Wedlich D. and Birchmeier W. (1998). Functional interaction of a Axin homolog, Conductin, with β-catenin, APC and GSK3β. *Science* **280**: 596-599

Ben-Ze'ev A. and Geiger B. (1998). Differential molecular interactions of β-catenin and plakoglobin in adhesion, signalling and cancer. *Curr Biol* **10**: 629-639

Berrueta L., Kraeft S-K., Tirnauer JS., Schuyler SC., Chen LB., Hill DE., Pellman D. and Bierer BE. (1998). The adenomatous polyposis coli-binding protein EB1 is associated with cytoplasmic and spindle microtubules. *Proc Natl Acad Sci USA* **95**: 10596-10601

Bhanot P., Brink M., Samos CH., Hsieh JC., Wang Y., Macke JP., Andrew D., Nathans J. and Nusse R. (1996). A new member of the frizzled family from Drosophila functions as a wingless receptor. *Nature* **382**: 225-230

Bilger A., Shoemaker AR., Gould KA. and Dove WF. (1996). *Semin Cancer Biol* **7**: 249-260

Bins M. and Takens F. (1985). A method to estimate the DNA content of whole nuclei from measurements made on thin tissue sections. *Cytometry* **6**:234-237

Birch JM. (1990). The Li-Fraumeni cancer family syndrome. *J Pathol* **161**: 1-2

Bishop JM. (1983). Cellular oncogenes and retroviruses. *Annu Rev Biochem* **52**: 301-354

Blackwell TK., Kretzner L., Backwood EM., Eisenman RN. and Weintraub H. (1990). Sequence-specific DNA binding by the c-myc protein. *Science* **250**: 1149-1151

Bleiberg H., Buyse M. and Galand P. (1985). Cell kinetics indicators of premalignant stages of colorectal cancer. *Cancer* **56**: 124-129

Bodrug SE., Warner BJ., Bath ML., Lindeman GJ., Harris AW. and Adams JM. (1994). Cyclin D1 transgene impedes lymphocyte maturation and collaborates in lymphomagenesis with the Myc gene. *EMBO J* **13**: 2124-2130

Borresen AL., Lothe RA., Meling GI., Lystad S., Morrison P., Lipford J., Kane MF., Rognum TO. and Kolodner RD. (1995). Somatic mutations in the hMSH2 gene in microsatellite unstable colorectal carcinomas. *Hum Mol Genet* **4**: 2065-2072

Bouffler SD., Kemp CJ., Balmain A. and Cox R. (1995). Spontaneous and ionizing radiation-induced chromosomal abnormalities in p53-deficient mice. *Cancer Res* **55**: 3883-3889

Bronner CE., Baker SM., Morrison PT., Warren G., Smith LG., Lescoe MK., Kane M., Earabino C., Lipford J., Lindblom A., Tannergard P., Bollag RJ., Godwin AR., Ward DC., Nordenskjold M., Fishel R., Kolodner R. and Linskay RM. (1994). Mutation in the DNA mismatch repair gene homologue hMLH1 is associated with hereditary nonpolyposis colon cancer. *Nature* **368**: 258-261

Browne SJ., Williams AC., Hague A., Butt AJ. and Paraskeva C. (1994). Loss of APC protein expressed by human colonic epithelial cells and the appearance of a specific low-molecular weight form is associated with apoptosis *in vitro*. *Int J Cancer* **59**: 56-64

Browne SJ., MacFarlane M., Cohen GM. and Paraskeva C. (1998). The adenomatous polyposis coli protein and retinoblastoma protein are cleaved early in apoptosis and are potential substrates for caspases. *Cell Death and Differentiation* **5**: 206-213

Buckley MF., Sweeney KJ., Hamilton JA., Sini RL., Manning DL., Nicholson RI., deFazio A., Watts CK., Musgrove EA. and Sutherland RL. (1993). Expression and amplification of cyclin genes in human breast cancer. *Oncogene* **8**: 2127-2133

Bunz F., Dutriaux A., Lengauer C., Waldman T., Zhou S., Brown JP., Sedivy JM., Kinzler KW. and Vogelstein B. (1998). Requirement for p53 and p21 to sustain G2 arrest after DNA damage. *Science* **282**: 1497-1501

Cadigan K. and Nusse R. (1998). Wnt signalling: a common theme in animal development. *Gene Dev* **11**: 3286-3305

Carder P., Wyllie AH., Purdie CA., Morris RG., White S., Piris J. and Bird CC. (1993). Stabilized p53 facilitates aneuploidy clonal divergence in colorectal cancer. *Oncogene* **8**: 1397-1401

Carlsson P., Waterman ML. and Jones KA. (1993). The hLEF/TCF-1 α HMG protein contains a context-dependent transcriptional activation domain that induces the TCR α enhancer in T cells. *Gene Dev* **7**: 2418-1430

Carnac G., Kodjabachian L., Gurdon JB. and Lemaire P. (1996). The homeobox gene *Siamois* is a target of the Wnt dorsalisation pathway and triggers organiser activity in the absence of mesoderm. *Development* **122**: 3055-3065

Castrop J., van Norren K. and Clevers HC. (1992). A gene family of HMG-box transcription factors with homology to Tcf-1. *Nucleic Acids Res* **20**: 611

Cavallo RA., Cox RT., Moline MM., Roose J., Polevoy GA., Clevers H., Peifer M. and Bejsovec A. (1998). *Drosophila* Tcf and groucho interacts to repress Wingless signalling activity. *Nature* **395**: 604-608

Chan SDH., Karpf DB., Fowlkes ME., Hooks M., Bradley MS., Vuong V., Bambino T., Liu MYC., Arnoud CD., Strewler GJ. and Nissenson RA. (1992). Two homologs of the Drosophila polarity gene frizzled (*fz*) are widely expressed in mammalian tissues. *J Biol Chem* **267**: 25202-25207

Clarke AR., Purdie CA., Harrison DJ., Morris RG., Bird CC., Hooper ML. and Wyllie AH. (1993). Thymocyte apoptosis induced by p53-dependent and independent pathways. *Nature* **362**: 849-852

Clarke AR., Gledhill S., Hooper ML., Bird CC. and Wyllie AH. (1994). p53 dependence of early apoptotic and proliferation response within the mouse intestinal epithelium following γ-irradiation. *Oncogene* **9**: 1767-1773

Clarke AR., Cummings MC. and Harrison DJ. (1995). Interaction between murine germline mutations in p53 and APC predisposes to pancreatic neoplasia but not to incrreased intestinal malignancy. *Oncogene* **11**: 1913-1920

Clarke AR., Howard LA., Harrison DJ. and Winton DJ. (1997). p53, mutation frequency and apoptosis in the murine small intestine. *Oncogene* **14**: 2015-2018

Clore GM., Omichinski JG., Sakaguchi K., Zambrano N., Sakamoto H., Appella E. and Gronenborn AM. (1994). High-resolution structure of the oligomerization domain of p53 by multidimensional NMR. *Science* **265**: 386-391

Cross SM., Sanchez CA., Morgan CA., Schimke MK., Ramel S., Idzerda RL., Raskind WH. and Reid BJ. (1995). A p53-dependent mouse spindle checkpoint. *Science* **267**: 1353-1356

D' Urso G. and Nurse P. (1995). Checkpoint in the cell cycle of fission yeast. *Curr Opin Genet Dev* **5**: 12-16

Damalas A., Ben-Ze'-ev A., Simcha I., Shtutman M., Fernando J., Leal M., Zhurinsky J., Geiger B. and Oren M. (1999). Excess β-catenin promotes accumulation of transcriptionally active p53. *EMBO J* **18**: 3054-3063

Damjanov I. and Linder J. (1996). Anderson's Pathology. 10th edition Mosby

de la Coste A., Romagnolo B., Billuart P., Renard C-A., Buendia M-A., Soubrane O., Fabre M., Chellly J., Beldjord C., Kahn A. and Perret C. (1998). Somatic mutations of the β-catenin gene are frequent in mouse and human hepatocellular carcinomas. *Proc Natl Acad Sci USA* **95**: 8847-8851

de Wind N., Dekker M., Berns A., Radman M. and Te Riele H. (1995). Inactivation of the mouse *Msh2* gene results in mismatch repair deficiency, methylation tolerance, hyperrecombination and predisposition to cancer. *Cell* **82**: 321-330

Dean M., Levine RA., Ran W., Kindy MS., Sonenshein GE. and Campisi J. (1986). Regulation of c-myc transcription and mRNA abundance by serum growth factors and cell contact. *J Biol Chem* **261**: 9161-9166

Devereux TR., Anna CH., Foley JF., White CM., Sills RC. and Barrett JC. (1999). Mutation of β-catenin is an early event in chemically induced mouse hepatocellular carcinogenesis. *Oncogene* **18**: 4726-4733

Diehl JA., Cheng M., Roussel MF. and Sherr CJ. (1998). Glycogen synthase kinase 3β regulates cyclin D1 proteolysis and subcellular localisation. *Gene Dev* **12**: 3499-3511

Dietrich WF., Lander ES., Smith JS., Moser AR., Gould KA., Luongo C., Borenstein N. and Dove W. (1993). Genetic identificatio of Mom-1, a major modifier locus affecting Min-induced intestinal neoplasia in the mouse. *Cell* **75**: 631-639

Donalies M., Cramer M., Ringwald M. and Starzinski-Powitz A. (1991). Expression of M-cadherin, a member of the cadherin multigene family, correlates with differentiation of skeletal muscle cells. *Proc Natl Acad Sci* **88**: 8024-8028

Donehower LA., Harvey M., Slagle BL., McArthur MJ., Montgomery CA., Butel JS. and Bradley A. (1992). Mice deficient for p53 developmentally normal but susceptible to spontaneous tumours. *Nature* **356**: 215-221

Dove WF., Luongo C., Connelly CS., Gould KA., Shoemaker AR., Moser AR. and Gardner RL. (1994). The adenomatous polyposis coli gene of the mouse in development and neoplasia. *Cold Spring Harbor Symposia on Quantitative Biology,* Volume LIX, page 501-507

Doyle DA., Lee A., Lewis J., Kim E., Sheng M. and MacKinnon R. (1996). Crystal structure of a complexed and peptide-free membrane protein-binding domain: molecular basis of peptide recognition by PDZ. *Cell* **85**: 1067-1076

Drummond JT., Li G., Longley MJ. and Modrich P. (1995). Isolation of an hMSH2-p160 heterodimer that restores DNA mismatch repair to tumour cells. *Science* **268**: 1909-1912

Drummond JT., Genschel J., Wolf E. and Modrich P. (1997). DHFR/MSH3 amplification in methotrexate-resistant cells alters the hMutS α/hMutS β ratio and reduces the efficiency of base-base mismatch repair. *Proc Natl Acad Sci USA* **94**: 10144-10149

Dulic V.,Kaufmann WK., Wilson SJ., Tlsty TD., Lees E., Harper JW., Elledge SJ. and Reed SI. (1994). p53 dependent inhibition of cyclin-dependent kinase activities in human fibroblasts during radiation-induced G1 arrest. *Cell* **76**: 1013-1023

Duval A., Gayet J., Zhou XP., Iacopetta B., Thomas G. and Hamellin R. (1999). Frequent frameshift mutations of the TCF-4 gene in colorectal cancers with microsatellite instability. *Cancer Res* **59**: 4213-4215

Eastman Q. and Grosschedl R. (1999). Regulation of *LEF-1/TCF* transcription factors by Wnt and other signals. *Curr Opin Cell Biol* **11**: 233-240

El-Deiry WS., Kern SE., Pretenpol IA., Kinzler KW. and Vogelstein B. (1992). Definition of a consensus binding site for p53. *Nat Genet* **1**: 45-49

El-Deiry WS., Harper JW., O'Conner PM., Velculescu VE., Canman CE., Jackman J., Pietenpol JA., Burrell M., Hill DE. and Wang Y. (1994). Waf-1/cip-1 is induced in p53-mediated G1 arrest and apoptosis. *Cancer Res* **54**: 1169-1174

Elledge RM. and Lee W-H. (1995). Life and death by p53. *BioEssays* **17**(11): 923-930

Evan GI., Wyllie AH., Gilbert CS., Littlewood TD., Land H., Brooks M., Waters CM., Penn LZ. and Hancock DC. (1992). Induction of apoptosis in fibroblasts by c-myc protein. *Cell* **69**: 119-128

Evan GI. and Littlewood TD. (1993). The role of c-myc in cell growth. *Curr Opin Genet Dev* **3**: 44-49

Evan GI. and Littlewood TD. (1998). A matter of life and cell death. *Science* **281**: 1317-1322

Fagotto F., Guger K. and Gumbiner BM. (1997). Induction of the primary dorsalising center in *Xenopus* by the Wnt/GSK/β-catenin signalling pathway, but not by Vg1, Activin, or Noggin. *Development* **124**: 453-460

Fagotto F., Gluck U. and Gumbiner BM. (1998). Nuclear localisation signal-independent and importin/karyopherin-independent nuclear import of β-catenin. *Curr Biol* **8**: 181-190

Fang L., Igarashi M., Leung J., Sugrue MM., Lee SW. and Aaronson SA. (1999). p21 $^{Waf1/Cip1/Sdi1}$ induces permanent growth arrest with markers of replicative senescence in human tumour cells lacking functional p53. *Oncogene* **18**: 2789-2797

Fang WH. and Modrich P. (1993). Human strand-specific mismatch repair occurs by a bidirectional mechanism similar to that of the bacterial reaction. *J Biol Chem* **268**: 11838-11844

Fearon ER. and Vogelstein B. (1990). A genetic model for colorectal tumorigenesis. *Cell* **61**: 759-767

Fields S. and Jang SK. (1990). Presence of a potent transcription activating sequence in the p53 protein. *Science* **249**: 1046-1049

Fishel R., Lescoe MK., Rao MR., Copeland NG., Jenkins NA., Garber J., Kane M. and Kolodner R. (1993). The human mutator gene homolog MSH2 and its association with hereditary nonpolyposis colon cancer. *Cell* **75**: 1027-1038

Fishel R., Ewel A. and Lescoe MK. (1994a). Purified human MSH2 protein binds to DNA containing mismatched nucleotides. *Cancer Res* **54**: 5539-5542

Fishel R., Ewel A., Lee S., Lescoe MK. and Griffith J. (1994b). Binding of mismatched microsatellite DNA sequences by the human MSH2 protein. *Science* **266**: 1403-1405

Fishel R. and Kolodner RD. (1995). Identification of mismatch repair genes and their role in the development of cancer. *Curr Opin Genet Dev* **5**: 382-395

Fisher AL. and Caudy M. (1998). Groucho protein: transcriptional corepressors for specific subsets of DNA binding transcription factors in vertebrates and invertebrates. *Gene Dev* **12**: 1931-1940

Fodde R., Edelmann W., Yang K., van Leeuwen C., Carlson C., Renault B., Breukel C., Alt E., Lipkin M. and Khan PM. (1994). A targeted chain-termination mutationin the mouse *Apc* gene results in multiple intestinal tumours. *Proc Natl Acad Sci USA* **91**: 8969-8973

Forsslund G. and Zetterberg A. (1990). Ploidy level determinations in high-grade and low-grade malignant variants of prostatic carcinoma. *Cancer Res* **50**:4281-4285

Friedberg EC., Walker GC. and Siede W. (1995). DNA Repair and Mutagenesis. Washington, DC: American Society for Microbiology

Froggatt NJ., Koch J., Davies R., Evans DGR., Clamp A., Quarrell OWJ., Weissenbach J., Hodgson SV., Ponder BAJ., Barton DE. and Maher ER. (1995). Genetic linkage analysis in hereditary non-polyposis colon cancer syndrome. *J Med Genet* **32**: 352-357

Fujii H. and Shimada T. (1989). Isolation and characterisation of cDNA clones derived from the divergently transcribed gene in the region upstream from the human dihydrofolate reductase gene. *J Biol Chem* **264**: 10057-10064

Fukasawa K., Choi T., Kuriyama R., Rulong S. and van de Woude GF. (1996). Abnormal centrosome amplification in the absence of p53. *Science* **271**: 1744-1747

Fukasawa K., Wiener F., Vande Woude GF. and Mai S. (1997). Genomic instability and apoptosis are frequent in p53 deficient young mice. *Oncogene* **15**: 1295-1302

Gausauge S., Gausauge F., Ramadani M., Stobbe H., Rau B., Harada N. and Beger HG. (1997). Overexpression of cyclin D1 in human pancreatic carcinoma is associated with poor prognosis. *Cancer Res* **57**: 1634-1637

Geiger B. and Ayalon O. (1992). Cadherins. *Annu Rev Cell Biol* **8**: 307-332

Giese K., Cox J. and Grosschedl R. (1992). The HMG domain of lymphoid enhancer factor 1 bends DNA and facilitates assembly of functional nucleoprotein structures. *Cell* **69**: 185-195

Giese K. and Grosschedl R. (1993). LEF-1 contains an activation domain that stimulates transcription only in a specific context of factor-binding sites. *EMBO J* **12**: 4667-4676

Giese K., Kingsley C., Kirschner JR. and Grosschedl R. (1995). Assembly and function of a TCR-α

enhancer complex is dependent on LEF-1 induced DNA bending and multiple protein-protein interactions. *Gene Dev* **9**: 995-1008

Glazer AN., Peck K. and Mathies RA. (1990). A stable double-stranded DNA ethidium homodimer complex: Application to picogram fluorescence detection of DNA in agarose gels. *Proc Natl Acad Sci USA* **87**: 3851-3855

Goodrich DW., Wang NP., Quian Y-W., Lee EY-HP. and Lee WH. (1991). The retinoblastoma gene product regulates progression through the G1 phase of the cell cycle. *Cell* **67**: 293-302

Going JJ. and Lamb RF. (1996). Practical histological microdissection for PCR analysis. *J Pathol* **179**: 121-124

Green DR. and Martin SJ. (1995). The killer and the executioner: how apoptosis controls malignancy. *Curr Opin Immunol* **7**: 694 –703

Greene DR., Taylor SR., Wheeler TM. and Scardino PT. (1991). DNA ploidy by image analysis of individual foci of prostate cancer: a preliminary report. *Cancer Res* **51**: 4084-4089

Groden J., Thliveris A., Samowitz W., Carlson M., Gelbert L., Albersen H., Joslyn G., Stevens J., Spirio L., Robertson M., Sargeant L., Krapcho K., Wolff E., Burt R., Hughes JP., Warrington J., McPherson J., Wasmuth J., LePaslier D., Abderrahim H., Cohen D., Leppert M. and White R. (1991). Identification and characterization of the familial adenomatous polyposis coli gene. *Cell* **66**: 589-600

Gualberto A., Aldape K., Kozakiewicz K. and Tlsty T. (1998). An oncogenic form of p53 confers a dominant, gain-of-function phenotype that disrupts spindle checkpoint control. *Proc Natl Acad Sci USA* **95**: 5166-5171

Guillouf C.,, Rosselli F., Krishnaraju K., Moustacchi E., Hoffman B. and Liebermann DA. (1995). p53 involvement in control of G2 exit of the cell cycle: role in DNA damage-induced apoptosis. *Oncogene* **10**: 2263-2270

Gumbiner BM. (1995). Signal transduction of β-catenin. *Curr Opin Cell Biol* **7**: 634-640

Gumbiner BM. (1996). Cell adhesion: the molecular basis of tissue architecture and morphogenesis. *Cell* **84**:345-357

Han EK., Lim JT., Arber N., Rubin MA., Xing WQ. and Weinstein IB. (1998). Cyclin D1 expression in human prostate carcinoma cell lines and primary tumours. *Prostate* **35**: 95-101

Hannigan GE., Leung-Hagesteijn C., Fitz-Gibbon L., Coppolino MG., Radeva G., Filmus J., Bell JC. and Dedhar S. (1996). Regulation of cell adhesion and anchorage-dependent growth by a new β(1)-integrin-linked protein kinase. *Nature (London)* **379**: 91-96

Hanson KD., Shichiri M., Follansbee MR. and Sedivy JM. (1994). Effects of c-myc expression on cell cycle progression. *Mol Cell Biol* **14**: 5748-5755

Haroske G., Dimmer V., Hermann WR., Kunze KD. and Meyer W. (1984). Metastatising APUD cell tumours of the human gastrointestinal tract. *Pathol Res Pract* **178**: 363-368

Hart MJ., de los Santos R., Albert IN., Rubinfeld B. and Polakis P. (1998). Downregulation of β-catenin by human Axin and its association with the APC tumour suppressor, β-catenin and GSK3β. *Curr Biol* **8**: 573-581

Hartley DA., PreissA. and Artavanis-Tsakonas S. (1988). A deduced gene product from the *Drosophila* neurogenic locus, enhancer of split, shows homology to mammalian G-protein β subunit. *Cell* **55**: 785-795

Hartwell LH. and Kastan MB. (1994). Cell cycle control and cancer. *Science* **266**: 1821-1828

Hattori K., Angel P., le Beau MM. and Karin M. (1988). Structure and chromosomal localisation of the functional intronless human JUN protooncogene. *Proc Natl Acad Sci USA* **85**: 9148-9152

Hawn MT., Umar A., Carethers JM., Marra G., Hunkel TA., Boland CR. and Koi M. (1995). Evidence for a connection between the mismatch repair system and the G_2 cell cycle checkpoint. *Cancer Res* **55**: 3721-3725

He T-C., Sparks AB., Rago C., Hermeking H., Zawel L., de la Costa LT., Morin PJ., Vogelstein B. and Kinzler KW. (1998). Identification of c-MYC as a target of the APC pathway. *Science* **281**: 1509-1512

He X., Saint-Jeannet J., Woodgett J., Varmus H. and David I. (1995). Glycogen synthase kinase-3 and dorsoventral patterning in Xenopus embryos. *Nature* **374**: 617-622

Heinen CD., Richardson D., White R. and Groden J. (1995). Microsatellite instability in colorectal adenocarcinoma cell lines that have full- length adenomatous polyposis coli protein. *Cancer Res* **55**: 4797-4799

Heinen CD. and Groden J. (1999). The APC tumour suppressor regulates progression through the G1 phasee of the cell cycle. Keystone Symposia 1999

Henriksson M. and Luscher G. (1996). Proteins of the Myc network: essential regulators of celll growth and differentiation. *Adv Cancer Res* **68**: 110-182

Hermeking H. and Eick D. (1994). Mediation of c-myc-induced apoptosis by p53. *Science* **265**: 2091-2093

Hinds PW., Dowdy SF., Eaton EN., Arnold A. and Weinberg RA. (1994). Function of human cyclin gene as an oncogene. *Proc Natl Acad Sci USA* **91**: 709-713

HMSO (1989). Cancer statistics. Registrations. England and Wales. London; HMSO

Hoang B., Moos M.Jr., Vukicevic S. and Luyten FP. (1996). Primary structure and tissue distribution of FRZB, a novel protein related to *Drosophila* frizzled, suggest a role in skeletal morphogenesis. *J Biol Chem* **271**: 26131-26137

Hoffmann B. and Liebermann DA. (1994). Molecular controls of apoptosis: differentiation, growth arrest primary response genes, proto-oncogenes, and tumour suppressor genes as positive and negative modulators. *Oncogene* **9**: 1807-1812

Hollstein M., Sidranksy D., Vogelstein B. and Harris CC. (1991). p53 mutations in human cancers. *Science* **253**: 49-53

Hsu B., Marin MC., El-Naggar AK., Stephens LC., Brisbay S. and McDonnell TJ. (1995). Evidence that c-myc mediated apoptosis does not require wild-type p53 during lymphomagenesis. *Oncogene* **11**: 175-179

Hsu S-C., Galceran J. and Grosschedl R. (1998). Modulation of transcriptional regulation by LEF-1 in response to Wnt-1 signalling and association with β-catenin. *Mol Cell Biol* **18**: 4807-4818

Huang J., Papadopoulos N., Mckinley AJ., Farrington SM., Curtis LJ., Wyllie AH., Zheng S., Willson JU., Markowitz SD., Morin P., Kinzler KW., Vogelstein B. and Dunlop MG. (1996). APC mutations in colorectal tumors with mismatch repair deficiency. *Proc Natl Acad Sci USA* **93**: 9049-9054

Huber AH., Neelson WJ. and Weis WI. (1997). Three-dimensional structure of the armadillo repeat region of β-catenin. *Cell* **90**: 871-882

Huber O., Kom R., McLaughlin J., Ohsugi M., Herrmann BG. and Kemler R. (1996). Nuclear localization of the β-catenin by interaction with transcription factor LEF-1. *Mech Dev* **59**: 3-10

Huber O., Bierkamp C. and Kemler R. (1996a). Cadherins and catenins in development. *Curr Opin Cell Biol* **8**: 685-691

Hulsken J., Birchmeier W. and Behrens J. (1994). E-cadherin and APC compete for the interaction with β-catenin and the cytoskeleton. *J Cell Biol* **127**: 2061-2069

Iaccarino I., Marra G., Palombo F. and Jiricny J. (1998). hMSH2 and hMSH6 play distinct roles in mis match binding and contribute differently to the ATPase activity of hMutS α. *EMBO J* **17**: 2677-2686

Iatropoulos MJ. and Williums GM. (1996). Proliferation markers. *Exp Toxicol Pathol* **48**: 175-181

Ikeda S., Kishida S., Yamamoto H., Murai H., Koyama S. and Kikuchi A. (1998). Axin, a negative regulator of the Wnt signalling pathway, forms a complex with GSK3β and β-catenin and promotes GSKβ-dependent phosphorylation of β-catenin. *EMBO J* **17**: 1371-1384

Ilyas M., Tomlinson IPM., Rowan A., Pignatelli M. and Bodmer WF. (1997). β-catenin mutations in cell lines established from human colorectal cancers. *Proc Natl Acad Sci USA* **94**: 10330-10334

Ionov Y., Peinado MA., Malkhosyan S., Shibata D. and Perucho M. (1993). Ubiquitous somatic mutations in simple repeated sequences reveal a new mechanism for colonic carcinogenesis. *Nature* **363**: 558-561

Jack T., Remington L., Williams BO., Schmitt EM., Halachmi S., Bronson RT. and Weinberg RA. (1994). Tumour spectrum analysis in p53-mutant mice. *Curr Biol* **4**: 1-7

Jacks T. and Weinberg RA. (1996). Cell cycle control and its watchman. *Nature* **381**: 643-644

Jiricny J. (1998). Replication errors: challenging the genome. *EMBO J* **17**: 6427-6436

Joslyn G., Richardson DS., White R. and Alber T. (1993). Dimer formation by an N-terminal coiled-coiled in the APC protein. *Proc Natl Acad Sci USA* **90**: 11109-11113

Justice MJ., Gilbert DJ., Kinzler KW., Vogelstein B., Buchberg AM., Ceci JD., Matsuda Y., Chapman VM., Muramatsu T., Jenkins NA. and Copeland NG. (1992). A molecular genetic linkage map of mouse chromosome 18 reveals extensive linkage conservation with human chromosome 5 and 18. *Genomics* **13**: 1281- 1288

Karn J., Watson JV., Lowe AD., Green SM. and Vedeckis W. (1989). Regulation of cell cycle duration by c-myc levels. *Oncogene* **4**: 773-787

Karran P. and Bignami M. (1994). DNA-damage tolerance, mismatch repair and genome instability. *BioEssays* **16**: 833-839

Kato GJ., Barrett J., Villa-Garcia M. and Dang CV. (1990). An amino-terminal c-myc domain required for neoplastic transformation activates transcription. *Mol Cell Biol* **10**: 5914-5920

Kemler R. (1992). Classical cadherins. *Semin Cell Biol* **3**: 149-155

Kerr JFR., Wyllie AH. and Currie AR. (1972). Apoptosis: a basic biological phenomenon with wide-ranging implication in tissue kinetics. *Br J Cancer* **26**: 239-257

Kerr JFR., Winterford CM. and Harmon BV. (1994). Apoptosis. *Cancer* **73**: 2013-2026

Kessel RG. (1998). Basic medical histology: the biology of cells, tissues and organs. *Oxford University Press*

Kim SH., Roth KA., Moser AR. and Gordon JI. (1993). Transgenic mouse models that explore the multistep hypothesis of intestinal neoplasia. *J Cell Biol* **123**: 877-893

Kinzler WK. and Vogelstein B. (1996). Lessons from hereditary colorectal cancer. *Cell* **87**: 159-170

Kishida M., Koyama S., Kishida S., Matsubara K., Nakashima S., Higano K., Takada R., Takada S. and Kikuchi A. (1998). Axin prevents Wnt-3a-induced accumulation of β-catenin. *Oncogene* **18**: 979-985

Klingensmith J., Nusse R. and Perrimon N. (1994). The *Drosophila* segment polarity gene *dishevelled* encodes a novel protein required for response to the *wingless* signal. *Gene Dev* **8**: 118-130

Ko LJ. and Prives C. (1996). p53: puzzle and paradigm. *Gene Dev* **10**: 1054-1072

Kolodner RD. (1995). Mismatch repair: mechanisms and relationship to cancer susceptibility. *Trends Biochem Sci* **20**: 397-401

Korinek V., Barker N., Morin PJ., van Wichen D., de Weger R., Kinzler KW., Vogelstein B. and Clevers H. (1997). Constitutive transcriptional activation by a β-catenin-Tcf complex in $APC^{-/-}$ colon carcinoma. *Science* **275**: 1784-1787

Kussel P. and Frasch M. (1995). Pendulin, a Drosophila protein with cell cycle-dependent nuclear localisation, is required for normal cell proliferation. *J Cell Biol* **129**: 1491-1507

Laird PW., Jackson-Grusby L., Fazeli A., Dickinson SL., Jung WE., Li E., Weinberg RA. and Jaenisch R. (1995). Suppression of intestinal neoplasia by DNA hypomethylation. *Cell* **81**: 197-205

Lajoie G., Zbieranowski I., Demianiuk C., Knape WA., Edinger MG. and Tubbs RR. (1993).
A comparative study of DNA quantitation in breast carcinoma with image cytometric analysis and *in vitro* fine needle aspiration with flow cytometric analysis. *Am J Clin Patho* **100**: 456-462

Lammie GA. and Peters G. (1991). Chromosome 11q13 abnormalities in human cancer. *Cancer Cells* **3**: 413-420

Lanni JS. and Jacks T. (1998). Characterisation of the p53-dependent postmitotic checkpoint following spindle disruption. *Mol Cell Biol* **18**: 1055-1064

Leach FS., Nicolaides, NC., Papadopoulos, N., Liu, B., Jen, J., Parsons, R., Peltomaki, P., Sistonen, P., Aaltonen, LA., Nystrom-Lahti, M., Guan X-Y., Zhang J., Meltzer PS., Yu J-W., Kao F-T., Chen DJ.,

Cerosaletti KM., Fournier REK., Todd S., Lewis T., Leach RJ., Naylor SL., Weissenbach J., Mecklin J-P., Jarvinen H., Petersen GM., Hamilton SR., Green J., Jass J., Watson P., Lynch HT., Trent JM., de la Chapelle A., Kinzler KW. and Volgestein B. (1993). Mutations of a mutS homologue in hereditary non polyposis colorectal cancer. *Cell* **75**: 1215-1225

Leach FS., Polyak K., Burrell M., Johnson KA., Hill D., Dunlop MG., Wyllie AH., Peltomaki P., de la Chapelle A., Hamilton SR., Kinzler KW. and Vogelstein B. (1996). Expression of the human mismatch repair gene hMSH2 in normal and neoplastic tissues. *Cancer Res* **56**: 235-240

Leahy DT., Salman R., Mulcahy H., Sheahan K., O'Donoghue DP. and Parfrey NA. (1996). Prognostic significance of p53 abnormalities in colorectal carcinoma detected by PCR-SSCP and immunohistochemical analysis. *J Pathol* **180**: 364-370

Lee JM. and Bernstein A. (1993). p53 mutations increase resistance to ionization radiation. *Proc Natl Acad Sci USA* **90**: 5742-5746

Lee SW. (1996). H-cadherin, a novel cadherin with growth inhibitory functions and diminished expression in human breast cancer. *Nat Med* **2**: 776-782

Lengauer C., Kinzler KW. and Vogelstein B. (1997). Genetic instability in colorectal cancers. *Nature* **386**: 623-627

Lengyel E., Wang H., Stepp E., Juarez J., Wang Y., Doe W., Pfarr CM. and Boyd D. (1996). Requirement of an upstream AP-1 motif for the constitutive and phorbol ester-inducible expression of the urokinase-type plasminogen activator receptor gene. *J Biol Chem* **271**: 23176-23184

Levanon D., Goldstein RE., Bernstein Y., Tang H., Goldenberg D., Stifani S., Paroush Z. and Groner Y. (1998). Transcriptional repression by AML1 and Lef-1 is mediated by the TLE/Groucho corepressors. *Proc Natl Acad Sci USA* **95**: 11590-11595

Levine AJ., Momand J. and Finlay CA. (1991). The p533 tumour suppressor gene. *Nature* **351**: 453-456

Levy DB., Smith KJ., Beazer-Barclay Y., Hamilton SR., Vogelstein B. and Kinzler KW. (1994). Inactivation of both APC alleles in human and mouse tumours. *Cancer Res* **54**: 5953-5958

Lew DJ. and Kornbluth S. (1996). Regulatory roles of cyclin dependent kinase phosphorylation in cell cycle control. *Curr Opin Cell Biol* **8**: 795-804

Lin K., Wang S., Julius MA., Kitajewski J. and Moos M. Jr. (1997). The cysteine-rich frizzled domain of Frzb-1 is reequired and sufficient for modulation of Wnt signalling. *Proc Natl Acad Sci USA* **94**: 11196-11200

Liu B., Nicolaides MC., Markowitz S., Willson JKV., Parsons RE., Jen J., Papadopoulos N., Peltomaki P., de la Chapelle A., Hamilton SR., Kinzler KW. and Vogelstein B. (1995). Mismatch repair gene defects in sporadic colorectal cancers with microsatellite instability. *Nat Genet* **9**: 48-55

Liu B., Parsons R., Papadopoulos N., Nicolaides MC., Lynch HT., Watson P., Lass JR., Dunlop M., Wyllie AH., Peltomaki P., de la Chapelle A., Hamilton SR., Vogelstein B. and Kinzler KW. (1996). Analysis of mismatch repair genes in hereditary non-polyposis colorectal cancer patients. *Nat Med* **2**: 169-174

Livingstone LR., White A., Sprouse J., Livanos E., Jacks T. and Tlsty TD. (1992). Altered cell cycle arrest and gene amplification potential accompany loss of wild-type p53. *Cell* **70**: 923-935

Love JJ., Li X., Case DA., Giese K., Grosschedl R. and Wright PE. (1995). Structural basis for DNA bending by the architectural transcription factor LEF-1. *Nature* **376**: 791-795

Lovec H., Grzeschiczek A., Kowalski MB. and Moroy T. (1994). Cyclin D1 bcl-1 cooperates with myc genes in the generation of B-cell lymphoma in transgenic mice. *EMBO J* **13**: 3487-34495

Lukes AS., Kohler MF., Pieper CF., Kerns BJ., Bentley R., Rodriguez GC., Soper JT., Clarkepearson DL., Bast RC. and Berchuck A. (1994). Multivariable analysis of DNA ploidy, p53, and HER-2/neu as prognostic factors in endometrial cancer. *Cancer* **73**: 2380-2385

Luongo C., Gould KA., Su L-K., Kinzler KW., Vogelstein B., Dietrich W., Lander ES. and Moser AR. (1993). Mapping of multiple intestinal neoplasia (Min) to proximal chromosome 18 of the mouse. *Genomics* **15**:3-8

Luongo C., Moser AR., Gledhill S. and Dove WF. (1994). Loss of Apc+ is necessary for intestinal adenoma formation in Min mice. *Cancer Res* **54**: 5947-5952

Lynch HT., Ens J., Lynch JF. and Watson P. (1988). Tumour variation in three extended Lynch syndrome II kindreds. *Am J Gastroenterol* **83**: 741-747

Lynch HT., Smyrk TC., Watson P., Lanspa SJ., Boman BM., Lynch PM., Lynch JF. and Cavalieri RT. (1991). Hereditary colorectal cancer. *Semin Oncol* **18**: 337-366

Lynch HT., Smyrk TC., Watson P., Lanspa SJ., Lynch JF., Lynch PM., Cavalieri RT. and Boland CR. (1993). Genetics, natural history, tumour spectrum, and pathology of hereditary nonpolyposis colorectal cancer: an updated review. *Gastroenterology* **104**: 1535-1549

Lynch HT. and Lynch JF. (1994). 25 years of HNPCC. *Anticancer Res* **14**: 1617-1624

Macleod KF. and Jacks T.(1999). Insights into cancer from transgenic mouse models. *J Pathol* **187**: 43-60

Maeda K., Chung Y., Kang S., Ogawa M., Onoda N., Nishiguchi Y., Ikehara T., Nakata B., Okuno M. and Sowa M. (1998). Cyclin D1 overeexpression and prognosis in colorectal adenocarcinoma. *Oncology* **55**: 145-151

Mahmoud NN., Boolbol SK., Bilinski RT., Martucci C., Chadburn A. and Bertagnolli MM. (1997). Apc gene mutation is associated with a dominant-negative effect upon intestinal cell migration. *Cancer Res* **57**: 5045-5050

Mairinger T., Gschwendtner A., Mikuz G. and Kampf V. (1994). Tissue section image analysis: comparison of different software releases (Letter of the editor). *Am J Clin Pathol* **101**: 673-680

Mallo M., Franco del Amo F. and Gridley T. (1993). Cloning and developmental expression of Grg, a mouse gene related to the groucho transcript of the Drosophila Enhancer of split complex. *Mech Dev* **42**: 67-76

Mandelkow E-M., Drewes G., Biernat J., Gustke N., van Lint J., Vandenheede JR. and Mandelkow E. (1992). Glycogen synthase kinase-3 and the Alzheimer-like state of microtubule-associated protein tau. *FEBS Lett.* **314**: 315-321

Mann B., Gelos M., Siedow A., Hanski ML., Gratchev A., Ilyas M., Bodmer WF., Moyer MP., Riecken EO., Buhr HJ. and Hanski C. (1999). Target genes of β-catenin-T cell-factor/lymphoid-enhancer-factor signalling in human colorectal carcinomas. *Proc Natl Acad Sci USA* **96**: 1603-1608

Martinez J., Georgoff I. and Levine AJ. (1991). Cellular localisation and cell cycle regulation by a temperature sensitive p53 protein. *Gene Dev* **5**: 151-159

Marra G. and Boland R. (1995). Hereditary nonpolyposis colorectal cancer: the syndrome, the genes, and historical perspectives. *J Natl Cancer Inst* **87**: 1114-1125

Marra G., Iaccarino I., Lettieri T., Roscilli G., Delmastro P. and Jiricny J. (1998). Mismatch repair deficiency associated with overexpression of the MSH3 gene. *Proc Natl Acad Sci USA* **95**: 8568-8573

Mateyak MK., Obaya AJ. and Sedivy JM. (1999). c-Myc regulates cyclin D-Cdk4 and -Cdk6 activity but affects cell cycle progression at multiple independent points. *Mol Cell Biol* **19**: 4672-4683

Matsumine A., Ogai A., Senda TON., Satoh K., Baeg G.-H., Kawahara T., Kobayashi S., Okada M., Toyoshima K. and Akiyama T. (1996). Binding of APC to the human homolog of the drosophila discs large tumour suppressor protein. *Science* **272**: 1020-1023

McCormack SJ., Weaver Z., Deming S., Natarajan G., Torri J., Johnson MD., Liyanage M., Ried T. and Dickson RB. (1998). Myc/p53 interactions in transgenic mouse mammary development, tumorigenesis and chromosomal instability. *Oncogene* **16**: 2755-2766

McCrea PD., Turck CW. and Gumbiner B. (1991). A homologue of the armadillo protein in Drosophila (plakoglobin) associated with E-cadherin. *Science* **254**: 1359-1361

Mecklin JP., Jaervinen HJ. and Peltokallio P. (1986). Cancer family syndrome: Genetic analysis of 22 Finnish kindreds. *Gastroenterology* **90**: 328-333

Mercer WE., Shields MT., Amin M., Sauve GJ., Appella E., Romano JW. and Ullrich SJ. (1990). Negative growth regulation in a glioblastoma tumour cell line that conditionally expresses human wild-type p53. *Proc Natl Acad USA* **87**: 6166-6170

Merritt AJ., Potten CS., Kemp CJ., Hickman JA., Balmain A., Lane DP. and Hall PA. (1994). The role of p53 in spontaneous and radiation-induced apoptosis in the gastrointestinal tract of normal and p53-deficient mice. *Cancer Res* **54**: 614-617

Merritt AJ., Allen TD., Potten CS. and Hickman CJ. (1997). Apoptosis in small intestinal epithelia from p53-null mice: evidence for a delayed, p53-independent G2/M-associated cell death after γ-irradiation. *Oncogene* **14**: 2759-2766

Midgley CA., Owens B., Briscoe CV., Thomas DB., Lane DP. and Hall PA. (1995). Coupling between γ irradiation, p53 induction and the apoptotic response depends upon cell type *in vivo*. *J Cell Sci* **108**: 1843-1848

Midgley CA., White S., Howitt R., Save V., Dunlop MG., Hall PA., Lane DP., Wyllie AH. and Bubb VJ. (1997). APC expression in normal human tissues. *J Pathol* **181**: 426-433

Miller JR. and Moon RT. (1996). Signal transduction through beta-catenin and specification of cell fate during embryogenesis. *Gene Dev* **10**: 2527-2539

Minsky M. (1961). Microscopy Apparatus. United States Patent 3,013,467, Dec 19, 1961 (Field Nov 7, 1957)

Mir R., Johnson H.,Jr, Margolis M., Teplitz S. and Wise L. (1992). Prognostic significance of DNA measurement determined by image analysis in human breast carcinoma. *J Surg Oncol* **50**: 168-172

Miyaki M., Konishi M., Muraoka M., Kikuchi-Yanoshita R., Tanaka K., Iwama T., Mori T., Koike M., Ushio K., Chiba M., Nomizu S. and Utsunomiya J. (1995). Germline mutations of hMSH2 and hMLH1 genes in Japanese families with hereditary nonpolyposis colorectal cancer (HNPCC): usefulness of DNA analysis for screening and diagnosis of HNPCC patients. *J Mol Med* **73**: 515-520

Miyashiro I., Senda T., Matsumine A., Baeg G-H., Kuroda T., Shimano T., Miura S., Noda T., Kobayashi S., Monden M., Toyoshima K. and Akiyama T. (1995). Subcellular localisation of the APC protein: immunoelectron microscopic study of the association of the APC protein with catenin. *Oncogene* **11**: 89-96

Moberger B., Auer G., Forsslund G. and Moberger G. (1984). The prognostic significance of DNA measurements in endometrial carcinoma. *Cytometry* **5**: 430-436

Modrich P. (1991). Mechanisms and biological effects of mismatch repair. *Annu Rev Genet* **25**: 229-253

Molenaar M., van de Wetering M., Ooterwegel M., Peterson-Maduro J., Godsave S., Korinek V., Roose J., Destree, O. and Clevers H. (1996). Xtcf-3 transcription factor mediates β-catenin-induced axis formation in Xenopus embryos. *Cell* **86**: 391-399

Momand I., Zambetti GP., Olson DC., George D. and Levine AI. (1992). The MDM2 oncogene product forms a complex with the p53protein and inhibits p53 mediated transactivation. *Cell* **69**: 1237-1245

Morais Cabral JH., Petosa C., Sutcliffe MJ., Raza S., Byron O., Poy F., Marfatia SM., Chishti AH. and Liddington RC. (1996). Crystal structure of a PDZ domain. *Nature* **382**: 649-652

Morin PJ., Vogelstein B. and Kinzler KW. (1996). Apoptosis and *APC* in colorectal tumorigenesis. *Proc Natl Acad Sci USA* **93**: 7950-7954

Morin PJ., Sparks AB., Korinek V., Barker N., Clevers H., Vogelstein B. and Kinzler KW. (1997). Activation of β-catenin-Tcf signalling in colon cancer by mutation in β-catenin or APC. *Science* **175**: 1787-1790

Morrison EE., Askham JM., Clissold P., Markham AF. and Meredith DM. (1997). The cellular distribution of the adenomatous polyposis coli tumour suppressor protein in neuroblastoma cells is regulated by microtubule dynamics. *Neuroscience* **81**: 553-563

Morrison EE., Wardleworth BN., Askham JM., Markham AF., Meredith DM. (1998). EB1, a protein which interacts with APC tumour suppressor, is associated with the microtubule cytoskeleton throughout the cell cycle. *Oncogene* **17**: 3471-3477

Morson B., Dawson I., Day D., Jass J., Price A. and Williums G. (1990). Morson and Dawson's gastro intestinal pathology. 3rd edn. Oxford: Blackwell Scientific Publications

Morton RA., Ewing CM., Nagafuchi A.,Tsukita S. and Isaacs WB. (1993). Reduction of E-cadherin levels and deletion of the α-catenin gene in human prostate cancer cells. *Cancer Res* **53**: 3585-3590

Moser AR., Pitot HC. and Dove WF. (1990). A dominant mutation that predisposes to multiple intestinal neoplasia in the mouse. *Science* **247**: 322-324

Moser AR., Dove WF., Roth KA., Gordon JI. (1992). The Min mutation: its effect on gut epithelial cell differentiation and interactions with a modifier system. *J Cell Biol* **116**: 1517-1526

Moser AR., Mattes EM., Dove WF., Lindstrom MJ., Haag, and Gould MN. (1993). Apc ^{Min}, a mutation in the murine Apc gene, predisposes to mammary carcinomas and focal alveolar hyperplasias. *Proc Natl Acad Sci* **90**: 8977-8981

Munemitsu S., Souza B., Muller O., Albert I., Rubinfeld B. and Polakis P. (1994). The APC gene product associates with microtubules in vivo and promotes their assembly in vitro. *Cancer Res* **54**: 3676-3681

Munemitsu S., Albert I., Sauza B., Rubinfeld B. and Polakis P. (1995). Regulation of intracellular β-catenin levels by the adenomatous polyposis coli (APC) tumour suppressor protein. *Proc Natl Acad Sci USA* **92**: 3046-3050

Munemitsu S., Albert I., Rubinfeld B. and Polakis P. (1996). Deletion of an amino-terminal sequence stabilised β-catenin *in vivo* and promotes hyperphosphorylation of the adenomatous polyposis coli tumour suppressor protein. *Mol Cell Biol* **16**: 4088-4094

Murray AW. (1995). The genetics of cell cycle checkpoints. *Curr Opin Genet Dev* **5**:5-11

Murre C., Schonleber-McCaw P. and Baltimore D. (1989). A new DNA-binding and dimerisation motif in immunoglobulin enhancer binding, daughterless, myod, and myc proteins. *Cell* **56**: 777-783

Nagar B., Overduin M., Ikura M. and Rini JM. (1996). Structural basis of calcium-induced E-cadherin rigidification and dimerization. *Nature* **380**: 360-364

Nagata S. (1997). Apoptosis by death factor. *Cell* **88**: 355-365

Nakamura Y. (1993). The role of the adenomatous polyposis coli (APC) gene in human cancers. *Adv Cancer Res* **62**: 65-87

Narayan S. and Jaiswal AS. (1997). Activation of adenomatous polyposis coli (APC) gene expression by the DNA-alkylating agent N-methyl-N-nitro-N-nitroguanidine requires p53. *J Biol Chem* **272**: 30619-30622

Nathke IS., Adams CL., Polakis P., Sellin JH. and Nelson WJ. (1996). The adenomatous polyposis coli tumour suppressor protein localises to plasma membrane sites involved in active cell migration. *J Cell Biol* **134**: 165-179

Neufeld KL. and White RL. (1997). Nuclear and cytoplasmic localisations of the adenomatous polyposis coli protein. *Proc Natl Acad Sci USA* **94**: 3034-3039

Nicolaides NC., Papadopoulos N., Liu B., Wei YF., Carter KC., Ruben SM., Rosen CA., Haseltine WA., Fleischmann RD., Fraser CM., Adams MD., Venter JC., Dunlop MG., Hamilton SR., Petersen GM., Delachapelle A., Vogelstein B. and Kinzler KW. (1994). Mutations of two PMS homologues in hereditary nonpolyposis colon cancer. *Nature* **371**: 75-80

Nollet F., Berx G., Molemans F. and van Roy F. (1996). Genomic organisation of the human β-catenin gene (CTNNB1). *Genomics* **32**: 413-424

Novak A., Hsu S., Leung-Hagesteijn C., Radeva G., Papkoff J., Montesano R., Roskelley C., Grosschedl R. and Dedhar S. (1998). Cell adhesion and the integrin-linked kinase regulate the LEF-1 and β-catenin signalling pathways. *Proc Natl Acad Sci USA* **95**: 4374-4379

Nusse R. and Varmus HE. (1992). Wnt genes. *Cell* **69**: 1073-1087

Nusse R. (1997). A versatile transcriptional effector of Wingless signalling. *Cell* **89**: 321-323

Ochiai A., Akimoto S., Kanai Y., Shibata T., Oyama T. and Hirohashi S. (1994). c-erbB2 gene product associates with catenins in human cancer cells. *Biochem Biophys Res Commun* **205**: 73-78

Okazaki M., Takeshita S., Kawai S., Kikuno R., Tsujimura A., Kudo A. and Amann E. (1994). Molecular cloning and characterisation of OB-cadherin, a new member of cadherin family expressed in osteoblasts. *J Biol Chem* **269**: 12092-12098

Oliner JD., Kinzler KW., Meltzer PS., George DL. and Vogelstein B. (1992). Amplification of a gene encoding a p53-associated protein in human sarcomas. *Nature* **358**: 80-83

Oliner JD., Pietenpol JA., Thiagalingam S., Gvuris J., Kinzler KW. and Vogelstein B. (1993). Oncoprotein MDM2 conceals the activation domain of tumour suppressor p53. *Nature* **362**: 857-860

Oosterwegel M., van de Wetering M., Timmerman J., Kruisbeek A., Destree O., Meijlink F. and Clevers H. (1993). Differential expression of the HMG box factors TCF-1 and LEF-1 during murine embryogenesis. *Development* **118**: 11-20

Orford K., Orford CC. and Byers SW. (1999). Exogenous expression of β-catenin regulates contact inhibition, anchorage-independent growth, anoikis and radiation-induced cell cycle arrest. *J Cell Biol* **146**: 855-867

Oshima M., Oshima H., Kitagawa K., Kobayashi M., Itakura C. and Taketo M. (1995). Loss of *Apc* herozygosity and abnormal tissue building in nascent intestinal polyps in mice carrying a truncated *Apc* gene. *Proc Natl Acad Sci USA* **92**: 4482-4486

Overduin M., Harvey T., Bagby S., Tong KI., Yau P., Takeichi M. and Ikura M. (1995). Solution structure of the epithelial cadherin domain responsible for selective cell adhesion. *Science* **267**: 386-389

Oyama T., Kanai Y., Ochiai A., Akimoto S., Oda T., Yanagihara K., Nagafuchi A., Tsukita S., Shibamoto S., Ito F., Takeichi M., Matsuda H. and Hirohashi S. (1994). A truncated β-catenin disrupts the interaction between E-cadherin and alpha-catenin: a cause of loss of intercellular adhesiveness in human cancer cell lines. *Cancer Res* **54**: 6282-6287

Palaparti A., Baratz A. and Stifani S. (1997). The Groucho/transducin-like enhancer of split transcriptional repressors interact with the genetically defined amino-terminal silencing domain of histone H3. *J Biol Chem* **7**: 230-237

Palombo F., Gallinari P., Laccarino I., Lettieri T., Hughes M., D'Arrigo A., Truong O., Hsuan JJ. and Jiricny J. (1995). GTBP, a 160 kilodalton protein essential for mismatch binding activity in human cells. *Science* **268**: 1912-1914

Papadopoulos N., Nicolaides NC., Wei YF., Ruen SM., Carter KC., Rosen CA., Haseltine WA., Fleischmann RD., Fraser CM., Adams MD., Venter JC., Hamilton SR., Petersen GM., Watson P., Lynch HT., Peltomaki P., Mecklin JP., Delachapelle A., Kinzler KW. and Vogelstein B. (1994). Mutation of a mutL homologue in hereditary colon cancer. *Science* **263**: 1625-1629

Parkhurst SM. (1998). Groucho: making its Marx as a transcriptional co-repressor. *Trends Genet* **14**: 130-132

Parkin DM., Muir CS., Whelan SL., Gao Y-T., Ferlay J. and Powell J. (1992). Cancer incidence in five continents. IARC Sci. Publication, vol 6, Lyon

Parson R., Li G-M., Longly M., Modrich P., Liu B., Berk T., Hamilton SR., Kinzler KW. and Vogelstein B. (1995). Mismatch repair deficiency in phenotypically normal human cells. *Science* **268**: 738-740

Parsons R., Li GM., Longley MJ., Fang W., Papadopoulos M., Jen J., de la Chapelle A., Kinzler KW., Vogelstein B. and Moddrich P. (1993). Hypermutability and mismatch repair eficiency in RER^+ tmour cells. Cell 75: 1227-1236

Paroush Z., Finley RL., Kidd T., Wainwright SM., Ingham PW., Brent R. and Ishhorowicz D. (1994). Groucho is required for *Drosophila* neurogenesis, segmentation and sex determination and interacts directly with hairy-related bHLH proteins. *Cell* **79**: 805-815

Paul R., Ewing CM., Robinson JC., Marshall FF., Johnson KR., Wheelock MJ. and Isaacs WB. (1997). Cadherin-6, a cell adhesion molecule specifically expressed in the proximal renal tubule and renal cell carcinoma. *Cancer Res* **57**: 2741-2748

Peifer M. (1996). Regulating cell proliferation: as easy as APC. *Science* **272**: 974-975

Peltomaki P., Lothe RA., Aaltonen LA., Pylkkanan L., Nystrom-Lahti M., Seruca R., David L., Holm R., Ryberg D., Haugen A., Brogger A., Borresen A-L. and de la Chapelle A. (1993). Microsatellite instability is associated with tumours that characterise the hereditary non-polyposis colorectal carcinoma syndrome. *Cancer Res* **53**: 5853-5855

Perez-Roger I., Solomon DLC., Sewing A. and Land H. (1997). Myc activation of cyclin E/Cdk2 kinase involves induction of cyclin E gene transcription and inhibition of $p27^{Kip1}$ binding to newly formed complexes. *Oncogene* **14**: 2373-2381

Perl A., Wilgenbus P., Dahl U., Semb H. and Christofori G. (1998). A causal role for E-cadherin in the transition from adenoma to carcinoma. *Nature* **392**: 190-193

Persson H. and Leder P. (1984). Nuclear localisation and DNA binding properties of a protein expressed by human c-myc oncogene. *Science* **225**: 718-721

Philipp A., Schneider A., Vasrik I., Finke K., Xiong Y., Beach D., Alitalo K. and Eilers M. (1994). Repression of cyclin D1: a novel function of Myc. *Mol Cell Biol* 14: 4032-4043

Piepenhagen PA. and Nelson WJ. (1995). Differential expression of cell-cell and cell-substratum adhesion proteins along the kidney nephron. *Am J Physiol* 269: (Cell Physiol. 38): C1443-C1449

Plyte SE., Hughes K., Nikolakaki E., Pulverer BJ. and Woodgett JR. (1992). Glycogen synthase kinase-3: functions in oncogenesis and development. *Biochem Biophys Acta* **1114**: 147-162

Polakis P. (1995). Mutation in the APC gene and their implications for protein structure and function. *Curr Opin Gen Dev* **5**: 66-71

Polakis P. (1997). The adenomatous polyposis coli (APC) tumour suppressor. *Biochem Biophys Acta* **1332**:F127-F147

Ponting CP. (1995). DHR domains in syntrophins, neuronal no synthases and other intracellular proteins. *Trends Biol Sci* **20**: 102-103

Ponting CP. (1996). Pleckstrin's repeat performance: a novel repeat in G-protein signalling? *Trends Biol Sci* **21**: 245-246

Potten CS., Owen G. and Roberts SA. (1990). The temporal and spatial changes in cell proliferation within

the irradiated crypts of the murine small intestine. *Int J Radiat Biol* **57**: 185-199

Prieve M., Guttridge K., Munguia J. and Waterman M. (1998). Differential importin-α recognition and nuclear transport by nuclear localisation signals within the high-mobility-group DNA binding domains of lymphoid enhancer factor 1 and T-cell factor 1. *Mol Cell Biol* **18**: 4819-4832

Purdie CA., O'Grady J., Piris J., Wyllie AH. and Bird CC. (1991). P53 expression in colorectal tumours. *Am J Pathol* **138**: 807-815

Purdie CA., Harrison DJ., Peter A., Dobbie L., White S., Howie SEM., Salter DM., Bird CC., Wyllie AH., Hooper ML. and Clarke AR. (1994). Tumour incidence: spectrum and ploidy in mice with a large deletion in the p53 gene. *Oncogene* **9**: 603-609

Radeva G., Petrocelli T., Behrend E., Leung-Hagesteijn C., Filmus J., Slingerland J. and Dedhar S. (1997). Overexpression of the integrin-linkedd kinase promotes anchorage-independent cell cycle progression. *J Biol Chem* **272**: 13937-13944

Raycroft L., Wu H. and Lozano G. (1990). Transcriptional activation by wild type but not transforming mutants of the p53 anti-oncogene. *Science* **249**: 1049-1051

Rayssiguier C., Thaler DS. and Radman M. (1989). The barrier to recombination between *Escherichia coli* and *Salmonella typhimurium* is disrupted in mismatch-repair mutants. *Nature* **342**: 396-401

Reenan RAG. and Kolodner RD. (1992). Isolation and characterisation of two Saccharomyces cerevisiae genes encoding homologs of the bacterial HexA and MutS mismatch repair proteins. *Genetics* **132**: 963-973

Reitmair AH., Scmits R., Ewel A., Bapat B., Redston M., Mitri A., Waterhouse P., Mittrucker H-W, Wakeman A., Liu B., Thomson A., Griesser H., Gallinger S., Ballhausen WG., Fishel R. and Mak TW. (1995). *MSH2* deficient mice are viable and susceptible to lymphoid tumours. *Nat Genet* **11**: 64-70

Reitmair AH., Cai J-C., Bjerknes M., Redston M., Cheng H., Pind MTL., Hay K., Mitri A., Bapat BV., Mak TW. and Gallinger S. (1996). Msh2 deficiency contributes to accumulated APC-mediated intestinal tumorigenesis. *Cancer Res* **56**: 2922-2926

Resnitzky D., Gossen M., Bujard H. and Reed SI. (1994). Acceleration of the G1/S phase-transition by expression of cyclin D1 and cyclin-E with an inducible system. *Mol Cell Biol* **14**: 1669-1679

Resnitzky D. and Reed SI. (1995). Different roles for cyclin D1 and cyclin-E regulation of the G1 to S transition. *Mol Cell Biol* **15**: 3463-3469

Roose J., Molenaar M., Peterson J., Hurenkamp J., Brantjes H., Moerer P., van der Wetering M., DestreeO. and Clevers H. (1998). The Xenopus Wnt effector XTcf3 interacts with Groucho-related transcriptional repressors. *Nature* **395**: 608-612

Rosenwald IB., Lazaris-Karatzas A., Sonenberg N. and Schmidt EV. (1993). Elevated levels of cyclin D1 protein in response to increased expression of eukaryotic initiation-factor 4E. *Mol Cell Biol* **13**: 7358-7363

Rubinfeld B., Souza B., Albert I., Munemitsu S. and Polakis P. (1995). The APC protein and E-cadherin form similar but independent complexes with α-catenin, β-catenin and plakoglobin. *J Biol Chem* **270**: 5549-5555

Rubinfeld B., Robbins P., El-Gamil M., Albert I., Porfiri E. and Polakis P. (1996). Binding of GSK-β to

the APC-catenin complex and regulation of complex assembly. *Science* **272**: 1023-1026

Rubinfeld B., Robbins P., EL-Gamil M., Albert I., Porfiri E. and Polakis P. (1997). Stabilization of β-catenin by genetic defects in melanoma cell line. *Science* **275**: 1790-1792

Ruel L., Bourouis M., Heitzler P., Pantesco V. and Simpson P. (1993). *Drosophila shaggy* kinase and rat glycogen synthase kinase-3 have conserved activities and act downstream of Notch. *Nature* **362**: 557-560

Rye HS., Yue S., Wemmer DE., Quesada MA., Haugland RP., Mathies RA. and Glazer AN. (1992). Stable fluorescent complexes of double-stranded DNA with bis-intercalating asymmetric cyanine dyes: Properties and applications. *Nucleic Acids Res* **20**: 2803-2812

Salomon D., Sacco PA., Guha Roy S., Simcha I., Johnson KR., Wheelock MJ. and Ben-Ze'ev A. (1997). Regulation of β-catenin levels and localization by overexpression of plakoglobin and inhibition of the ubiquitin-proteasome system. *J Cell Biol* **139**: 1325-1335

Salomon R. and Diaz-Cano, S. (1995). Introduction to apoptosis. *Diagn Mol Pathol* **4**: 235-238

Samowitz WS., Powers MD., Spirio LN., Nollet F., van Roy F. and Slattery ML. (1999). β-catenin mutations are more frequently in small colorectal adenomas than in larger adenomas and invasive carcinomas. *Cancer Res* **59**: 1442-1444

Sancar A. and Hearst JE. (1993). Molecular matchmakers. *Science* **259**: 1415-1420

Sapi Z., Hendricks JB., Pharis PG. and Wilkinson EJ. (1993). Tissue sections image analysis of breast neoplasms: evidence of false aneuploidy. *Am J Clin Pathol* **99**: 714-720

Shapiro L., Fannon AM., Kwong PD.,Thomson A., Lehmann MS., rubel G., Legrand JF., Alsnielsen J., Colman DR. and Hendrickson WA. (1995). Structural basis of cell-cell adhesion by cadherins. *Nature* **374**: 327-337

Shaulsky G., Goldfinger N., Ben-Zelev A. and Rotter V. (1990a). Nuclear accumulation of p53 protein is mediated by several nuclear localization signals and plays a role in tumorigenesis. *Mol Cell Biol* **10**: 6565-6577

Shaulsky G., Benzeev A. and Rotter V. (1990b). Subcellular distribution of the p53 protein during the cell cycle of Balb/c 3T3 cells. *Oncogene* **5**: 1707-1711

Sheng H., Shao J., Williams CS., Pereira MA., Taketo MM., Oshima M., Reynolds AB., Washington MK., DuBois RN. and Beauchamp RD. (1998). Nuclear translocation of β-catenin in hereditary and carcinogen induced intestinal adenomas. *Carcinogenesis* **19**: 543-549

Sherr CJ. (1994). G_1 phase progression: cyclin on cue. *Cell* **79**: 551-555

Shibamoto S., Hayakawa M., Takeuchi K., Hori T., Oku N. and Miyazawa K. (1994). Tyrosine phosphorylation of β-catenin and plakoglobin enhanced by hepatocyte growth factor and epidermal growth factor in human carcinoma cells. *Cell Adhes Commun* **1**: 295-305

Shibata T., Toyama K., Shioya H., Ito M., Hirota M., Hasegawa S., Matsumoto H., Takano H., Akiyama T., Toyoshima K., Kanamura R., Kanegae Y., Saito I., Nakamura Y., Shiba K. and Noda T. (1997). Rapid colorectal adenoma formation initiated by conditional targeting of the Apc gene. *Science* **278**: 120-123

Shichiri M., Hanson KD. and Sedivy JM. (1993). Effects of *c-myc* expression on proliferation, quiescence,

and the G_0 to G_1 transition in nontransformed cells. *Cell Growth Differ* **4**: 93-104

Shiozaki H., Kadowaki T., Doki Y., Inoue M., Tamura S., Oka H., Iwazawa T., Matsui S., Shimaya K., Takeichi M. and Mori T. (1995). Effect of epidermal growth factor on cadherin-mediated adhesion in a human oesophageal cancer cell line. *Br J Cancer* **71**: 250-258

Shoemaker AR., Gould KA., Luongo C., Moser AR. and Dove WF. (1997). Studies of neoplasia in the Min mouse. *Biochem Biophys Acta* **1332**: F25-F45

Siegfried E., Chou TB. and Perrimon N. (1992). Wingless signalling acts through zeste-white 3, the Drosophila homologue of glycogen synthase kinase-3, to regulate engrailed and establish cell fate. *Cell* **71**: 1167-1179

Smith KJ., Johnson KA., Bryan TM., Hill DE., Markowitz S., Willson JKV., Paraskeva C., Petersen GM., Hamilton SR., Vogelstein B. and Kinzler KW. (1993). The APC gene product in normal and tumour cells. *Proc Natl Acad Sci USA* **90**: 2846-2850

Smith KJ., Levy DB., Maupin P., Pollard TD., Vogelstein B. and Kinzler KW. (1994). Wild type but not mutant APC associates with microtubules cytoskeleton. *Cancer Res* **54**: 3672-3675

Solomon DLC., Philipp A., Land H. and Eilers M. (1995). Expression of cyclin D1 mRNA is not Upregulated by Myc in rat fibroblasts. *Oncogene* **11**: 1893-1897

Sparks AB., Morin PJ., Vogelstein B. and Kinzler KW. (1998). Mutational analysis of the APC/β-catenin/ Tcf pathway in colorectal cancer. *Cancer Res* **58**: 1130-1134

Sperb RA., Arnold W., Bahr GF., Lonign T. and Gebbers JO. (1993). Comparative DNA image cytometry imprint, cytospin and tissue section preparations of breast carcinoma. *An Cell Pathol* **5**: 265-275

Stifani S., Blaumueller CM., Redhead NJ., Hill RE. and Artavanis-Tsakonas S. (1992). Human homologues of a Drosophila enhancer of split gene product define a novel family of nuclear proteins. *Nat Genet* **2**: 119-127

Strand M., Prolla TA., Liskay RM. and Petes TD. (1993). Destabilisation of tracts of simple repetitive DNA in yeast by mutations affecting DNA mismatch repair. *Nature* **365**: 274-276

Sturzbecher HW., Brain R., Addison C., Rudge K., Remm M., Grimaldi M., Keenan E. and Jenkins JR. (1992). A C-terminal α-helix plus basic region motif is the major structural determinant of p53 tetramerization. *Oncogene* **7**: 1513-1523

Su LK., Kinzler KW., Vogelstein B., Preisinger AC., Moser AR., Luongo C., Gould KA. and Dove WF. (1992). Multiple intestinal neoplasia caused by a mutation in the murine homolog of the APC gene. *Science* **256**: 668-670

Su LK., Johnson KA., Smith KJ., Hill DE., Vogelstein B. and Kinzler KW. (1993). Association between wild type and mutant APC gene products. *Cancer Res* **53**: 2728-2731

Su LK., Burrell M., Hill DE., Gyuris J., Brent R., Wiltshire R., Trent J., Vogelstein B. and Kinzler KW. (1995). APC binds to the novel protein EB1. *Cancer Res* **55**: 2972-2977

Sussman DJ., Klingensmith J., Salinas P., Adams PS., Nusse R. and Perrimon N. (1994). Isolation and characterisation of a mouse homologue of the *Drosophila* segment polarity gene *dishevelled*. *Dev Biol* **166**: 73-86

Syljuasen RG., Krolewski B. and Little JB. (1999). Loss of normal G1 checkpoint control is an early step in carcinogenesis, independent of p53 status. *Cancer Res* **59**: 1008-1014

Takahashi E., Hori T., O'Connell P., Leppert M. and White R. (1991). Mapping of the Myc gene to band 8q24.12-q24.13 by R-banding and distal to fra(8)(q24.11), FRA8E, by fluorescence in situ hybridization. *Cytogenet Cell Genet* **57**: 109-111

Takayama T., Shiozaki H., Shibamoto S., Oka H., Kimura Y., Tamura S., Inoue M., Monden T., Ito F. and Monden M. (1996). β-catenin expression in human cancers. *Am J Pathol* **148**: 39-46

Takeichi M. (1987). Cadherins: a molecular family essential for selective cell-cell adhesion and animal morphogenesis. *Trends Genet* **3**: 213-217

Takeichi M. (1991). Cadherin cell adhesion receptors as a morphogenic regulator. *Science* **251**: 1451-1455

Takeichi M. (1995). Morphogenetic roles of classic cadherins. *Curr Opin Cell Biol* **7**: 619-627

Tam SW., Theodoras AM., Shay JW., Draetta GF. and Pagano M. (1994). Differential expression and regulation of cyclin D1 protein in normal and tumour human cells-association with CDK4 is required for cyclin D1 function in G1 progression. *Oncogene* **9**: 2663-2674

Tanaka S., Akiyoshi T., Mori M., Wands JR. and Sugimachi K. (1998). A novel frizzled gene identified in human oesophageal carcinoma mediated APC/β-catenin signals. *Proc Natl Acad Sci USA* **95**: 10164-10169

Tanergard P., Lipford JR., Kolodner R., Frodin JE., Nordenskjold M. and Lindblom A. (1996). Mutation screening in the hMLH1 gene in Swedish hereditary nonpolyposis colon cancer families. *Cancer Res* **55**: 6092-6096

Tekola P., Baak JPA., Belien JAM. and Brugghe J. (1994). Highly sensitive, specific, and stable new fluorescent DNA stains for confocal laser microscopy and image processing of normal paraffin sections. *Cytometry* **17**: 191-195

Teich N., Wyke J., Mak T., Bernstein A. and Hardy W. (1984). Pathogenesis of retrovirus induced disease, in RNA tumour viruses. (Weiss R, Teich N, Varmus H, Coffin J, eds) pp 785-998. Cold Spring Harbor Laboratory, Cold Spring Harbor, USA

Tetsu O. and McCormick F. (1999). β-catenin regulates expression of cyclin D1 in colon carcinoma cells. *Nature* **398**: 422-426

Thibodeau SN., Bren G. and Schaid D. (1993). Microsatellite instability in cancer of the proximal colon. *Science* **260**: 816-819

Toft NJ., Winton DJ., Kelly J., Howard LA., Dekker M., Riele HT., Arends MJ., Wyllie AH., Margison GP. and Clarke AR. (1999). *Msh2* status modulates both apoptosis and mutation frequency in the murine small intestine. *Proc Natl Acad Sci USA* **96**: 3911-3915

Travis A., Amsterdam A., Belanger C. and Grosschedl R. (1991). Lef-1, a gene encoding a lymphoid-specific protein with an HMG domain, regulates T-cell receptor α enhancer function. *Gene Dev* **5**: 880-894

Trzepacz C., Lowy AM., Kordich JJ. and Groden J. (1997). Phosphorylation of the tumour suppressor

adenomatous polyposis coli (APC) by the cyclin-dependent kinase $p34^{cdc2}$. *J Biol Chem* **272**: 21681-21684

Uyterlinde AM., Smeulders AWM. and Baak JPA. (1989). Reproducibility and comparison of quantitative DNA histogram features obtained with a scanning microdensitometer and flow cytometer in breast cancers. *Anal Quant Cytol Histol* **11**: 353-360

van de Wetering M., Oosterwegel M., Dooijes D. and Clevers H. (1991). Identification and cloning of TCF-1, a T cell-specific transcription factor containing a sequence-specific HMG box. *EMBO J* **10**: 123-132

Vasen HF., Offerhaus GT., den Hartog Jager FC., Menko FH., Nagengast FM., Griffioen G., van Hogezand RB. and Heintz AP. (1990). The tumour spectrum in hereditary non-polyposis colorectal cancer: a study of 24 kindreds in the Netherlands. *Int J Cancer* **46**: 31-34

Vatanasapt V., Martin N., Sriplung H., Chindavijak K., Soontipong S., Sriamporn S., Parkin DM. and Ferlay J. (1993). Cancer in Thailand. IARC technical report no. 16. Lyon.

Venkatachalam S., Shi Y-P., Jones SN., Vogel H., Bradley A., Pinkel D. and Donehower LA. (1998). Retention of wild type p53 in tumours from p53 heterozygous mice: reduction of p53 dosage can promote cancer formation. *EMBO J* **17**: 4657-4667

Vestweber D., Kemler R. and Ekblom P. (1985). Cell-adhesion molecule uvomorulin during kidney development. *Dev Biol* **112**: 213-221

Vleminckx K., Vakaet L.Jr., Mareel M., Fiers W. and Vanroy F. (1991). Genetic manipulation of E-cadherin expression by epithelial tumor cells reveals an invasion suppressor role. *Cell* **66**: 107-119

Wang TC., Cardiff RD., Zukerberg L., Lees E., Arnold A. and Schmidt EV. (1994). Mammary hyperplasia and carcinoma in MMTV-cyclin D1 transgenic mice. *Nature* **369**: 669-671

Wang Y., Szekely L., Okan I., Klein G. and Wiman KG. (1993). Wild-type p53-triggered apoptosis is inhibited by bcl-2 in a v-myc-induced T-cell lymphoma line. *Oncogene* **8**: 3427-3431

Wang Y., Macke JP., Abella BS., Andreasson K., Worley P., Gilbert DJ., Copeland NG., Jenkins NA. and Nathans J. (1996). A large family of putative transmembrane receptors homologous to the product of the *Drosophila* tissue polarity gene *frizzled*. *J Biol Chem* **271**: 4468-44766

Wasan HS., Park H-S., Liu KC., Mandir NK., Winnett A., Sasieni P., Bodmer WF., Goodlad RA. and Wright NA. (1998). APC in the regulation of intestinal crypt fission. *J Pathol* **185**: 246-255

Waters CM.., Littlewood TD., Hancock DC., Moore JP. and Evan GI. (1991). C-myc protein expression in untransformed fibroblasts. *Oncogene* **6**: 797-805

Waterman ML., Fisher WH. and Jones KA. (1991). A thymus-specific member of the HMG protein family regulates the human T cell receptor Cα enhancer. *Gene Dev* **5**: 656-669

Watson P. and Lynch HT. (1993). Extracolonic cancer in hereditary nonpolyposis colorectal cancer. *Cancer (Phila)* **71**: 677-685

Webb SJ., Nicholson D., Bubb VJ. and Wyllie AH. (1999). Caspase-mediated cleavage of APC results in an amino-terminal fragment with an intact armadillo repeat domain. *FASEB J* **13**: 339-346

Weinberg RA. (1995). The retinoblastoma protein and cell cycle control. *Cell* **81**: 323-330

White E. (1996). Life, death, and pursuit of apoptosis. *Gene Dev* **10**: 1-15

White RL. (1997). Colon cancer. Molecular Biology of the APC protein. *Path Biol* **45**: 240-244

Wieschaus E. and Riggleman R. (1987). Autonomous requirements for the segment polarity gene armadillo during Drosophila embryogenesis. *Cell* **49**: 177-184

Willert K. and Nusse R. (1998). β-catenin: A key mediator of Wnt signalling. *Curr Opin Genet Dev* **8**: 95-102

Wilson TM., Ewel A., Duguid JR., Eble JN., Lescoe MK., Fishel R., and Kelly MR. (1995). Differential cellular expression of the human MSH2 repair enzyme in small and large intestine. *Cancer Res* **55**: 5146-5150

Woodgett JR. (1990). Molecular cloning and expression of glycogen synthase kinase-3/Factor A. *EMBO J* **9**: 2431-2438

Wu C., Keightley S., Leung-Hagesteijn C., Radeva G., Coppolino M., Goicoechea S., McDonald J. and Dedhar S. (1998). Integrin-linked protein kinase regulates fibronectin matrix assembly, E-cadherin expression, and tumorgenicity. *J Biol Chem* **273**: 528-536

Wyllie AH., Kerr JFR. and Currie AR. (1980). Cell death: The significance of apoptosis. *Int Rev Cytol* **68**: 251-305

Yamamoto H., Kishida S., Uochi T., Ikeda S., Koyama S., Asashima M. and Kikuchi A. (1998). Axil, a member of the Axin family, interacts with both glycogen synthase kinase 3β and β-catenin and inhibits axis formation of *Xenopus* embryo. *Mol Cell Biol* **18**: 2867-2875

Yanakawa S., van Leeuwen F., Wodarz A., Klingensmith J. and Nusse R. (1995). The Dishevelled protein is modified by Wingless signalling in Drosophila. *Gene Dev* **9**: 1087-1097

Yang S-D., Song JS., Hsieh Y-T., Liu H-W. and Chan W-H. (1992). Identification of the ATP-Mg-dependent protein phosphatase activator (F_A) as a synapsin I kinase that inhibits cross-linking of synapsin I with brain microtubules. *J Protein Chem* **11**: 539-546

Yang-Snyder J., Miller JR., Brown JD., Lai CJ. and Moon RT. (1996). A frrizzled homologue functions in a vertebrate Wnt signalling pathway. *Curr Biol* **6**: 1302-1306

Yin XY., Grove L., Datta NS., Long MW. and Prochownik EV. (1999). C-myc overexpression and p53 loss cooperate to promote genomic instability. *Oncogene* **18**: 1177-1184

Yost C., Torres M., Miller JR., Huang E., Kimelman D. and Moon RT. (1996). The axin inducing activity, stability, and subcellular distribution of β-catenin is regulated in Xenopus embryos by glycogen synthase kinase 3. *Gene Dev* **10**: 1443-1454

Young CS., Kitamura M., Hardy S. and Kitajewski J. (1998). Wnt-1 induced growth, cytosolic β-catenin, and Tcf/Lef transcriptional activation in rat-1 fibroblasts. *Mol Cell Biol* **18**: 2474-2485

Zeng L., Fagotto F., Zhang T., Hsu W., Vasicek TJ., Perry WL., Lee JJ., Tilghman SM., Gumbiner BM. and Costantini F. (1997). The mouse fused locus encoded axin, an inhibitor of the Wnt signalling pathway that regulates embryonic axis formation. *Cell* **90**: 181-192

Zhang H., Richards B., Wilson T., Lloyd M., Cranston A., Thorburn A., Fishel R. and Meuth M. (1999). Apoptosis induced by overexpression of h MSH2 or hMLH1. *Cancer Res* **59**: 3021-3027

Zhang T., Nanney LB., Peeler MO., Williams CS., Lamps L., Heppner KJ., DuBois RN. and Beauchamp RD. (1997). Decreased transforming growth factor β type II receptor expression in intestinal adenomas from *Min*/+ mice is associated with increased cyclin D1 and cyclin-dependent kinase 4 expression. *Cancer Res* **57**: 1638-1643

Zhao Z., Lee CC., Baldini A. and Caskey CT. (1995). A human homologs for the Drosophila polarity gene frizzled has been identified and mapped to 17q21.1. *Genomics* **27**: 370-373

Zhu Q., Tekola P., Baak JPA. and Belien JAM. (1994). Measurement of confocal laser scanning microscopy of the volume of epidermal nuclei in thick skin sections. *Anal Quant Cytol Histol* **16**: 145-152

Oncogene (1999) 18, 7219–7225

http://www.stockton-press.co.uk/onc

Dysregulated expression of β-catenin marks early neoplastic change in Apc mutant mice, but not all lesions arising in Msh2 deficient mice

Rungtiva Kongkanuntn[1], Vivien J Bubb[1], Owen J Sansom[1], Andrew H Wyllie[1], David J Harrison[1] and Alan R Clarke*,[1]

[1]*CRC Laboratories, Department of Pathology, University Medical School, Teviot Place, Edinburgh, EH8 9AG, Scotland*

We have analysed the pattern of β-catenin expression by immunohistochemistry in mice singly or multiply mutant for *Apc*, *p53* and *Msh2*. We observed increased expression of β-catenin in all intestinal lesions arising on an $Apc^{Min}+/-$ background. In all categories of lesion studied mosaic patterns of β-catenin expression were observed, with the proportion of cells showing enhanced expression decreasing with increasing lesion size. p53 status did not alter these patterns. We also show that β-catenin dysregulation marks pancreatic abnormalities occurring in $Apc^{Min}+/-$ and ($Apc^{Min}+/-$, p53−/−) mice. In these mice both adenomas and adenocarcinomas of the pancreas arose and were characterized by increased expression of β-catenin. We have extended these analyses to intestinal lesions arising in mice mutant for the mismatch repair gene *Msh2*. In these mice, increased expression of β-catenin was again observed. However, in contrast with $Apc^{Min}+/-$ mice, a subset of lesions retained normal expression. Taken together, these findings show that increased expression of β-catenin is an efficient marker of early neoplastic change in both murine intestine and pancreas in *Apc* mutant mice. However, we also show that dysregulation of β-catenin is not an obligate step in the development of intestinal lesions, and therefore that genetic events other than the loss of Apc function may initiate the transition from normal to neoplastic epithelium.

Keywords: β-catenin; Apc; p53; Msh2; intestine; pancreas

Introduction

Germline mutations in the adenomatous polyposis coli gene (APC) gene at 5q21 characterize an inherited disorder known as familial adenomatous polyposis coli (FAP) (Kinzler *et al.*, 1991). FAP patients develop numerous adenomas throughout both the small and large intestine, some of which ultimately progress to carcinoma. However, a more general role for APC mutations in neoplasia is suggested by the fact that FAP patients have an increased predisposition to tumours of the brain, thyroid and bone and also to focal proliferative lesions ('desmoid tumours') of the connective tissue. Mutated APC has also been reported in a range of sporadic tumours, including pancreatic and gastric tumours and the majority of adenomas and carcinomas of the colorectum (Miyoshi *et al.*, 1992; Horii *et al.*, 1992; Nakatsuru *et al.*, 1992). Furthermore, loss of heterozygosity at 5q21 has been observed in sporadic tumours of the breast and oesophagus (Boynton *et al.*, 1992; Thompson *et al.*, 1993; Kashiwaba *et al.*, 1994).

Several different murine models of FAP have been generated by random chemical carcinogenesis (Moser *et al.*, 1992), conventional gene targeting (Fodde *et al.*, 1994; Oshima *et al.*, 1995) and by the use of Cre-Lox technology (Shibata *et al.*, 1997). All of these models are characterized by high levels of spontaneous intestinal neoplasia, confirming a role for *Apc* in the development of these lesions. Several observations using these models support the notion that *Apc* has more widespread tumour suppressor activity. First, desmoid tumours have been reported to occur spontaneously in *Apc* mutant mice (Shoemaker *et al.*, 1997; Smits *et al.*, 1998). Second, Apc^{Min} heterozygotes show an increased susceptibility to mammary carcinoma both spontaneously and following genotoxic stress such as carcinogen treatment or X irradiation (Moser *et al.*, 1993, 1995; van der Houven *et al.*, 1997). Finally, *Apc* heterozygosity on a *p53* null background has been shown to strongly predispose to pancreatic neoplasia (Clarke *et al.*, 1995).

How loss of function of Apc predisposes to malignancy remains unclear, however disruption of the normal function of β-catenin has been implicated in this process (Rubinfeld, 1993; Su *et al.*, 1993). Levels of β-catenin are modulated by Apc through the mammalian Wnt signalling pathway, where Apc interacts with both glycogen synthase kinase 3β (GSK3β) and β-catenin. The central portion of Apc contains sites at which it can be phosphorylated by GSK3β and also through which it complexes with β-catenin. Phosphorylation by GSK3β increases the stability of the Apc/β-catenin complex and is thereby thought to increase the rate of β-catenin degradation (Rubinfeld *et al.*, 1996).

From the above it is clear that disruption of Apc function can lead to an increase in the cellular levels of β-catenin. However, this is not the only potential mechanism for such an increase. Wnt-1 has been shown to regulate free pools of catenin (Papkoff *et al.*, 1996) and both axin and the axin homologue conductin have been reported to alter β-catenin activity through interaction with Apc, β-catenin and GSK3β (Behrens *et al.*, 1998; Ikeda *et al.*, 1998; Kishida *et al.*, 1998). The potential relevance of increased levels of β-catenin becomes clear in the light of findings which show that β-catenin functionally interacts with and activates members of the Tcf family of DNA binding

*Correspondence: AR Clarke
Received 16 March 1999; revised 20 August 1999; accepted 23 August 1999

transcription factors, including both Lef-1 and Tcf 4 (Behrens *et al*., 1998; Korinek *et al*., 1997). Activation of transcriptional signalling by β-catenin-Tcf complexes has been shown to occur as a consequence of mutations in both *Apc* and β-catenin (Morin *et al*., 1997; Rubinfeld *et al*., 1997) and mutations of β-catenin have been reported in human colorectal cancers (Sparks *et al*., 1998). Dysregulated transcription has therefore been proposed as the basis for early neoplastic change, although the target genes through which this may be mediated remain as yet undetermined (Nusse, 1997).

β-catenin also regulates E-cadherin in conjunction with α-catenin, and loss of function of any of these proteins abrogates E-cadherin activities, including maintenance of the adherens junction complex. Amongst other activities this complex mediates cell-to-cell adhesion and thereby the control of cell motility (Chen *et al*., 1997). Modulation of cell adhesion appears to be a common mechanism in neoplastic change, and altered E-cadherin activity has been found in a number of cancers of epithelial origin including lobular breast carcinoma, colorectal carcinoma and gastric adenocarcinoma (Birchmeier and Behrens, 1994). In a transgenic murine model of pancreatic β-cell carcinogenesis, loss of function of E-cadherin has been shown to be a critical step in the transition from adenoma to carcinoma (Perl *et al*., 1998).

Immunohistochemical analysis of both human and murine intestinal tumours has shown that both adenomas and well differentiated carcinomas are characterized by high levels of β-catenin (Inomata *et al*., 1996; Takayama *et al*., 1996). However, both β-catenin and E-cadherin are reported to be expressed at significantly lower levels in more aggressive malignancies, strongly suggesting that over-expression of β-catenin is only crucial in early tumour development (Takayama *et al*., 1996).

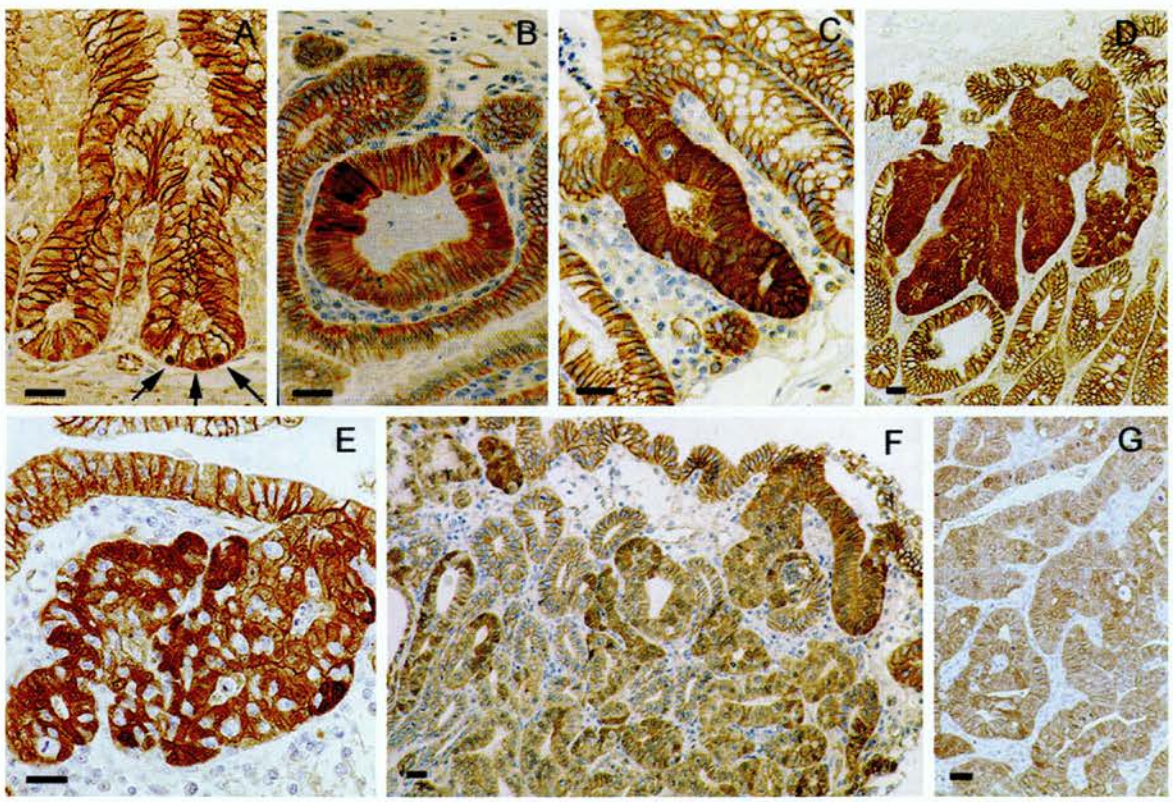

Figure 1 The pattern of β-catenin staining in the intestine of $Apc^{Min}+/-$ and ($Apc^{Min}+/-$, p53−/−) animals. Mice mutant for *Msh2* (De Wind *et al*., 1995), *p53* (Clarke *et al*., 1993) and Apc^{Min} (Moser *et al*., 1992) were maintained as outbred colonies segregating for Ola/129, Balb C, SWR and C57Bl/6 genomes. Mice were monitored on a daily basis for signs of ill health and were killed when they showed signs of disease. All tissues were paraffin embedded using standard methods after overnight fixation in either buffered formalin or methacarn (four parts methanol, two parts chloroform, one part acetic acid v/v). High temperature antigen retrieval was performed (Alman *et al*., 1997), sections were cooled to room temperature and immersed in 1.5%H_2O_2 solution to block endogenous peroxidase for 15 min. Sections were then incubated with 1 : 50 mouse monoclonal β-catenin antibody (IgG_1, clone 14, Transduction Laboratories, USA) for 60 min, and subsequently with 1 : 400 Rabbit Anti-Mouse Biotinylated secondary antibody (DAKO) for 30 min. The sections were incubated in StrepABComplex/HRP (DAKO) for 30 min. The labelled complex was developed with diaminobenzidine (DAB, 0.5 mg/ml) for 5–8 min. at room temperature. (**a**–**g**) Photographs demonstrating the various features observed in animals with these genotypes. All the features illustrated here were observed irrespective of *p53* status. All scale bars represent 10 μm (**a**) β-catenin staining in morphologically normal crypts of the small intestine. β-catenin was detected throughout the cytoplasm of epithelial cells but was strongly localized to the lateral borders. Strong nuclear localization was observed in cells at the crypt base (arrows). (**b**) Heterogeneous expression in a type I lesion. The majority of cells show the normal pattern of staining, with localization to the lateral borders. A subset of cells show increased cytoplasmic and nuclear staining. (**c**) Uniformly increased β-catenin staining within a type 1 lesion. (**d**) Increased β-catenin staining in a type II lesion. (**e**) Heterogeneous expression in a type II lesion. Cells showing increased β-catenin showed localized to the cytoplasm and in some instances localization to the nucleus. (**f**) Heterogeneous expression of β-catenin within a type III lesion. (**g**) Reduced expression within a type IV lesion. Where expression of β-catenin was retained this was often localized to the nucleus

In order to further characterize the association between tumourigenesis and dysregulation of β-catenin we have analysed the pattern of β-catenin expression in normal and neoplastic tissue derived from mice mutant for the tumour suppressor genes *p53* and *Apc*. This analysis is performed on mice which carry a mutant *Apc* allele. Loss of the remaining wild type *Apc* allele results in dysregulated expression of β-catenin. Because we also wished to address the possibility that dysregulation of β-catenin is not an obligate step in intestinal neoplasia, we also analysed mice deficient for the DNA mismatch repair gene *Msh2* (De Wind *et al*., 1998), a murine model of hereditary non-polyposis colorectal cancer (HNPCC). *Msh2*−/− mice develop lymphomas with a peak incidence at 2–3 months of age (De Wind *et al*., 1995; Reitmair *et al*., 1996). Of the 50% of *Msh2*−/− mice which survive beyond 6 months of age, 70% develop intestinal neoplasms (Reitmair *et al*., 1996). We report here the pattern of β-catenin expression in lesions arising in mice mutant for *Msh2*−/− and (*Msh2*−/−, Apc^{Min}+/−).

We first investigated the pattern of expression of β-catenin in intestinal lesions arising in Apc^{Min} and p53/Apc^{Min} mutants. In morphologically normal epithelium, β-catenin was localized at the cell membrane. Nuclear localization was observed in some cells: these were always located at the crypt base (Figure 1a). This observation suggests a role for β-catenin in the base of the crypt as β-catenin is thought to mediate transcriptional regulation within the nucleus, and indeed interaction with the transcription factor Lef-1 is known to promote nuclear localization of β-catenin (Huber *et al*., 1996).

In both Apc^{Min}+/− and (Apc^{Min}+/−, p53−/−) mice, expression of β-catenin is more intense in dysplastic crypts and small adenomas. To control for staining variability between sections, changes in the intensity of expression were always scored relative to normal epithelium within the same section. The lesions were subclassified as in Clarke *et al*. (1995): (i) single dysplastic crypts, showing nuclear pleomorphism and stratification; (ii) complex lesions, comprising several architecturally distorted crypts in the lamina propria with virtually normal overlying surface epithelium; (iii) small adenomas, identified by the overall disturbance of architecture including the surface and distinguished from the previous category on the basis of increased size and surface involvement; (iv) large adenomas, and (v) adenocarcinoma. The pattern of β-catenin staining, summarised in Figure 2, was essentially identical in Apc^{Min}+/− and (Apc^{Min}+/−, p53−/−) mice, with all features described below noted in both groups. A substantial proportion of all lesion types showed heterogeneous expression of β-catenin expression, even where only single crypts were involved (type I lesions, Figure 1b,e and 2). The term 'heterogeneous' is used here to describe lesions in which only a proportion of cells were characterized by increased expression. Although heterogeneous β-catenin was observed in all lesions types, the proportion of cells overexpressing β-catenin were at their highest in type I-III lesions (Figure 1c–d and 2). Mosaic type IV lesions showed the lowest proportion of cells staining positive for β-catenin (Figure 1f). Large areas of reduced staining were observed in some late stage lesions, including those categorized both as type IV and V (Figure 1g). In all categories of lesion the predominant pattern was of increased β-catenin staining within the nucleus, within the cytoplasm and also at the cell membrane. However a pattern of strong nuclear localization without concomitant cytoplasmic staining was also observed within some lesions as has been previously reported (Sheng *et al*., 1998).

These results show that high levels of β-catenin are present in the majority of intestinal lesions, presumably as a direct consequence of perturbation of the Wnt pathway. Furthermore, areas showing high levels of β-catenin included those composed of heterogeneous or single dysplastic crypts in the intestine, supporting the notion that dysregulated β-catenin expression is an extremely efficient marker of early neoplastic change in the murine intestine. Lower levels of expression were seen in focal areas within some larger adenomas and adenocarcinomas, suggesting that genotypic changes which lead to elevated β-catenin are only relevant to the early stages of neoplasia. This concept is supported by observations of localized areas of reduced or absent β-catenin expression within some adenomas; and also by studies of human tumorigenesis, where down-regulation of both β-catenin and E-cadherin has been reported in a range of carcinomas (Takayama *et al*., 1996).

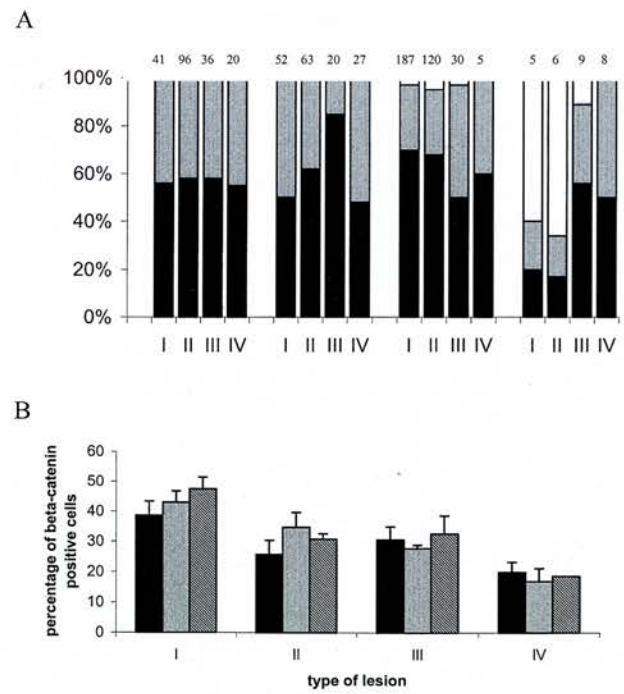

Figure 2 β-catenin expression patterns within each class of intestinal lesion. (**a**) Percentage of each lesion type showing either upregulation of β-catenin in all cells (black bars); a mosaic or heterogeneous pattern of upregulation as defined in the text (grey bars); or no upregulation (open bars). The number of lesions scored is shown over each column. Insufficient numbers of category V lesions were identified to permit scoring. (**b**) Histogram showing the percentage of cells expressing high levels of β-catenin within lesions characterized by mosaic expression of β-Catenin. Black bars, Apc^{Min}+/−; Grey bars (Apc^{Min}+/−, *p53*−/−); Hatched bars (Apc^{Min}+/−, *Msh2*−/−). Mean values are given for each lesion category, as defined in the text. Error bars represent SEM. Insufficient numbers of mosaic lesions were identified in *Msh2*−/− mice to permit analysis

We next investigated the pattern of expression of β-catenin in intestinal lesions arising in Msh2 mutant animals and Msh2/Apc^{Min} mutants (summarized in Figure 2). Previous studies have shown that the Msh2 mutation predisposes to intestinal tumorigenesis and also accelerates neoplasia in Apc^{Min}+/− mice (De Wind *et al*., 1995, 1998; Reitmair *et al*., 1996). In Msh2−/− animals we identified type I , II and III lesions which showed normal β-catenin expression (Figure 3b), a phenomenon we did not observe in Apc^{Min}+/−mice (Figure 3a). However, all type IV adenomas were characterized by increased levels of β-catenin expression. No type V lesions were identified. In (Msh2−/−, Apc^{Min}+/−) mice there was a significant increase in the frequency of adenomas, as has been previously reported (Reitmair *et al*., 1996). The majority of these lesions stained strongly for β-catenin (Figure 3c), however we again identified a small number of type I,II and III lesions (×10%) with the pattern of β-catenin expression characteristic of normal cells (Figure 3d). All type IV lesions analysed showed altered β-catenin expression, with an almost identical pattern to that observed in Apc^{Min}+/−mice. No type V lesions were identified.

We therefore successfully identified small lesions in both *Msh2* and *Msh2*/*Apc*^{Min} mice which showed normal levels and distribution of β-catenin. These findings show that dysregulated β-catenin is not an obligate event in early lesion formation, and furthermore that *Msh2* deficiency predisposes to such apparent β-catenin-independent events. Thus, *Msh-2* deficiency may predispose to dysplasia through mutations in other components of the Wnt signalling pathway which do not affect β-catenin levels or indeed through mutations in other path-

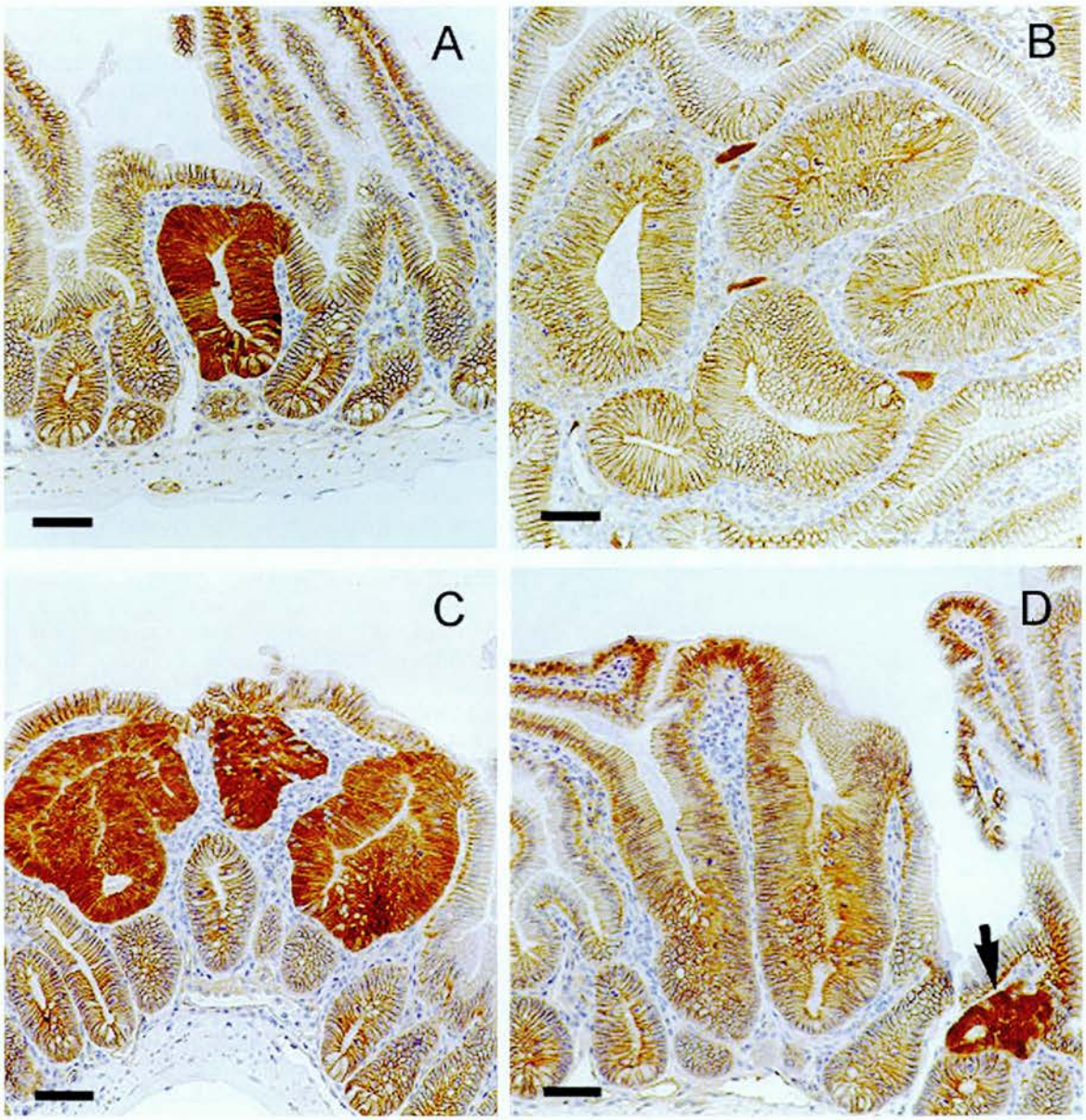

Figure 3 The pattern of β-catenin expression in the intestine of Msh2−/− mice (**a**,**b**) and (Msh2−/−, Apc^{Min}+/−) mice (**c**,**d**). Immunohistochemical analysis was performed as described in the legend to Figure 1. All scale bars represent 10 μm. (**a**) Increased β-catenin staining in a type I lesion. (**b**) Normal pattern of β-catenin expression in a type II lesion, with β-catenin strongly localized to the lateral borders. (**c**) Increased β-catenin expression in a type II lesion. (**d**) Normal β-catenin expression in a type II lesion, with retained localization to the lateral borders. A type I lesion showing β-catenin dysregulation is indicated for comparison (arrow)

ways. All large adenomas (type IV) were characterized by increased β-catenin, showing that this degree of morphological change is absolutely associated with events which dysregulate β-catenin levels.

We have previously described the phenotype of mice mutant for both *p53* and *Apc* (Clarke *et al*., 1995). In addition to intestinal lesions these mice develop pancreatic neoplasia, either adenoma or acinar adenocarcinoma, with almost 100% penetrance. The cell type observed in these lesions was predominantly acinar, although some foci showed ductal transdifferentiation. The involvement of *Apc* in the development of pancreatic lesions was confirmed by loss of the remaining wild type allele in adenocarcinomas (Clarke *et al*., 1995). We therefore next wished to assess the extent of dysregulation of β-catenin in these lesions.

Within morphologically normal pancreatic cells, β-catenin was observed at the cell membrane, with no obvious nuclear localization. In ($Apc^{Min}+/-$p53$-/-$) mice all foci showing histological change were characterized by high levels of β-catenin. Increased staining was also seen in foci which were virtually histologically normal. Such increased staining was never observed in pancreas samples derived from wild type mice. Foci varied in size, with some containing only single or a few cells in the plane of section (Figure 4a,b). The observation of few or single cell lesions strongly suggests that dysregulated expression occurs very early in neoplasia.

In lesions identified in formalin fixed tissues, increased β-catenin expression was seen within both the nucleus and cytoplasm (Figure 4c). However, cytoplasmic staining was rarely observed in Methacarn fixed sections, suggesting that the observed cytoplasmic localisation was an artefact of tissue fixation. Using either fixation protocol we observed rare (<1%) lesions which did not show increased nuclear staining (Figure 4d). Nuclear atypia was seen in the majority of lesions, although the extent of nuclear pleomorphism varied considerably from mild to severe within each lesion (Figure 4b,e). Acinar cell lesions classified as adenoma were also characterized by increased β-

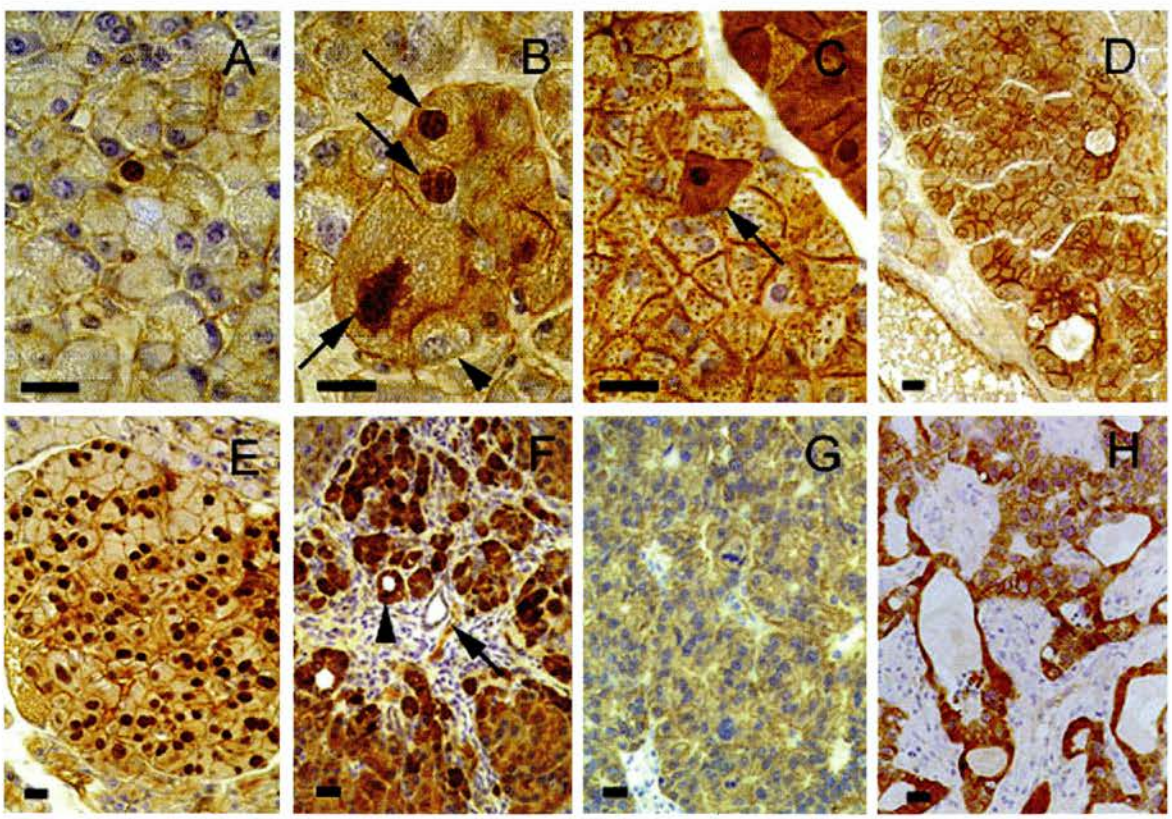

Figure 4 The pattern of β-catenin staining in the pancreas of $Apc^{Min}+/-$ and ($Apc^{Min}+/-$, p53$-/-$) mice. Immunohistochemical analysis was performed as described in the legend to Figure 1. (**a**–**e**) are representative of the patterns of β-catenin staining and histological atypia observed in the pancreas of both $Apc^{Min}+/-$mice and ($Apc^{Min}+/-$, *p53*$-/-$) mice. (**f**–**h**) are representative of these patterns in pancreatic adenomas and adenocarcinomas arising in ($Apc^{Min}+/-$, *p53*$-/-$) mice. All scale bars represent 10 μm. (**a**) Methacarn fixed. A single pancreatic acinar cell characterised by increased nuclear and cytoplasmic expression. The surrounding acinar cells are representative of the normal pattern of β-catenin staining, with localization to the cell borders. (**b**) Methacarn fixed. Small focus of acinar cells with increased expression. These foci were often composed of cells with increased nuclear size, prominent examples of which are indicated by arrows. This focus also contains a cell (short arrow) with no increase in nuclear levels of β-catenin. (**c**) This picture demonstrates the pattern of staining observed in formalin fixed tissues. Cells (arrowed or restricted to the upper right hand portion of this photograph) showing increased nuclear and cytoplasmic levels of β-catenin staining. (**d**) Methacarn fixed. A dysplastic adenoma showing increased β-catenin expression, but with no apparent nuclear localization. (**e**) Methacarn fixed. Increased β-catenin staining in a pancreatic focus, showing strong nuclear localization. Again, these foci were often composed of cells with increased nuclear size. (**f**) Methacarn fixed. Heterogeneous β-catenin expression in an adenoma containing areas of acinar-ductal transdifferentiation (arrowhead). No increase in β-catenin staining was detectable in normal ducts (arrow). (**g**) Low levels of β-catenin within an acinar adenocarcinoma. (**h**) Methacarn fixed. Areas of ductal differentiation within an acinar adenocarcinoma which have retained high levels of β-catenin expression

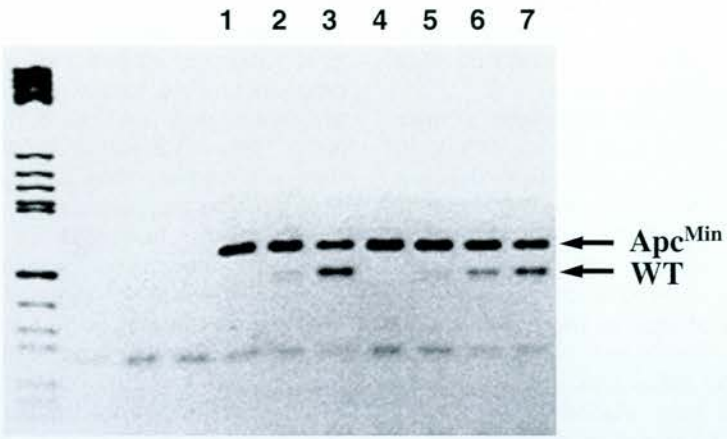

Figure 5 PCR amplification of Apc alleles from microdissected lesions. PCR analysis. Histological microdissection was performed as previously described (Going and Lamb, 1996). Samples were digested in proteinase K (1 mg/ml) and 1% Tween 20. The proteinase K was subsequently heat-inactivated at 95°C, for 10 min. PCR amplification was then performed essentially as previously described (Luongo *et al* 1994) using the primers (5′TCTCTT CTGAGAG CAGAAGTT) and (5′ATAGCCAA AGTTATGGAA GAAGTATCA). Representative results from PCR analysis of microdissected lesions. Determination of Min status was by PCR and *Hind*III digest of PCR product as previously described (Luongo *et al*., 1994). WT, the amplification product from the wild type *Apc* allele. Apc^{Min}, the amplification product from the mutant allele. Samples were all derived form lesions arising within Apc^{Min} mutant mice and were as follows: lanes 1 and 2, pancreatic foci showing β-catenin dysregulation; lane 3 normal pancreas; lanes 4 and 5, small intestinal lesions; lanes 6 and 7 normal intestinal epithelium. All results were obtained using microdissected areas containing a minimum of 50 cells

catenin staining. Some of these lesions contained areas of acinar-ductal transdifferentiation which were also strongly stained (Figure 4f). Adenocarcinomas contained areas in which β-catenin intensity was reduced (Figure 4g), however areas of ductal differentiation within these tumours retained high levels of β-catenin (Figure 4h).

These results prompted us to analyse Apc^{Min} mice. When these animals are maintained on a wild type background they do not develop pancreatic adenomas (Clarke *et al*., 1995). Surprisingly, although we confirmed absolute absence of neoplasms of the pancreas, we did find multiple foci of β-catenin dysregulation identical to those observed in (Apc^{Min} +/−p53−/−) mice. Our previous analysis (Clarke *et al*., 1995) had identified focal mild dysplasia in one out of seven *ApcMin* heterozygotes. Subsequent re-examination of these sections showed multiple ill-defined areas containing cells characterized by nuclear size variation. These areas overexpressed β-catenin. Thus, β-catenin immunohistochemistry efficiently highlighted focal areas of early histological change in the pancreas of both (Apc^{Min}+/−p53−/−) and Apc^{Min}+/−mice. We also analysed pancreatic tissue derived from *Msh2*−/−mice and (*Msh2*−/−, Apc^{Min}+/−) mice, neither of which develop spontaneous pancreatic neoplasms. No abnormal expression of β-catenin or histological atypia was observed in *Msh2*−/−mice. However, in (*Msh2*−/−, Apc^{Min}+/−) mice we again identified foci of β-catenin overexpression, and these did not differ in morphological appearance from those seen in Apc^{Min}+/−animals.

In the pancreas, dysregulated β-catenin expression was seen in 100% of lesions which appeared morphologically abnormal. Previously, we had noted the presence of these lesions at high frequency only in (*p53*−/−, Apc^{Min}+/−) mice and rarely in wild type mice. The occurrence of high β-catenin expression in areas of minimal histological abnormality in Apc^{Min} heterozygotes allows an order of genetic events to be proposed for this model of pancreatic neoplasia. In the presence of wild type *p53* such dysregulated expression does not lead to neoplasia, but it is associated with nuclear size variation, raising the possibility that loss of Apc function may promote chromosomal instability. We are currently characterizing this phenomenon in greater detail. By contrast, a *p53* null environment allows progression to adenoma and then adenocarcinoma. Loss of *p53* is therefore essential for adenoma formation in the time frame analysed here. Notably, the requirement for genetic change differs between pancreas and intestine, as within the murine intestine *p53* loss does not increase either adenoma burden or neoplastic progression (Clarke *et al*., 1995).

To characterize the status of the remaining *Apc* allele in both the intestinal and pancreatic lesions arising in Apc^{Min}+/− mice we performed PCR analysis on microdissected foci. Serial sections were generated and areas of increased β-catenin staining identified. These areas were microdissected and DNA isolated. Loss of the remaining Apc^{wt} allele was assessed following PCR amplification. This approach allowed us to analyse intestinal and pancreatic lesions of, at the lowest limit, approximately 50 cells per cross section. Using this method we demonstrate loss of the remaining wild type *Apc* allele in both the intestinal and pancreatic lesions analysed from Apc^{Min}+/− and Apc^{Min}+/−, *p53*−/− mice (Figure 5). This finding is consistent with the concept that β-catenin dysregulation occurs as a consequence of loss of Apc function.

Taken together, these results show that β-catenin dysregulation occurs in both the intestine and pancreas, and that where present it is associated with the very first steps in the development of neoplasia. These findings demonstrate that altered expression of β-catenin is a key marker of *Apc* dysregulation in both these tissues, and suggest that altered β-catenin expression may be a useful diagnostic marker of early

neoplastic change in human disease. However, we also show that β-catenin dysregulation is not an obligate step in the generation of intestinal lesions in an *Msh2* deficient background, and therefore that other mechanisms may underlie such early neoplastic change.

Acknowledgements
We wish to thank Hein te Riele for supply of *Msh-2* deficient mice, James Going for assistance with microdissection and John Verth and his staff for animal maintenance. AR Clarke is a Royal Society University Research Fellow. This work was supported by SHERT, the Cancer Research Campaign and by a grant from the government of Thailand to R Kongkanuntn.

References

Alman BA, Li C, Pajerski ME, Diaz-Cano S and Wolfe HJ. (1997). *Am. J. Path.*, **151,** 329–334.

Behrens J, Jerchow BA, Wurtele M, Grimm J, Asbrand C, Wirtz R, Kuhl M, Wedlich D and Birchmeier W. (1998). *Science,* **280,** 596–599.

Boynton R, Blout P, Yin J, Brown V, Huang Y, Tong Y, McDaniel T, Newkirk C, Resau J, Raskind W, Haggitt R, Ried B and Meltzer S. (1992). *Proc. Natl. Acad. Sci. USA,* **89,** 1–4.

Birchmeier W and Behrens J. (1994). *Biochimica Et Biophysica Acta.*, **1198,** 11–26.

Chen H, Paradies N, Fedor-Chaiken M and Brackenbury R. (1997). *J. Cell Sci.*, **110,** 345–356.

Clarke AR, Cummings MC and Harrison D. (1995). *Oncogene,* **11,** 1913–1920.

Clarke AR Purdie CA, Harrison DJ, Morris RG, Bird CC, Hooper ML and Wyllie AH. (1993). *Nature,* **362,** 849–851.

De Wind N, Dekker M, Berns A Radman M and te Riele H. (1995). *Cell,* **82,** 321–330.

De Wind N, Dekker M, VanRossum A, VanderValk M and Riele HT. (1998). *Cancer Res.*, **58,** 248–255.

Fodde R, Edelmann W, Yang K, Vanleeuwen C, Carlson C, Renault B, Breukel C, Alt E, Lipkin M, Khan PM and Kucherlapati R. (1994). *Proc. Natl. Acad. Sci. USA.*, **91,** 8969–8973.

Going JJ and Lamb RF. (1996). *J. Pathol.* **179,** 121–124.

Horii A, Nakatsuru S, Miyoshi Y, Ichii S, Nagase H, Ando H, Yanagisawa A, Tsuchiya E, Kato Y and Nakamura Y. (1992). *Cancer Res.*, **52,** 6696–6698.

Huber O, Korn R, McLaughlin J, Ohsugi M, Herrmann BG and Kemler R. (1996). *Mech. Dev.*, **59,** 3–10.

Ikeda S, Kishida S, Yamamoto H, Murai H, Koyama S and Kikuchi A. (1998). *EMBO J.*, **17,** 1371–1384.

Inomata M, Ochiai A, Akimoto S, Kitano S and Hirohashi S. (1996). *Cancer Res.*, **56,** 2213–2217.

Kashiwaba M, Tamura G and Ishida M. (1994). *J. Cancer Res. Clin. Oncol.*, **120,** 727–731.

Kinzler K *et al.* (1991). *Science,* **253,** 661–664.

Kishida S, Yamamoto H, Ikeda S, Kishida M, Sakamoto I, Koyama S and Kikuchi A. (1998). *J. Biol. Chem.*, **273,** 10823–10826.

Korinek V, Barker N, Morin PJ, van Wichen D, de Weger R, Kinzler KW, Vogelstein B and Clevers H. (1997). *Science,* **275,** 1784–1787.

Luongo C, Moser AR, Gledhill S and Dove WF. (1994). *Cancer Res.*, **54,** 5947–5952.

Morin PJ, Sparks AB, Korinek V, Barker N, Clevers H, Vogelstein B and Kinzler KW. (1997). *Science,* **275,** 1787–1790.

Moser AR, Luongo C, Gould KA, McNeley MK, Shoemaker AR and Dove WF. (1995). *Eur. J. Cancer,* **31,** 1061–1064.

Moser AR, Mattes EM, Dove WF, Lindstrom MJ, Haag JD and Gould MN. (1993). *Proc. Natl. Acad. Sci. USA,* **90,** 8977–8981.

Moser AR, Dove WF, Roth KA and Gordon JI. (1992). *J. Cell. Biol.*, **116,** 1517–1526.

Miyoshi Y, Nagase H, Ando H, Horii A, Ichii S, Nakatsuru S, Aoki T, Miki Y, Mori T and Nakamura Y. (1992). *Hum. Mol. Genet.*, **1,** 229–233.

Nakatsuru S, Yanagisawa A, Ichii S, Tahara E, Kato Y, Nakamura Y and Horii A. (1992). *Hum. Mol. Genet.*, **1,** 559–563.

Nusse R. (1997). *Cell,* **89,** 321–323.

Oshima M, Oshima H, Kitagawa K, Kobayashi M, Itakura C, Taketo M. (1995). *Proc. Natl. Acad. Sci.*, **92,** 4482–4486.

Papkoff J Rubinfeld B, Schryver B and Polakis P. (1996). *Mol. Cell. Biol.*, **16,** 2128–2134.

Perl A-K Wilgenbus P, Dahl U, Semb H and Christofori G. (1998). *Nature,* **392,** 190–193.

Reitmair AH, Cai JC, Bjerknes M, Redston M, Cheng H, Pind MTL, Hay K, Mitri A, Bapat BV, Mak TW and Gallinger S. (1996). *Cancer Res.*, **56,** 2922–2926.

Rubinfeld B, Souza B, Albert I, Muller O, Chamberlain SH, Masiarz Fr, Munemitsu S and Polakis P. (1993). *Science,* **262,** 1731–1734.

Rubinfeld B, Albert I, Porfiri E, Fiol C, Munemitsu S and Polakis P. (1996). *Science,* **272,** 1023–1026.

Rubinfeld B, Robbins P, El-Gamil M, Albert I, Porfiri E and Polakis P *et al.* (1997). *Science,* **275,** 1790–1792.

Smits R, van der Houven van Oordt W, Luz A, Zurcher C, Jagmohan-Changur S, Breukel C, Khan PM, Fodde R. (1998). *Gastroenterology,* **114,** 275–283.

Sparks AB, Morin PJ, Vogelstein B, Kinzler KW. (1998). *Cancer Res.*, **58,** 1130–1134.

Sheng H, Shao J, Williams CS, Pereira MA, Taketo MM, Oshima M, Reynolds AB, Washington MK, DuBois RN and Beauchamp RD. (1998). *Carcinogenesis.*, **19,** 543–550.

Shibata H, Toyama K, Shioya H, Ito M, Hirota M, Hasegawa S, Matsumoto H, Takano H, Akiyama T, Toyoshima K, Kanamaru R, Kanegae Y, Saito I, Nakamura Y, Shiba K and Noda T. (1997). *Science,* **278,** 120–123.

Shoemaker AR, Gould KA, Luongo C, Moser AR and Dove WF. (1997). *Biochim Biophys Acta,* **1332,** 25–48.

Su LK, Vogelstein B and Kinzler KW. (1993). *Science,* **262,** 1734–1737.

Takayama T, Shiozaki H, Shibamoto S, Oka H, Kimura Y, Tamura S, Inoue M, Mondon T, Ito F, Monden M. (1996). *Am. J. Pathol.* **148,** 39–46.

Thompson AM, Morris RG, Wallace M, Wyllie AH, Steel CM and Carter DC. (1993). *Br. J. Cancer, (1993).* **68,** 64–68.

van der Houven, van Oordt CW, Smits R, Williamson SL, Luz A, Khan PM, Fodde R, van der Eb AJ and Breuer ML. (1997). *Carcinogenesis.*, **18.** 2197–2203.